Robert G. Byram
Senior Vice President and
Chief Nuclear Officer

PPL Susquehanna, LLC
Two North Ninth Street
Allentown, PA 18101-1179
Tel. 610.774.7502 Fax 610.774.6092
rgbyram@pplweb.com

FEB 0 4 2002

U.S. Nuclear Regulatory Commission
Attn: Document Control Desk
Mail Station OP1-17
Washington, DC 20555

SUSQUEHANNA STEAM ELECTRIC STATION
SUPPLEMENT TO PROPOSED AMENDMENT NO. 239
TO LICENSE NPF-14 AND PROPOSED
AMENDMENT NO. 204 TO LICENSE NPF-22:
HPCI AUTOMATIC TRANSFER TO SUPPRESSION
POOL LOGIC ELIMINATION
PLA-5425

Docket No. 50-387
and 50-388

Reference: 1) PLA-5322, R. G. Byram (PPL) to USNRC Document Control Desk, "Proposed Amendment No. 239 to License NPF-14 and Proposed Amendment No. 204 to License NPF-22: HPCI Automatic Transfer to Suppression Pool Logic Elimination", dated June 8, 2001.

2) Letter, NRC to R. G. Byram (PPL), "Susquehanna Steam Electric Station, Units 1 and 2 - Request for Additional Information Re: Elimination of Automatic Transfer of High-Pressure Coolant Injection Pump Suction Source (TAC Nos. MB2190 and MB2191)", dated December 18, 2001.

The purpose of this letter is to provide supplemental information necessary for the NRC staff to complete its review of the license amendment proposed in Reference 1.

PLA-5322 proposed deletion from the Unit 1 and Unit 2 Technical Specification Table 3.3.5.1-1 the "High Pressure Coolant Injection (HPCI) System Suppression Pool Water Level – High" (Function 3e). Implementation of this proposed change eliminates automatic transfer of the HPCI pump suction source from the Condensate Storage Tank to the Suppression Pool for a high Suppression Pool level. Implementation of the proposed change and the associated plant modifications are essential to eliminate a vulnerability identified by the PPL Susquehanna (PPL) Individual Plant Evaluation (IPE).

A001

The Nuclear Regulatory Commission staff has reviewed Reference 1 and has determined that additional information is required in order to complete the NRC review. The additional information requested is documented in a Request for Additional Information (RAI) dated December 18, 2001, (Reference 2).

Attachment 1 to this letter contains responses to the NRC Request for Additional Information (Reference 2), and supplemental support documents referenced in the responses.

Both Attachments 2 and 3 contain information proprietary and/or confidential to PPL. Accordingly, it is respectfully requested that the information which is proprietary and/or confidential to PPL be withheld from public disclosure in accordance with 10 CFR 2.790 of the Commission's regulations. In addition, Attachment 3 contains information which should be withheld from disclosure in the interest of national defense and to protect the security of the Susquehanna Steam Electric Station. This request is supported by an affidavit which sets forth the basis on which the information may be withheld from public disclosure by the Commission and addresses with specificity the considerations listed in paragraphs (a)(1) and (a)(4) of 10 CFR 2.790 of the Commission's regulations.

A non-proprietary/non-confidential version of calculation EC-RISK-1083, "Risk Associated with the Removal of the HPCI Automatic Suction Swap from the CST to the Suppression Pool" is included as Attachment 4.

We trust that this information is sufficient for NRC to complete its review by May 1, 2002 to support implementation of the modifications, procedure changes, and operator training in September 2002. If you have any questions, please contact Mr. D. L. Filchner at (610) 774-7819.

Sincerely,

R. G. Byram

Attachment

cc: NRC Region I w/o attachment
Mr. S. L. Hansell, NRC Sr. Resident Inspector w/o attachment
Mr. D. S. Collins, NRC Project Manager w/o attachment

BEFORE THE
UNITED STATES NUCLEAR REGULATORY COMMISSION

In the Matter of :

PPL Susquehanna, LLC: Docket No. 50-387

SUPPLEMENT TO PROPOSED AMENDMENT NO. 239
TO LICENSE NPF-14: HPCI AUTOMATIC TRANSFER TO SUPPRESSION POOL LOGIC ELIMINATION
UNIT NO. 1

Licensee, PPL Susquehanna, LLC, hereby files a supplement Proposed Amendment No. 239 in support of a revision to its Facility Operating License No. NPF-14 dated July 17, 1982.

This amendment involves a revision to the Susquehanna SES Unit 1 Technical Specifications.

PPL Susquehanna, LLC
By:

R. G. Byram
Sr. Vice-President and Chief Nuclear Officer

Sworn to and subscribed before me
This 4th day of February, 2002.

Notary Public

Notarial Seal
Nancy J. Lannen, Notary Public
Allentown, Lehigh County
My Commission Expires June 14, 2004

BEFORE THE
UNITED STATES NUCLEAR REGULATORY COMMISSION

In the Matter of :

PPL Susquehanna, LLC : Docket No. 50-388

SUPPLEMENT TO PROPOSED AMENDMENT NO. 204
TO LICENSE NPF-22: HPCI AUTOMATIC TRANSFER TO SUPPRESSION POOL LOGIC ELIMINATION
UNIT NO. 2

Licensee, PPL Susquehanna, LLC, hereby files a supplement to Proposed Amendment No. 204 in support of a revision to its Facility Operating License No. NPF-22 dated March 23, 1984.

This amendment involves a revision to the Susquehanna SES Unit 2 Technical Specifications.

PPL Susquehanna, LLC
By:

R. G. Byram
Sr. Vice-President and Chief Nuclear Officer

Sworn to and subscribed before me
this 4th day of February, 2002.

Notary Public

Notarial Seal
Nancy J. Lannen, Notary Public
Allentown, Lehigh County
My Commission Expires June 14, 2004

Attachment 1 to PLA-5425

Response to RAI Questions

Attachment 1 – Response to RAI Questions

NRC Question 1a, 1b, 1c, and 1d

The licensee stated that this change would address a potential vulnerability identified in the individual plant examination that is associated with a specific scenario involving an anticipated transient without scram. The licensee also indicates that this change would reduce operator burden during a station blackout event. However, if this automatic feature were removed, new operator actions may be necessary during a small-break loss-of-coolant accident (LOCA) to manually transfer the suction from the CST to the SP on high SP level. Because there are potentially negative as well as positive risk impacts associated with the proposed change, the Nuclear Regulatory Commission (NRC) staff requires the following information to support its review:

NRC Question 1a

> Provide the plant's current core damage frequency (CDF) and large early release frequency (LERF) and the plant's revised (i.e. assuming the proposed change is implemented) CDF and LERF. In addition, the licensee should provide a breakdown of the current and revised CDF and LERF contribution by initiating event and needs to provide a discussion of the impacts of the proposed change on the individual event sequences/initiating events.

PPL Response

The current and revised CDF and LERF values are contained in calculation EC-RISK-1083, which is included as Attachment 4 to this correspondence. The calculation determines that the CDF and LERF are reduced by 12% (from 4.45 E-7 to 3.92 E-7) and 85% (from 5.52 E-8 to 8.49 E-9) respectively if the automatic suction swap is changed to a manual suction swap for mean and the upper 95% confidence level operator error rates.

The calculation determines that CDF reduction decreases from 12% to 7% and the LERF remains at 85% when the operator error associated with making the manual suction swap and controlling RPV water level with HPCI is assumed to be 100%.

The breakdown of current and revised CDF and LERF initiating event contributions are provided in Attachment 4, Calculation EC-RISK-1083, "Risk Associated with the Removal of the HPCI Automatic Suction Swap from the CST to the Suppression Pool", Section 5.3.

NRC Question 1b

Provide a description of how the licensee assures that the current probabilistic risk analysis (PRA) models reflect the as-built, as-operated plant and if the current PRA has been through an industry peer review certification process. If there was a peer review, please provide the overall findings of the review (by element) and discuss any elements rated low (e.g., less than a 3 on a scale of 1 to 4) or any findings that potentially affect the sequences impacted by the licensee's proposed change. The licensee will need to address any identified weaknesses in the PRA models that might affect the results associated with this license amendment.

PPL Response

The PPL approach to risk assessment is to develop an accurate and definitive description of each accident sequence and to realistically portray the role of human intervention as defined by Emergency Operating Procedures (EOPs) to terminate accident progression. The original PRA model was developed under the auspices of the PPL Quality Assurance Program. The program requires each calculation to be prepared and reviewed by qualified engineers and approved by qualified supervision. This process assured the original model was consistent with the as built and as operated plant. A discussion of how plant changes are incorporated in the model follows.

There are four ways plant changes can impact the model: design changes, procedure changes, configuration changes and reliability data changes. Each activity is captured and its impact reflected in the model.

Risk Management is a design consideration for all plant modifications. The design engineer is required to evaluate the impact of each design change on the plant risk model using a screening checklist. The design engineer is required to contact the Risk Analysis Subgroup for any design changes that do not pass the screening. The Risk Analysis Subgroup then analyzes the impact of the change on the model. This process ensures that the model will be consistent with design changes.

The Risk Analysis Subgroup is responsible for the generation of the Emergency Operating Procedure (EOP) basis, preparation of the 50.59 evaluations, and validation of the procedure changes in the plant simulator. EOP changes are well understood by the Risk Analysis Group and have often been motivated by risk reduction initiatives. This close coupling between the Risk Analysis Subgroup and the plant EOPs ensures that EOP procedure changes are reflected in the model.

Changes in plant configuration and reliability data are linked to the risk model through the Maintenance Rule (10 CFR 50.65). The plant configuration is controlled using an on-line risk monitor (currently ORAM/SENTENAL but transitioning to EOOS). The monitor is based upon ensuring defense in depth for both Core Damage (CDF) and Large Early Release (LERF). The EOOS model under development will include a real time calculation of both CDF and LERF. Thus, plant configuration is controlled within the bounds of the risk model using an online monitor.

Finally the reliability and availability criteria used to evaluate the performance of plant Systems, Structures and Components (SSC) were derived from the PRA study. SSCs which do not satisfy the criteria are placed into Maintenance Rule Category a1 where a recovery plan is developed to restore the SSC to the value consistent with the PRA study. Thus, the reliability database used for the PRA model is validated via implementation of the Maintenance Rule.

The PRA has not been certified through an industry PRA certification program. In accordance with Reg. Guide 1.174, Section 2.2.3.3, July 1998, "An Approach for Using Probabilistic Risk Assessment in Risk-Informed Decisions on Plant Specific Changes to the Licensing Basis", a peer review or certification process should be used as the basis to justify PRA adequacy in terms of scope and quality. The PPL IPE received an expert peer review by Dr. William Vesely. Additionally, the NRC issued a revised SER for the Susquehanna IPE. The review by Dr. Vesely and the SER are included within this Attachment.

NRC Question 1c

Provide a description of the revised PRA modeling and/or assumptions used to reflect the proposed change. This description should address the specific thermal hydraulic conditions that are impacted and were analyzed and any changes in success criteria or sequence / timing events.

PPL Response

In the PRA model, based on current Susquehanna design, Manual Rod Insertion (MRI) is assumed failed and HPCI will automatically swap its suction source to the suppression pool on high pool level. MRI is a relatively slow process to shutdown the reactor and is only successful if HPCI is available for makeup. If an ATWS occurs, the suppression pool temperature will rise above 190°F, the short-term HPCI limit, before the reactor can be brought to Hot Shutdown by MRI. When the automatic suction transfer occurs due to high suppression pool level, there are not enough rods driven into the core to shut down the reactor. HPCI is assumed failed shortly after the automatic transfer occurs due to the

high suction temperature. Without HPCI adding water, the Reactor Pressure Vessel (RPV) level will drop and the RPV must be depressurized while critical, which will cause core damage.

In the revised PRA model, applicable after the proposed change to remove the HPCI automatic suction swap for high suppression pool level, success of MRI is allowed. The manual suction swap imposes an operator action for the small liquid LOCAs. With a small liquid LOCA the suppression pool level rises due to the liquid from the break and the HPCI exhaust steam. The level will exceed the manual transfer point (25 feet suppression pool level) in a minimum of 21 minutes. However, the temperature of the pool does not exceed 140°F. A suppression pool level above 25 feet does not automatically fail HPCI. HPCI will continue to exhaust steam into the suppression pool and the suppression pool level will not exceed the suppression pool load limit. However, if the operator does not control RPV level with HPCI, level 8 will be reached and HPCI will trip. HPCI will automatically restart if the RPV water level reaches level 2. The restart of HPCI with high suppression pool level permits water to enter the horizontal portion of the HPCI exhaust line and could cause a waterhammer upon restart of the system.

The current Emergency Operating Procedure directs the operator to ensure HPCI and Reactor Core Isolation Cooling (RCIC) are running when the suppression pool reaches 26'. (The 26' will be changed to 25' in the next revision of the subject procedure.) This action is not modeled in PPL's Computerized Fault Tree Analysis (CAFTA) because there is complete dependence between the operator manually initiating the suction swap and also assuring that HPCI is running. Therefore, one operator action is sufficient for modeling this event.

The HPCI level concerns outlined above are addressed in the changes to the fault tree model as described below:

An AND Gate, 152-II-N-LVLFAIL was added to the HPCI OR Gate, 152. The AND Gate has four inputs: a small liquid LOCA initiator, a basic event of an operator error to control RPV water level, a basic event of an operator error to manually swap the HPCI suction from the CST to the suppression pool and a switch to defeat this logic for the case using the automatic transfer. Both operator actions need to fail during a small liquid break LOCA to fail HPCI. If either RPV level is controlled or the operator transfers the HPCI suction to the suppression pool, HPCI will not fail due to water intrusion into the exhaust line. If the operator controls RPV level below level 8, HPCI will not trip and try to restart. Continued operation of HPCI when the suppression pool level is above the automatic suction swap level is not a problem, as the exhaust steam will maintain the turbine exhaust piping free of water.

A small liquid break is the only scenario when it is desirable to align the HPCI suction to the suppression pool. For other initiators, the suppression pool level does not reach the HPCI suction manual transfer point of 25 feet or the pool level is above the manual transfer point but the suppression pool temperature exceeds 190°F (the ATWS sequence using MRI).

NRC Question 1d

Provide a description of any new operator actions that are required as a result of the proposed change (e.g., manual swap-over from the CST to the SP for small-break LOCA events), including the associated human error probabilities (HEP's) and the human reliability analysis bases for the HEP's (e.g., cause-based versus time-based, time available, proceduralized, difficulty of diagnosis and implementation, etc.) based on NRC Information Notice 97-78, "Crediting of Operator Actions in Place of Automatic Actions and Modifications of Operator Actions, including Response Times," the licensee should provide for each of these operator actions: (1) the specific operator actions required; (2) the potentially harsh or inhospitable environmental conditions expected; (3) a general discussion of the ingress/egress paths taken by the operators to accomplish functions; (4) the procedural guidance for required actions; (5) the specific operator training necessary to carry out actions, including any operator qualifications required to carry out actions; (6) any additional support personnel and/or equipment required by the operator to carry out actions; (7) description of information required by the control room staff to determine whether such operator action is required, including qualified instrumentation used to diagnose the situation and to verify that the required action has successfully been taken; (8) the ability to recover from credible errors in performance of manual actions, and the expected time required to make such a recovery; and (9) consideration of the risk significance of the proposed operator actions.

PPL Response

(1) New Operator Actions - There are two operator actions credited in the removal of the HPCI automatic suction transfer modification: (1) RPV level control after a transient and (2) manual suction transfer. The manual suction transfer is a new action not currently part of the Emergency Operating Procedures (EOP). This new action will be added to the procedures in accordance with the administrative program that governs EOP changes. It is anticipated that the step will read as follows: When the suppression pool level reaches 25', ensure HPCI and RCIC are running. If HPCI is injecting into the RPV and Suppression Pool Temperature can be maintained less than 140°F, transfer HPCI suction from the CST to the Suppression Pool. Success of either the RPV level control action or manual suction transfer will prevent loss of HPCI.

(2) Harsh/Inhospitable Environments - There are no harsh or inhospitable environments for the new operator action. The new operator action, manual suction transfer, is accomplished in the control room by turning an existing electrical switch on panel 1(2) C601, an inner ring panel.

(3) Ingress/Egress - The new operator action is in the control room, therefore, there is no ingress/egress path.

(4) Procedural Guidance - Guidance for the RPV level control currently exists in the Emergency Operating Procedures. Also, HPCI manual suction transfer will be added to the Emergency Operating Procedures when the modification is installed.

(5) Operator Training - This modification will not be implemented prior to training the operators. A Licensed Reactor Operator will perform the new operator action in the control room. The operators will require training on the manual suction transfer. Simulator exercises will be used to validate that a Licensed Reactor Operator would perform this action properly.

(6) Additional Support - There are no additional support personnel or additional equipment required for these actions.

(7) Control Room Staff Information - Operators control RPV level by any entry condition for the RPV Control or Level/Power Control emergency operating procedures, step RC/L-4. The cue for initiating the HPCI suction transfer is suppression pool high level. The suppression pool high level condition is alarmed in the control room. The level switches that actuate the alarm are safety related and powered by a Class 1E 125VDC power. A 1E battery powers the control room annunciator; however, it is via a non-1E electrical panel. There are also two safety related suppression pool level indicators in the control room on 1/2C601. The operator will receive indication of a successful suction transfer by the valve position indicating lights in the control room.

(8) Recovery from Credible Errors - A credible error in implementing the manual suction transfer is an error closing the suction source from the CST without the suppression pool suction valve being open. If this error occurs, HPCI will trip on low suction pressure. If this valve is inadvertently closed and there still is a valid HPCI initiation signal, this valve will automatically reopen and HPCI will automatically restart when the low suction pressure condition clears. The hand switch, which initiated the close signal, is a spring return to "auto" so the close signal is not continuous. Hence, the potential operator error of closing the CST

suction source is of no consequence. The duration of the less than full suction flow condition is expected to be approximately 27 seconds. Loss of flow for 27 seconds has no impact on core cooling during small break LOCAs where HPCI is required to operate.

It should be noted that if the HPCI suction valve from the suppression pool is opened, the 100% open limit switch on this valve will initiate a close signal to the HPCI suction valve from the CST.

(9) Risk Significance of Proposed Actions - The proposed operator action, manual HPCI suction transfer, is not risk significant. There is no change in CDF for the operator action always being successful and there is only a 5% increase in CDF if the operator action always fails. The LERF is insensitive to the manual HPCI suction transfer.

NRC Question 2

The SABRE code is relied upon to assess the impact of the proposed change on the intermediate – and small-break LOCA and inadvertent main steam isolation valve closure sequences. This code has not previously been reviewed or approved by the staff. In order for the staff to complete its review of the proposed change, please submit the code and associated documentation. The submittal should include the source code, available user documentation, and input data used to evaluate the sequences noted above.

PPL Response:

Included in Attachment 1 to PLA-5425 are PPL Calculations EC-ATWS-0505, Rev. 8; EC-052-0593, Rev. 0; EC-SIMU-0501, Rev. 0; and EC-SATH-1007, Rev. 1 which provide software QA documentation for the SABRE computer code. Also supplied are Calculations EC-052-1018, Rev. 2 and EC-052-1025, Rev. 2 which support the proposed Technical Specification change to delete automatic HPCI suction transfer on high suppression pool level.

The SABRE source code and SABRE input files are considered proprietary and are provided on 4mm tape along with instructions for code installation and execution in Attachment 2.

UNITED STATES
NUCLEAR REGULATORY COMMISSION
WASHINGTON, D.C. 20555-0001

August 11, 1998

Mr. Robert G. Byram
Senior Vice President-Generation
and Chief Nuclear Officer
Pennsylvania Power and Light Company
2 North Ninth Street
Allentown, PA 18101

SUBJECT: REVIEW OF THE SUSQUEHANNA STEAM ELECTRIC STATION, UNITS 1 AND 2, INDIVIDUAL PLANT EXAMINATION SUBMITTAL - INTERNAL EVENTS (TAC NOS. M74478 AND M74479)

Dear Mr. Byram:

Enclosed is the NRC staff's supplement to the October 27, 1997, staff evaluation report (SER) of the Susquehanna Steam Electric Station (SSES), Units 1 and 2, Individual Plant Examination (IPE) submittal for internal events, including internal flooding.

On October 27, 1997, the NRC forwarded to Pennsylvania Power & Light Company (PP&L) an SER stating that the NRC staff could not conclude that the SSES IPE submittal met the intent of Generic Letter (GL) 88-20. In response, you submitted additional information and on February 27, 1998, briefed the staff on revisions made to address the issues identified in the SER. On April 1, 1998, the staff audited the SSES IPE at your offices in Allentown, Pennsylvania.

The enclosed SER supplement addresses the final resolution of the issues raised by the staff in its original SER. In the revised IPE, the calculated mean core damage frequency (CDF) is about 7E-7/reactor-cycle of 15 months (or about 5E-7/reactor-year), which is about a factor of seven higher than the original IPE CDF of 1E-7/reactor-cycle. Anticipated transient without scram contributes about 63% to the CDF, loss of decay heat removal contributes about 23%, internal flooding contributes about 10%, station blackout contributes about 2%, and transients contribute about 2%. The contribution of loss-of-coolant-accident (LOCA) and interfacing systems LOCA is less than 1%.

You have implemented all of the plant improvements identified in the original IPE, as well as additional improvements. On the basis of the information provided, the staff concludes that the revised SSES IPE process is adequate to meet the following four objectives of GL 88-20:

(1) To develop an appreciation for severe accident behavior,
(2) To understand the most likely severe accident sequences that could occur at the plant,
(3) To gain a more quantitative understanding of the overall probabilities of core damage and fission product releases, and
(4) If necessary, to reduce the overall probabilities of core damage and fission product releases by modifying, where appropriate, hardware and procedures that would help prevent or mitigate severe accidents.

Therefore, the staff concludes that the SSES IPE submittal, as supplemented, meets the intent of GL 88-20. The staff notes your commitment to identify instances of plant improvements in order to maintain a low CDF or further decrease the CDF, at SSES. The staff also notes PP&L's strong in-house PRA capability. The SSES IPE was performed almost entirely in-house; also, according to PP&L, it is continually using and updating the SSES PRA. Although the NRC staff had several concerns about the original SSES IPE approach, because of the revisions performed in the front-end portion, the ongoing use of the PRA in conjunction with PP&L's defense-in-depth approach, and the ongoing identification and implementation of improvements, the staff believes that the current front-end analysis of the SSES IPE presents an exemplary analysis. The staff encourages you to continually confirm the IPE's reliability of equipment and operator performance ensuring that it portrays SSES plant capability under severe accident conditions.

However, some weaknesses still remain in the IPE's back-end analysis. The staff believes that it is unlikely that these remaining weaknesses have affected the overall conclusion from the revised analysis or the capability of identifying vulnerabilities; it may, however, limit its usefulness in other regulatory applications, especially in applications related to containment performance. The staff believes that PP&L can enhance the usefulness of the SSES IPE by addressing the weaknesses discussed in the enclosed SER supplement.

It should be noted, that the staff focused its review primarily on your ability to examine SSES Units 1 and 2 for severe accident vulnerabilities. Although certain aspects of the IPE were explored in more detail than others, the review is not intended to validate the accuracy of the detailed findings (or quantification estimates) that stemmed from the examination. Therefore, this SER does not constitute NRC approval or endorsement of any IPE material for purposes other than those associated with meeting the intent of GL 88-20.

If you have any questions regarding the enclosed SER supplement, please contact me at (301) 415-1484.

Sincerely,

Victor Nerses

Victor Nerses, Senior Project Manager
Project Directorate I-2
Division of Reactor Projects - I/II
Office of Nuclear Reactor Regulation

Docket Nos. 50-387/50-388

Enclosure: As stated

cc w/encl: See next page

cc:

Jay Silberg, Esq.
Shaw, Pittman, Potts & Trowbridge
2300 N Street N.W.
Washington, D.C. 20037

Bryan A. Snapp, Esq.
Assistant Corporate Counsel
Pennsylvania Power & Light Company
2 North Ninth Street
Allentown, Pennsylvania 18101

Regional Administrator, Region I
U.S. Nuclear Regulatory Commission
475 Allendale Road
King of Prussia, Pennsylvania 19406

General Manager
Susquehanna Steam Electric Station
Pennsylvania Power and Light Company
Box 467
Berwick, Pennsylvania 18603

Licensing Group Supervisor
Pennsylvania Power & Light Company
2 North Ninth Street
Allentown, Pennsylvania 18101

Mr. Herbert D. Woodeshick
Special Office of the President
Pennsylvania Power and Light Company
Rural Route 1, Box 1797
Berwick, Pennsylvania 18603

Senior Resident Inspector
U. S. Nuclear Regulatory Commission
P.O. Box 35
Berwick, Pennsylvania 18603-0035

George T. Jones
Vice President-Nuclear Operations
Pennsylvania Power and Light Company
2 North Ninth Street
Allentown, Pennsylvania 18101

Director-Bureau of Radiation
Protection
Pennsylvania Department of
Environmental Resources
P. O. Box 8469
Harrisburg, Pennsylvania 17105-8469

Dr. Judith Johnsrud
National Energy Committee
Sierra Club
433 Orlando Avenue
State College, PA 16803

Mr. Jesse C. Tilton, III
Allegheny Elec. Cooperative, Inc.
212 Locust Street
P.O. Box 1266
Harrisburg, Pennsylvania 17108-1266

Chairman
Board of Supervisors
738 East Third Street
Berwick, PA 18603

UNITED STATES
NUCLEAR REGULATORY COMMISSION
WASHINGTON, D.C. 20555-0001

STAFF EVALUATION REPORT SUPPLEMENT SUSQUEHANNA STEAM ELECTRIC STATION, UNITS 1 AND 2 INDIVIDUAL PLANT EXAMINATION (INTERNAL EVENTS ONLY)

I. INTRODUCTION

On December 13, 1991, Pennsylvania Power & Light Company (PP&L) (the licensee) submitted the Susquehanna Steam Electric Station (SSES), Units 1 and 2, Individual Plant Examination (IPE) in response to Generic Letter (GL) 88-20 and associated supplements. On November 4, 1992, and on December 17, 1996, the staff met with the licensee to discuss the Nuclear Regulatory Commission's (NRC) concerns regarding the SSES IPE. On January 11, 1993, the licensee submitted Volume 6 of the IPE and on June 23, 1997, the licensee provided additional information regarding issues raised by the staff.

The staff performed a "Step 1" review of the SSES IPE submittal and was supported by the Brookhaven National Laboratory. On October 27, 1997, the staff sent its evaluation report to the licensee in which it was stated that the staff could not conclude that the SSES IPE met the intent of GL 88-20. In response to this staff evaluation report (SER), the licensee revised its IPE. On February 27, 1998, the licensee briefed the staff on the revisions it had made and on April 1, 1998, the staff audited the SSES IPE at the licensee's headquarters in Allentown, Pennsylvania. The staff's audit focused on whether the licensee addressed the concerns documented in the October 27, 1997, SER. This supplement, therefore, documents the staff's findings and conclusions regarding the licensee's resolution of its concerns.

In accordance with GL 88-20, PP&L had proposed in its original IPE to resolve Unresolved Safety Issue (USI) A-45, "Shutdown Decay Heat Removal Requirements." The licensee had also proposed to resolve USI A-17, "System Interactions," as part of its IPE. No other specific USIs or generic safety issues were proposed for resolution as part of the IPE.

II. EVALUATION

In the revised IPE, the licensee calculated a core damage frequency (CDF) of about 7E-7/reactor-cycle, which is about a factor of seven larger than the CDF of 1E-7/reactor cycle of the original submittal. Anticipated transients without scram (ATWS) contribute about 63% to the CDF, loss of decay heat removal (DHR) contributes about 23%, internal flooding contributes about 10%, station blackout (SBO) contributes about 2%, transients contribute about 2%. The contribution from loss-of-coolant-accident (LOCA) and interfacing systems LOCA (ISLOCA) is less than 1%.

In the SER of October 27, 1997, the staff expressed concerns in several areas. In particular, it was noted that the licensee did not provide sufficient evidence for the staff to conclude that the following areas were appropriately treated: common-cause failures (CCFs), human reliability analysis (HRA), plant-specific failures, and back-end (i.e., containment performance) analysis, including the lack of sensitivity analyses. The licensee addressed these concerns by revising its CCF, HRA, and plant-specific data analysis, and performing a sensitivity study for the back-end analysis.

Regarding the CCF analysis, the staff found that the original submittal treated CCFs inadequately for active components (e.g., diesels, valves, pumps, and batteries); did not examine single failures to identify those that have a potential for common coupling; did not treat cross-system CCFs, particularly between the high-pressure coolant injection (HPCI) and the reactor core isolation cooling (RCIC) pumps; and did not consider CCFs due to test and maintenance.

In response to these concerns, the licensee reviewed the SSES operational history and revised its approach to CCF by incorporating in the IPE model CCFs for active components of important systems (residual heat removal (RHR), emergency service water (ESW), RHR service water (RHRSW), and diesel generators); examining single failures for common coupling; and including CCFs for RCIC and HPCI and CCFs due to test and maintenance. (The licensee identified a single failure with common-coupling potential, an ESW pump failure due to end bell erosion; it inspected the other pumps and indeed identified end bell erosion in those pumps as well, although they were in operable condition. The licensee accounted this failure as a CCF for ESW.) Overall, it appears that the licensee performed a reasonable search for CCFs.

In order to address the concern regarding low CCF values, the licensee used generic data (NUREG-1150) instead of plant-specific data (estimated on the basis of examining SSES's procedures and practices). In a similar manner, in order to address the concern for the low plant-specific failure rates, the licensee substituted them with generic values. The licensee did not provide a justification as to why these values are appropriate for SSES; therefore, although the licensee demonstrated the impact of the use of higher values on the IPE's results, they did not demonstrate their applicability to SSES. The staff believes that this is a weakness of the revised IPE approach. The licensee, however, performed uncertainty analysis throughout the IPE. Therefore, the staff believes that it is unlikely that this weakness has affected the licensee's overall conclusion from its revised analysis or its capability for identifying vulnerabilities. It may, however, have limited its ability to gain insights.

Regarding the IPE's HRA, the staff found that the revisions in the treatment of both routine human actions (pre-initiator human events) and actions in response to an initiating event (post-initiator human events) are appropriate.

Pre-initiator human events were explicitly modeled in the revised IPE and were segregated from random equipment failures to allow a better assessment of the contribution of human reliability to CDF and, therefore, the development of a better understanding of the role of human reliability on plant safety. According to licensee document EC-RISK-1063, "the maintenance records were re-examined to identify specific instances of undetected system unavailabilities caused by pre-initiator human errors" (PP&L Calculation, pg. 34) for the period from July 1987 to January 1990. This search uncovered three instances of post-maintenance restoration errors. As a result, the licensee revised its IPE model to include post-maintenance restoration human errors in specific components of the systems: HPCI, RCIC, low-pressure coolant injection (LPCI), diesel generators, alternate control rod drive pump, and standby liquid control system. A human error probability (HEP) mean value was estimated on the basis of plant-specific data.

The licensee treated miscalibration errors, which have a common-cause potential, using, as mentioned above, generic, NUREG-1150, data. The staff notes that even a generic treatment of miscalibration is better than no treatment at all because it allows the performance of sensitivity analyses for deriving insights regarding the importance of miscalibration. But, as noted above, the generic treatment of miscalibration is a weakness in the licensee's HRA.

Regarding post-initiator human actions, the licensee revised its IPE model to explicitly include them on the event trees. The licensee's document, EC-RISK-1063, gives a detailed description of the process used to identify and quantify these actions. Accordingly, the licensee identified post-initiator human actions through a review of emergency procedures and its defense-in-depth criteria that provide a reliable and updated source of actions performed in response to an initiating event. The licensee used two different approaches to quantify these actions. For those actions that could be quantified using plant-specific data documented in "Susquehanna Operator Response Data for Actual Events," or in "Susquehanna Operator Response Data From Simulated Events," an HEP was estimated on the bases of these data. For the remaining actions, data from NUREG/CR-4835 were used "because the method generation and its application are generally consistent with the approach being pursued at Susquehanna."

The staff finds the licensee's approach of using plant-specific data for estimating HEPs a strength of the licensee's HRA. In general, the staff found that the licensee appropriately considered critical factors, such as the layout and accessibility of manipulated components, operator training for a specific action, the potential for confusion and misinterpretation of an emergency operator procedure entry condition, and time needed versus time available to perform an action. Furthermore, the dependencies between human actions and the influence of the accident progression on human performance appear to have been treated appropriately.

On the basis of these findings, the staff concludes that the front-end analysis of the revised SSES IPE is reasonable.

In the original submittal, the licensee presented an approach to resolve USI A-45, "Decay Heat Removal Reliability." Taking into consideration the changes in the licensee's front-end analysis and quantitative results, its review of SSES plant-specific features, and the strategy it developed and implemented regarding this issue, the staff concludes that the licensee's IPE process used to search for DHR vulnerabilities is reasonable.

The licensee also proposed to resolve USI A-17, "System Interactions," as part of the IPE. The licensee did not identify any vulnerabilities with respect to A-17. According to GL 88-20, if a licensee concludes "that no vulnerability exists at its plant that is topically associated with any USI or generic safety issue (GSI), the staff will consider the USI or GSI resolved for a plant upon review and acceptance of the results of the IPE." The staff concludes, therefore, that the licensee has resolved USIs A-45 and A-17.

Regarding the back-end analysis, the licensee conducted limited sensitivity studies to investigate the conditional probability of containment failure given conditions of vessel breach at high pressure. With the combination of core damage and vessel failure not at high pressure, the licensee calculated a conditional probability of containment failure of 9 percent. By contrast, the combination of core damage and vessel failure at high pressure resulted in a conditional probability of containment failure of 54 percent. This result appears to be reasonable.

One specific aspect of the SSES IPE is the credit taken for preventing vessel failure with the core damaged under station blackout conditions through local operator actions focusing on providing alternate power (ac) or restoring ac power. According to EC-RISK-1063, the licensee relies on operators stationed locally for performing these actions and the actions are well proceduralized and practiced. In estimating pertinent HEPs, plant conditions and time needed versus time available to perform these actions were taken into consideration. The staff notes that it was the intent of GL 88-20 for licensees to identify all potential means of accident mitigation. Therefore, the staff finds this aspect as a strength of the SSES IPE. It is noted however, that these actions contribute to a high probability of vessel failure prevention. Therefore, the staff encourages the licensee to continually confirm the reliability of operator performance used in the IPE, ensuring that the IPE portrays SSES performance under severe accident conditions.

In general, the licensee indicated that core debris is 14 times more likely to be quenched in-vessel if core damage progresses in a manner consistent with the core relocation model used in the BWRSAR code, which the licensee used in the IPE, compared to the core blockage model employed in the industry-developed MAAP code. The staff believes that code input assumptions, such as success criteria, may play a role in the reduction of vessel breach likelihood at SSES compared to other Mark II plants.

Regarding the containment performance improvement (CPI) program recommendations, the SSES design includes a 30-day supply of compressed nitrogen for safety-relief valve actuation. The licensee has also installed a mobile diesel generator to recharge the 125-volt dc batteries. These plant capabilities provide enhanced depressurization system reliability.

The licensee has also provided threaded connections on the RHR service water system, which allow for alignment of the diesel-driven fire protection system pumps to the RHR system, thus providing an alternate water source for injection.

The licensee examined the issue of venting using an existing soft vent (i.e., the heating, ventilation, and air conditioning (HVAC) ducts). The HVAC piping will fail at expected vent pressures, now estimated at approximately 60 psig (based on the revised venting procedure) instead of at the 15 psig vent pressure proposed in the original IPE. The licensee indicated that it has developed procedures to maintain core cooling in the event that most reactor building equipment is lost by aligning systems external to the reactor building. In addition, the licensee is evaluating a conceptual venting strategy that will provide a framework, based upon input such as the estimated source term and combustible gas challenges, to help decide if venting is a viable option. This appears reasonable.

On the basis of this review, the staff concludes that the licensee's response to the CPI program recommendations is reasonable and consistent with the intent of GL 88-20.

Some weaknesses exist, however, in the licensee's back-end analysis:

1. In the licensee's analysis, the accident sequence progression was terminated if the containment failed prior to core damage; all sequences were then assumed to go to core damage in the reported CDF. Radionuclide releases were not calculated for these containment failures nor was a detailed understanding of plant response obtained.

2. The impact on conditional containment failure probability of some severe accident phenomena and resulting containment failure modes appear to have been understated. As a result, all early and late containment failures, other than the containment failures resulting from loss of DHR discussed in item 1 above, are reported by the licensee to occur in less than one percent of core damage events, including ATWS and station blackout.

   Appendix 1 to GL 88-20 recommended that licensees consider a maximum coolable debris bed to be 25 cm. For depths in excess of that (as proposed in the SSES IPE) both coolable and noncoolable outcomes should be considered and documented, even in the presence of a water layer provided by the drywell sprays, because of the possibility of the formation of a noncoolable debris crust. Noncoolable outcomes may lead to the occurrence of phenonema such as containment overpressure failure from noncondensible gas generation due to core-concrete interaction or containment failure from corium attack on the drywell liner/concrete containment boundary.

   The licensee assumed, however, that core debris released from the vessel post-accident will always be quenched on the drywell floor and, consequently, core-concrete interactions with the drywell floor, steel liner, or concrete containment will be prevented, as long as the drywell sprays provide a water pool on the drywell floor. Similarly, core debris attack on other structures, such as the downcomer vents, resulting in suppression pool bypass or loss of pool scrubbing, would not be possible, according to the licensee, given spray operation. Additionally, the licensee did not consider the possible negative effects of water on the drywell floor, such as containment pressurization due to ex-vessel steaming resulting from fuel-coolant interactions.

3. The treatment of ISLOCA was characterized as limited in the staff's October 27, 1997, SER. The licensee has not revised its ISLOCA analysis and, consequently, it remains a weakness.

III. CONCLUSION

On the basis of the information submitted by the licensee through either direct discussion with the staff or in writing, the staff concludes that the licensee's IPE is complete with regard to the information requested by GL 88-20 (and associated NUREG-1335), and that the licensee's IPE process is adequate to meet the objectives of the IPE program as stated in GL 88-20:

1. To understand the most likely severe accident sequences that could occur at the plant.

2. To develop an appreciation for severe accident behavior.

3. To gain a more quantitative understanding of the overall probabilities of core damage and fission product releases.

4. If necessary, to reduce the overall probabilities of core damage and fission product releases by modifying, where appropriate, hardware and procedures that would help prevent or mitigate severe accidents.

Therefore, the staff now concludes that the SSES IPE submittal meets the intent of GL 88-20. The staff notes PP&L's commitment to identify instances of plant improvements in order to maintain a low CDF or further decrease the CDF, at SSES. The staff also notes PP&L's strong in-house PRA capability. The SSES IPE was performed almost entirely in-house; also, according to PP&L, its staff is continually using and updating the SSES PRA. Although the staff had several concerns about the original SSES IPE approach, because of the revisions performed in the front-end portion, the ongoing use of the PRA in conjunction with PP&L's defense-in-depth approach, and the ongoing identification and implementation of improvements, the staff believes that the current front-end analysis of the SSES IPE presents an exemplary analysis. The staff encourages the licensee to continually confirm the IPE's reliability of equipment and operator performance ensuring that it portrays SSES plant capability under severe accident conditions.

However, some weaknesses still remain in the IPE's back-end analysis. The staff believes that it is unlikely that these remaining weaknesses have affected the licensee's overall conclusion from its revised analysis or its capability of identifying vulnerabilities; it may, however, limit its usefulness in other regulatory applications, especially in applications related to containment performance. The staff believes that the licensee can enhance the usefulness of its IPE by addressing these issues, discussed in this document.

It should be noted, that the staff focused its review primarily on the licensee's ability to examine SSES Units 1 and 2 for severe accident vulnerabilities. Although certain aspects of the IPE were explored in more detail than others, the review is not intended to validate the accuracy of the licensee's detailed findings (or quantification estimates) that stemmed from the examination. Therefore, this SER does not constitute NRC approval or endorsement of any IPE material for purposes other than those associated with meeting the intent of GL 88-20.

Principal Contributors: E. Lois
J. Lane

Date: July 15, 1998

PLA-5425
ATTACHMENT 1

REVIEW OF THE SUSQUEHANNA IPE

W. E. VESELY

May 29, 1997

REVIEW OF THE SUSQUEHANNA IPE

W. E. Vesely

My conclusion overall is that the SSES IPE is a very detailed and competent analysis. Based on my review of the accident sequences and based on my discussions with the chief engineer responsible for the IPE, I am convinced that the IPE models are thorough, detailed, and accurate. The accident sequences that are defined are developed to the detail required to include all the contributing component failures and human errors. The accident sequences are not binned as in the usual PRA, but instead each individual sequence is followed in the evaluations and quantifications to determine the consequences of the sequence. The plant damage state associated with each sequence is determined from the thermal-hydraulics of the sequence. Sequences resulting in similar consequences which result in the same damage state are combined to give the total frequency of the damage state. This detailed analysis was necessary because of the defense-in-depth criteria utilized in the SSES IPE which required that specific, multiple equipment be identified which could mitigate each accident sequence.

In carrying out its detailed treatments, the SSES IPE uses modeling approaches and quantification approaches which are different from those used in the usual PRA. Instead of focusing on the physical consequences and events which are associated with the accident sequences, the focus is on the plant damage state associated with the sequence. The comprehensive set of plant damage states defined in the SSES IPE are: (1) core damage from inadequate cooling, (2) mechanical cladding damage, (3) core melt with

reactor vessel breach, (4) containment failure with core damage in-vessel, (5) containment failure with mechanical cladding damage in-vessel, (6) core melt with reactor vessel breach and containment failure, (7) wetwell venting without core damage, and (8) containment overpressure failure without prior core damage, and (9) core damage from inadequate cooling with vessel failure and containment overtemperature failure. The IPE focus on the plant damage states is done at the expense of a de-emphasis of the physical event and consequence descriptions. For example, direct containment heating (DCH) is not explicitly evaluated in the SSES IPE. This makes the review of the sequences difficult with regard to the physical variables and events associated with the sequences, however the event bases for the sequences can be found in the IPE.

The results of the SSES IPE are different from other PRAs and IPEs in that very low frequencies are calculated for core damage (1.1×10^{-7} per year), for core damage plus vessel failure (3.7×10^{-9} per year) and for core damage, vessel failure, and containment breach (7.9×10^{-11} per year). These calculated values are of the order of a factor of 50 to 100 lower than the corresponding values calculated in other PRAs and IPEs. Specific accident sequence frequencies for transients, ATWS, and LOCAs calculated in the SSES IPE are also low, ranging from one to several orders of magnitude lower than for other PRAs and IPEs.

The very low accident frequencies reflect the significant design and procedure improvements that have been incorporated in the SSES plant. These significant improvements include:

1. Controlling the water level in the RPV within a wider band (from -60 to -161) during an ATWS as opposed to the narrow band used in other BWRs. This more flexible water level control not only reduces operator error but frees one operator for manual insertion of the rods which can significantly reduce the contribution from ATWS.

2. Adding an RCS bypass switch to allow immediate manual rod insertion which significantly reduces the contribution from ATWS which otherwise would be significant as it is in other BWRs.

3. Installation of a fifth, self-contained swing diesel which has its own DC system and which can be linked to any of the four ESS buses when other power sources fail. This significantly reduces the frequencies of accidents from loss of emergency power, which are significant contributors in other BWRs.

4. Eliminating the requirement to depressurize RPV on HCTL or PCPL which allows the operator approximately forty minutes to initiate SLCS in a full ATWS and approximately sixty minutes in a partial ATWS. This large time window significantly reduces the probability of an operator error of failing to initiate SLCS. In other BWRs the time window is significantly shorter, on the order of a factor of ten shorter, resulting in a significantly higher operator error probability which importantly contributes to the accident frequencies in other BWRs.

5. Using the RWCU in the blowdown mode to remove decay heat from the containment which significantly reduces the requirement for venting the containment and significantly reduces the probability of containment failure given core damage.

6. Early controlled RPV depressurization to allow operation of the fire main if HPCI and RCIC fail, and early connection of the fire main using installed threaded attachments for RPV/PC injection. This significantly reduces the contribution from HPCI/RCIC failure which is an important contributor in other BWRs.

7. Controlling the RPV water level so that it is in the TAF +5 feet range and hence above the ADS set point. This basically eliminates the human errors of failing to inhibit the ADS and failing to initiate the ADS when there is a loss of high pressure injection. These human errors are significant contributors in other BWRs.

In all, more than a dozen significant design and procedure improvements have been instituted at the SSES plant compared to other BWRs. The NRC has issued a number of letters recommending that the SSES improvements be instituted at other plants. As a part of this review, a separate evaluation was carried out to determine the benefits of the SSES improvements by re-evaluating the Peach Bottom 1150 PRA assuming the SSES improvements were in place. The Peach Bottom CDF was determined to be 4.51×10^{-6} per year in the 1150 PRA and hence was already low. For the re-evaluation, the Peach Bottom 1150 data were used where applicable and SSES data were used for those events not covered by the Peach Bottom analyses. With the SSES improvements in place, the dominant accident sequence contributions to CDF in the Peach Bottom PRA were

reduced by a factor of 10 to a factor of greater than 1000. This again confirms that the improvements instituted at the SSES plant are significant from a CDF reduction and risk reduction standpoint. The 1150 PRA re-evaluations that were performed are attached.

In spite of its many good points, however, the SSES IPE poses a quantification problem. The difficulty lies with the low CDF and low accident frequency values calculated in the SSES IPE. These low values have little credibility in the way they are presented because they seemingly don't incorporate present PRA experience. The PRAs and IPEs which have been conducted to date have provided a data base of equipment failure rates, human error rates, ccf probabilities, and resulting system failure probabilities and accident sequence frequencies. Because of the different modeling used in the SSES IPE, this experience data base has not been accessed to the degree it could have been. The extra time allowed for post-initiator operator actions and the less demanding, but different, responses required from the operator result in human error probabilities which are not directly relatable to human error probabilities used for other BWRs. It is thus difficult to differentiate design and procedure differences from modeling differences. The SSES IPE presents best estimates of the human error probabilities based on knowledgeable assessments. However, these estimates need to recognize the possibility for higher human error probabilities existing, based on the experience data base to date. This does not necessarily involve changing the point estimates but instead assigning ranges to cover the possibility of having higher human error probabilities. These ranges will also account for quantification uncertainties in post-initiator scenarios. These ranges can then be used to calculate adjusted results in sensitivity analyses and uncertainty analyses.

The very low accident frequencies calculated in the SSES IPE also increase the potential dominance of ccf contributions. The added equipment redundancies in the SSES plant result in low probabilities from multiple equipment failures. However, because of the low failure probabilities, there is a greater sensitivity to ccf contributions and to failure dependencies. The SSES IPE included particular ccf contributions when these contributions were assessed to be compatible with SSES plant data. However the SSES plant data which was used to show compatibility with independent failure assumptions can also be used to show compatibility with a potential ccf probability existing. This potential for ccf probabilities, although it is low, will significantly increase the ranges the accident frequencies can have. The low failure rates used for certain equipment will also have wider ranges when data uncertainties are considered. Based on reviews of the SSES IPE quantifications, I believe the above adjustments when incorporated in the evaluations will provide a basis for the quantifications and will significantly increase the credibility of the SSES IPE numerical values.

As an additional consideration, in the SSES IPE modeling of the accident sequences to determine the plant damage state, the range of events considered is truncated since only the most likely events are selected. The selection of the most likely events gives the most likely responses and most likely system success states. However, this most likely event analysis neglects other less likely events which can result in greater consequences and greater demands on the system and on the operator. The accident sequences therefore need to be reviewed to check for these variations in events. For example, as a sensitivity

study the results from the MAAP code should be compared with the results of the SSES IPE which utilized the BWRSAR code.

The above issues with the SSES IPE quantification should not be the cause for the IPE being redone. Rejection of the IPE models and engineering analyses would lose the valuable and valid information in the IPE. The SSES IPE represents a state of advancement of plant design and procedures to reduce core damage frequency, to reduce the frequency of vessel failure and to reduce the frequency of containment failure. The SSES IPE also represents a valuable tool for risk management applications. The SSES IPE should not be redone.

To address the difficulties with the SSES IPE, the quantification needs to be extended to include uncertainties and to recognize the different possibilities in the present experience data base. It is not the point values in themselves which provide confidence in the quantification, but their bases and the assigned ranges which account for uncertainties in the values. These uncertainties can be used to define adjusted values and to determine the ranges and adjusted values for the results. The re-evaluation of the numerical values is not a major effort and should entail approximately six man months worth of effort. This work will be worthwhile since it will upgrade the quantifications performed in the SSES IPE so that they have increased credibility. This will in turn upgrade the credibility of the SSES IPE.

ANALYSIS OF THE PEACH BOTTOM NUREG-1150 PRA WITH THE SSES MODIFICATIONS INCORPORATED

The following pages present a re-analysis of the Peach Bottom NUREG-1150 PRA[1] with the SSES modifications incorporated. The re-analysis was done in two ways 1) incorporating the SSES equipment and procedure modifications but using the 1150 models and data and 2) also incorporating and taking credit for the SSES IPE differences in models and data. These analyses were requested from the chief engineer responsible for the SSES IPE and have been reviewed. The first two tables present the summary results from the re-analysis. The accident sequence indices are those used in the NUREG-1150. The "Delta for Methods" represents the factor difference due to differing methods and the "Delta for Modifications" represents the factor difference due to SSES equipment and procedure modifications. The subsequent pages give the analyses of the individual sequences. Additional sensitivity analyses are also carried out for the probability of failing to actuate SLCS.

[1] "Analysis of Core Damage Frequency: Peach Bottom, Unit 2 Internal Events", NUREG/CR-4550, August 1989.

No Credit for Modeling Differences

Accident Sequence	NUREG-1150	Delta Methods	New Frequency	Delta Modifications	With PP&L Mods	note
1	1.64E-06	1	1.64E-06	0.0001824	2.99E-10	See Sensitivity 2
2	1.40E-06	1	1.40E-06	0.001	1.40E-09	See Sensitivity 1
3	2.79E-07	1	2.79E-07	0.28	7.81E-08	See Sensitivity 3
4	2.12E-07	1	2.12E-07	0.01	2.12E-09	See Sensitivity 4
5	1.90E-07	1	1.90E-07	1	1.90E-07	DGs use batteries from either unit
6	1.30E-07	1	1.30E-07	0.0001824	2.37E-11	See Sensitivity 2
7	1.25E-07	1	1.25E-07	0.0001824	2.28E-11	See Sensitivity 5
8	1.14E-07	1	1.14E-07	0.001	1.14E-10	See Sensitivity 1
9	8.73E-08	1	8.73E-08	0.01	8.73E-10	See Sensitivity 4
10	5.72E-08	1	5.72E-08	0.01	5.72E-10	See Sensitivity 4
11	6.41E-08	1	6.41E-08	0.01	6.41E-10	See Sensitivity 4
12	4.63E-08	1	4.63E-08	0.01	4.63E-10	See Sensitivity 4
13	4.37E-08	1	4.37E-08	0.001	4.37E-11	See Sensitivity 1
14	3.29E-08	1	3.29E-08	0.001	3.29E-11	See Sensitivity 1
15	2.69E-08	1	2.69E-08	0.001	2.69E-11	See Sensitivity 1
16	2.45E-08	1	2.45E-08	0.01	2.45E-10	See Sensitivity 4
17	2.20E-08	1	2.20E-08	0.28	6.16E-09	See Sensitivity 3
18	1.70E-08	1	1.70E-08	1	1.70E-08	DGs use batteries from either unit
Totals	4.51E-06		4.51E-06		2.98E-07	

Delta due to modifications = (2.98E-7)/(4.51E-6) = 0.06608239

Credit for Modeling Differences and Modifications

Accident Sequence	NUREG-1150	Delta Methods	New Frequency	Delta Modifications	With PP&L Mods	note
1	1.64E-06	1	1.64E-06	0.0001824	2.99E-10	See Sensitivity 2
2	1.40E-06	1	1.40E-06	0.001	1.40E-09	See Sensitivity 1
3	2.79E-07	0.055	1.53E-08	0.28	4.30E-09	See Sensitivity 3 & 7
4	2.12E-07	1	2.12E-07	0.01	2.12E-09	See Sensitivity 4
5	1.90E-07	0.1	1.90E-08	1	1.90E-08	See Sensitivity 6
6	1.30E-07	1	1.30E-07	0.0001824	2.37E-11	See Sensitivity 2
7	1.25E-07	1	1.25E-07	0.0001824	2.28E-11	See Sensitivity 5
8	1.14E-07	1	1.14E-07	0.001	1.14E-10	See Sensitivity 1
9	8.73E-08	1	8.73E-08	0.01	8.73E-10	See Sensitivity 4
10	5.72E-08	1	5.72E-08	0.01	5.72E-10	See Sensitivity 4
11	6.41E-08	1	6.41E-08	0.01	6.41E-10	See Sensitivity 4
12	4.63E-08	1	4.63E-08	0.01	4.63E-10	See Sensitivity 4
13	4.37E-08	1	4.37E-08	0.001	4.37E-11	See Sensitivity 1
14	3.29E-08	1	3.29E-08	0.001	3.29E-11	See Sensitivity 1
15	2.69E-08	1	2.69E-08	0.001	2.69E-11	See Sensitivity 1
16	2.45E-08	1	2.45E-08	0.01	2.45E-10	See Sensitivity 4
17	2.20E-08	1	2.20E-08	0.28	6.16E-09	See Sensitivity 3
18	1.70E-08	0.1	1.70E-09	1	1.70E-09	See Sensitivity 6
Totals	4.51E-06		4.06E-06		3.80E-08	

Delta due to modifications = (3.80E-8)/(4.51E-6) = 0.009363433

Sensitivity 1
Impact of Manual Rod Insertion and ATWS Procedure Changes on ATWS CDF

NUREG 1150 Cut Set #	NUREG 1150 PE	Point Estimate Frequency	Cut Set	SLCS sensitivity	
				0.005	0.001
1	8.00E-07	7.98E-07	T3A*RPSM*SLCS8	7.98E-07	7.98E-07
2	5.00E-07	5.00E-07	T3A*RPSM*SLCS9	1.25E-07	2.50E-08
6	8.50E-08	8.50E-08	T3A*RPSM*SLCS10	8.50E-08	8.50E-08
9	6.10E-08	6.06E-08	T3C*RPSM*SLCS8	6.06E-08	6.06E-08
13	3.80E-08	3.80E-08	T3C*RPSM*SLCS9	9.50E-09	1.90E-09
NS-1		6.46E-09	T3C*RPSM*SLCS10	6.46E-09	6.46E-09
		1.49E-06		1.08E-06	9.76E-07

PP&L Modifications designed to mitigate these sequences

1. Add RSCS bypass switch to allow immediate manual rod insertion
2. Change level control band to –60 to –161 – Frees operator to insert rods. BWROG procedures requires one operator to control pressure and one to control level
3. Eliminate requirement to depressurize on HCTL & PSP – avoids unnecessary and potentially core damaging depressurization during MRI. Operator has at least 40 minutes in full and 60 minutes in partial ATWS to start SLCS.

These modifications to the equipment and procedures allow the operator to successfully complete MRI.

Sensitivity 2
Impact of Susquehanna Modes on Accident Sequence #1

NUREG 1150 Cut Set #	NUREG 1150 PE	Point Estimate Frequency
14	3.70E-08	3.70E-08
P(CD/SBO) =		0.001832

Modifications

1. Early controlled RPV depressurization to allow success of fire main should HPCI/RCIC fail to run (EO-1/200-030).
2. Early connection of the fire main, using installed threaded attachment for RPV/PC injection (ES-013-001).
3. Early connection of 100kw generator to supply DC power to DC busses (EO-1/200-030 & ES-002-001).
4. Elimination of HPCI suction swap from CST to the Suppression Pool on high pool water level, prevents failure of HPCI on high water temperature.
5. Early alignment of HPCI in pressure control mode to reduce chance of SORV & multiple starts HPCI and RCIC (EO-1/200-030).
6. Installation of a maintenance swing diesel generator that can be substituted into any of the 4 ESS busses (OP-024-004). E diesel has self-contained DC system.
7. Modified Emergency Service Water System so that 4 diesel must fail for SBO rather than two combinations of two diesel.

We have two self-contained diesel driven fire pumps and over 12 hours to connect fire main

NUREG-1150 Cut Set 14

T1	ESW-XHE-FO-EHS	ACP-DGE-FR-EDGB	ACP-DGE-FR-EDGC	INJ-Fails	DGHWN R12HR	LOSPNR18HR

INJ-Fails HPCI and RCIC = 0.5, due to either harsh environment or loss of batteries.

Modifications and procedure changes 1, 2, 4, 5 significantly reduce the loss injection.
Based upon these mod INJ-Fails becomes:

INJ-Fails (HPCI and RCIC fail to run 24 hours) and (Both diesel driven fire pumps fail to start and run 23 hours)
INJ-Fails $(0.1 \times 0.1) \times \{(0.003 + 0.016) \times (0.067 + 0.01 + 0.016)\}$ = 1.77E-05

Sensitivity 2
Impact of Susquehanna Modes on Accident Sequence #1 (continued)

Modification 3 significantly reduces the chance of loss of DC power.

Using NUREG 1150 numbers for the charger diesel we get 0.003 + 0.016 = 0.019

These modifications change the NUREG 1150 sequence by replacing the term INJ-Fails with failure: failure of either the charge diesel or the new injection capability, or (0.019 + 1.80E-05) = 0.019

Therefore the NUREG 1150 sequence becomes:

P(cd cut set 14) = (3.70E-8/0.5) × 0.019 = 1.41E-09

Risk reduction from these models = 2.07E-09/3.70E-08 = 0.037959

Modification 6 allows onsite AC power to be recovered in less than 2 hours.
Lighting is available to perform the manipulation of these breakers
P(swing diesel) = 0.3

Risk reduction from this diesel becomes a straight multiplier of 0.3

P(cd cut set 14) = (3.70E-08/0.5) × 0.019 × 0.3 = 4.22E-10

Risk reduction from 1, 2, 3, 4, 5 & 6 = 0.011388

Modification 7 result in the requirement that all four diesel fail for SBO.
NUREG 1150 does not report common cause failure of 4 diesel to run. Therefore, I'll assume a common cause couple of 1.0 for the fourth given the third.

Risk reduction for third and fourth diesel = 0.016 (NUREG-1150 diesel fails to run)

P(cd cut set 14) = 3.70E-08/0.5) × 0.028 × 0.3 × 0.016 = 6.75E-12

Risk reduction from 1, 2, 3, 4, 5, 6 & 7 = 0.000182

Sensitivity 3
Impact of Susquehanna Design on Accident Sequence #3

Analysis of Susquehanna plant scram data shows that the loss of feedwater given plant trip with the MSIVs open is 0.28. In NUREG-1150 a value of 1.0 was used since the water level is lowered below the MSIV isolation. Susquehanna procedures keep the water level above the level 1 isolation; plus a bypass switch has been installed that bypasses the MSIV isolation on level 1. The MSIV isolation on high drywell pressure has also been removed. Therefore credit for feedwater is appropriate.

Modifications

1. Level control band target above MSIV isolation set point.
2. Installation of a bypass switch that bypasses MSIV isolation on Level 1.
3. Removal of MSIV isolation on high drywell pressure.

Note: Susquehanna modeling would have all low pressure ATWS events with uncontrolled LPI proceed to core damage.

Risk Reduction from modifications = 0.28

Sensitivity 4
Impact of Modifications on Accident Sequence #4

Modifications:

1. Installation of a bypass switch that allows the operator to bypass the low pressure permissive
2. change to the Aux Load shed (LOCA load shed) scheme that allows the operator to reload the D condensate pump and inject water into the RPV. Failure of the low pressure permissive has no impact on the ability of the condensate pump to inject to the vessel.

NOTE: The low pressure permissive circuit consists of two division which forms a one out of two taken twice logic. Division I uses Barksdale pressure sensors, which uses a bordon tube for pressure measurement. Division II uses a Barton pressure sensor which uses a diaphragm for pressure measurement. Since different instruments are used for pressure measurement, one would anticipate a less likely incident rate for CCF.

Medium break LOCA calculations demonstrate that the operator has at least 648 seconds after the RPV pressure decays to the HPCI low pressure trip. This provides the operator ample time to establish vessel injection from either condensate of 1 of 8 low pressure ECCS pumps. Two different operators control condensate and ECCS flow. With 10 minutes to establish flow the operator is at least as likely to initiate injection flow as to inject SLCS. Therefore a conservative value of 0.01 is applied.

Risk reduction from Modifications > 0.01

Sensitivity 5
Impact of modifications on Accident #7.

This sensitivity is just like Sensitivity 2 except in this case HPCI is already failed. Therefore no credit is taken for the risk reduction associated with continued HPCI operation.

INJ-Fails $(1.0 \times 0.1) \times \{(0.003 + 0.016) \times (0.067 + 0.01 + 0.016)\} = 0.000177$

These modifications change the NUREG 1150 sequence by replacing the term INJ-Fails with failure: failure of either the charger diesel or the new injection capability, or (0.019 + 1.70E-04) = 0.019

Early failure of HPCI has little impact on the injection success rate due to the diversity on injection systems provided by the modifications. Therefore the risk reduction is the same as Sensitivity #2.

Sensitivity 6
Treatment of Battery Common Cause Failure

Development of the battery failure rates used in the Susquehanna IPE are discussed in volume 3 Section C.7.2.3. The analysis was based upon a review of LER through 6/31/87 and NPRDS data from 1/1/84 through 12/31/89. Based upon this data a battery failure rate on demand was estimated to be 2.40E-7/hr. The authors of NUREG/CR-3831 report following values for battery failure from their investigations: 3.80E-08/hr (low), 6.40E-07 (recommended) and 3.00E-06/hr (high). Clearly the Susquehanna value is within this range. A value of 3.00E-06 was used in NUREG-1150. Susquehanna did not include a common cause couple for batteries. A common cause couple of 0.0023 was applied for failure of 4 batteries given failure of the first. This common cause couple is based upon work in NUREG-0666, and is largely attributed to common maintenance errors. The diesel generators at Susquehanna can utilize DC power from either unit. Maintenance is generally performed on the batteries during refueling outages due to the 2 hour AOT associated with a battery being inoperable. Therefore this common cause couple should not apply across units. The batteries used to start the diesel are selected using a selector switch in the diesel bay. Upon LOOP with failure of the diesel to start a non-licensed operator (NPO) will be dispatched to the diesel bayes in alphabetical order to manually initiate the diesel EO-1/200/030). Time studies show that no more than 10 minutes is required for the control room operator to observe the SBO, dispatch the NPO to the diesel bays and have the NPO at the A diesel panel. BWRSAR calculations show that given power uprate conditions, core damage will occur in 79 minutes following reactor trip and a high pressure boil off. Therefore the NPO has 69 minutes to identify the loss of DC on the engine panel, change the position of the DC power selector switch, place the engine in local and push the start button. The failure to recover offsite power in 68 minutes is estimated to be 0.1 in NUREG-1150. This is considered a conservative estimate for diesel recovery since there are many causes of loop that require many hours to restore, where this recovery action requires positioning two selector switches and pushing the start button.

Based upon this evaluation the NUREG-1150 common mode failure is applied to only one unit and an operator error of 0.1 is applied to the selection of the alternate battery supply.

Sensitivity 7
Impact of Modeling Differences and
Low Pressure ECCS Control Logic on Accident Sequence 3

Susquehanna ATWS calculations, as well as BWROG EPG documentation, identify the potential for severe core damage if the reactor is depressurized while either unborated or slightly borated. In the case where SLCS is successful, but low pressure injection cannot be controlled, the injection flow may flush the boron out of the core and cause a power excursion. For this reason without modification to the ECCS control logic, all low pressure ATWS events which rely on ECCS for core cooling result in core damage. PP&L has modified the ECCS control logic in a manner that allows the operator to control the low pressure ECCS flow within the requirements of ATWS. Therefore with success of SLCS, the operator can feed the vessel with 2-3000 gpm using LPCI. Prior to this modification the operator had to either lockout ECCS flow for five minutes or stop and start pumps. This modification was required to satisfy defense in depth. The operator has about 300 seconds in full ATWS and 460 seconds in partial ATWS to initiate a rapid depressurization to avoid core damage. An error rate of 0.001 was assigned to failure to depressurize the reactor during ATWS based upon the time allowed. The operator can either feed with condensate or LPCI given installation of the control circuit modification. The probability of failure to control low pressure injection is assigned at 0.01, given the ability to control flow and the 101 inch control band.

Crediting the operator for initiating rapid blowdown has allowed us to uncover additional potential significant operator errors during ATWS. Discovery of this error has led to a plant modification to allow the operator to control low pressure flow and a level control band that assures core cooling and reactivity control, while providing the operator with a procedure that can be implemented.

Replace NUREG-1150 operator error - ESF-XHE-FO-DATWS = 0.2 with

{operator fails to depressurize or operator fails control low pressure injection} = {0.001 + 0.01} = 0.011

Risk Reduction becomes: 0.011/0.2 = 0.055

This risk reduction is placed in the modeling column due to the different treatment in low pressure ATWS operation.

Comparison of NUREG-1150 and Susquehanna Analysis

Item	Description	Peach Bottom	Susquehanna	note
T3A	Transient with PCS initially available	2.5	2	
T3C	IORV	0.19	0.01	1
RPSM	Mechanical ATWS	1.00E-05	1.80E-05	2
SLCS-XHE-RE-Driver	Operator fails to restore SLCS after test	3.19E-02	2.00E-03	3
SLCS-XHE-FO-Driver	Operator fails to initiate SLCS	2.00E-02	2.00E-03	3
SLC-SYS-TE-SLC	SLCS system unavailable due to test	3.40E-03		3
ESF-XHE-FO-DATWS	Operator fails to depressurize during ATWS	0.2		
HCI-TDP-FS-20S37	Turbine Driven Pump Fails to start	3.00E-02	1.70E-02	
T1	Loss of Offsite Power	0.079	0.071	
ESW-XHE-FO-EHS	Operator fails to start Emergency heat Sink	0.9	na	
ACP-DGE-FR-EDGB	Emergency Diesel Generator fails to run	0.016	0.024	
ACP-DGE-FR-EDGC	Emergency Diesel Generator fails to run	0.016	0.024	
INJ-Fails	Failure of Injection Systems	0.5	1	
DGHWN R12HR	Failure to recover Diesel at 12 hours	0.55	1	
LOSPNR18HR	Failure to recover offsite power at 18 hours	0.0074	0.069	

CONTENTS

1. SABRE Computer Code Documentation:
   - Calculation EC-ATWS-0505, Rev. 8
   - Calculation EC-052-0593, Rev. 0
   - Calculation EC-SIMU-0501, Rev. 0
   - Calculation EC-SATH-1007, Rev. 1

2. SABRE Calculations Supporting Technical Specification Change Deleting Automatic HPCI Suction Transfer on High Suppression Pool Level:
   - Calculation EC-052-1018, Rev. 2
   - Calculation EC-052-1025, Rev. 2

CALCULATION / STUDY COVER SHEET and NUCLEAR RECORDS TRANSMITTAL SHEET

1. Page 1 of 353
Total Pages 365

➢2. TYPE: Calc. ➢3. NUMBER: EC-ATWS-0505 ➢4. REVISION: 8

5. TRANSMITTAL#: K0009051 *➢6. UNIT: 3 *➢7. QUALITY CLASS: Q

➢9. DESCRIPTION: SABRE: A Computer Code for Simulation of Boiling Water Reactor Dynamics Under Failure-to-Scram Conditions *➢8. DISCIPLINE: T

SUPERSEDED BY: EC-

10. Alternate Number: RA-B-NA-045 11. Cycle:

12: Computer Code or Model used: SABRE, SIMULATE, SIMTRAN Fichee x Dis ☐ Am't 4 Rockets

13. Application:

*➢14 *Affected Systems:* 058 , , , , ,

* If N/A then line 15 is mandatory.

**➢15. NON-SYSTEM DESIGNATOR: ATWS EOPC THYD

**If N/A then line 14 is mandatory

16. Affected Documents:

☒ SAR Change Req'd

17. References: PLA-4480, FSAR Section 15.8

18. Equipment / Component #:

19. DBD Number:

➢20. PREPARED BY	Mark A. Chaiko *Print Name*	Mark A. Chaiko *Signature*
➢21. REVIEWED BY	Kevin W. Brinckman *Print Name*	Kevin W. Brinckman *Signature*
➢21A. VERIFIED BY	Kevin W. Brinckman *Print Name*	Kevin W. Brinckman *Signature*
➢22. APPROVED BY	Casimir A. Kukielka *Print Name*	Casimir A. Kukielka 9/27/00 *Signature*
➢23. ACCEPTED BY PP&L / DATE	 *Print Name*	 *Signature / DATE*

RECEIVED

TO BE COMPLETED BY NUCLEAR RECORDS

NR-DCS SIGNATURE/DATE: Ruth Charnitz SEP 27 2000

NUCLEAR REC. SERVICES

ADD A NEW COVER PAGE FOR EACH REVISION
FORM NEPM-QA-0221-1, Revision 3, Page 1 of 2, ELECTRONIC FORM

* Verified Fields ➢ REQUIRED FIELDS

PPL, Inc	ENGINEERING CALCULATION STUDY REVISION DESCRIPTION SHEET
REVISION NO: 8	CALCULATION NUMBER: EC-ATWS-0505

This form shall be used to record the purpose or reason for the revision, indicate the revised pages and / or affected sections and give a short description of the revision. Check (x) the appropriate function to add, replace or remove the affected pages.

Revised Pages	Affected Sections	Add	Rpl	Rmv	Description / Purpose of Revision
4	Contents		x		Added Section 5.15
6	Computer Case Summary		x		Reran last SIMULATE case in Table (new Run# is 0002019)
13	1		x		Provided overall description of code changes.
21	2.1		x		Fixed typos in Eq. (2.1-3)
83	2.10		x		Modified equation (2.10-1) because of addition of "rainout" model.
84	2.10		x		Changed Eq. (2.10-4). Added definition of enthalpy of water vapor at surface of drywell pool. Also incorporated "rainout" model.
85	2.10		x		Incorporated "rainout" model.
85a	2.10	x			Incorporated "rainout" model.
87,91	2.10		x		Incorporated "rainout" model.
110	3.2		x		Corrected typos in Eqs. (3.2-3), (3.2-4), and (3.2-6).
122, 123, 124, 125	5.1		x		Reran SABRE Case 01.
128, 129, 130, 131	5.2		x		Reran SABRE Case 02.
134, 135, 136	5.3		x		Reran SABRE Case 03.
139, 140	5.4		x		Reran SABRE Case 04.
141, 142, 143, 144, 145, 146,	5.5		x		Reran SABRE Case 05. Also modified Case 05 to get drywell conditions and break conditions that would initiate rainout.
149, 150,	5.6		x		Reran SABRE Case 06.
153, 155, 156, 157, 158	5.7		x		Reran SABRE Case 07.
159, 160, 163-172	5.8		x		Reran SABRE Case 08.

REVISION TYPE: (check one)	☐ SUPERSEDED BY CALCULATION NUMBER EC- ☐ FULL REVISION ☒ PAGE FOR PAGE

PPL, Inc	ENGINEERING CALCULATION STUDY REVISION DESCRIPTION SHEET
REVISION NO: 8	**CALCULATION NUMBER:** EC-ATWS-0505

This form shall be used to record the purpose or reason for the revision, indicate the revised pages and / or affected sections and give a short description of the revision. Check (x) the appropriate function to add, replace or remove the affected pages.

Revised Pages	Affected Sections	Add	Rpl	Rmv	Description / Purpose of Revision
179, 181-185	5.10		x		Reran SABRE Case 10. Reduced max step size from 100 msec to 50 msec.
188, 189	5.11		x		Reran SABRE Case 11.
191, 194, 195-199	5.12		x		Reran SABRE Case 12.
203-212	5.13		x		Reran SABRE Case 13.
213, 214, 216, 217, 218, 219, 220, 221	5.14		x		Reran SABRE Case 14.
221a-221l	5.15	x			Added SABRE Case 15 to check drywell temperature response to small steam break.
324	F.69		x		Corrected typos.
1	N/A		x		Revised cover sheet.
1a	N/A		x		Changed revision page
1b	N/A	x			Added revision page

REVISION TYPE: (check one)

☐ SUPERSEDED BY CALCULATION NUMBER EC-

☐ FULL REVISION ☒ PAGE FOR PAGE

CONTENTS

COMPUTER CASE SUMMARY
(SIMULATE-E CASES)

Run #	Diskette	Micro-fiche	Description
9904110		X	U2C7 3-D Cross-section and Power distribution calculation. Run includes 7 cross-section cases for the following rod patterns: 1.) 4 rods in ÷ 4 rods at notch 10 2.) 8 rods in ÷ 4 rods at notch 10 3.) 12 rods in ÷ 4 rods at notch 10 4.) 20 rods in ÷ 4 rods at notch 10 5.) 36 rods in ÷ 4 rods at notch 10 6.) 68 rods in ÷ 4 rods at notch 10 7.) all rods in Run #9904110 was restarted from data set r9507299.0012 Cycle exposure = 11.562 GWD/MTU
9904111		X	U2C9 3-D Cross-section and Power distribution calculation. Run includes 7 cross-section sets for the following rod patterns: 1.) all rods out 2.) 4 rods in 3.) 8 rods in 4.) 16 rods in 5.) 32 rods in 6.) 64 rods in 7.) all rods in. Run #9904111 was restarted from data set r9602506.0002 Cycle exposure = 15.700 GWD/MTU
9904112		X	U2C10 3-D Cross-section and Power distribution calculation. Run includes 7 cross-section sets for the following rod patterns: 1.) all rods out 2.) 4 rods in 3.) 8 rods in 4.) 16 rods in 5.) 32 rods in 6.) 64 rods in 7.) all rods in. Run #9904112 was restarted from data set r9808566.0001 Cycle exposure = 15.2 GWD/MTU
9905326		X	U1C12 3-D Cross-section and Power distribution calculation. Run includes 7 cross-section sets for the following rod patterns: 1.) all rods out 2.) 4 rods in 3.) 8 rods in 4.) 16 rods in 5.) 32 rods in 6.) 64 rods in 7.) all rods in. Run #9904113 was restarted from data set r9903464.0001 Cycle exposure = 14.800 GWD/MTU
0002019		X	U2C10 Core power calculation with 16 rods inserted. Run #0002019 was restarted from data set r9808566.0001 Cycle exposure = 15.2 GWD/MTU Power result is compared against SABRE in Section 5.14.

COMPUTER CASE SUMMARY
(SIMTRAN-E CASES)

Run #	Diskette	Micro-fiche	Description
9900339		X	U2C7 1-D Cross-section set calculation Run includes 7 cross-section sets for the following rod patterns: 1.) 4 rods in + 4 rods at notch 10 2.) 8 rods in + 4 rods at notch 10 3.) 12 rods in + 4 rods at notch 10 4.) 20 rods in + 4 rods at notch 10 5.) 36 rods in + 4 rods at notch 10 6.) 68 rods in + 4 rods at notch 10 7.) all rods in SIMTRAN Run #9900339 was run using SIMULATE restart file generated from SIMULATE Run#9904110. Cycle exposure = 11.562 GWD/MTU
9900340		X	U2C9 1-D Cross-section set calculation Run includes 7 cross-section sets for the following rod patterns: 1.) all rods out 2.) 4 rods in 3.) 8 rods in 4.) 16 rods in 5.) 32 rods in 6.) 64 rods in 7.) all rods in. SIMTRAN Run #9900340 was run using SIMULATE restart file generated from SIMULATE Run#9904111 Cycle exposure = 15.700 GWD/MTU
9900341		X	U2C10 1-D Cross-section set calculation Run includes 7 cross-section sets for the following rod patterns: 1.) all rods out 2.) 4 rods in 3.) 8 rods in 4.) 16 rods in 5.) 32 rods in 6.) 64 rods in 7.) all rods in. SIMTRAN Run #9900342 was run using SIMULATE restart file generated from SIMULATE Run#9904112 Cycle exposure = 15.2 GWD/MTU
9900369		X	U1C12 1-D Cross-section set calculation Run includes 7 cross-section sets for the following rod patterns: 1.) all rods out 2.) 4 rods in 3.) 8 rods in 4.) 16 rods in 5.) 32 rods in 6.) 64 rods in 7.) all rods in. SIMTRAN Run #9900343 was run using SIMULATE restart file generated from SIMULATE Run#9904113 Cycle exposure = 14.800 GWD/MTU
9900370		X	U2C7 1-D Cross-section set calculation. Same as Run #9900339 except that input parameter limnft was set to 13 instead of 50 to eliminate warning message in output. Comparison of output files showed that there was no difference in kinetics parameters. The cross-section sets for Run #9900339 and 9900370 are identical.

COMPUTER CASE SUMMARY
(CASMO-3 CASES)

Run #	Diskette	Micro-fiche	Description
9900755		X	Lattice calculations to determine dependency of macroscopic B-10 thermal absorption cross section on boron concentration and void fraction. Calculations are for ATRIUM-10 fuel at hot zero power conditions and lattice type 92. Void fraction ranges from 0 to .80 and boron concentration ranges from 0 to 800 ppm. Cycle exposure ranges from 0 to 60 GWD/MTU.

COMPUTER CASE SUMMARY
(SABRE CASES)

Case #	Diskette	Micro-fiche	Description
01		X	MSIV Closure with scram - comparison to plant data (§ 5.1) SABRE input file is c01.dat kinetics file is u2c7.simtran.out (SIMTRAN Run#9900339)
02		X	Containment response for unmitigated ATWS - comparison against CONTAIN code(§ 5.2) SABRE input file is c02.dat Kinetics file is u2c10.simtran.out (SIMTRAN Run#9900341)
03		X	MSIV closure ATWS - Comparison to PP&L RETRAN Calculations (§ 5.3) SABRE input file is c03.dat Kinetics file is u2c9.simtran.out (SIMTRAN Run#9900340)
04		X	Inventory Boildown with Scram Failure - Comparison to SIMULATE-E static calculations(§ 5.4) SABRE input file is c04.dat Kinetics file is u2c9.simtran.out (SIMTRAN Run#9900340)
05		X	Containment response to a Small break LOCA - Comparison to CONTAIN Results (§ 5.5) SABRE input file is c05.dat Kinetics file is u2c7.simtran.out (SIMTRAN Run# 9900339)
06		X	Turbine trip ATWS from MEOD rod line - Comparison to GE TRAC Results (§ 5.6) SABRE input file is c06.dat Kinetics file is u2c7.simtran.out (SIMTRAN Run#9900339)
07		X	ATWS Initiated by Pressure Regulator Failure Open - Comparison to GE Results (§ 5.7) SABRE input file is c07.dat Kinetics file is u2c7.simtran.out (SIMTRAN Run#9900339)
08		X	MSIV closure ATWS with Boron Injection - Comparison to GE Calculations. (§ 5.8) SABRE input file is c08.dat Kinetics file is u2c7.simtran.out (SIMTRAN Run#9900339)
08a		X	Same as Case 08 but one SRV out of service.
08b		X	Same as Case 08 but hydraulic time step size changed from 25 msec to 20 msec for t>30sec.
08c		X	Same as Case 08 but hydraulic time step size changed from 25 msec to 30 msec for t>30sec.
08d		X	Same as Case 08 but hydraulic time step size changed from 25 msec to 35 msec for t>30sec.
08e		X	Same as Case 08 but hydraulic time step size changed from 5 msec to 10 msec for t<30sec.
08f		X	Same as Case 08 but hydraulic time step size changed from 5 msec to 2.5 msec for t<30sec.
08g		X	Same as Case 08 but number of boron mixing nodes in core changed from 10 to 9.
08h		X	Same as Case 08 but number of boron mixing nodes in core changed from 10 to 8.
08i		X	Same as Case 08 but hydraulic time step size changed from 5 msec to 1.25 msec for t<30sec.

COMPUTER CASE SUMMARY
(SABRE CASES)

Case #	Diskette	Micro-fiche	Description
08j		X	Same as Case 08 but error control parameters, RTOL and ATOL, for kinetics solution are increased from 1.E-05 to 5.E-05.
08k		X	Same as Case 08 but error control parameters for kinetics solution, RTOL and ATOL, are decreased from 1.E-05 to 5.E-06.
08l		X	Same as Case 08 but boron entrainment exponent *b* in Eq. (2.4.6-1) is set to ½.
08m		X	Same as Case 08 but boron entrainment exponent *b* in Eq. (2.4.6-1) is set to 2.
10		X	Suppression Pool heatup from decay heat - Comparison to Heat Balance Calculation. (§ 5.10) SABRE input file is c10.dat Kinetics file is u2c10.simtran.out (SIMTRAN Run#9900341)
11		X	Small break LOCA compared to GE results (§ 5.11) SABRE input file is c11.dat Kinetics file is.u2c7.simtran.out (SIMTRAN Run#9900339)
12		X	Check of SABRE mass/energy balances with Core Spray injection (§ 5.12) SABRE input file is c12.dat Kinetics file is u2c9.simtran.out (SIMTRAN Run#9900340)
13		X	Check of SABRE Fuel/Clad Temperature Calculations with partial length fuel rods (§ 5.13) SABRE input file is c13.dat Kinetics file is u2c10.simtran.out (SIMTRAN Run#9900341)
14		X	MSIV-Closure ATWS with SLCS failure—Shutdown with MRI. (§ 5.14) SABRE input file is c14.dat Kinetics file is u2c10.simtran.out (SIMTRAN Run#9900341)
14a		X	Same as Case 14 except that run was made using SABRE Version 2.4 (Point Kinetics model)

COMPUTER CASE SUMMARY
(CONTAIN CASES)

Case #	Diskette	Micro-fiche	Description
02		x	Containment response for unmitigated ATWS - comparison against SABRE code(§ 5.2) Mass and energy source tables are developed from SABRE output for SABRE Case 02.
05		x	Containment response to a Small break LOCA - Comparison to SABRE Results (§ 5.5) Mass and energy source tables are developed from SABRE output for SABRE Case 05.

COMPUTER CASE SUMMARY
(SABRE Source Code Listing and Input Files)

Diskette	Micro-fiche	Description
X	X	filename=sabre_30.f – FORTRAN source code listing of SABRE code Version 3.0
X	X	filename=common.txt – Common blocks for SABRE code Version 3.0
X		filename=c01.dat – input file for SABRE Case 01
X		filename=c02.dat – input file for SABRE Case 02
X		filename=c03.dat – input file for SABRE Case 03
X		filename=c04.dat – input file for SABRE Case 04
X		filename=c05.dat – input file for SABRE Case 05
X		filename=c06.dat – input file for SABRE Case 06
X		filename=c07.dat – input file for SABRE Case 07
X		filename=c08.dat – input file for SABRE Case 08
X		filename=c08a.dat – input file for SABRE Case 08a
X		filename=c08b.dat – input file for SABRE Case 08b
X		filename=c08c.dat – input file for SABRE Case 08c
X		filename=c08d.dat – input file for SABRE Case 08d
X		filename=c08e.dat – input file for SABRE Case 08e
X		filename=c08f.dat – input file for SABRE Case 08f
X		filename=c08g.dat – input file for SABRE Case 08g
X		filename=c08h.dat – input file for SABRE Case 08h
X		filename=c08i.dat – input file for SABRE Case 08i
X		filename=c08j.dat – input file for SABRE Case 08j
X		filename=c08k.dat – input file for SABRE Case 08k
X		filename=c08l.dat – input file for SABRE Case 08l
X		filename=c08m.dat – input file for SABRE Case 08m
X		filename=c10.dat – input file for SABRE Case 10
X		filename=c11.dat – input file for SABRE Case 11
X		filename=c12.dat – input file for SABRE Case 12
X		filename=c13.dat – input file for SABRE Case 13
X		filename=c14.dat – input file for SABRE Case 14
X		filename=u2c9.base.dat – base 9x9 core model
X		filename=u2c10.base.dat – base 10x10 core model

1. INTRODUCTION

Revision 8 (SABRE version 3.1) to this calculation incorporates a correction to the primary containment temperature/pressure calculation. In previous versions of SABRE, the specific enthalpy of steam in the drywell and wetwell atmospheres was approximated by the specific enthalpy of saturated steam at the drywell/wetwell temperature. Although this approximation was acceptable for analysis of transients involving liquid breaks and/or steam discharge to the suppression pool via SRVs, it was found to produce significant error in drywell temperature response in the case of a steam break. Therefore, a function routine for computing superheated enthalpy as a function of temperature and pressure was added to SABRE. Enthalpy is computed using the ASME FORTRAN function *hss*. When adding the function routine *hss*, the lower level routines *hfp* and *hgp* (saturated liquid and vapor enthalpy as a function of pressure) also had to be included. This generated a conflict with existing function routines of the same name. Consequently, *hfp* and *hgp* were replaced with the corresponding ASME routines. This correction involving the superheated steam enthalpy does not affect any calculation of record as no steam-break analyses have previously been performed with SABRE.

As part of this revision, two additional corrections were made. It was found that the input data defining the parameters ΔP_{open} and ΔP_{FO} in Eqs. (2.10-11)-(2.10-13) were not passed correctly to subroutine *concal.f* because of incorrect naming of the variables in the main program. The variable names were changed in the main program. This error caused these parameters to take the value 0.0 in previous versions of SABRE. As a result, the vacuum breakers opened somewhat earlier than they should have. From rerunning benchmark problems in §5, it was determined that the effect of this coding error is not significant. The second correction involves adding a "rainout" model to prevent the primary containment atmospheres from becoming supersaturated with water. This model can be important when simulating containment respose to liquid breaks in which the break flow becomes subcooled relative to the drywell atmosphere conditions. If this occurs, the drywell will start to cool down and atmosphere conditions may become saturated. The rainout model removes excess water from the atmosphere and deposits it in the pool thus preventing the relative humidity from exceeding 100%.

This calculation package provides documentation of the SABRE code and benchmarking of the SABRE reactor and primary containment models. In addition, two base-case SABRE input decks and four 1-D cross-section files are developed in this calculation package. The two base case SABRE input decks correspond to an ANF 9x9-2 core model and to a Siemens ATRIUM-10 core model. SABRE can only model the physical characteristics of one fuel type. Therefore, mixed cores of 9x9 and 10x10 fuel are modeled by approximating the core as a full core of the dominant fuel type. An effective fuel-clad gap conductance is used to make the thermal response of the core model consisting of the dominant fuel type consistent with the actual mixed core. In addition, the cross-section data is developed from a SIMULATE model of the actual mixed core.

Overview of SABRE Code

In an ATWS (Anticipated Transient Without Scram) event, a BWR (boiling water reactor) may be operated over a wide range of conditions far removed from those encountered during normal operation. In a non-isolation ATWS (main steam isolation valves open) for instance, the reactor operates in natural circulation with large reductions in feedwater enthalpy caused by loss of turbine extraction steam flow to feedwater

heaters. Decreased make-up-flow enthalpy results in increased core-inlet subcooling which can lead to unstable power oscillations.[1]

If the ATWS event involves closure of the main steam isolation valves (MSIVs), a drop in water level occurs due to loss of feedwater flow. Vessel makeup is then provided by the HPCI (high pressure coolant injection) system which supplies highly subcooled water to the vessel at a reduced flow rate. At the low reactor water levels which result with HPCI injection, the feedwater spargers become uncovered and cold make-up coolant is injected directly into a region occupied by saturated steam. The development of condensation on the injection flow has a significant modulating influence on increasing core-inlet subcooling.

An ATWS may also involve depressurization of the reactor vessel as a mitigative response to failure of certain equipment. For example, should HPCI fail to function, the reactor could be depressurized below ~600 psia to allow coolant injection by intermediate-pressure-range condensate pumps.

In order to properly formulate a mitigative strategy for response to an ATWS event, an understanding of the reactor dynamic behavior over the wide range of conditions described above is required. Consequently, the SABRE (Simulation of ATWS in Boiling-Water Reactors) computer code was developed by PP&L to simulate BWR transient behavior under natural circulation conditions with failure to scram. SABRE contains thermal-hydraulic models of the reactor jet pump, lower plenum, core, bypass, upper plenum, riser, separator, steam dome, and downcomer regions of the reactor vessel. A three-node, radially-lumped parameter model describes fuel-to-coolant heat transfer in each of the axial nodes within the core region. Nuclear heating effects are simulated using a two-group, one-dimensional kinetics model. 1-D cross section files are developed for U2C7, U2C9, U2C10, and U1C12 cores.

The SABRE code also includes a model of the primary containment. In an isolation ATWS, reactor steam is discharged to the primary containment where it is condensed within the suppression pool. As pool temperature rises, the containment begins to pressurize, and alternate methods of reactor shutdown (boron injection or manual insertion of control rods) are required to maintain containment structural integrity.

It is important to emphasize, in the context of emergency operating procedure development, that SABRE results are not used to justify reactor operation under conditions where core dynamics are poorly behaved by demonstrating that fuel integrity can be maintained. On the contrary, at PP&L, the SABRE calculations are used to identify operating regimes where core/containment integrity is likely to be threatened. The mitigative strategy for ATWS is then constructed to avoid these severe operating

---

[1] Wulff, W., Cheng, H.S., and Mallen, A.N., "Causes of Instability at LaSalle and Consequences from Postulated Scram Failure", in Proceedings of International Workshop on Boiling Water Reactor Stability, Holtsville, New York, October 17-19, 1990.

regimes whenever possible. Consequently, the reactor is maintained within an operating domain where there is confidence that core and containment integrity will be preserved.

Although SABRE was developed to study reactor behavior under ATWS conditions, it can also be used to investigate reactor and containment response to small break LOCAs or anticipated reactor transients such as an MSIV closure with scram.

The NRC has examined SABRE results for ATWS scenarios as part of their review of proposed changes to the BWR Owners' Group Emergency Procedure Guidelines.[2] ATWS simulations were performed by the NRC using the TRAC-BF1 and RAMONA-4B computer codes. When discussing their results in the Safety Evaluation Report, the NRC makes the following statement, "Results obtained with these two codes were reasonably consistent and were also comparable to PP&L findings for Susquehanna BWRs using SABRE, after making adjustments to compensate for different procedural assumptions." It is concluded, based on this Safety Evaluation, and subsequent conversations with the NRC[3], that SABRE can be used for ATWS analysis.

The FORTRAN listing of the SABRE code and the base-case SABRE input files are included on diskette (see Computer Case Summary). In addition, the SABRE neutron kinetics data bases which were developed with the SIMULATE-E code, are also included on microfiche as indicated in the Computer Case Summary.

The basic assumptions and modeling features used in the SABRE code are summarized below:

Reactor Model

1. The flow is one-dimensional, and each flow region (core, bypass, upper plenum etc.) has an axially-uniform flow area.

2. Acoustic waves travel at infinite speed.

3. Potential and kinetic energy effects are neglected.

4. Slip between phases is governed by a Drift-Flux model.

5. Complete vapor-liquid separation occurs at exit of steam separator (steam dryer not explicitly modeled).

6. Flow regime can be co-current or counter-current.

---

[2] Nuclear Regulatory Commission, "Safety Evaluation Report Modifications to the Boiling Water Reactor (BWR) Emergency Procedure Guidelines to Address Reactor Core Instabilities," June 6, 1996.

[3] PLA-4480, "Unit 2 Cycle 9 ATWS Evaluation," File R41-2, Docket No. 50-388, July 23, 1996.

7. The axial power shape is non-uniform and time varying.

8. The 764 fuel bundles are averaged into a single channel.

9. Gamma heating within fuel bundles is specified as part of input data.

10. Gamma heating in bypass channel is specified as part of input data.

11. Efficiency of steam condensation is 95% when downcomer level is a meter or more below the feedwater nozzles.

12. Twenty-seven axial hydraulic nodes are used for the core region.

13. Twenty-five axial and two radial nodes are used to model the fuel. The cladding is modeled with twenty-five axial nodes and one radial node. The number of fuel pins can vary axially along the core.

14. In the outer radial node of the fuel, the volumetric heat generation rate is 10% greater than the radially-averaged heat generation rate to account for self-shielding effects.

15. Core power is computed using a two-group 1-D kinetics model with six delayed-neutron groups.

16. The kinetics model includes reactivity contributions from control rod insertion, boron injection, and variations in moderator density and fuel temperature,.

17. Axial power shape for fission power changes with core conditions based on the 1-D kinetics model, but the power shape for decay power remains equal to the initial axial power shape.

18. Injected boron stagnates in lower plenum if total core flow is less than 5 MLb/hr.

19. Stagnated boron re-mixes if total core flow exceeds 15 MLb/hr.

20. Perfect mixing occurs in each boron mixing node.

21. Dissolved boron does not affect coolant density. The density of injected boron solution is assumed to be the same as water at the same temperature.

22. Boron volatility is neglected.

23. Boron transport is calculated from coolant flow.

24. In general, a boron mixing node consists of several hydraulic nodes.

25. The thermal absorption cross section for B-10 is assumed to be a linear function of the boron concentration in the fuel channels and the bypass region.

26. Model includes thermal capacitance of reactor vessel and vessel internal structures. Sensible heat given off by these structures is superimposed on core power.

27. Pump power decays exponentially following a recirculation pump trip.

28. For a recirculation pump runback, pump power decays exponentially to a lower value which maintains the desired total core flow.

29. An inertial flow model describes steam flow through closing MSIVs.

30. Pressure wave phenomena in steam lines is neglected.

31. HPCI/RCIC extraction steam flow is included in steam dome mass/energy balances.

32. SRV flow and break flow during a LOCA are computed with homogeneous critical flow model.

33. A proportional controller approximates the feedwater controller response.

34. Upon loss of feedwater heating, the decrease in feedwater temperature is approximated by a delayed exponential decay.

35. CRD flow reaches thermal equilibrium with coolant in lower plenum; flow enters reactor in lower node of bypass region.

36. RPV injection systems consist of feedwater, HPCI, RCIC, condensate, Core Spray, SLCS, and CRD.

Containment Model

37. The drywell and wetwell are each modeled with a single control volume.

38. Model includes thermal capacitance of structural steel and liner plate, but thermal capacitance of concrete structures is neglected.

39. Pressure within drywell and wetwell is computed with Ideal Gas equation of state.

40. Vacuum breakers and downcomer vents are modeled.

41. Drywell coolers and suppression pool cooling system are modeled.

42. Suppression pool letdown can be described by specifying a constant letdown flow rate.

43. Model includes heat transfer from SRV tailpipes to suppression chamber atmosphere.

44. Heat structure model includes natural convection, condensation, and radiation heat transfer effects.

45. Drywell heat load includes dissipation from reactor vessel.

46. Wetwell air space varies with suppression pool level.

47. Pool layer can form on drywell floor. Depth of pool layer can reach top of downcomer pipes.

48. Condensation on liner plate and structural steel drains into drywell/wetwell pool.

49. Effect of pool formation on drywell free volume is negligible.

50. Model includes heat transfer/evaporation effects at surface of drywell/wetwell pool.

51. For LOCA, break flow comes to pressure equilibrium with drywell.

In this calculation references are generally provided in the form of footnotes. Please be aware that all footnotes begin with the number 1 in each section of the calculation. Within a section of the calculation, there is no cross reference to footnotes outside that particular section.

2. MODEL DESCRIPTION

Figure 2-1 shows a schematic diagram of the SABRE model of the SSES reactor. A single core channel is used to represent the average flow and power conditions within the 764 fuel bundles. Models of the bypass, upper plenum, riser, separator, steam dome, downcomer, jet pump, and lower plenum regions are also included. Vessel coolant sources consist of feedwater flow, high pressure injection, condensate, core spray, SLCS (Standby liquid control), and CRD (control rod drive) flow. In this Section, the governing thermal-hydraulic equations for the various regions of the reactor vessel are presented. A description of the fuel and cladding heat balance equations and the nuclear heating model are then given.

2.1 Fluid Dynamics Equations for Jet Pump, Lower Plenum, Core, Bypass, Upper Plenum, Riser, and Separator Regions

Within the scope of the present model, the fluid at a particular location within a region can consist of liquid (subcooled or saturated), vapor (saturated or superheated), or two-phase mixture. The flow is one-dimensional and each region of the reactor is characterized by an axially-uniform flow area. Over each cross section of a region, it is assumed that the fluid is in thermodynamic equilibrium which implies that subcooled boiling effects are neglected. Locally, the fluid is treated as incompressible so that all acoustic phenomena are neglected (i.e., acoustic waves are assumed to travel at infinite speed). The fluid is, however, globally compressible in the sense that fluid properties vary with the overall system pressure. This description allows modeling of transient reactor behavior involving overall pressure variations which occur on a time scale which is considerably slower than that associated with the propagation of pressure waves. Potential and kinetic energy effects are neglected in the present analysis. The model considers slip between phases, a non-uniform, time-varying axial power profile, local pressure losses at the inlet and outlet of the various regions, and wall and fuel-spacer frictional effects. With these assumptions the mixture continuity and energy equations, respectively, for a flow region of the reactor are given by[1]

$$\frac{\partial \rho}{\partial t} + \frac{\partial G}{\partial z} = \gamma_s, \tag{2.1-1}$$

and

$$\frac{\partial(\rho \bar{h})}{\partial t} + \frac{\partial\left[(1-\alpha)u_\ell \rho_\ell h_\ell + \alpha u_g \rho_g h_g\right]}{\partial z} = \frac{1}{J}\frac{dP^*}{dt} + q''' + \frac{P_h q''}{A} + \gamma_s h_s . \tag{2.1-2}$$

---

[1]Lahey, R.T. and Moody, F.J., *The Thermal-Hydraulics of a Boiling Water Nuclear Reactor*, Second Edition, American Nuclear Society, La Grange Park, Illinois, 1993, Equations 5.57 & 5.96, pp. 208-219.

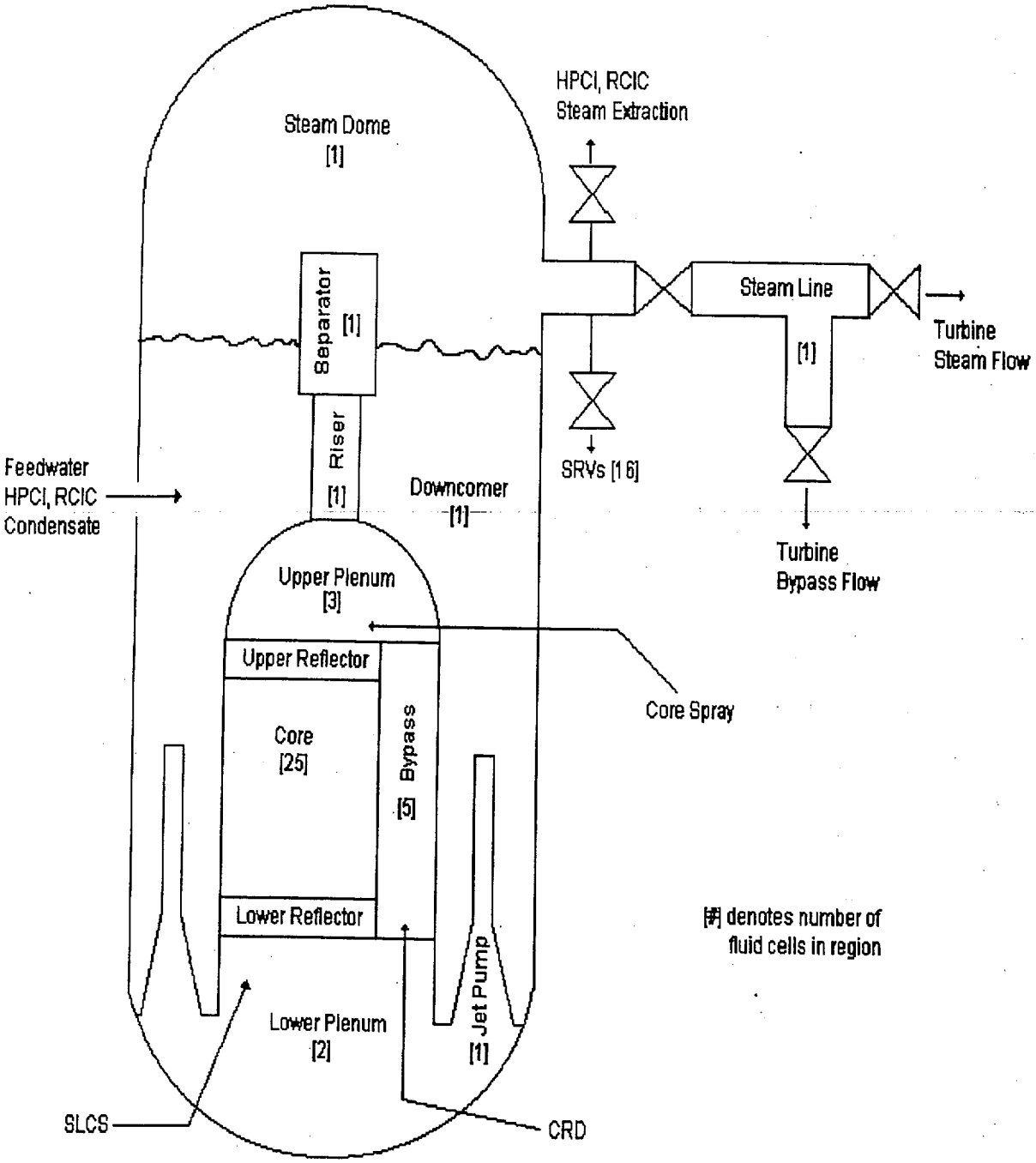

Figure 2-1 SABRE Model of Susquehanna reactor.

The mixture momentum equation is given by[2]

$$\frac{\partial G}{\partial t}+\frac{\partial\left[(1-\alpha)\rho_\ell u_\ell^2+\alpha\rho_g u_g^2\right]}{\partial z}+g_c\frac{\partial P}{\partial z}+\rho g+\frac{G|G|}{2\rho_\ell}\left[\frac{f_w\varphi}{D_h}+\frac{f_s\Phi}{D_h}+K_1\Phi\delta(z-0)+K_2\Phi\delta(z-L)\right]=0. \quad \textbf{(2.1-3)}$$

The subscripts g and ℓ designate gas and liquid phases. In the momentum equation (2.1-3), the sign of the elevation term ρgL is negative for the jet pump region since the normal flow direction for the jet pump region is downward. Also, the elevation change along the lower plenum differs from the flow path length. Therefore, for the lower plenum region, the value of [elevation at core inlet]-[elevation at jet pump outlet] is used in place of the flow path length L in the term ρgL of Eq. (2.1-3). In addition, the fuel spacer frictional pressure drop term $f_s\Phi/D_h$ appears only in the momentum equation for the core region. The Dirac delta function $\delta(z-\xi)$, where $\xi=0$ and $\xi=L$, designates the location of the local pressure losses at the region inlet and outlet. Additional variables in the above conservation equations are defined below:

G(z,t)	=	fluid mass flux $\left(\frac{Lb_m}{ft^2\,\text{sec}}\right)$,
h_g	=	gas-phase enthalpy (Btu/Lb_m),
h_ℓ	=	liquid-phase enthalpy (Btu/Lb_m),
$\bar{h}$(z,t)	=	volume-weighted enthalpy (Btu/Lb_m),
h_s	=	enthalpy associated with mass source γ_s (Btu/Lb_m),
P(z,t)	=	local fluid pressure (Lb_f/ft^2),
P^*(t)	=	system pressure = steam dome pressure (Lb_f/ft^2),
t	=	time (sec),
u(z,t)	=	fluid velocity (ft/sec),
z	=	axial coordinate (ft) $(0 \le z \le L)$,
α	=	void fraction,
ρ_g	=	gas-phase density (Lb_m/ft^3),
ρ_ℓ	=	liquid-phase density (Lb_m/ft^3), and
γ_s	=	volumetric source of mass per unit time $(Lb_m/ft^3\,\text{sec})$.

The mixture density $\rho(z,t)$, the volume-weighted enthalpy $\bar{h}(z,t)$, and the fluid mass flux $G(z,t)$ are defined through

---

[2]Lahey, R.T. and Moody, F.J., *The Thermal-Hydraulics of a Boiling Water Nuclear Reactor*, Second Edition, American Nuclear Society, La Grange Park, Illinois, 1993, Equation 5.65 p. 212.

$$\rho = \alpha\rho_g + (1-\alpha)\rho_\ell, \tag{2.1-4}$$

$$\bar{h} = \left[\alpha\rho_g h_g + (1-\alpha)\rho_\ell h_\ell\right]/\rho \text{, and} \tag{2.1-5}$$

$$G = \rho_\ell(1-\alpha)u_\ell + \rho_g \alpha\, u_g. \tag{2.1-6}$$

The system pressure $P^*(t)$ is a known function of t from additional mass and energy balance equations describing the steam dome and downcomer regions.

Closure of the thermal-hydraulic system is accomplished through use of the drift-flux relation:

$$(\alpha C_0 - 1)u_g + C_0(1-\alpha)u_\ell = -V_{gj}. \tag{2.1-7}$$

where C_0 is the radial bubble concentration parameter, and V_{gj} is the drift velocity. In SABRE, C_0 and V_{gj} are computed from the Ohkawa-Lahey void model which accurately predicts the counter-current flooding limit.[3]

The unknowns in this system of 7 equations consist of $\rho, G, \bar{h}, u_g, u_\ell, \alpha, and P$. The vapor and liquid phase densities and specific enthalpies are determined from the equations of state as described below:

Subcooled Liquid Region

This thermodynamic region is defined by $\bar{h}(z,t) < h_f(P^*)$ where $h_f(P^*)$ is the specific enthalpy of saturated liquid at the system pressure P^*. In this thermodynamic region, the liquid phase density and liquid-phase specific enthalpy are given by

$$\rho_\ell(z,t) = \rho_\ell\left[P^*(t), \bar{h}(z,t)\right] \quad and \quad h_\ell(z,t) = \bar{h}(z,t). \tag{2.1-8}$$

Saturated Region

This thermodynamic region is defined by $h_f(P^*) \le \bar{h}(z,t) \le h_v(P^*)$ where $h_v(P^*)$ is the specific enthalpy of saturated vapor at the system pressure P^*. In this region, the liquid-phase and vapor-phase densities and enthalpies are given by

$$h_\ell(z,t) = h_f\left[P^*(t)\right],\ \rho_\ell(z,t) = \rho_f\left[P^*(t)\right],\ h_g(z,t) = h_v\left[P^*(t)\right],\ and\ \rho_g(z,t) = \rho_v\left[P^*(t)\right] \tag{2.1-9}$$

---

[3]Ohkawa, K. and Lahey, R.T., "The Analysis of CCFL Using Drift-Flux Models", Nuclear Engineering and Design, 61, 245-255, 1980.

Superheated Vapor Region

The superheated vapor region is defined by $h_v[P^*(t)] < \bar{h}$. Here the gas-phase specific enthalpy and density are determined from

$$h_g(z,t) = \bar{h}(z,t), \; and \; \rho_g(z,t) = \rho_g[P^*(t), \bar{h}(z,t)] \qquad \textbf{(2.1-10)}$$

Appropriate boundary conditions for Equations (2.1-1)-(2.1-3) are formulated by specifying the local pressure on the boundaries of the region and the volume-weighted enthalpy on any boundary where fluid (liquid or vapor) enters the region.

Under natural circulation conditions, the pressure in the downcomer at the elevation of the jet pump throat is calculated as the steam dome pressure plus the static head of the fluid above the jet pump throat. Obviously, the natural circulation flow rate depends strongly on the height of the water column above the jet pump throat. Therefore, in order to accurately model the downcomer water level, a level-versus-volume table (see Appendix D, Section D.1.9) is used to determine level from the calculated fluid volume. The downcomer level-volume table consists of 18 data points which incorporate the cross-sectional flow area variation of the region. Conservation equations which yield the downcomer fluid volume are described in Section 2.2.

In Eq. (2.1-2) the heat flux term q"(z,t) is zero for all regions of the reactor except the core where it accounts for heat transfer from the fuel rods to the coolant. (Heat transfer to and from the vessel structures is also included in this term; see discussion in Section 2.4.7) In the single-phase region of the core (liquid or superheated vapor), the Dittus-Boelter[4] correlation is used to calculate the coolant-film heat transfer coefficient. In the bulk boiling region of the core, where the coolant is saturated, the film coefficient is computed from the Thom correlation.[5]

$$H_{2\varphi} = \frac{(T_{surf} - T_{cool})}{18.66} \exp\left(\frac{P^*}{90{,}720}\right) \qquad \textbf{(2.1-11)}$$

where

$H_{2\varphi}$ = film coefficient for boiling region (Btu/sec·ft^2·°F),

T_{surf} = clad surface temperature (°F),

P^* = system pressure (lb$_f$/ft^2), and

T_{cool} = coolant temperature (°F).

In the subcooled-boiling region, the film coefficient is calculated as a linear combination of the liquid-phase and bulk-boiling coefficients. The onset of nucleation within the subcooled region

---

[4]Burmeister, L.C., *Convective Heat Transfer*, Wiley, New York, p. 486, 1983.

[5]Thom, J.R.S., Walker, W.M., Fallon, T.A., and Reising, G.F.S., "Boiling in Subcooled Water During Flow in Tubes and Annuli", Proc. Inst. Mech. Eng., 3C180, 1966.

is determined from the nucleation model of Davis and Anderson[6] as described by Lahey and Moody.[7] The methodology for identifying departure from nucleate boiling is taken from the RAMONA-3B code.[8] RAMONA uses a combination of two critical heat flux correlations[9,10] to cover the expected range of flow conditions within the core channels. In the transition boiling region, where the cladding surface temperature is greater than the value corresponding to DNB and less than the rewetting temperature, the film coefficient is calculated as a linear combination of the nucleate-boiling and film-boiling coefficients. The clad rewetting temperature T_{RW} associated with the break down of stable film boiling is estimated from the following empirical correlation,[11]

$$\frac{T_{RW}}{T_{Crit}} = 0.13\frac{P}{P_{Crit}} + 0.86 \qquad \textbf{(2.1-12)}$$

where T_{Crit} and P_{Crit} are the critical temperature and pressure of water, and P is the pressure. The film boiling heat transfer coefficient is obtained from the Dittus-Boelter correlation using the mass flux and fluid properties associated with the steam flow.

$q'''(z,t)$ in the energy equation [see Eq. (2.1-2)] represents the local volumetric heat generation rate within the coolant. For the present model, this quantity is zero for all regions except for the core and bypass where it accounts for gamma heating of the coolant. The heat generation rate within each of these two regions is specified as part of the code input. The magnitude of gamma heating is assumed to be a constant fraction of the total core power.

In the momentum equation, the two-phase friction multiplier φ is calculated from the Martinelli-Nelson correlation which includes the flow correction developed by Jones[12]. φ is correlated as

$$\varphi = \Gamma(G,P^*)\left[1.2\left(\rho_\ell/\rho_g - 1.0\right)x^{0.824}\right] + 1.0\ , \qquad \textbf{(2.1-13)}$$

where

---

[6]Davis, E.J. and Anderson, G.H., "The Incipience of Nucleate Boiling in Forced Convection," *AIChE J.*, 12 , 1966.

[7]Lahey, R.T. and Moody, F.J., *The Thermal-Hydraulics of a Boiling Water Nuclear Reactor*, Second Edition, p. 253, American Nuclear Society, La Grange Park, Illinois, 1993.

[8]Wulff, W., Cheng, H.S., Diamond, D.J., and Khatib-Rahbar, M., "A Description and Assessment of RAMONA-3B Mod. 0 Cycle 4: A Computer Code with Three-Dimensional Neutron Kinetics for BWR Systems Transients," NUREG/CR-3664, p. 100, January 1984.

[9]Condie, K.G. and Bengston, S.G., "Development of the Mod 7 Correlation," EG&G Report, Attachment PN-181-78.

[10]Smith, R.A. and Griffith, P., "A Simple Model for Estimating Time to CHF in a PWR LOCA," Natl. Heat Transfer Conference, ASME paper 76-HT-9.

[11]Hsu, Y., Graham, R.W., *Transport Processes in Boiling and Two-Phase Systems*, p. 118, Hemisphere, Washington, 1976.

[12]Lahey, R.T. and Moody, F.J., *The Thermal-Hydraulics of a Boiling Water Nuclear Reactor*, Second Edition, p. 270, American Nuclear Society, La Grange Park, Illinois, 1993.

$$\Gamma(G,P^*)=1.36+3.47x10^{-6}P^*+3.60x10^{-4}G-1.79x10^{-8}P^*G \quad if G<194 \qquad \textbf{(2.1-14)}$$

and

$$\Gamma(G,P^*)=1.26-2.78x10^{-6}P^*+3.31/G+5.40x10^{-4}P^*/G \quad if G>194 \qquad \textbf{(2.1-15)}$$

For local pressure losses such as those occurring across a fuel spacer and the inlet or outlet of a flow region, the homogeneous two-phase multiplier Φ is used in computing the pressure drop, where

$$\Phi=1+x(v_g-v_\ell)/v_\ell \qquad \textbf{(2.1-16)}$$

In (2.1-16) v_g is the vapor-phase specific volume and v_ℓ is the liquid-phase specific volume. The flow quality x is defined by

$$x=\frac{w_g}{w_\ell+w_g}. \qquad \textbf{(2.1-17)}$$

where w_g *and* w_ℓ are the mass flow rates of vapor and liquid respectively. Under counter-current flow regimes $(w_g>0$ *and* $w_\ell<0)$, x can be greater than 1 or less than 0. In the SABRE calculation, x is set to 1 if it becomes greater than 1, and x is set to 0 if it becomes less than 0.

Pressure changes associated with flow area differences between adjoining flow regions are neglected in SABRE. This is not a serious code limitation because SABRE employs momentum equations which are integrated over the entire natural circulation loop. If large axial gradients in mass flow do not occur, then the reversible losses tend to cancel in the integrated momentum equations. This simplifying approximation of neglecting reversible pressure losses is also used in the RAMONA-3B code.[13]

---

13 Wulff, W., Cheng, H.S., Diamond, D.J., and Khatib-Rahbar, M., "A Description and Assessment of RAMONA-3B Mod. 0 Cycle 4: A Computer Code with Three-Dimensional Neutron Kinetics for BWR Systems Transients," NUREG/CR-3664, p. 84, January 1984.

2.2 Fluid Dynamics Equations for Downcomer and Steam Dome Regions

Both the downcomer and steam dome are variable-volume regions. The combined volume of these two regions is, however, fixed and is denoted as V_0. In the following discussion, the subscript "DC" refers to the downcomer region and the subscript "SD" refers to the steam dome region. In the downcomer, coolant can be added by means of injection flow and by means of the liquid exiting the steam separator region. Furthermore, when the downcomer water level drops below the feedwater spargers, coolant is injected directly into a region occupied by saturated steam. In this case the steam condensing on the cold make-up flow provides an additional source of mass to the downcomer region. Fluid exits the downcomer through the entrance to the jet pump region. In depressurization transients, where flashing occurs in the downcomer, vapor separation at the fluid surface also contributes to mass loss from this region. The mass and energy balances for the downcomer region can be written as

$$-\rho_{DC}\frac{dV_{SD}}{dt}+(V_0-V_{SD})\frac{\partial\rho_{DC}}{\partial\bar{h}_{DC}}\frac{d\bar{h}_{DC}}{dt}+\left[(V_0-V_{SD})\frac{\partial\rho_{DC}}{\partial P^*}\right]\frac{dP^*}{dt}= W_{inj}+W_{cond}+W_{tS}(L_S,t)-W_{tJ}(0,t)-W_{gJ}(0,t)-W_{vs}-W_{break} \tag{2.2-1}$$

and

$$-\rho_{DC}\bar{h}_{DC}\frac{dV_{SD}}{dt}+(V_0-V_{SD})\left(\rho_{DC}+\bar{h}_{DC}\frac{\partial\rho_{DC}}{\partial\bar{h}_{DC}}\right)\frac{d\bar{h}_{DC}}{dt}+\left[(V_0-V_{SD})\left(\bar{h}_{DC}\frac{\partial\rho_{DC}}{\partial P^*}-\frac{1}{J}\right)\right]\frac{dP^*}{dt} = W_{inj}h_{inj}+W_{cond}h_{gSD}+W_{tS}(L_S,t)h_{tS}(L_S,t)-W_{tJ}(0,t)h_{tJ}(0,t)-W_{gJ}(0,t)h_{gJ}(0,t) - W_{vs}h_{gDC}-W_{break}\bar{h}_{DC} \tag{2.2-2}$$

where ρ_{DC} is the downcomer fluid density, V_{SD} is the steam dome fluid volume, W_{inj} is the injection flow rate, W_{VS} is the rate of vapor loss from the downcomer region due to buoyancy effects, W_{cond} is the mass addition rate due to steam condensation, and W_{break} is the break flow rate which is used in the simulation of small break LOCAs. W_J and W_S refer to the mass flow rates within the jet pump and separator regions respectively. The relation $V_{DC} = V_o - V_{SD}$, where V_{DC} is the downcomer fluid volume and V_{SD} is the steam dome fluid volume, has been used in obtaining (2.2-1) and (2.2-2). In (2.2-2) $\bar{h}_{DC}$ is the downcomer volume-weighted enthalpy, h_{inj} is the injection-flow enthalpy, h_{tS} and h_{tJ} are the liquid-phase enthalpies in the separator and jet pump regions, h_{gDC} and h_{gJ} are the gas-phase enthalpies in the downcomer and jet pump regions. Potential and kinetic energy effects are neglected in (2.2-2). Also, it is assumed that the latent heat associated with condensation is completely absorbed by the injection flow.

Similarly, the mass and energy balance equations, respectively, for the steam dome region are given by

$$\rho_{SD}\frac{dV_{SD}}{dt}+V_{SD}\frac{\partial\rho_{SD}}{\partial\bar{h}_{SD}}\frac{d\bar{h}_{SD}}{dt}+\left[V_{SD}\frac{\partial\rho_{SD}}{\partial P^*}\right]\frac{dP^*}{dt}=W_{gS}(L_S,t)+W_{VS}-W_{stm}-W_{cond}-W_{break} \tag{2.2-3}$$

and

$$\rho_{SD}\bar{h}_{SD}\frac{dV_{SD}}{dt}+V_{SD}\left[\rho_{SD}+\bar{h}_{SD}\frac{\partial\rho_{SD}}{\partial\bar{h}_{SD}}\right]\frac{d\bar{h}_{SD}}{dt}+\left[V_{SD}\left(\bar{h}_{SD}\frac{\partial\rho_{SD}}{\partial P^*}-\frac{1}{J}\right)\right]\frac{dP^*}{dt}= \tag{2.2-4}$$
$$W_{gS}(L_S,t)h_{gS}(L_S,t)+W_{vs}h_{gDC}-(W_{stm}+W_{break})\bar{h}_{SD}-W_{cond}h_{gSD}$$

where ρ_{SD} and $\bar{h}_{SD}$ are the density and volume-weighted enthalpy of the fluid in the steam dome region. W_{stm} is the rate at which steam exits the vessel through the steam lines, and h_{gSD} denotes the enthalpy of vapor in the steam dome region. Note that W_{stm} consists of the steam flow through the turbine stop valve, the bypass valve, the safety relief valves, and the HPCI/RCIC steam admission valves. Derivations of (2.2-1)-(2.2-4) are given in Appendix A.

The homogeneous, equilibrium critical flow model is used to compute W_{stm} under isolation conditions where steam is discharged through SRVs. For the unisolated case, the steam flow rate is calculated from a pressure regulator model (see Section 2.6).

The steam condensation rate W_{cond} is defined in terms of a condensation efficiency η. If η=0, no condensation occurs on the subcooled injection flow; if η=1, the injection flow is heated to the saturation state by the condensing steam. Also, W_{cond} accounts for steam condensation on the water exiting the steam separators when this liquid is subcooled, and the downcomer level is below the separator outlet (this effect is only important under conditions where the reactor is shutdown and operated under forced-flow conditions). Accounting for condensation on subcooled liquid exiting the separators, and using the above definition of η, the steam condensation rate W_{cond} is given by

$$W_{cond}=\frac{\eta W_{inj}(h_f-h_{inj})}{h_{gSD}-h_{inj}-\eta(h_f-h_{inj})}+\eta_{sep}W_S(L_S,t)[h_f-h_S(L_S,t)]/h_{fg} \tag{2.2-5}$$

where

η_{sep} = efficiency of condensation on subcooled liquid exiting separators.

For purposes of computational simplicity, η is taken to be a linear function of the water level in the downcomer region. η=0 if level is greater than or equal to the elevation of the feedwater spargers, and $\eta=\eta_{max}$ (η_{max} is typically 0.95; See Section D.4) if water level is less than or equal to a specified elevation (which is below the spargers) denoted

by L_{max}. The parameter L_{max} is measured in inches above TAF and is supplied as part of the input data. A similar approach is used to calculate η_{sep}.

Under conditions where flashing occurs in the bulk downcomer region, the vapor separation rate W_{VS} is computed from

$$W_{vs} = V_{br}\, A_{DC}\, \alpha_{DC}\, \rho_{gDC} \qquad \textbf{(2.2-6)}$$

where

V_{br} = bubble rise velocity (ft/sec)

A_{DC} = downcomer flow area at interface between downcomer and steam dome regions (ft^2)

α_{DC} = downcomer void fraction

ρ_{gDC} = gas phase density in downcomer (lbm/ft^3)

In Eq. (2.2-6), the bubble rise velocity is computed from Equations (2.1-6) and (2.1-7) using the Ohkawa-Lahey void model. At the surface of the vapor-liquid mixture in the downcomer, $u_f = 0$ and $G = \rho_g \alpha u_g$. Using these relations, and the fact that $w_g = \rho_g \alpha u_g A$, Equations (2.1-6) and (2.1-7) lead to the following expression for the bubble-rise velocity:

$$V_{br} = \frac{V_{gj,DC}}{1 - \alpha_{DC} C_{0,DC}}. \qquad \textbf{(2.2-7)}$$

2.3 Fuel and Cladding Heat Balance Equations

The heat transfer model presented here describes the transient temperature behavior within an average power fuel rod within the core. Axial conduction within the fuel rod is neglected since the dominant temperature gradient occurs in the radial direction. A lumped-parameter model is used to describe the radial flow of heat from the fuel to the coolant. The overall resistance to heat transfer from fuel to coolant consists of the thermal resistance of the fuel, the fuel-cladding gap, the cladding, and the coolant convective film at the outer surface of the cladding. The radially-lumped parameter model employed here is a generalization of the model formulated by Tong.[1] With two equal-volume radial fuel nodes, the governing fuel heat transfer equations are given by

$$\rho_{fa} C_{pfa} r_a^2 \frac{\partial T_{fa}}{\partial t} = -\frac{2k_{fa}\left(T_{fa} - T_{fb}\right)}{\ln\left(\frac{r_a + r_b}{\sqrt{2}\, r_a}\right)} + r_a^2 \bar{q}'''_{fa}, \qquad \text{and} \qquad \textbf{(2.3-1)}$$

$$\rho_{fb} C_{pfb}\left(r_b^2 - r_a^2\right)\frac{\partial T_{fb}}{\partial t} = \frac{2k_{fa}\left(T_{fa} - T_{fb}\right)}{\ln\left(\frac{r_a + r_b}{\sqrt{2}\, r_a}\right)} - \frac{\left(T_{fb} - T_{cl}\right)}{\left[\frac{\left(r_b - r_a\right)}{4r_b\, k_{fb}} + \frac{1}{2r_{ci} H_g} + \frac{\left(r_{co} - r_{ci}\right)}{4r_{co}\, k_{cl}}\right]} + \left(r_b^2 - r_a^2\right)\bar{q}'''_{fb} \qquad \textbf{(2.3-2)}$$

where

ρ_f	=	fuel density (lbm/ft^3),
C_{pf}	=	fuel specific heat (Btu/lbm·°F),
r_a	=	radius of inner fuel node (ft),
r_b	=	fuel pellet radius (ft),
$T_f(z_c,t)$	=	fuel temperature (°F),
k_f	=	fuel thermal conductivity (Btu/sec·ft·°F),
$\bar{q}'''_{fa}(z_c,t)$	=	volumetric heat generation rate within inner radial fuel node (Btu/sec·ft^3),
$\bar{q}'''_{fb}(z_c,t)$	=	volumetric heat generation rate within outer fuel node (Btu/sec·ft^3),

[1]Tong, .L.S., "Simplified Calculation of Thermal Transient of a Uranium Dioxide Fuel Rod," Nuclear Science and Engineering, Vol. 11, pp. 340-343, 1961.

r_{ci}, r_{co} = cladding inside and outside radii respectively (ft),

$T_{cl}(z_c,t)$ = cladding temperature (°F),

H_g = gap conductance (Btu/ft^2·sec·°F), and

k_{cl} = cladding thermal conductivity (Btu/ft·sec·°F).

In Equations (2.3-1) and (2.3-2), the subscript "a" refers to the inner fuel node, and the subscript "b" refers to the outer fuel node. In the outer fuel node, the volumetric heat generation rate is specified as 10% greater than the radially-averaged volumetric heat generation rate to account for self-shielding effects within the fuel (C_s = 0.9 in §3.1.4). Note that the volumetric heat generation rates $\bar{q}'''_{fa}(z_c,t)$ and $\bar{q}'''_{fb}(z_c,t)$ include the effects of the axial power shape. Similarly, the heat balance equation for the bulk temperature of the cladding can be written as

$$\rho_{cl}\, C_{pcl}\left(r_{co}^2 - r_{ci}^2\right)\frac{\partial T_{cl}}{\partial t} = \frac{\left(T_{fb} - T_{ci}\right)}{\left[\frac{\left(r_b - r_a\right)}{4\, r_b\, k_{fb}} + \frac{1}{2\, r_{ci}\, H_g} + \frac{\left(r_{co} - r_{ci}\right)}{4\, r_{co}\, k_{cl}}\right]} - \frac{\left(T_{cl,surf} - T_{cool}\right)}{\left[\frac{1}{2\, r_{co}\, H_{film}}\right]} \qquad \textbf{(2.3-3)}$$

where

ρ_{cl} = cladding density (lbm/ft^3)

$C_{p,cl}$ = cladding specific heat (Btu/lbm·°F)

$T_{cool}(z_c,t)$ = coolant temperature within core region (°F)

$T_{cl,surf}(z_c,t)$ = clad surface temperature (°F), and

H_{film} = coolant film heat transfer coefficient (Btu/ft^2·sec·°F).

The governing equation for the surface temperature of the cladding $T_{cl,surf}$ is obtained from (2.3-3) with an appropriate adjustment of the resistance terms so that the rate of energy flow into and out of the cladding is referenced to the outer surface of the cladding.

The resulting expression is

$$\rho_{cl}\, C_{pcl}\left(r_{co}^2 - r_{ci}^2\right)\frac{\partial T_{cl,surf}}{\partial t} = \frac{\left(T_{fb} - T_{cl,surf}\right)}{\left[\frac{\left(r_b - r_a\right)}{4\, r_b\, k_{fb}} + \frac{1}{2\, r_{ci}\, H_g} + \frac{\left(r_{co} - r_{ci}\right)}{2\, r_{co}\, k_{cl}}\right]} - \frac{\left(T_{cl,surf} - T_{cool}\right)}{\left[\frac{1}{2\, r_{co}\, H_{film}}\right]} \qquad \textbf{(2.3-4)}$$

Derivations of Equations. (2.3-1)—(2.3-4) are given in Appendix B.

2.4. Neutron Kinetics

A one-dimensional neutron kinetics model based on the two-group, one-dimensional neutron diffusion equations is used in SABRE to compute core power. The kinetics equations are solved using a finite-difference procedure. The model includes lower and upper reflector regions in addition to the active core region. Within the active core region, there are twenty-five material regions having spatially-independent neutronics parameters. The kinetics model can simulate the effects of boron addition by reactor scram, manual control rod insertion (MRI), and Standby Liquid Control System injection.

2.4.1 Neutron Kinetics Parameters

Neutron kinetics parameters are obtained from output of the SIMTRAN-E[1] computer code. SIMTRAN-E collapses the 3-D cross-sections calculated by the SIMULATE-E[2] code to a 1-D (axial) cross section set. In the active core region, 1-D parameters are constant over 6" axial segments referred to as material regions. The core is designed such that the radially-averaged fuel composition does not vary axially within these 6" segments. The neutronics parameters obtained from the SIMTRAN-E code are in the form of polynomial curve fits. The polynomials give the cross sections, diffusion coefficients, and delayed neutron fraction as functions of perturbations in fuel temperature and moderator density. Curve fit equations are provided for the following kinetics parameters:

D_1 = diffusion coefficient for fast neutrons (cm),

Σ_{a1} = macroscopic absorption cross section for fast neutrons (cm^{-1}),

Σ_s = macroscopic down-scattering cross section for fast neutrons (cm^{-1}),

$\nu_1 \Sigma_{f1}$ = [average number of neutrons produced in a fission induced by a neutron in fast group] x [macroscopic fission cross section for fast group] (cm^{-1}),

$\kappa \Sigma_{f1}$ = [energy per fission conversion factor] x [macroscopic fission cross section for fast group] (cm^{-1}),

D_2 = diffusion coefficient for thermal group (cm),

---

[1]McClure, J.A., and Gose, G.C., "SIMTRAN-E: A SIMULATE-E to RETRAN-02 Datalink," NP-5509-CCM, Electric Power Research Institute, Palo Alto, California (1987).

[2]Ver Planck, D.M., Cobb, W.R., Borland, R.S., and Versteegen, P.L., "SIMULATE-E: A Nodal Core Analysis Program for Light Water Reactors," NP-2792-CCM, Electric Power Research Institute, Palo Alto, California (1983).

Σ_{a2} = macroscopic absorption cross section for thermal group (cm^{-1}),

$\nu_2 \Sigma_{f2}$ =[average number of neutrons produced in a fission induced by a thermal neutron] x [macroscopic fission cross section for thermal group] (cm^{-1}),

$\kappa \Sigma_{f2}$ = [energy per fission conversion factor] x [macroscopic fission cross section for thermal group] (cm^{-1}),

υ_1 = average speed of fast neutrons (cm/sec),

υ_2 =average speed of thermal neutrons (cm/sec), and

β = delayed neutron fraction.

In the Susquehanna SIMTRAN model, the reactor core is divided axially into 27 material regions. In each of these material regions, the 12 parameters listed above are functions of time only. The material regions consist of the lower and upper reflectors and twenty-five 6" axial segments within the active core (region containing fuel). For each of the 27 material regions, the kinetics parameters are approximated by polynomials in fuel temperature and moderator density fluctuations. For example, the polynomial representation of D_1 in neutronic region j, where $j \in \{1,\ldots,27\}$, is

$$D_{1,j}(t) = c_{j,0} + c_{j,1}\,\Delta\sqrt{T_{f,j}} + c_{j,2}\,\Delta u_j + c_{j,3}\,\Delta u_j\,\Delta\sqrt{T_{f,j}} + c_{j,4}\,\Delta u_j\,\Delta u_j + c_{j,5}\,\Delta\sqrt{T_{f,j}}\,\Delta u_j\,\Delta u_j \qquad (2.4.1\text{-}1)$$

where

$$\Delta\sqrt{T_{f,j}} = \sqrt{T_{f,j}(t)} - \sqrt{T_{f,j}(0)} \qquad (2.4.1\text{-}2)$$

and

$$\Delta u_j = \frac{\rho_j(t) - \rho_j(0)}{\rho_j(0)}. \qquad (2.4.1\text{-}3)$$

Here $T_{f,j}$ (K) is the average fuel temperature in material region j, and ρ_j is the average moderator density in material region j (Lbm/ft^3). The constants $c_{j,i}$ in (2.4.1-1) are computed by the SIMTRAN-E code and given in the SIMTRAN output file. The other eleven neutronics parameters are represented by expressions identical to (2.4.1-1). Within the present calculation, four cycle-specific (EOC) cross-section sets are developed: U2C7, U2C9, U2C10, and U1C12. These are discussed in detail in §2.4.8.

2.4.2 Governing Equations

With the assumption that all neutrons are born in the fast group, the two-group, time-dependent, one-dimensional neutron diffusion equations are[3]

Fast Group (Group 1)

$$\frac{1}{\upsilon_1(z,t)}\frac{\partial\varphi_1(z,t)}{\partial t}=\frac{\partial}{\partial z}\left[D_1(z,t)\,\frac{\partial\varphi_1(z,t)}{\partial z}\right]-D_1(z,t)\,B_R^2(z)\varphi_1(z,t)-\Sigma_{a1}(z,t)\,\varphi_1(z,t)$$

$$+\ (1-\beta)\nu_1\Sigma_{f1}(z,t)\,\varphi_1(z,t)+(1-\beta)\nu_2\Sigma_{f2}(z,t)\ \varphi_2(z,t)$$

$$-\Sigma_s(z,t)\,\varphi_1(z,t)+\sum_{m=1}^{6}\lambda_m\,C_m(z,t) \qquad (2.4.2\text{-}1)$$

and

Thermal Group (Group 2)

$$\frac{1}{\upsilon_2(z,t)}\frac{\partial\varphi_2(z,t)}{\partial t}=\frac{\partial}{\partial z}\left[D_2(z,t)\,\frac{\partial\varphi_2(z,t)}{\partial z}\right]-\Sigma_{a2}(z,t)\,\varphi_2(z,t)+\Sigma_s(z,t)\varphi_1(z,t) \qquad (2.4.2\text{-}2)$$

where

φ_1 = group-1 (fast) neutron flux ($cm^{-2}sec^{-1}$),

φ_2 = group-2 (thermal) neutron flux ($cm^{-2}sec^{-1}$), and

$B_R^2(z)$ = radial buckling (cm^{-2}).

The radial buckling $B_R^2(z)$ is time-independent and is listed in the SIMTRAN output file. The neutron flux is assumed to go to zero at the inlet of the lower reflector and the outlet of the upper reflector. Therefore, boundary conditions for the fast and thermal flux consist of

$$\varphi_1(0,t)=\varphi_1(L,t)=0 \qquad (2.4.2\text{-}3)$$

and

$$\varphi_2(0,t)=\varphi_2(L,t)=0. \qquad (2.4.2\text{-}4)$$

Note that z=0 corresponds to bottom of lower reflector region, z=L corresponds to top of upper reflector region.

---

[3] Stacey, W.M., *Space-Time Nuclear Reactor Kinetics*, Academic Press, New York, 1969.

Conservation equations for delayed neutron precursors consist of

$$\frac{\partial C_m(z,t)}{\partial t} = \beta_m\left[\nu_1 \Sigma_{f1}(z,t)\,\varphi_1(z,t) + \nu_2 \Sigma_{f2}(z,t)\varphi_2(z,t)\right] - \lambda_m C_m(z,t) \quad m \in \{1,\ldots,6\}\,. \tag{2.4.2-5}$$

where

$\beta = \sum_{m=1}^{6} \beta_m$ = delay fraction,

λ_m = decay constant for delayed neutron precursor group m (sec^{-1}), and

C_m = concentration of group m delayed neutron precursors,

Initial conditions for the fast and thermal flux, and for the delayed precursor concentrations are obtained by the methodology discussed in §2.4.3.

The reactor thermal power is computed from[4]

$$Q(t) = \int_0^L dz \left[\kappa\, \Sigma_{f1}(z,t)\ \varphi_1(z,t) + \kappa\, \Sigma_{f2}(z,t)\ \varphi_2(z,t)\ \right] \tag{2.4.2-6}$$

where

κ = energy per fission conversion factor.

Since the initial flux is computed as the solution of an eigenvalue problem, the amplitude of the initial flux is arbitrary (only the flux shape is relevant), and therefore, a scaling factor is included in the SABRE code so that the power computed from the integral in (2.4.2-6) is equal to the initial specified core power.

2.4.3 Methodology for Initial Flux Distribution

The initial flux distribution, initial precursor concentrations, and the initial neutron multiplication factor k_{eff} are obtained by solving the eigenvalue problem associated with the steady-state, 1-D, two-group diffusion equations. The eigenvalue problem is expressed as

[4] J.A. McClure, and G.C. Gose, SIMTRAN-E: A SIMULATE-E to RETRAN-02 Datalink, NP-5509-CCM, p. II-25, Electric Power Research Institute, Palo Alto, CA, 1987.

$$-\frac{d}{dz}\left[D_1(z)\,\frac{d\varphi_1(z)}{dz}\right]+D_1(z)\,B_R^2(z)\,\varphi_1(z)+\Sigma_{a1}(z)\,\varphi_1(z)$$

$$+\Sigma_s(z)\varphi_1(z)=\left[\nu_1\,\Sigma_{f1}(z)\varphi_1(z)+\nu_2\,\Sigma_{f2}(z)\,\varphi_2(z)\right]/k_{eff}\,, \qquad (2.4.3\text{-}1)$$

$$-\frac{d}{dz}\left[D_2(z)\,\frac{d\varphi_2(z)}{\partial z}\right]+\Sigma_{a2}(z)\,\varphi_2(z)=\Sigma_s(z)\varphi_1(z)\,, \qquad (2.4.3\text{-}2)$$

$$C_m(z)=\frac{\beta_m}{\lambda_m}\left[\nu_1\,\Sigma_{f1}(z)\,\varphi_1(z)+\nu_2\,\Sigma_{f2}(z)\,\varphi_2(z)\right], \qquad (2.4.3\text{-}3)$$

and

$$\varphi_1(0)=\varphi_1(L)=\varphi_2(0)=\varphi_2(L)=0\,. \qquad (2.4.3\text{-}4)$$

The terms on the left hand side of (2.4.3-1) represent neutron loss due to axial and radial leakage, absorption and scattering. The two terms in the numerator on the right hand side of (2.4.3-1) represent neutron production due to fast and thermal fission. Thus the eigenvalue k_{eff} in (2.4.3-1) is the ratio of neutron production to neutron destruction which is the definition of the effective neutron multiplication factor.[5] The factor $1/k_{eff}$ has been introduced into the steady-state neutron diffusion equations in order to facilitate calculation of a steady-state flux distribution. Eqs. (2.4.3-1), (2.4.3-2), and (2.4.3-4) are homogeneous in the fast and thermal flux, and therefore, a non-trivial solution to these equations will exist only for a specific value of the neutron multiplication factor k_{eff}.

In the SABRE code, the power method[6] is used to calculate the initial flux shape and the corresponding neutron multiplication factor. These results provide the necessary initial conditions for the transient kinetics problem.

Power Method for Solution of Eigenvalue Problem

The kinetics parameters in (2.4.3-1) and (2.4.3-2) are defined on 27 material regions within the core. These material regions consist of the lower and upper reflectors and the 25 axial cells within the active core region. The equations (2.4.3-1) and (2.4.3-2) are solved, using a finite-difference procedure, on each of these 27 material regions. The solutions are coupled by requiring continuity of the fast and thermal neutron flux and the neutron current density at the interface of any two material regions. These interfacial coupling conditions consist of

$$\varphi_{1,j}(0)=\varphi_{1,j-1}(L_{j-1}) \qquad j\in\{2,3,\ldots,N\}\,, \qquad (2.4.3\text{-}5)$$

---

[5] J. J. Duderstadt and L.J. Hamilton, *Nuclear Reactor Analysis*, p. 216, Wiley, New York, 1976.

[6] J. J. Duderstadt and L.J. Hamilton, *Nuclear Reactor Analysis*, pp. 216-218, Wiley, New York, 1976.

$$\varphi_{2,j}(0) = \varphi_{2,j-1}(L_{j-1}). \qquad j \in \{2,3,\ldots,N\}, \qquad (2.4.3\text{-}6)$$

$$-D_{1,j}\left.\frac{d\varphi_{1,j}(z_j)}{dz_j}\right|_{z_j=0} = -D_{1,j-1}\left.\frac{d\varphi_{1,j-1}(z_{j-1})}{dz_{j-1}}\right|_{z_{j-1}=L_{j-1}} \qquad j \in \{2,3,\ldots,N\}, \qquad (2.4.3\text{-}7)$$

and

$$-D_{2,j}\left.\frac{d\varphi_{2,j}(z_j)}{dz_j}\right|_{z_j=0} = -D_{2,j-1}\left.\frac{d\varphi_{2,j-1}(z_{j-1})}{dz_{j-1}}\right|_{z_{j-1}=L_{j-1}} \qquad j \in \{2,3,\ldots,N\}, \qquad (2.4.3\text{-}8)$$

where the subscript j denotes the material region within the core ($j \in \{1,2,\ldots,N\}$ where N = number of material regions = 27), and L_j is the length of each material region such that $z_j \in (0, L_j)$.

Within a material region, the diffusion coefficients and cross sections in (2.4.3-1) and (2.4.3-2) are constant. Therefore, within material region j, (2.4.3-1) and (2.4.3-2) become

$$-D_{1,j}\frac{d^2\varphi_{1,j}(z_j)}{dz_j^2} + D_{1,j}\ B_{R,j}^2\ \varphi_{1,j}(z_j) + \Sigma_{a1,j}\ \varphi_{1,j}(z_j) + \Sigma_{s,j}\varphi_{1,j}(z_j)$$

$$= \left[\nu_{1,j}\Sigma_{f1,j}\varphi_{1,j}(z_j) + \nu_{2,j}\Sigma_{f2,j}\ \varphi_{2,j}(z_j)\right]/k_{eff}, \qquad (2.4.3\text{-}9)$$

and

$$-D_{2,j}\frac{d^2\varphi_2(z_j)}{dz_j^2} + \Sigma_{a2,j}\ \varphi_{2,j}(z_j) = \Sigma_{s,j}\varphi_{1,j}(z_j). \qquad (2.4.3\text{-}10)$$

The second-order, central-difference formula,

$$D_{kj}\frac{d^2\varphi_{k,j}}{dz_j^2} = D_{kj}\frac{\varphi_{k,j}^{i+1} - 2\varphi_{k,j}^{i} + \varphi_{k,j}^{i-1}}{\Delta z_j^2} + O\left(\Delta z_j^2\right) \qquad i \in \{2,3,\ldots,M_j - 1\} \qquad (2.4.3\text{-}11)$$

is used to approximate the diffusion terms in (2.4.3-9) and (2.4.3-10). In (2.4.3-11), the subscript k defines the flux group (1=fast group and 2=thermal group), j denotes the material region, and i specifies the mesh point within the material region. Each material region can have a different number of mesh points. That is, M_j can be different for each of the 27 material regions and is really a function of j. At the interior mesh points of a material region, the finite-difference approximation to Eqs. (2.4.3-9) and (2.4.3-10) are

$$D_{1,j}\varphi_{1,j}^{i-1}+\left[-2D_{1,j}-\Delta z_j^2 D_{1,j}B_{Rj}^2-\Delta z_j^2\Sigma_{a1,j}+\Delta z_j^2\nu_{1,j}\frac{\Sigma_{f1,j}}{k_{eff}}-\Delta z_j^2\,\Sigma_{s1,j}\right]\varphi_{1,j}^{i}$$

$$+D_{1,j}\varphi_{1,j}^{i+1}=-\Delta z_j^2\nu_{2,j}\frac{\Sigma_{f2,j}}{k_{eff}}\varphi_{2,j}^{i}\qquad i\in\{2,3,\ldots,M_j-1\}\qquad\text{(2.4.3-12)}$$

and

$$D_{2,j}\varphi_{2,j}^{i-1}+\left[-2D_{2,j}-\Delta z_j^2\,\Sigma_{a2,j}\right]\varphi_{2,j}^{i}+D_{2,j}\varphi_{2,j}^{i+1}=-\Delta z_j^2\,\Sigma_{s,j}\varphi_{1,j}^{i}\qquad i\in\{2,3,\ldots,M_j-1\}.\qquad\text{(2.4.3-13)}$$

Equations (2.4.3-12) and (2.4.3-13) provide relations for determining the fast and thermal neutron flux at the interior grid points of each material region. The flux on the boundary points of each material region is determined from boundary conditions (2.4.3-4) and matching conditions (2.4.3-5) through (2.4.3-8). A 3-point sloping difference formula is used to obtain the following finite-difference approximations to (2.4.3-7) and (2.4.3-8):

$$-\frac{D_{1,j}}{2\Delta z_j}\left[-3\varphi_{1,j}^{1}+4\varphi_{1,j}^{2}-\varphi_{1,j}^{3}\right]=-\frac{D_{1,j-1}}{2\Delta z_{j-1}}\left[3\varphi_{1,j-1}^{M_{j-1}}-4\varphi_{1,j-1}^{M_{j-1}-1}+\varphi_{1,j-1}^{M_{j-1}-2}\right]\qquad\text{(2.4.3-14)}$$

and

$$-\frac{D_{2,j}}{2\Delta z_j}\left[-3\varphi_{2,j}^{1}+4\varphi_{2,j}^{2}-\varphi_{2,j}^{3}\right]=-\frac{D_{2,j-1}}{2\Delta z_{j-1}}\left[3\varphi_{2,j-1}^{M_{j-1}}-4\varphi_{2,j-1}^{M_{j-1}-1}+\varphi_{2,j-1}^{M_{j-1}-2}\right]\qquad\text{(2.4.3-15)}$$

where $j\in\{2,3,\ldots,N\}$. In terms of the values of the flux at the boundary grid points, Eqs. (2.4.3-5) and (2.4.3-6) become

$$\varphi_{1,j}^{1}=\varphi_{1,j-1}^{M_{j-1}}\qquad j\in\{2,3,\ldots,N\},\qquad\text{(2.4.3-16)}$$

$$\varphi_{2,j}^{1}=\varphi_{2,j-1}^{M_{j-1}}\qquad j\in\{2,3,\ldots,N\},\qquad\text{(2.4.3-17)}$$

Substituting (2.4.3-16) into (2.4.3-14) and (2.4.3-17) into (2.4.3-15) leads to the following expressions for the fast and thermal flux at the interface of the material regions in terms of the values at interior mesh points:

$$\varphi_{1,j}^{1}=\varphi_{1,j-1}^{M_{j-1}}=\frac{4\mu_{1,j}\varphi_{1,j}^{2}-\mu_{1,j}\varphi_{1,j}^{3}+4\varphi_{1,j-1}^{M_{j-1}-1}-\varphi_{1,j-1}^{M_{j-1}-2}}{3(1+\mu_{1,j})}\qquad j\in\{2,3,\ldots,N\}$$

$$\text{(2.4.3-18)}$$

and

$$\varphi_{2,j}^{1} = \varphi_{2,j-1}^{M_{j-1}} = \frac{4\mu_{2,j}\varphi_{2,j}^{2} - \mu_{2,j}\varphi_{2,j}^{3} + 4\varphi_{2,j-1}^{M_{j-1}-1} - \varphi_{2,j-1}^{M_{j-1}-2}}{3(1+\mu_{2,j})} \qquad j \in \{2,3,\ldots,N\} \tag{2.4.3-19}$$

where

$$\mu_{1,j} = \frac{\Delta z_{j-1}}{\Delta z_j}\left(\frac{D_{1,j}}{D_{1,j-1}}\right) \quad \text{and} \quad \mu_{2,j} = \frac{\Delta z_{j-1}}{\Delta z_j}\left(\frac{D_{2,j}}{D_{2,j-1}}\right). \tag{2.4.3-20}$$

The additional relations,

$$\varphi_{1,j}^{M_j} = \frac{4\mu_{1,j+1}\varphi_{1,j+1}^{2} - \mu_{1,j+1}\varphi_{1,j+1}^{3} + 4\varphi_{1,j}^{M_j-1} - \varphi_{1,j}^{M_j-2}}{3(1+\mu_{1,j+1})} \qquad j \in \{1,2,\ldots,N-1\} \tag{2.4.3-21}$$

and

$$\varphi_{2,j}^{M_j} = \frac{4\mu_{2,j+1}\varphi_{2,j+1}^{2} - \mu_{2,j+1}\varphi_{2,j+1}^{3} + 4\varphi_{2,j}^{M_j-1} - \varphi_{2,j}^{M_j-2}}{3(1+\mu_{2,j+1})}, \qquad j \in \{1,2,\ldots,N-1\} \tag{2.4.3-22}$$

result from incrementing j by 1 in equations (2.4.3-18) and (2.4.3-19).

It is convenient to rewrite Eqs. (2.4.3-12) and (2.4.3-13) as

$$c_{1,j}^{i}\ \varphi_{1,j}^{i-1} + a_{1,j}^{i}\ \varphi_{1,j}^{i} + b_{1,j}^{i}\ \varphi_{1,j}^{i+1} = d_{1,j}^{i} \qquad (i=2,\ 3,\ \ldots,\ M_j\text{-}1) \tag{2.4.3-23}$$

and

$$c_{2,j}^{i}\ \varphi_{2,j}^{i-1} + a_{2,j}^{i}\ \varphi_{2,j}^{i} + b_{2,j}^{i}\ \varphi_{2,j}^{i+1} = d_{2,j}^{i} \qquad (i=2,\ 3,\ \ldots,\ M_j\text{-}1) \tag{2.4.3-24}$$

where

$$c_{1,j}^{i} = D_{1,j},$$

$$a_{1,j}^{i} = -2D_{1,j} - \Delta z_j^2 D_{1,j} B_{R,j}^2 - \Delta z_j^2 \Sigma_{a1,j} + \Delta z_j^2 \frac{\nu_{1j}\Sigma_{f1,j}}{k_{eff}} - \Delta z_j^2 \Sigma_{s1,j},$$

$$b_{1,j}^{i} = D_{1,j},$$

$$d^i_{1,j} = -\Delta z_j^2 \frac{\nu_{2,j}\Sigma_{f2,j}}{k_{eff}} \varphi^i_{2,j},$$

$$c^i_{2,j} = D_{2,j},$$

$$a^i_{2,j} = -2D_{2,j} - \Delta z_j^2 \Sigma_{a2,j},$$

$$b^i_{2,j} = D_{2,j}, \text{ and}$$

$$d^i_{2,j} = -\Delta z_j^2 \, \Sigma_{s,j} \, \varphi^i_{1,j}.$$

The power iteration method for computing the neutron flux shape and the associated eigenvalue k_{eff} proceeds as follows:

Step 1

An initial guess, consistent with the boundary conditions, $\varphi^1_{1,1} = 0$, $\varphi^1_{2,1} = 0$, $\varphi^{M_N}_{1,N} = 0$, and $\varphi^{M_N}_{2,N} = 0$, is made for the fast and thermal flux $\varphi^i_{1,j}$. Also, an initial guess is made for the eigenvalue k_{eff}.

Step 2

The neutron generation rate is integrated numerically, using Simpson's Rule, over the length of the core region to obtain the source integral S,

$$S = \int_0^{L_C} dz \left[\nu_1 \Sigma_{f1}(z) \varphi_1(z) + \nu_2 \Sigma_{f2}(z) \, \varphi_2(z)\right]$$

Step 3

The Thomas algorithm[7] is used to solve for the fast flux at the interior mesh points of the N material regions of the core. For each material region ($j \in \{1,\ldots,N$), the solution proceeds as follows:

Define $\delta(1) = \varphi^1_{1,j}$ and $F(1) = 0$

[7] Anderson, D.A., Tannehill, J.C., and Pletcher, R.H., *Computational Fluid Mechanics and Heat Transfer*, p. 99, Hemisphere, New York, 1984.

Compute $F(i+1)=\dfrac{-b_{1,j}^{i+1}}{a_{1,j}^{i}+c_{1,j}^{i+1}F(i)}$ for $i\in\{1,2,\ldots,M_j-2\}$

Compute $\delta(i+1)=\dfrac{d_{1,j}^{i+1}-c_{1,j}^{i+1}\delta(i)}{a_{1,j}^{i+1}+c_{1,j}^{i+1}F(i)}$ for $i\in\{1,2,\ldots,M_j-2\}$

Compute $\varphi_{1,j}^{i}=F(i)\,\varphi_{1,j}^{i+1}+\delta(i)$ for $i\in\{M_j-1,M_j-2,\ldots,2\}$

Step 4

The constants $d_{2,j}^{i}$ are computed from the fast flux calculated in Step 3. An improved estimate for the thermal flux is obtained by solving the tri-diagonal system (2.4.3.-24) using the Thomas Algorithm.

Step 5

The source integral S in Step 2 is recomputed with the improved estimates of the fast and thermal flux. An improved estimate for k_{eff} is calculated from the iteration formula[8]

$$k_{eff}^{(n+1)}=\frac{S^{(n+1)}}{\dfrac{1}{k_{eff}^{(n)}}S^{(n)}}$$

where n denotes the iteration index.

Step 6

A check is made for convergence of the multiplication factor k_{eff}. If $\left|k_{eff}^{(n+1)}-k_{eff}^{(n)}\right|<\varepsilon$, the calculation process is stopped. Otherwise, the calculation proceeds to Step 7.

Step 7

$S^{(n)}$ takes the value of $S^{(n+1)}$ and $k_{eff}^{(n)}$ takes the value of $k_{eff}^{(n+1)}$. The calculation then transfers back to Step 3 and proceeds until the acceptance criterion in Step 6 is satisfied.

After the initial neutron flux is computed as described above, a second level of flux initialization is performed to remove any initial perturbations from the numerical solution. This is accomplished by performing internal time steps within the SABRE code prior to initiating the transient simulation. The transient solution is started at t = -40

[8] J. J. Duderstadt and L.J. Hamilton, *Nuclear Reactor Analysis*, p. 217, Wiley, New York, 1976.

seconds and all of the governing kinetic and thermal-hydraulic equations are numerically integrated up to t=0. During the time that t<0, small adjustments are made to the value of k_{eff} (typically a few tenths of a mk) and the pressure regulator setpoint so that when t=0 the power and reactor pressure are acceptably close to the values specified in the SABRE input file. When the transient simulation is initiated at t=0, all initial perturbations have been removed through the dynamic initialization process.

Table 2.4.3-1 and Figure 2.4.3-1 compare the initial axial power shape calculated by SABRE for Case 03 (see Computer Case summary) against the SIMTRAN-calculated power shape. SABRE Case 03 was calculated using the U2C9 kinetics file (u2c9.simtran.out) which is the output file for SIMTRAN Run#9900340. The normalized power shape calculated by SIMTRAN was obtained from this output file. The SABRE-calculated power shape was obtained from the output file for SABRE Case 03. The mesh spacing used in the SABRE finite-difference solution of the two-group diffusion equations is essentially the same as that used in the PP&L SIMTRAN model. In SABRE, 33 grid points are used in each of the two reflector regions and 13 grid points are used in each of the active core material regions. In the SIMTRAN model, 12 grid points are used in each of the 25 active core material regions. Thirteen points were used in SABRE because the number of grid points must be odd since spatial integration of the flux is performed using Simpson's rule. The results in Figure 2.4.3-1 show reasonably close agreement. Sensitivity studies were performed on the grid point spacing in SABRE, and little change in the solution was observed upon increasing the number of grid points.

The RMS difference between SABRE and SIMTRAN is computed from the values in Table 2.4.3-1 as follows:

$$\text{RMS} = (100\%)\text{x}\sqrt{\frac{1}{25}\sum_{i=1}^{25}(SABRE_i - SIMTRAN_i)^2} = 4.86\%$$

Comparison of PP&L Nuclear Fuels' predictions for core axial power shape against TIP (Traversing In-Core Probe) measurements show that the RMS uncertainty associated with the predictions ranges from 5% to 12%.[9] Therefore, the differences between SABRE and SIMTRAN are well within the uncertainty of the core-physics methodology.

[9] PP&L Report PL-NF-90-001A, "Application of Reactor Analysis Methods for BWR Design and Analysis," pp. 85-90, July, 1992.

Table 2.4.3-1
Normalized Axial Power Predicted by SABRE and SIMTRAN

Core Node	SABRE	SIMTRAN	(SABRE-SIMTRAN)^2
25	0.1509	0.163	0.000146
24	0.4473	0.482	0.001204
23	0.7748	0.834	0.003505
22	0.9415	1.01	0.004692
21	1.0693	1.14	0.004998
20	1.163	1.23	0.004489
19	1.2283	1.29	0.003807
18	1.2741	1.33	0.003125
17	1.2987	1.35	0.002632
16	1.3276	1.36	0.00105
15	1.3141	1.34	0.000671
14	1.288	1.30	0.000144
13	1.2512	1.25	1.44E-06
12	1.2055	1.19	0.00024
11	1.1535	1.13	0.000552
10	1.1007	1.07	0.000942
9	1.05	1.01	0.0016
8	1.005	0.955	0.0025
7	0.9708	0.914	0.003226
6	0.9506	0.892	0.003434
5	0.946	0.885	0.003721
4	0.9444	0.883	0.00377
3	0.9231	0.863	0.003612
2	0.8195	0.761	0.003422
1	0.4022	0.362	0.001616

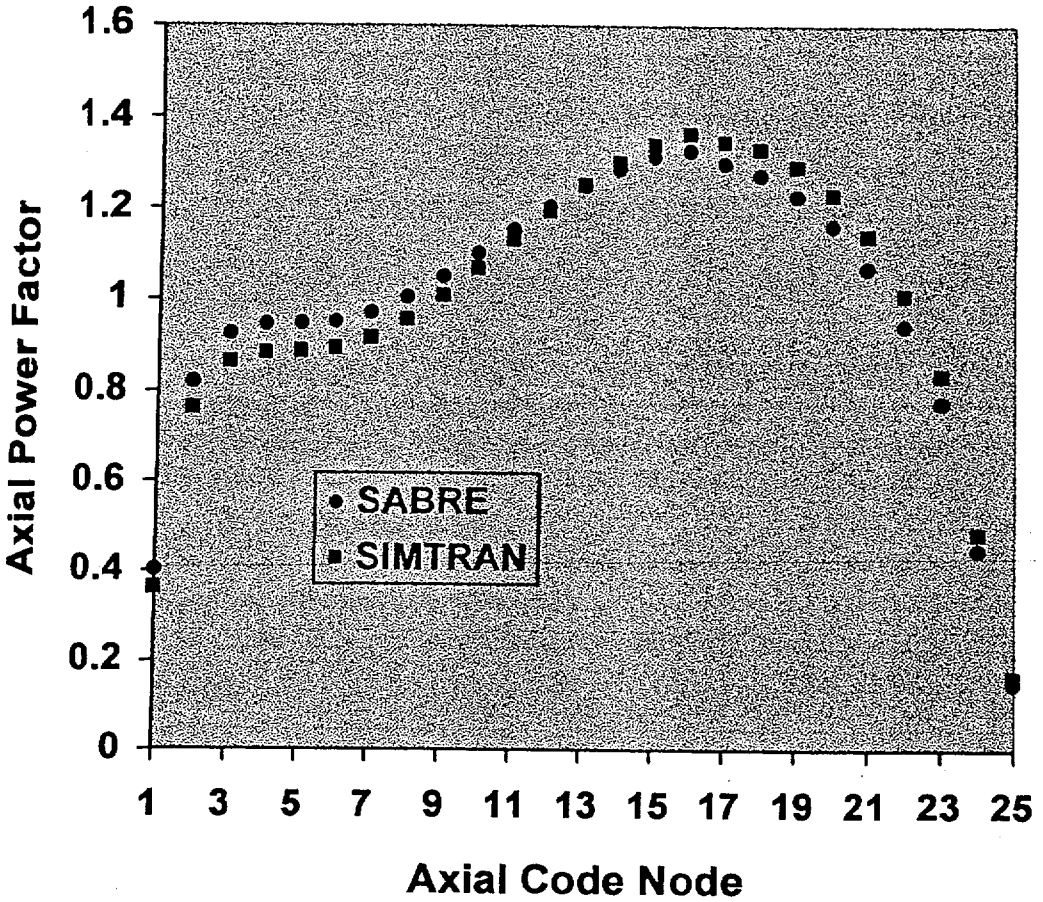

Figure 2.4.3-1 Comparison of initial core axial power shape for SABRE Case 03 against SIMTRAN-calculated power shape.

2.4.4 Methodology for Transient Flux

Since the kinetics parameters are constant over each of the N material regions comprising the core, the time-dependent, two-group diffusion equations are written for each material region denoted by the subscript j. The regional fast and thermal group equations, respectively, are

$$\frac{1}{\upsilon_{1,j}(t)}\frac{\partial\varphi_{1,j}(z_j,t)}{\partial t}=D_{1,j}(t)\frac{\partial^2\varphi_{1,j}(z_j,t)}{\partial z_j^{\,2}}-D_{1,j}(t)\,B_{R,j}^2\,\varphi_{1,j}(z_j,t)-\Sigma_{a1,j}(t)\varphi_{1,j}(z_j,t)$$

$$+(1-\beta)\frac{\nu_{1,j}(t)}{k_{eff}}\Sigma_{f1,j}(t)\varphi_{1,j}(z_j,t)+(1-\beta)\frac{\nu_{2,j}(t)}{k_{eff}}\Sigma_{f2,j}(t)\;\varphi_{2,j}(z_j,t)$$

$$-\Sigma_{s,j}(t)\;\varphi_{1,j}(z_j,t)+\sum_{m=1}^{6}\lambda_m C_{m,j}(z_j,t) \qquad (2.4.4\text{-}1)$$

and

$$\frac{1}{\upsilon_{2,j}(t)}\frac{\partial\varphi_{2,j}(z_j,t)}{\partial t}=D_{2,j}(t)\frac{\partial^2\varphi_{2,j}(z_j,t)}{\partial z_j^{\,2}}-\Sigma_{a2,j}(t)\;\varphi_{2,j}(z_j,t)+\Sigma_{s,j}(t)\;\varphi_{1,j}(z_j,t)\,. \qquad (2.4.4\text{-}2)$$

Similarly, the delayed-neutron precursor equations for each neutronic region consist of

$$\frac{\partial C_{m,j}(z_j,t)}{\partial t}=\beta_m\left[\frac{\nu_{1,j}(t)}{k_{eff}}\Sigma_{f1,j}(t)\varphi_{1,j}(z_j,t)+\frac{\nu_{2,j}(t)}{k_{eff}}\Sigma_{f2,j}(t)\varphi_{2,j}(z_j,t)\right]-\lambda_m C_{m,j}(z_j,t)\,. \qquad m\in\{1,2,\ldots,6\} \qquad (2.4.4\text{-}3)$$

The index j defining the material regions ranges from 1 to N where N=27 for the Susquehanna core model. Region 1 is the lower reflector, region 27 is the upper reflector, and regions 2-26 constitute the active core. The length of each region is denoted as L_j. The subscript m ranges from 1 to 6, since there are six delayed neutron groups. Inclusion of the factor $1/k_{eff}$ in (2.4.4-1) and (2.4.4-3) ensures that the reactor simulation starts from a critical condition. Fast and thermal flux boundary conditions consist of

$$\varphi_{1,1}(0,t)=0 \quad \text{and} \quad \varphi_{1,N}(L_N,t)=0 \qquad (2.4.4\text{-}4)$$

and

$$\varphi_{2,1}(0,t) = 0 \quad \text{and} \quad \varphi_{2,N}(L_N,t) = 0. \tag{2.4.4-5}$$

At each interface between neutronic regions the flux and the normal component of the neutron current density are continuous.[10] Therefore, the interfacial conditions consist of

$$\varphi_{1,j}(0,t) = \varphi_{1,j-1}(L_{j-1}, t) \qquad j \in \{2,3,\ldots,N\}, \tag{2.4.4-6}$$

$$\varphi_{2,j}(0,t) = \varphi_{2,j-1}(L_{j-1}, t). \qquad j \in \{2,3,\ldots,N\}, \tag{2.4.4-7}$$

$$-D_{1,j}\left.\frac{\partial\varphi_{1,j}(z_j,t)}{\partial z_j}\right|_{z_j=0} = -D_{1,j-1}\left.\frac{\partial\varphi_{1,j-1}(z_{j-1},t)}{\partial z_{j-1}}\right|_{z_{j-1}=L_{j-1}} \qquad j \in \{2,3,\ldots,N\}, \tag{2.4.4-8}$$

and

$$-D_{2,j}\left.\frac{\partial\varphi_{2,j}(z_j,t)}{\partial z_j}\right|_{z_j=0} = -D_{2,j-1}\left.\frac{\partial\varphi_{2,j-1}(z_{j-1},t)}{\partial z_{j-1}}\right|_{z_{j-1}=L_{j-1}} \qquad j \in \{2,3,\ldots,N\},. \tag{2.4.4-9}$$

As shown for the steady-state problem in §2.4.3, these relations lead to the matching conditions (2.4.3-18), (2.4.3-19), (2.4.3-21), and (2.4.3-22) which express the interfacial flux in terms of the flux at interior grid points. Initial conditions for the neutron flux and precursor concentrations are obtained as described in Section 2.4.3.

A method of lines (MOL) approach is used to solve the transient equations (2.4.4-1)-(2.4.4-3). In the MOL, finite-difference approximations are applied only to the spatial derivatives in equations (2.4.4-1)-(2.4.4-3) thus converting PDEs (2.4.4-1)-(2.4.4-3) into a coupled set of ODEs with time as the independent variable. At the interior grid points of each material region, the spatial derivatives are approximated with a second-order, central-difference formula. Application of the MOL yields the following set of ODEs for the neutron flux and precursor concentrations at the interior grid points of each material region:

[10] Lamarsh, J.R., *Introduction to Nuclear Reactor Theory*, pp. 135-136, Addison-Wesley, Reading, MA, 1966.

$$\frac{1}{\upsilon_{1,j}(t)}\frac{d\varphi^i_{1,j}(t)}{dt}=D_{1,j}(t)\frac{\varphi^{i+1}_{1,j}(t)-2\varphi^i_{1,j}(t)+\varphi^{i-1}_{1,j}(t)}{\Delta z_j^2}-D_{1,j}(t)\,B^2_{R,j}\varphi^i_{1j}(t)-\Sigma_{a1,j}(t)\varphi^i_{1,j}(t)$$

$$+(1-\beta)\frac{\nu_{1,j}(t)}{k_{eff}}\Sigma_{f1,j}(t)\varphi^i_{1j}(t)+(1-\beta)\frac{\nu_{2,j}(t)}{k_{eff}}\Sigma_{f2,j}(t)\,\varphi^i_{2j}(t)$$

$$-\Sigma_{s,j}(t)\,\varphi^i_{1,j}(t)+\sum_{m=1}^{6}\lambda_m C^i_{m,j}(t) \qquad (2.4.4\text{-}10)$$

and

$$\frac{1}{\upsilon_{2,j}(t)}\frac{d\varphi^i_{2,j}(t)}{dt}=D_{2,j}(t)\frac{\varphi^{i+1}_{2,j}(t)-2\varphi^i_{2,j}(t)+\varphi^{i-1}_{2,j}(t)}{\Delta z_j^2}-\Sigma_{a2,j}(t)\varphi^i_{2,j}(t)+\Sigma_{s,j}(t)\,\varphi^i_{1,j}(t)\,. \qquad (2.4.4\text{-}11)$$

Similarly, the delayed-neutron precursor equations for each neutronic region consist of

$$\frac{dC^i_{m,j}(t)}{dt}=\beta_m\left[\frac{\nu_{1,j}(t)}{k_{eff}}\Sigma_{f1,j}(t)\varphi^i_{1,j}(t)+\frac{\nu_{2,j}(t)}{k_{eff}}\Sigma_{f2,j}(t)\,\varphi^i_{2j}(t)\right]-\lambda_m C^i_{mj}(t)\,. \qquad m\in\{1,2,\ldots,6\} \qquad (2.4.4\text{-}12)$$

Here j denotes the particular material region, and i specifies the grid point within the material region. In the transient solution, the fast and thermal flux at the interface between two adjacent material regions is computed from (2.4.3-18), (2.4.3-19), (2.4.3-21), and (2.4.3-22). The flux on the lower boundary of the lower reflector and the upper boundary of the upper reflector is specified in accordance with boundary conditions (2.4.4-4) and (2.4.4-5). The ODEs approximating the transient reaction-diffusion system are integrated with the ODE solver LSODES (Livermore Solver for Ordinary Differential Equations with General Sparse Jacobian Matrices).[11] A relative error criterion of 1.E-05 is specified in the SABRE code. LSODES automatically selects time-step size and method order as the computation proceeds in order to optimize the computational efficiency. For temporal integration of the ODEs, an implicit solution option based on the backward differentiation formulas proposed by Gear[12] was chosen (LSODES input parameter mf=222). Thirty-three grid points were used in the upper and lower reflector regions, and 13 grid points were used in each of the 25 axial nodes within the active fuel region. This mesh spacing is consistent with that used to solve the 1-D kinetics equations in the PP&L RETRAN model of Susquehanna.

---

[11] A.C. Hindmarsh, ODEPACK, A Systematized Collection of ODE Solvers. In Scientific Computing (R.S. Stepleman et al. eds.), Vol. 1, pp. 55-64. IMACS Trans. on Scientific Computation, North-Holland Publ., Amsterdam, 1983.

[12] Gear C.W., *Numerical Initial Value Problem in Ordinary Differential Equations*, Prentice-Hall, Englewood Cliffs, NJ (1971).

2.4.5 Modification of Thermal Absorption Cross Section to Account for Dissolved Boron

The 1-D thermal absorption cross section Σ_{a2} obtained from the output file of the SIMTRAN code depends only on changes in moderator density and fuel temperature; there is no boron dependency built into this cross section. Since SABRE is used primarily to simulate reactor response during ATWS events in which the reactor is shutdown by injecting borated water via the SLCS, it is necessary to incorporate boron dependency into the SIMTRAN 1-D cross-section set. Rather than modifying the underlying lattice physics calculations to build boron dependency into the cross-section set, a much simpler approach is taken in this calculation. This approach is described as follows.

For each fuel cycle, the PP&L Nuclear Fuels' Group supplies a Hot Shutdown Boron Concentration (HSBC) for use in cycle-specific ATWS analyses. The HSBC is the boron concentration measured in ppm required to bring the reactor from hot full-power to hot zero power (no voids) with the Xenon concentration at the hot full-power condition. The cycle-specific value of the HSBC obtained from the Nuclear Fuels' Group is used to empirically modify the boron-free thermal absorption cross section generated by SIMTRAN. In SABRE, a modified cross section of the form

$$\tilde{\Sigma}_{a2,j} = \Sigma_{a2,j} + \mu \, \mathbf{F}(C_{B,C,j};\ C_{B,B,j};\ \alpha_{C,j};\ \alpha_{B,j}) \qquad (2.4.5\text{-}1)$$

is used where

$$\mathbf{F}(C_{B,C,j};\ C_{B,B,j};\ \alpha_{C,j};\ \alpha_{B,j}) \equiv C_{B,C,j}\left(1-\alpha_{C,j}\right)\frac{A_C}{A_C + A_B} + C_{B,B,j}\left(1-\alpha_{B,j}\right)\frac{A_B}{A_C + A_B}. \qquad (2.4.5\text{-}2)$$

In (2.4.5-1), $\Sigma_{a2,j}$ represents the boron-free, 1-D thermal absorption cross-section computed by SIMTRAN for material region j, and $\tilde{\Sigma}_{a2,j}$ is the modified thermal absorption cross-section which includes dependency on dissolved boron. $C_{B,C,j}$ is the concentration of boron (ppm) in the coolant within the fuel bundle, $C_{B,B,j}$ is the concentration of boron in the bypass coolant, $\alpha_{C,j}$ is the void fraction within fuel channel, $\alpha_{B,j}$ is the bypass void fraction, A_C is the fuel channel flow area, A_B is the bypass channel flow area, and the subscript j denotes a particular axial material region $j \in \{1,2,\ldots,27\}$.

The parameter μ is determined from the requirement that the core is critical at hot zero-power conditions with the boron concentration equal to HSBC, i.e., when $C_{B,C,j}=C_{B,B,j}=HSBC$, $\alpha_{C,j}=\alpha_{B,j}=0$, and the fuel and moderator temperatures are equal to the saturation temperature corresponding to rated reactor pressure. The parameter μ is computed in an iterative fashion by SABRE during the initialization phase of the calculation. This is accomplished by varying μ in accordance with a bisection procedure

and repeatedly solving the eigenvalue problem defined by (2.4.3-1), (2.4.3-2), and (2.4.3-3) at hot zero power conditions with the boron concentration equal to the HSBC until the eigenvalue k_{eff} converges to the hot full power eigenvalue (target k_{eff}) with no boron. The value of μ computed in this manner is used in the transient calculation to compute the thermal absorption cross section from (2.4.5-1) and (2.4.5-2). This approach forces the reactor core to shutdown in a manner consistent with the value of the HSBC.

The functional form of (2.4.5-1) is verified by performing lattice physics calculations using the CASMO-3 computer code[13] with various void fractions and boron concentrations (CASMO Run#9900755 in Computer Case Summary). The input data file and *mem* file (job control file) for this CASMO case are documented in Tables 2.4.5-1 and 2.4.5-2. Lattice calculation results for the macroscopic boron thermal absorption cross section for ATRIUM-10 fuel with lattice type 92[14] are presented in Table 2.4.5-3. Also contained within this table is the value of **F** calculated from (2.4.5-2). In computing **F**, the values of the core and bypass flow areas A_C and A_B are taken from the base ATRIUM-10 input deck for SABRE which is listed in Appendix G (A_C=78.19 ft^2 and A_B=66.04 ft^2).

In Figure 2.4.5-1, the B-10 thermal absorption cross sections computed with CASMO-3 are plotted against the function **F** for bundle exposures of 10 and 20 GWD/MTU. A straight line connecting the largest and smallest CASMO-calculated cross sections is included in each plot in order to assess the linearity of the relationship between the B-10 thermal cross section and the function **F**. It can be seen from Figure 2.4.5-1 that this relationship is indeed very nearly linear, and therefore, Eqs. (2.4.5-1) and (2.4.5-2) represent a valid model of the boron dependency in the 1-D thermal absorption cross section.

---

[13] Malte Edenius and Bengt H. Forssen, "CASMO-3 A Fuel Assembly Burnup Program," User's Manual, STUDSVIK/NFA-89/3, Studsvik of America, Inc., 1087 Beacon St., Suit 301, Newton MA.

[14] See Nuclear Fuels' Calculation NFE-2-10-001, Rev. 0, p. C.6 for description of assembly and lattice type.

Table 2.4.5-1
CASMO Input File for Run#9900755

```
DIM,10/
TIT,VOI=40,TFU=840.0,TMO=562.2,IDE='9240' *lt92--10x10--e=4.19 13Gd6 - .40 VB
FUE, 1, 9.91010/2.550
FUE, 2, 9.91010/3.050
FUE, 3, 9.91010/3.400
FUE, 4, 9.91010/3.800
FUE, 5, 9.91010/4.150
FUE, 6, 9.70209/4.150,7301= 6.00
FUE, 7, 9.91010/4.450
FUE, 8, 9.91010/4.680
BAD,7301,1
BWR,10,1.29540,13.40612, .20320, .71374, .71374,1.1684
PDQ,'BND',1,0,1, -77//92235, 92236, 92238, 94239, 94240, 94241, 94242
    54135, 62149, 7300, 93237, 94238
THE,0
RUN,0,2
PIN, 1, .44196, .50254,
PIN, 2,1.67767,1.75006/'MOD','BOX'//-9
LPI
 1
 1 1
 1 1 1
 1 1 1 1
 1 1 1 1 2
 1 1 1 1 2 2
 1 1 1 1 2 2 2
 1 1 1 1 1 1 1 1
 1 1 1 1 1 1 1 1 1
 1 1 1 1 1 1 1 1 1 1
LFU
 1
 3 7
 5 6 8
 5 8 8 8
 5 7 6 8 0
 5 8 8 8 0 0
 4 6 8 8 0 0 0
 3 8 7 8 8 8 7 6
 1 7 6 8 6 7 6 8 7
 1 3 5 7 7 7 7 3 2 1
SPA,6.970,,,6.980/302=82.46,718=17.54 * inconel spacer
can,,,576.0
PDE,24.513
DEP,0,.1,.5,1,1.5,2,2.5,3,3.5,4,4.5,5,5.5,6,6.5,7,7.5,8,8.5,9,9.5,10,
    10.5,11,11.5,12,12.5,13,13.5,14,14.5,15,15.5,16,16.5,17,17.5,18,
     18.5,19,19.5,20,-40,42.5,45,47.5,50,52.5,55,57.5,60.0
STA
TIT,IDE='924A' *+Hot 000.0 PPM  0 Voids Branch
RES,'9240',0,5,10,15,20,25,30,40,50,60
VOI,0 TMO,561.22 TFU,561.22 PDE,0
CAN,,,293.15
BOR, 000.0
XEN,0
STA
TIT,IDE='924B' *+Hot 000.0 PPM  40 Voids Branch
RES,'9240',0,5,10,15,20,25,30,40,50,60
VOI,40 TMO,561.22 TFU,561.22 PDE,0
CAN,,,293.15
BOR, 000.0
XEN,0
STA
TIT,IDE='924C' *+Hot 000.0 PPM  80 Voids Branch
RES,'9240',0,5,10,15,20,25,30,40,50,60
VOI,80 TMO,561.22 TFU,561.22 PDE,0
CAN,,,293.15
BOR, 000.0
XEN,0
STA
TIT,IDE='924D' *+Hot 200.0 PPM  0 Voids Branch
RES,'9240',0,5,10,15,20,25,30,40,50,60
VOI,0 TMO,561.22 TFU,561.22 PDE,0
CAN,,,293.15
BOR, 200.0
XEN,0
STA
TIT,IDE='924E' *+Hot 200.0 PPM  40 Voids Branch
RES,'9240',0,5,10,15,20,25,30,40,50,60
VOI,40 TMO,561.22 TFU,561.22 PDE,0
CAN,,,293.15
BOR, 200.0
```

```
XEN,0
STA
TIT,IDE='924F' *+Hot 200.0 PPM  80 Voids Branch
RES,'9240',0,5,10,15,20,25,30,40,50,60
VOI,80 TMO,561.22 TFU,561.22 PDE,0
CAN,,,293.15
BOR, 200.0
XEN,0
STA
TIT,IDE='924G' *+Hot 400.0 PPM  0 Voids Branch
RES,'9240',0,5,10,15,20,25,30,40,50,60
VOI,0 TMO,561.22 TFU,561.22 PDE,0
CAN,,,293.15
BOR, 400.0
XEN,0
STA
TIT,IDE='924H' *+Hot 400.0 PPM  40 Voids Branch
RES,'9240',0,5,10,15,20,25,30,40,50,60
VOI,40 TMO,561.22 TFU,561.22 PDE,0
CAN,,,293.15
BOR, 400.0
XEN,0
STA
TIT,IDE='924I' *+Hot 400.0 PPM  80 Voids Branch
RES,'9240',0,5,10,15,20,25,30,40,50,60
VOI,80 TMO,561.22 TFU,561.22 PDE,0
CAN,,,293.15
BOR, 400.0
XEN,0
STA
TIT,IDE='924J' *+Hot 800.0 PPM  0 Voids Branch
RES,'9240',0,5,10,15,20,25,30,40,50,60
VOI,0 TMO,561.22 TFU,561.22 PDE,0
CAN,,,293.15
BOR, 800.0
XEN,0
STA
TIT,IDE='924K' *+Hot 800.0 PPM  40 Voids Branch
RES,'9240',0,5,10,15,20,25,30,40,50,60
VOI,40 TMO,561.22 TFU,561.22 PDE,0
CAN,,,293.15
BOR, 800.0
XEN,0
STA
TIT,IDE='924L' *+Hot 800.0 PPM  80 Voids Branch
RES,'9240',0,5,10,15,20,25,30,40,50,60
VOI,80 TMO,561.22 TFU,561.22 PDE,0
CAN,,,293.15
BOR, 800.0
XEN,0
STA
END
```

Table 2.4.5-2
CASMO MEM File for Run#9900755

```
1 lt92.4.out
2 lt92.4.error
3 *none*
4 *none*
5 *none*
6 3
7 ,VOI=40,TFU=840.0,TMO=562.2,IDE="9240" *lt92--10x10--e=4.19 13Gd6 - .40 VB
8 *none*
9 *none*
11
1 long
2 *now*
3 *none*
4 *all*
7 /users/NF/scripts/casmo-job.ksh
8 /users/NF/bin/casmo3v4p7.out
9
10
11
12
5
1 *none*
2 *none*
3 /users/chaiko/casmo
5 lt92.4
6 *none*
7 lt92.4.ci
8 /users/NF/Midburn3/lt92.gadfile
9 *required*
10 *required*
11 *none*
```

Table 2.4.5-3
CASMO Results for Run#9900755

CASMO State Point	Burnup[†] (GWD/MTU)	Fuel Channel Void Fraction[‡]	Boron Concentration (ppm)	Boron Thermal Absorption Cross Section (cm^{-1})	$\Sigma^a(C_{B,Cj}, C_{B,Bj}, \alpha_{Cj}, \alpha_{Bj})$
61	10	0.0	0	3.0745E-22	0
71	10	0.4	0	3.0077E-22	0
81	10	0.8	0	2.9146E-22	0
91	10	0.0	200	2.4945E-03	200
101	10	0.4	200	1.9878E-03	156.630382
111	10	0.8	200	1.5196E-03	113.2607641
121	10	0.0	400	4.9665E-03	400
131	10	0.4	400	3.9572E-03	313.2607641
141	10	0.8	400	3.0253E-03	226.5215281
151	10	0.0	800	9.8461E-03	800
161	10	0.4	800	7.8428E-03	626.5215281
171	10	0.8	800	5.9967E-03	453.0430562
63	20	0.0	0	3.0696E-22	0
73	20	0.4	0	3.0119E-22	0
83	20	0.8	0	2.9293E-22	0
93	20	0.0	200	2.4903E-03	200
103	20	0.4	200	1.9750E-03	156.630382
113	20	0.8	200	1.4962E-03	113.2607641
123	20	0.0	400	4.9589E-03	400
133	20	0.4	400	3.9323E-03	313.2607641
143	20	0.8	400	2.9793E-03	226.5215281
153	20	0.0	800	9.8331E-03	800
163	20	0.4	800	7.7960E-03	626.5215281
173	20	0.8	800	5.9078E-03	453.0430562

[†] Void history is 0.4.
[‡] Bypass void is zero in all cases.

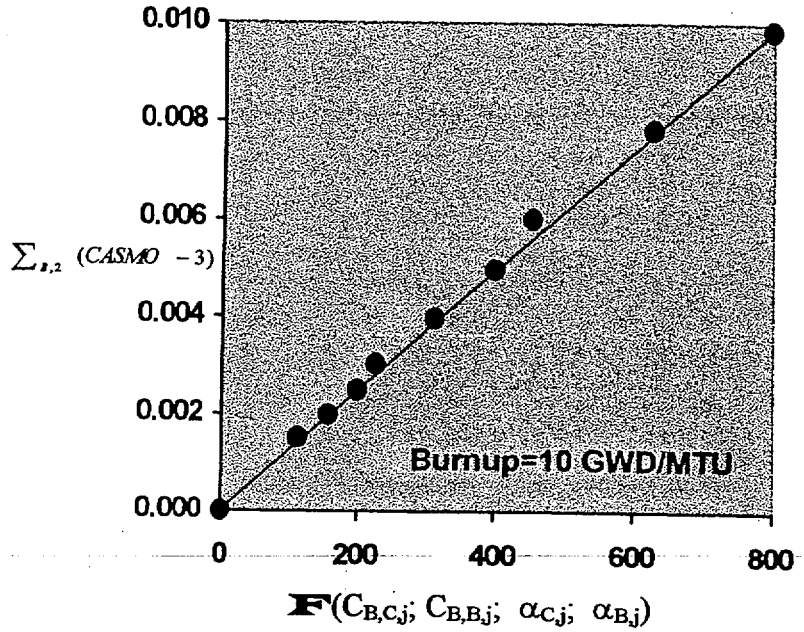

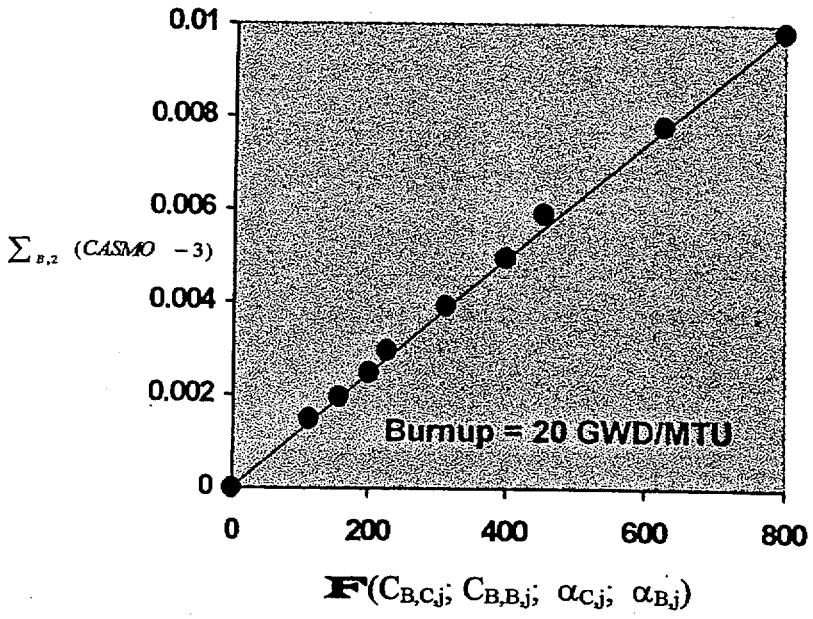

Figure 2.4.5-1 CASMO-3 calculated macroscopic thermal absorption cross section for B-10 plotted against the function $\mathbf{F}$ given in Eq. (2.4.5-2). Line segments included to illustrate the nearly linear relationship between B-10 cross section and $\mathbf{F}$. Calculations are for ATRIUM-10 fuel with lattice type 92. (CASMO Run#9900755)

2.4.6 Boron Transport Model

In the SABRE model, boron is transported throughout the reactor by the coolant flow. A control-volume approach, with up to eighteen control volumes (see Table 2.4.6-1), is used in calculating the local boron concentration. Boron in each control volume is assumed to be perfectly mixed. In the SABRE boron mixing model, boron is only transported by liquid flow; the volatility of boron is neglected.

For boron mixing and transport, fine noding is used within the core region, because within this region, there is generally a large gradient in coolant void fraction due to heat addition from the fuel. Since boron is only contained within the liquid phase of the coolant, variations in void fraction are accompanied by variations in boron concentration. In the other regions of the reactor vessel such as the upper plenum, riser, and separator, large spatial variations in void fraction do not typically occur and therefore coarse nodalization is used.

In the Susquehanna reactors, boron is injected by the SLCS into the lower plenum region of the vessel. Since the borated water injected by the SLCS is more dense than the reactor coolant, there is concern that under low-flow conditions boron may stagnate in the lower head of the vessel. Experimental studies on boron mixing efficiency, carried out by Dias, Yan, and Theofanous, [15,16] indicate that complete upward entrainment of boron into the core "is 100% efficient and complete, down to flows of at least 6% (of rated), perhaps even as low as 4%." The discussion in the Technical Evaluation Report[17] supporting the NRC's Safety Evaluation Report[18] on ATWS mitigation strategies corroborates this view on boron mixing efficiency. When referring to the boron mixing data of Dias et al., the TER states: "The new data suggests that mixing is almost perfect (i.e., 100% efficiency) even for flows as low as 4% to 5%." Here 100% core flow corresponds to 100 MLb/hr.

SABRE simulates boron injection by adding boron to the upper node of the lower plenum region since this corresponds to the location of the injection standpipe within the reactor. If the total core flow is greater than W_2, which is specified as part of the SABRE input data, then the injected boron becomes completely mixed within this upper control volume. On the other hand, if the total core flow is less than a specified value W_1, then the injected boron is immediately transferred to the bottom node of the lower plenum to simulate boron stagnation under low-flow conditions. Thus, boron entrainment is 100% complete if the total core flow is greater than W_2, and there is no entrainment of boron if the total core flow drops below W_1.

---

[15] Dias, M.P., Yan, H., and Theofanous, T.G., "The Management of ATWS by Boron Injection," Proceedings, NURETH-5, Sept. 21-24, 1992, Salt Lake City, Utah.
[16] Dias, M.P., Yan, H., and Theofanous, T.G., "The Management of ATWS by Boron Injection," NUREG/CR-5951, March 1993.
[17] March-Leuba, J., "Technical Evaluation Report ORNL/NRC/LTR-94/28, Revision 2, November 1995.
[18] "Safety Evaluation Report: Modifications to the Boiling Water Reactor (BWR) Emergency Procedure Guidelines to Address Reactor Core Instabilities," Letter from D.B. Matthews (NRC) to K.P. Donovan (Centerior Energy), June 6, 1996.

Based on the boron mixing studies referred to above, the core flow W_2 has a value of 6 Mlbm/hr. The value of W_1 is conservatively taken as 4 MLb/hr since there is no available information on boron entrainment for core flows less than 4 MLb/hr. For flows between W_1 and W_2, the fraction χ_B of injected boron that is entrained upward into the core is computed from

$$\chi_B = \left(\frac{W - W_1}{W_2 - W_1}\right)^b \qquad (W_1 < W < W_2) \qquad (2.4.6\text{-}1)$$

where W represents the total core flow rate (fuel channel and bypass flow). Note that χ_B=1 for $W>W_2$ and χ_B=0 for $W<W_1$. When b=1 in Eq. (2.4.6-1), the fraction of the injected boron which is entrained upward into the core decreases linearly from 1.0 to 0.0 as the total core flow decreases from W_2 (6 MLb/hr) to W_1 (4 MLb/hr). Since the boron mixing experiments of Dias et al. suggest that 100% of the injected boron may be entrained at core flows as low as 4 MLb/hr, it is conservative to use the linear entrainment model represented by Eq. (2.4.6-1) with b=1. Unless otherwise stated, all ATWS simulations in this calculation package are performed with b=1. A sensitivity study with respect to the exponent b is performed for an MSIV closure ATWS in §5.8. Figure 2.4.6-1 shows the boron entrainment fraction χ_B for b=1/2, b=1, and b=2.

Remixing of stagnated boron is also an important phenomenon considered in the SABRE model. If the total core flow is less than the remixing threshold W_0 (a value of 15 Mlbm/hr[19] is used, but as with W_1 and W_2, any value can be specified as part of the code input data), the flow exiting the jet pumps is assumed to pass directly into the upper node of the lower plenum so that the bottom node of the lower plenum is completely bypassed. Thus, there is no remixing of stagnated boron if the total core flow is less than W_0.

The experimental studies on boron mixing indicate that little flow reaches the bottom of the lower head if the total core flow is less than the threshold value W_0 (15 Mlbm/hr). For flow rates greater than W_0 it is not clear what fraction of flow extends into the region near the bottom of the lower head. Therefore, in the SABRE boron mixing model, the following assumptions are made with regard to the flow distribution in the lower plenum:

- No recirculation flow passes through the bottom node of the lower plenum if the total core flow W is less than W_0.
- The flow through the bottom node of the lower plenum is W- W_0 if the total core flow is greater than W_0.

[19] See Section F.29.8.

Table 2.4.6-1

Description of Control Volumes Used in Calculating Local Boron Concentration in Reactor Coolant

Reactor Flow Region	Number of Node Used in Boron Mixing Model
Jet Pumps	1
Lower Plenum	2
Lower Reflector	1
Active Core[20]	1 to 10
Upper Reflector	1
Bypass	1
Upper Plenum, Riser, & Separator	1
Downcomer	1

[20] Number of nodes is specified as part of the input data.

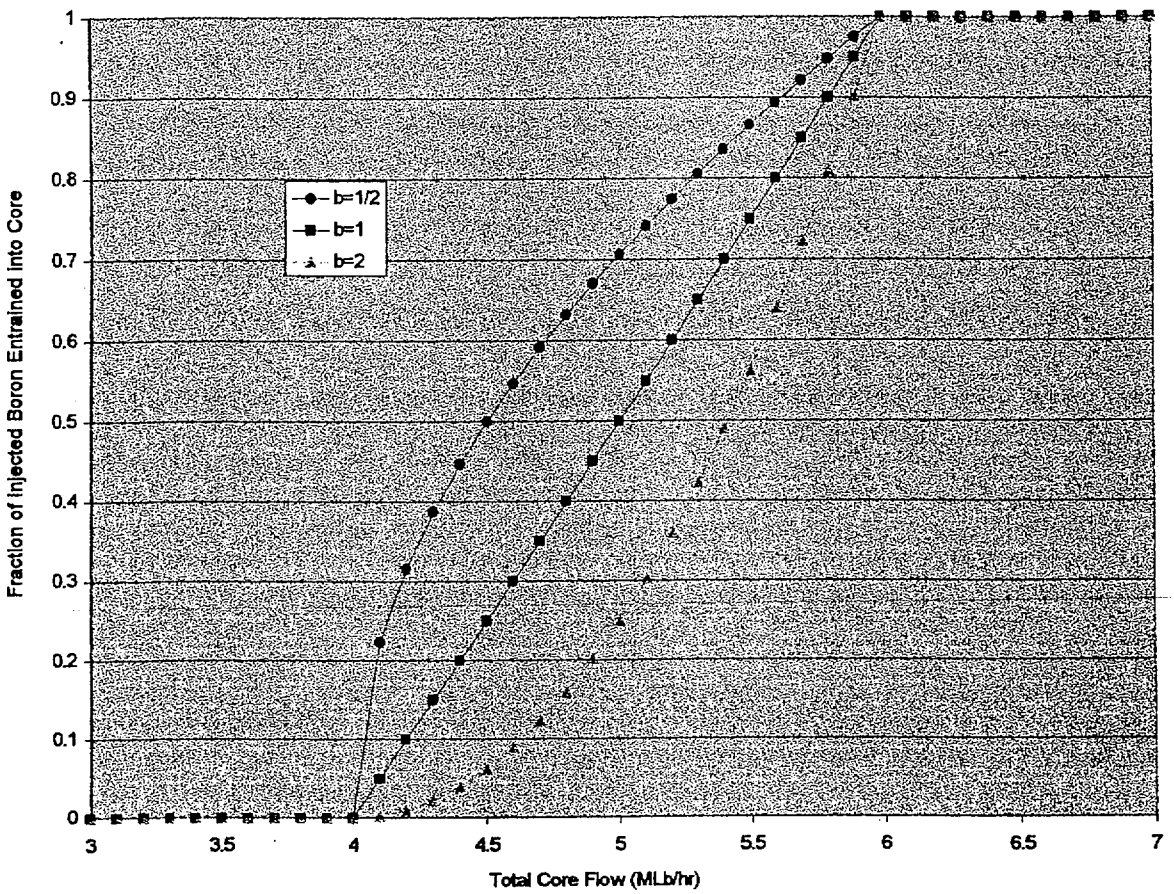

Figure 2.4.6-1 Boron entrainment factor χ_B as a function of the exponent b in Eq. 2.4.6-1.

2.4.7 Decay Heat Fraction

In addition to the fission power, heat is generated within the fuel as a result of fission product decay. In SABRE, decay power is computed from the eleven-equation decay model used in the RETRAN code:[21]

$$Q_{decay}(t) = Q_{fiss}(0) \sum_{i=1}^{11} \gamma_i(t)\, \bar{\lambda}_i \qquad \textbf{(2.4.7-1)}$$

where the decay heat group "concentrations" $\gamma_i(t)$ are obtained from the solution of

$$\frac{d\gamma_i(t)}{dt} + \bar{\lambda}_i \gamma_i(t) = Y_i \frac{Q_{fiss}(t)}{Q_{fiss}(0)} \qquad \textbf{(2.4.7-2)}$$

with

$$\gamma_i(0) = Y_i / \bar{\lambda}_i \quad i \in \{1, 2, \ldots, 11\} \,. \qquad \textbf{(2.4.7-3)}$$

In the above decay heat equations,

$Q_{decay}(t)$	=	decay power (Btu/sec),
$Q_{fiss}(t)$	=	total fission power = $q'''_{fiss}(t)\, V_f$ (Btu/sec),
V_f	=	volume of fuel (ft^3),
$\gamma_i(t)$	=	"concentration" of i-th decay heat group (sec),
$\bar{\lambda}_i$	=	decay constant for the i-th group (sec^{-1}), and
Y_i	=	yield fraction for the i-th group (dimensionless).

Values for the $\bar{\lambda}_i$ and Y_i are given in the RETRAN code description manual. Summation of the fission power, decay power, and heat dissipation from the reactor vessel Q_{Rx} and vessel internals Q_{VI} (see Section 2.11), gives the total heat generation rate $Q(t)$ within the reactor,

$$Q(t) = Q_{fiss}(t) + Q_{decay}(t) + Q_{Rx}(t) + Q_{VI}(t) \,. \qquad \textbf{(2.4.7-4)}$$

---

[21] McFadden, J.H., "RETRAN-02 - A Program for Transient Thermal-Hydraulic Analysis of Complex Fluid Flow Systems," Volume 1, NP-1850-CCMA, Electric Power Research Institute, Palo Alto, California, November 1984.

2.4.8 Control Rod Model

The kinetics file for SABRE consists of a SIMTRAN output file containing seven 1-D cross-section sets with each set corresponding to a different control rod pattern. The differences among the seven cross-section sets are solely due to the presence of control rods. Void and fuel temperature feedback effects are maintained constant across the seven cross-section sets. That is, control rod position is assumed to change instantaneously relative to the initial or base rod configuration which typically corresponds to an all-rods-out configuration. In each cross-section set, dependency on moderator density and fuel temperature is explicitly included through polynomial expressions of the form shown in Eq. (2.4.1-1). The effect of control rod movement is incorporated into the SABRE 1-D diffusion theory model by interpolating between appropriate cross-section sets within the SIMTRAN output.

The seven cross-section sets in the SIMTRAN output consist of the following:

1. Initial control rod configuration (typically all rods out or a small number of fully or partially inserted rods)

2. Set 1 with four additional rods completely inserted (The four additional rods are quarter-core symmetric)

3. Set 1 with eight additional quarter-core-symmetric rods completely inserted

4. Set 1 with sixteen additional quarter-core-symmetric rods completely inserted

5. Set 1 with thirty-two additional quarter-core-symmetric rods completely inserted

6. Set 1 with sixty-four additional quarter-core-symmetric rods completely inserted

7. All rods in

Generation of the SIMTRAN output with these seven cross-section sets is a two-step process. First, a SIMULATE restart file is obtained from the PP&L Nuclear Fuels' Group for the desired cycle, initial rod pattern, and cycle exposure. A SIMULATE run specifying the six additional rod patterns is then made using this restart file. The SIMULATE calculation generates a second restart file which is then used by SIMTRAN, along with a SIMTRAN input file, to generate the 1-D cross-section file used by SABRE. As part of the present calculation, four 1-D cross-section sets are generated. These sets are described in Table 2.4.8-1.

SABRE includes two different control rod models. The first is a scram model in which all control rods move simultaneously into the reactor core over a specified time period. The scram time is specified as part of the SABRE input data. In the case of a reactor scram, only Sets 1 and 7 out of the seven cross-section sets contained within the SIMTRAN output file are used. As the bank of rods moves into the core, interpolation

between cross-section sets 1 and 7 is carried out on a nodal basis. That is, a control rod fraction is computed for each axial node (material region) of the core. If the control rod bank has not reached a particular axial node, then the control rod fraction for that node is 0, and cross-section Set 1 is used for that material region. If, on the other hand, the rods have passed through a particular material region, then the control rod fraction for that region is 1 and cross-section Set 7 is used. Note that the 1-D cross-section sets generated by SIMTRAN are defined on a nodal basis. If the control rod bank is passing through an axial node of the core, then the control rod fraction for that material region is between 0 and 1 depending on how far the rods have moved through the node. In this case, the cross-section set for that material region is computed by interpolating between cross-section Sets 1 and 7 using the control rod fraction as the interpolation parameter.

The second control rod model contained in SABRE is used to describe reactor shutdown by manual control rod insertion (MRI) using the Control Rod Drive (CRD) system. In an ATWS event in which the SLCS fails to initiate and the CRD pumps are available, the control room operator can individually select and insert control rods from the Control Room bench board using the Reactor Manual Control System. The acceptance criteria for CRD Stroke Time Test (TP-055-001, Rev. 7) indicates that the insertion time for a single control rod is ≤ 60 seconds. In the SABRE code, the rate of control rod insertion for MRI is specified as part of the input data.

It is assumed that the operator will drive rods so that they are distributed fairly uniformly about the core. Since MRI is a relatively slow process, the important changes in core flux occur on a global basis. That is, it is not necessary to describe detailed changes in neutron flux as individual rods move through the core. The only relevant effect which needs to be described is the gradual decrease in core average power as rods are individually inserted as this is the only factor which influences suppression pool heat up during an ATWS with SLCS failure. During MRI, the effect of gradually increasing control rod density within the core is captured by interpolating, on a core wide basis, between the appropriate SIMTRAN cross-section sets. Seven different cross-section sets with increasing control rod fraction are generated in order to obtain a fairly detailed description of overall core response during MRI.

Table 2.4.8-1
Description of 1-D Cross Section Sets for SABRE

Unit/Cycle	Nuclear Fuels' SIMULATE Restart File Used in Generating Cross-Section Set	SIMULATE Input File	SIMTRAN Input File
U2C7 End of Cycle	r9507299.0012	u2c7.simulate.in (Listed in Table 2.4.8-2)	u2c7.simtran.in (Listed in Table 2.4.8-6)
U2C9 End of Cycle	r9602506.0002	u2c9.simulate.in (Listed in Table 2.4.8-3)	u2c9.simtran.in (Listed in Table 2.4.8-7)
U2C10 End of Cycle	r9808566.0001	u2c10.simulate.in (Listed in Table 2.4.8-4)	u2c10.simtran.in (Listed in Table 2.4.8-8)
U1C12 End of Cycle	r9903464.0001	u1c12.simulate.in (Listed in Table 2.4.8-5)	u1c12.simtran.in (Listed in Table 2.4.8-9)

Table 2.4.8-2

SIMULATE Input File (u2c7.simulate.in)Used in Generating U2C7 Cross-Section File

```
 15 15 25  5  0  0  0  0  0 15 16216 43172 24 72100 10 80 13  0  0  0  0mcas2920
  2  0  2  0  0  2  2  2  2  2  2  2  2  2  2
ddisk U2C7 ATWS (01  BOC)
                BEGEXP ENDEXP DELEXP POWER   WT    SUB   PRES
          1     11.562 11.562 00.000

                   (1)  Execute INPUT & NUCLER
          2          0

                   (2)  1=Initialize Hailing to present distrib & reset to 2
                   (7)  0=input value of subcool used to calc density
         20     S1   1
         20     S4   0

                   (3)  0=Use restart Xe  2=Use equil Xe
         21     S2   0

                   (5)  Search Option  0=No Search  2=Pwr Search  7=use file power distr
          21     S1   0

                   (9)  0=No DP Calc   3=Detl FIBWR   4=Apprx FIBWR
         21     S3   3

                   (27) 0=Control blade depletion has no effect
          21     S17  0

         99
ddisk U2C7 ATWS (02  4 rods in)
                   (25) Limit on nodal power distribution peak
          2      S24   100.

                   (2)  2=Carry existing Hailing files from prev case w/o change
                   (2)  1=Initialize Hailing to present distrib & reset to 2
         20      S1   1

                   (3)  0=Use restart Xe  2=Use equil Xe
         21      S2   0

                   (5)  Search Option  0=No Search  2=Pwr Search  7=use file power distr
          21     S1   7

         30   8  S7  -- -- -- -- -- -- -- --
         30   9  S7  -- 00 -- -- -- -- -- --
         30  10  S7  -- -- -- -- -- -- -- --
         30  11  S7  -- -- 10 -- -- -- -- --
         30  12  S7  -- -- -- -- -- -- --
         30  13  S7  -- -- -- -- -- --
         30  14  S7  -- -- -- -- --
         30  15  S7  -- -- -- --
         99
ddisk U2C7 ATWS (03  8 rods in)
                   (25) Limit on nodal power distribution peak
          2      S24   100.

                   (2)  2=Carry existing Hailing files from prev case w/o change
         20      S1   2

                   (3)  0=Use restart Xe  2=Use equil Xe
         21      S2   0

                   (5)  Search Option  0=No Search  2=Pwr Search  7=use file power distr
          21     S1   7

         30   8  S7  -- -- -- -- -- -- -- --
         30   9  S7  -- 00 -- -- -- -- -- --
         30  10  S7  -- -- -- -- -- -- -- --
         30  11  S7  -- 00 10 -- -- -- -- --
         30  12  S7  -- -- -- -- -- -- --
         30  13  S7  -- -- -- -- -- --
         30  14  S7  -- -- -- -- --
         30  15  S7  -- -- -- --
         99
ddisk U2C7 ATWS (04  16 rods in)
                   (25) Limit on nodal power distribution peak
          2      S24   100.

                   (2)  2=Carry existing Hailing files from prev case w/o change
         20      S1   2

                   (3)  0=Use restart Xe  2=Use equil Xe
         21      S2   0

                   (5)  Search Option  0=No Search  2=Pwr Search  7=use file power distr
          21     S1   7
```

```
          30   8  S7  -- -- -- -- -- -- -- --
          30   9  S7  -- 00 -- 00 -- -- -- --
          30  10  S7  -- -- -- -- -- -- -- --
          30  11  S7  -- 00 10 00 -- -- -- --
          30  12  S7  -- -- -- -- -- -- --
          30  13  S7  -- -- -- -- -- --
          30  14  S7  -- -- -- -- --
          30  15  S7  -- -- -- --
          99
ddisk U2C7 ATWS (05  32 rods in)
                (25) Limit on nodal power distribution peak
           2      S24   100.

                (2)  2=Carry existing Hailing files from prev case w/o change
          20      S1    2

                (3)  0=Use restart Xe  2=Use equil Xe
          21      S2    0

                (5)  Search Option  0=No Search  2=Pwr Search  7=use file power distr
            21      S1    7

          30   8  S7  -- -- -- -- -- -- -- --
          30   9  S7  -- 00 -- 00 -- 00 -- --
          30  10  S7  -- -- -- -- -- -- -- --
          30  11  S7  -- 00 10 00 -- 00 -- --
          30  12  S7  -- -- -- -- -- -- --
          30  13  S7  -- 00 -- 00 -- --
          30  14  S7  -- -- -- -- --
          30  15  S7  -- -- -- --
          99
ddisk U2C7 ATWS (06  64 rods in)
                (25) Limit on nodal power distribution peak
           2      S24   100.

                (2)  2=Carry existing Hailing files from prev case w/o change
          20      S1    2

                (3)  0=Use restart Xe  2=Use equil Xe
          21      S2    0

                (5)  Search Option  0=No Search  2=Pwr Search  7=use file power distr
            21      S1    7

          30   8  S7  -- -- 00 -- -- -- 00 --
          30   9  S7  -- 00 -- 00 -- 00 -- --
          30  10  S7  00 -- 00 -- 00 -- 00 --
          30  11  S7  -- 00 10 00 -- 00 -- --
          30  12  S7  -- -- 00 -- 00 -- --
          30  13  S7  -- 00 -- 00 -- --
          30  14  S7  00 -- 00 -- --
          30  15  S7  -- -- -- --
          99
ddisk U2C7 ATWS (07  All Rods in)
                (25) Limit on nodal power distribution peak
           2      S24   100.

                (2)  2=Carry existing Hailing files from prev case w/o change
          20      S1    2

                (3)  0=Use restart Xe  2=Use equil Xe
          21      S2    0

                (5)  Search Option  0=No Search  2=Pwr Search  7=use file power distr
            21      S1    7

          30   8  S7  00 00 00 00 00 00 00 00
          30   9  S7  00 00 00 00 00 00 00 00
          30  10  S7  00 00 00 00 00 00 00 00
          30  11  S7  00 00 00 00 00 00 00 00
          30  12  S7  00 00 00 00 00 00 00
          30  13  S7  00 00 00 00 00 00
          30  14  S7  00 00 00 00 00
          30  15  S7  00 00 00 00
          99
ILAST
```

Table 2.4.8-3
SIMULATE Input File (u2c9.simulate.in) Used in Generating U2C9 Cross-Section File

```
 15 15 25  5  0  0  0  0  0 15 16216 43172 24200100 10 80  0  0  0  0  0mcas2920
  2  0  2  0  0  2  2  2  2  2  2  2  2  2  2
ddisk U2C9 ATWS (01  All Rods Out)
                BEGEXP ENDEXP DELEXP POWER   WT    SUB   PRES
          1     15.700 15.700 00.000

                  (1)  Execute INPUT & NUCLER
          2         0

                  (2)  1=Initialize Hailing to present distrib & reset to 2
                  (7)  0=input value of subcool used to calc density
         20    S1   1
         20    S4   0

                  (3)  0=Use restart Xe  2=Use equil Xe
         21    S2   0

                  (5)  Search Option  0=No Search  2=Pwr Search  7=use file power distr
         21    S1   0

                  (9)  0=No DP Calc   3=Detl FIBWR   4=Apprx FIBWR
         21    S3   3

                 (27) 0=Control blade depletion has no effect
         21    S17  0

         30   8  S7  -- -- -- -- -- -- -- --
         30   9  S7  -- -- -- -- -- -- -- --
         30  10  S7  -- -- -- -- -- -- -- --
         30  11  S7  -- -- -- -- -- -- -- --
         30  12  S7  -- -- -- -- -- -- --
         30  13  S7  -- -- -- -- -- -- --
         30  14  S7  -- -- -- -- --
         30  15  S7  -- -- -- --
         99
ddisk U2C9 ATWS (02  4 rods in)
                 (25) Limit on nodal power distribution peak
          2    S24   100.

                  (2)  2=Carry existing Hailing files from prev case w/o change
                  (2)  1=Initialize Hailing to present distrib & reset to 2
         20    S1   1

                  (3)  0=Use restart Xe  2=Use equil Xe
         21    S2   0

                  (5)  Search Option  0=No Search  2=Pwr Search  7=use file power distr
         21    S1   7

         30   8  S7  -- -- -- -- -- -- -- --
         30   9  S7  -- 00 -- -- -- -- -- --
         30  10  S7  -- -- -- -- -- -- -- --
         30  11  S7  -- -- -- -- -- -- -- --
         30  12  S7  -- -- -- -- -- -- --
         30  13  S7  -- -- -- -- -- -- --
         30  14  S7  -- -- -- -- --
         30  15  S7  -- -- -- --
         99
ddisk U2C9 ATWS (03  8 rods in)
                 (25) Limit on nodal power distribution peak
          2    S24   100.

                  (2)  2=Carry existing Hailing files from prev case w/o change
         20    S1   2

                  (3)  0=Use restart Xe  2=Use equil Xe
         21    S2   0

                  (5)  Search Option  0=No Search  2=Pwr Search  7=use file power distr
         21    S1   7

         30   8  S7  -- -- -- -- -- -- -- --
         30   9  S7  -- 00 -- -- -- -- -- --
         30  10  S7  -- -- -- -- -- -- -- --
         30  11  S7  -- 00 -- -- -- -- -- --
         30  12  S7  -- -- -- -- -- -- --
         30  13  S7  -- -- -- -- -- --
         30  14  S7  -- -- -- -- --
         30  15  S7  -- -- -- --
         99
ddisk U2C9 ATWS (04  16 rods in)
                 (25) Limit on nodal power distribution peak
          2    S24   100.
```

```
                (2)  2=Carry existing Hailing files from prev case w/o change
          20      S1    2

                (3)  0=Use restart Xe  2=Use equil Xe
          21      S2    0

                (5)  Search Option  0=No Search  2=Pwr Search  7=use file power distr
           21      S1    7

          30   8  S7  -- -- -- -- -- -- -- --
          30   9  S7  -- 00 -- 00 -- -- -- --
          30  10  S7  -- -- -- -- -- -- -- --
          30  11  S7  -- 00 -- 00 -- -- -- --
          30  12  S7  -- -- -- -- -- -- --
          30  13  S7  -- -- -- -- -- --
          30  14  S7  -- -- -- -- --
          30  15  S7  -- -- -- --
          99
ddisk U2C9 ATWS (05  32 rods in)
                (25) Limit on nodal power distribution peak
           2      S24   100.

                (2)  2=Carry existing Hailing files from prev case w/o change
          20      S1    2

                (3)  0=Use restart Xe  2=Use equil Xe
          21      S2    0

                (5)  Search Option  0=No Search  2=Pwr Search  7=use file power distr
           21      S1    7

          30   8  S7  -- -- -- -- -- -- -- --
          30   9  S7  -- 00 -- 00 -- 00 -- --
          30  10  S7  -- -- -- -- -- -- -- --
          30  11  S7  -- 00 -- 00 -- 00 -- --
          30  12  S7  -- -- -- -- -- -- --
          30  13  S7  -- 00 -- 00 -- --
          30  14  S7  -- -- -- -- --
          30  15  S7  -- -- -- --
          99
ddisk U2C9 ATWS (06  64 rods in)
                (25) Limit on nodal power distribution peak
           2      S24   100.

                (2)  2=Carry existing Hailing files from prev case w/o change
          20      S1    2

                (3)  0=Use restart Xe  2=Use equil Xe
          21      S2    0

                (5)  Search Option  0=No Search  2=Pwr Search  7=use file power distr
           21      S1    7

          30   8  S7  -- -- 00 -- -- -- 00 --
          30   9  S7  -- 00 -- 00 -- 00 -- --
          30  10  S7  00 -- 00 -- 00 -- 00 --
          30  11  S7  -- 00 -- 00 -- 00 -- --
          30  12  S7  -- -- 00 -- 00 -- --
          30  13  S7  -- 00 -- 00 -- --
          30  14  S7  00 -- 00 -- --
          30  15  S7  -- -- -- --
          99
ddisk U2C9 ATWS (07  All Rods in)
                (25) Limit on nodal power distribution peak
           2      S24   100.

                (2)  2=Carry existing Hailing files from prev case w/o change
          20      S1    2

                (3)  0=Use restart Xe  2=Use equil Xe
          21      S2    0

                (5)  Search Option  0=No Search  2=Pwr Search  7=use file power distr
           21      S1    7

          30   8  S7  00 00 00 00 00 00 00 00
          30   9  S7  00 00 00 00 00 00 00 00
          30  10  S7  00 00 00 00 00 00 00 00
          30  11  S7  00 00 00 00 00 00 00 00
          30  12  S7  00 00 00 00 00 00 00
          30  13  S7  00 00 00 00 00 00
          30  14  S7  00 00 00 00 00
          30  15  S7  00 00 00 00
          99
```

Table 2.4.8-4

SIMULATE Input File (u2c10.simulate.in) Used in Generating U2C10 Cross-Section File

```
 15 15 25  5  0  0  0  0  0 15 16216 43172 24200100 10 80  0  0  0  0 0mcas2920
  2  0  2  0  0  2  2  2  2  2  2  2  2  2  2
ddisk U2C10 ATWS (01  All Rods Out)
                BEGEXP ENDEXP DELEXP POWER   WT    SUB   PRES
          1     15.200 15.200 00.000

                  (1)  Execute INPUT & NUCLER
          2         0

                  (2)  1=Initialize Hailing to present distrib & reset to 2
                  (7)  0=input value of subcool used to calc density
         20    S1   1
         20    S4   0

                  (3)  0=Use restart Xe  2=Use equil Xe
         21    S2   0

                  (5)  Search Option  0=No Search  2=Pwr Search  7=use file power distr
         21    S1   0

                  (9)  0=No DP Calc   3=Detl FIBWR   4=Approx FIBWR
         21    S3   3

                 (27) 0=Control blade depletion has no effect
         21    S17  0

        30   8  S7  -- -- -- -- -- -- -- --
        30   9  S7  -- -- -- -- -- -- -- --
        30  10  S7  -- -- -- -- -- -- -- --
        30  11  S7  -- -- -- -- -- -- -- --
        30  12  S7  -- -- -- -- -- -- --
        30  13  S7  -- -- -- -- -- --
        30  14  S7  -- -- -- -- --
        30  15  S7  -- -- -- --
        99
ddisk U2C10 ATWS (02  4 rods in)
                 (25) Limit on nodal power distribution peak
         2     S24   100.

                  (2)  2=Carry existing Hailing files from prev case w/o change
                  (2)  1=Initialize Hailing to present distrib & reset to 2
        20    S1   1

                  (3)  0=Use restart Xe  2=Use equil Xe
        21    S2   0

                  (5)  Search Option  0=No Search  2=Pwr Search  7=use file power distr
         21    S1   7

        30   8  S7  -- -- -- -- -- -- -- --
        30   9  S7  -- 00 -- -- -- -- -- --
        30  10  S7  -- -- -- -- -- -- -- --
        30  11  S7  -- -- -- -- -- -- -- --
        30  12  S7  -- -- -- -- -- -- --
        30  13  S7  -- -- -- -- -- --
        30  14  S7  -- -- -- -- --
        30  15  S7  -- -- -- --
        99
ddisk U2C10 ATWS (03  8 rods in)
                 (25) Limit on nodal power distribution peak
         2     S24   100.

                  (2)  2=Carry existing Hailing files from prev case w/o change
        20    S1   2

                  (3)  0=Use restart Xe  2=Use equil Xe
        21    S2   0

                  (5)  Search Option  0=No Search  2=Pwr Search  7=use file power distr
         21    S1   7

        30   8  S7  -- -- -- -- -- -- -- --
        30   9  S7  -- 00 -- -- -- -- -- --
        30  10  S7  -- -- -- -- -- -- -- --
        30  11  S7  -- 00 -- -- -- -- -- --
        30  12  S7  -- -- -- -- -- -- --
        30  13  S7  -- -- -- -- -- --
        30  14  S7  -- -- -- -- --
        30  15  S7  -- -- -- --
        99
ddisk U2C10 ATWS (04  16 rods in)
                 (25) Limit on nodal power distribution peak
         2     S24   100.

                  (2)  2=Carry existing Hailing files from prev case w/o change
```

```
          20      S1    2

                        (3)  0=Use restart Xe  2=Use equil Xe
          21      S2     0

                        (5)  Search Option  0=No Search  2=Pwr Search  7=use file power distr
           21      S1     7

          30   8  S7  -- -- -- -- -- -- -- --
          30   9  S7  -- 00 -- 00 -- -- -- --
          30  10  S7  -- -- -- -- -- -- -- --
          30  11  S7  -- 00 -- 00 -- -- -- --
          30  12  S7  -- -- -- -- -- -- --
          30  13  S7  -- -- -- -- -- --
          30  14  S7  -- -- -- -- --
          30  15  S7  -- -- -- --
          99
ddisk U2C10 ATWS (05  32 rods in)
                        (25) Limit on nodal power distribution peak
           2      S24   100.

                        (2)  2=Carry existing Hailing files from prev case w/o change
          20      S1     2

                        (3)  0=Use restart Xe  2=Use equil Xe
          21      S2     0

                        (5)  Search Option  0=No Search  2=Pwr Search  7=use file power distr
           21      S1     7

          30   8  S7  -- -- -- -- -- -- -- --
          30   9  S7  -- 00 -- 00 -- 00 -- --
          30  10  S7  -- -- -- -- -- -- -- --
          30  11  S7  -- 00 -- 00 -- 00 -- --
          30  12  S7  -- -- -- -- -- -- --
          30  13  S7  -- 00 -- 00 -- --
          30  14  S7  -- -- -- -- --
          30  15  S7  -- -- -- --
          99
ddisk U2C10 ATWS (06  64 rods in)
                        (25) Limit on nodal power distribution peak
           2      S24    100.

                        (2)  2=Carry existing Hailing files from prev case w/o change
          20      S1     2

                        (3)  0=Use restart Xe  2=Use equil Xe
          21      S2     0

                        (5)  Search Option  0=No Search  2=Pwr Search  7=use file power distr
           21      S1     7

          30   8  S7  -- -- 00 -- -- -- 00 --
          30   9  S7  -- 00 -- 00 -- 00 -- --
          30  10  S7  00 -- 00 -- 00 -- 00 --
          30  11  S7  -- 00 -- 00 -- 00 -- --
          30  12  S7  -- -- 00 -- 00 -- --
          30  13  S7  -- 00 -- 00 -- --
          30  14  S7  00 -- 00 -- --
          30  15  S7  -- -- -- --
          99
ddisk U2C10 ATWS (07  All Rods in)
                        (25) Limit on nodal power distribution peak
           2      S24    100.

                        (2)  2=Carry existing Hailing files from prev case w/o change
          20      S1     2

                        (3)  0=Use restart Xe  2=Use equil Xe
          21      S2     0

                        (5)  Search Option  0=No Search  2=Pwr Search  7=use file power distr
           21      S1     7

          30   8  S7  00 00 00 00 00 00 00 00
          30   9  S7  00 00 00 00 00 00 00 00
          30  10  S7  00 00 00 00 00 00 00 00
          30  11  S7  00 00 00 00 00 00 00 00
          30  12  S7  00 00 00 00 00 00 00
          30  13  S7  00 00 00 00 00 00
          30  14  S7  00 00 00 00 00
          30  15  S7  00 00 00 00
          99
ILAST
```

Table 2.4.8-5
SIMULATE Input File (u1c12.simulate.in) Used in Generating U1C12 Cross-Section File

```
 15 15 25  5  0  0  0  0  0 15 16216 43172 24200100 10 80  0  0  0  0  0mcas2920
  2  0  2  0  0  2  2  2  2  2  2  2  2  2  2
ddisk U1C12 ATWS (01  All Rods Out)
                BEGEXP ENDEXP DELEXP POWER   WT    SUB   PRES
          1     14.800 14.800 00.000

                   (1)  Execute INPUT & NUCLER
          2          0

                   (2)  1=Initialize Hailing to present distrib & reset to 2
                   (7)  0=input value of subcool used to calc density
         20     S1   1
         20     S4   0

                   (3)  0=Use restart Xe  2=Use equil Xe
         21     S2   0

                   (5)  Search Option  0=No Search  2=Pwr Search  7=use file power distr
         21     S1   0

                   (9)  0=No DP Calc   3=Detl FIBWR   4=Apprx FIBWR
         21     S3   3

                  (27)  0=Control blade depletion has no effect
         21     S17  0

         30   8 S7  -- -- -- -- -- -- -- --
         30   9 S7  -- -- -- -- -- -- -- --
         30  10 S7  -- -- -- -- -- -- -- --
         30  11 S7  -- -- -- -- -- -- -- --
         30  12 S7  -- -- -- -- -- -- --
         30  13 S7  -- -- -- -- -- --
         30  14 S7  -- -- -- -- --
         30  15 S7  -- -- -- --
         99
ddisk U1C12 ATWS (02  4 rods in)
                  (25)  Limit on nodal power distribution peak
          2      S24   100.

                   (2)  2=Carry existing Hailing files from prev case w/o change
                   (2)  1=Initialize Hailing to present distrib & reset to 2
         20     S1   1

                   (3)  0=Use restart Xe  2=Use equil Xe
         21     S2   0

                   (5)  Search Option  0=No Search  2=Pwr Search  7=use file power distr
         21     S1   7

         30   8 S7  -- -- -- -- -- -- -- --
         30   9 S7  -- 00 -- -- -- -- -- --
         30  10 S7  -- -- -- -- -- -- -- --
         30  11 S7  -- -- -- -- -- -- -- --
         30  12 S7  -- -- -- -- -- -- --
         30  13 S7  -- -- -- -- -- --
         30  14 S7  -- -- -- -- --
         30  15 S7  -- -- -- --
         99
ddisk U1C12 ATWS (03  8 rods in)
                  (25)  Limit on nodal power distribution peak
          2      S24   100.

                   (2)  2=Carry existing Hailing files from prev case w/o change
         20     S1   2

                   (3)  0=Use restart Xe  2=Use equil Xe
         21     S2   0

                   (5)  Search Option  0=No Search  2=Pwr Search  7=use file power distr
         21     S1   7

         30   8 S7  -- -- -- -- -- -- -- --
         30   9 S7  -- 00 -- -- -- -- -- --
         30  10 S7  -- -- -- -- -- -- -- --
         30  11 S7  -- 00 -- -- -- -- -- --
         30  12 S7  -- -- -- -- -- -- --
         30  13 S7  -- -- -- -- -- --
         30  14 S7  -- -- -- -- --
         30  15 S7  -- -- -- --
         99
ddisk U1C12 ATWS (04  16 rods in)
                  (25)  Limit on nodal power distribution peak
          2      S24   100.
```

```
                    (2)  2=Carry existing Hailing files from prev case w/o change
          20      S1    2

                    (3)  0=Use restart Xe  2=Use equil Xe
          21      S2    0

                    (5)  Search Option  0=No Search  2=Pwr Search  7=use file power distr
            21      S1    7

          30   8  S7  -- -- -- -- -- -- -- --
          30   9  S7  -- 00 -- 00 -- -- -- --
          30  10  S7  -- -- -- -- -- -- -- --
          30  11  S7  -- 00 -- 00 -- -- -- --
          30  12  S7  -- -- -- -- -- -- --
          30  13  S7  -- -- -- -- -- --
          30  14  S7  -- -- -- -- --
          30  15  S7  -- -- -- --
          99
ddisk U1C12 ATWS (05  32 rods in)
                    (25) Limit on nodal power distribution peak
          2       S24   100.

                    (2)  2=Carry existing Hailing files from prev case w/o change
          20      S1    2

                    (3)  0=Use restart Xe  2=Use equil Xe
          21      S2    0

                    (5)  Search Option  0=No Search  2=Pwr Search  7=use file power distr
            21      S1    7

          30   8  S7  -- -- -- -- -- -- -- --
          30   9  S7  -- 00 -- 00 -- 00 -- --
          30  10  S7  -- -- -- -- -- -- -- --
          30  11  S7  -- 00 -- 00 -- 00 -- --
          30  12  S7  -- -- -- -- -- -- --
          30  13  S7  -- 00 -- 00 -- --
          30  14  S7  -- -- -- -- --
          30  15  S7  -- -- -- --
          99
ddisk U1C12 ATWS (06  64 rods in)
                    (25) Limit on nodal power distribution peak
          2       S24   100.

                    (2)  2=Carry existing Hailing files from prev case w/o change
          20      S1    2

                    (3)  0=Use restart Xe  2=Use equil Xe
          21      S2    0

                    (5)  Search Option  0=No Search  2=Pwr Search  7=use file power distr
            21      S1    7

          30   8  S7  -- -- 00 -- -- -- 00 --
          30   9  S7  -- 00 -- 00 -- 00 -- --
          30  10  S7  00 -- 00 -- 00 -- 00 --
          30  11  S7  -- 00 -- 00 -- 00 -- --
          30  12  S7  -- -- 00 -- 00 -- --
          30  13  S7  -- 00 -- 00 -- --
          30  14  S7  00 -- 00 -- --
          30  15  S7  -- -- -- --
          99
ddisk U1C12 ATWS (07  All Rods in)
                    (25) Limit on nodal power distribution peak
          2       S24   100.

                    (2)  2=Carry existing Hailing files from prev case w/o change
          20      S1    2

                    (3)  0=Use restart Xe  2=Use equil Xe
          21      S2    0

                    (5)  Search Option  0=No Search  2=Pwr Search  7=use file power distr
            21      S1    7

          30   8  S7  00 00 00 00 00 00 00 00
          30   9  S7  00 00 00 00 00 00 00 00
          30  10  S7  00 00 00 00 00 00 00 00
          30  11  S7  00 00 00 00 00 00 00 00
          30  12  S7  00 00 00 00 00 00 00
          30  13  S7  00 00 00 00 00 00 00
          30  14  S7  00 00 00 00 00
          30  15  S7  00 00 00 00
          99
ILAST
```

Table 2.4.8-6

SIMTRAN Input File (u2c7.simtran.in) Used in Generating U2C7 Cross-Section File

```
/users/chaiko/SIMULATE/u2c7.simulate.restart 1 2 3 4 5 6 7
9999
U2C7 ATWS SIMTRAN EC-ATWS-0505 Rev 7
 1  1  1  0  6                jdisk,ibwr,krs,krout,krin
 2  3  4  5  6  7
10 80  0  0 14100             dimensions
 0  0  0  0  0  0  0  0       edit flags
24  0  1  1  2  2  0          iter,kdflag,kpflag,ksolv,krwtf,ktwtf,kphiwt
 6  4                         ndu,ndtf
   45.8244                   rhoref
 1 11                        lstscm / nscmm
 0.60        1.20        2.40        3.60        4.80        6.00
 7.20        8.40        9.60       10.80       12.00
33 12 12 12 12 12 12 12 12 12 12 12 12 12 12 12 12 12 12 12 12 12 12 12
33
     1.057       1.131
 1 25
  0.00  -0.10   .100   .200   .300   .400
 1 25
   0.0  -100.    60.   225.
SIGTR1   312001 5 1 0
         312001 .2 .4 .6 .8 1.0 0. .17030   .21132   .25230   .29339
         312001 .33458
SIGA1    312002 5 1 0
         312002 .2 .4 .6 .8 1.0 0. .0043117 .0043622 .0044160 .0044720
         312002 .0045297
SIGR1    312003 5 1 0
         312003 .2 .4 .6 .8 1.0 0. .0049850 .010767  .016879  .023234
         312003 .029769
SIGTR2   312004 5 1 0
         312004 .2 .4 .6 .8 1.0 0. .46027   .68728   .91722  1.14790
         312004 1.3788
SIGA2    312005 5 1 0
         312005 .2 .4 .6 .8 1.0 0. .067142  .068668  .070216  .071771
         312005 .073326
VEL2     312006 3 1 0
         312006 .33478 .61987 1.0 0.  3.7710E+05 3.6944E+05 3.6396E+05
VEL1     312007 3 1 0
         312007 .33478 .61987 1.0 0.  1.5278E+07 1.4839E+07 1.4492E+07
SIGTR1   312008 5 1 0
         312008 .2 .4 .6 .8 1.0 0. .085254  .11156   .13784   .16418
         312008 .19060
SIGA1    312009 5 1 0
         312009 .2 .4 .6 .8 1.0 0. .00048065 .00051302 .00054752
         312009 .00058343 .00062040
SIGR1    312010 5 1 0
         312010 .2 .4 .6 .8 1.0 0. .0030222 .0067297 .010649  .014724
         312010 .018915
SIGTR2   312011 5 1 0
         312011 .2 .4 .6 .8 1.0 0. .20390   .34945   .49690   .64482
         312011 .79289
SIGA2    312012 5 1 0
         312012 .2 .4 .6 .8 1.0 0. .0053686 .0063474 .0073403 .0083368
         312012 .0093342
VEL2     312013 3 1 0
         312013 .33478 .61987 1.0 0.  3.7710E+05 3.6944E+05 3.6396E+05
VEL1     312014 3 1 0
         312014 .33478 .61987 1.0 0.  1.5278E+07 1.4839E+07 1.4492E+07
BLANK
         550101 1  4 1 0 2 2001   ( GROUP 1 TOTAL REMOVAL - REFLECTOR1)
         550201 2  4 1 0 2 2002   ( GROUP 1 ABSORPTION    - REFLECTOR1)
         550301 3  4 1 0 2 2003   ( GROUP 1 DOWNSCATTER   - REFLECTOR1)
         550401 6  4 1 0 2 2004   ( GROUP 2 TOTAL REMOVAL - REFLECTOR1)
         550501 7  4 1 0 2 2005   ( GROUP 2 ABSORPTION    - REFLECTOR1)
         550601 21 4 1 0 2 2006   ( GROUP 2 VELOCITY      - REFLECTOR1)
         550701 20 4 1 0 2 2007   ( GROUP 1 VELOCITY      - REFLECTOR1)
         550102 1  4 1 0 2 2008   ( GROUP 1 TOTAL REMOVAL - REFLECTOR2)
         550202 2  4 1 0 2 2009   ( GROUP 1 ABSORPTION    - REFLECTOR2)
         550302 3  4 1 0 2 2010   ( GROUP 1 DOWNSCATTER   - REFLECTOR2)
         550402 6  4 1 0 2 2011   ( GROUP 2 TOTAL REMOVAL - REFLECTOR2)
         550502 7  4 1 0 2 2012   ( GROUP 2 ABSORPTION    - REFLECTOR2)
         550602 21 4 1 0 2 2013   ( GROUP 2 VELOCITY      - REFLECTOR2)
         550702 20 4 1 0 2 2014   ( GROUP 1 VELOCITY      - REFLECTOR2)
         99
```

Table 2.4.8-7
SIMTRAN Input File (u2c9.simtran.in) Used in Generating U2C9 Cross-Section File

```
/users/chaiko/SIMULATE/u2c9.simulate.restart 1 2 3 4 5 6 7
9999
U2C9 ATWS SIMTRAN EC-ATWS-0505 Rev 7
 1  1  1  0  6                jdisk,ibwr,krs,krout,krin
 2  3  4  5  6  7
10 80  0  0 14100             dimensions
 0  0  0  0  0  0  0  0       edit flags
24  0  1  1  2  2  0          iter,kdflag,kpflag,ksolv,knwtf,ktwtf,kphiwt
 6  4                         ndu,ndtf
   45.8244                   rhoref
 1 11                        lstscm / nscrm
 0.60        1.20        2.40        3.60        4.80        6.00
 7.20        8.40        9.60       10.80       12.00
33 12 12 12 12 12 12 12 12 12 12 12 12 12 12 12 12 12 12 12 12 12 12 12
33
     1.057       1.131
 1 25
  0.00  -0.10   .100   .200   .300   .400
 1 25
   0.0  -100.    60.   225.
SIGTR1   312001 5 1 0
         312001 .2 .4 .6 .8 1.0 0. .17030   .21132   .25230   .29539
         312001 .33458
SIGA1    312002 5 1 0
         312002 .2 .4 .6 .8 1.0 0. .0043117 .0043622 .0044160 .0044720
         312002 .0045297
SIGR1    312003 5 1 0
         312003 .2 .4 .6 .8 1.0 0. .0049850 .010767  .016879  .023234
         312003 .029769
SIGTR2   312004 5 1 0
         312004 .2 .4 .6 .8 1.0 0. .46027   .68728   .91722  1.14790
         312004 1.3788
SIGA2    312005 5 1 0
         312005 .2 .4 .6 .8 1.0 0. .067142  .068668  .070216  .071771
         312005 .073326
VEL2     312006 3 1 0
         312006 .33478 .61987 1.0 0.  3.7710E+05 3.6944E+05 3.6396E+05
VEL1     312007 3 1 0
         312007 .33478 .61987 1.0 0.  1.5278E+07 1.4839E+07 1.4492E+07
SIGTR1   312008 5 1 0
         312008 .2 .4 .6 .8 1.0 0. .085254  .11156   .13784   .16418
         312008 .19060
SIGA1    312009 5 1 0
         312009 .2 .4 .6 .8 1.0 0. .00048065 .00051302 .00054752
         312009 .00058343 .00062040
SIGR1    312010 5 1 0
         312010 .2 .4 .6 .8 1.0 0. .0030222 .0067297 .010649  .014724
         312010 .018915
SIGTR2   312011 5 1 0
         312011 .2 .4 .6 .8 1.0 0. .20390   .34945   .49690   .64482
         312011 .79289
SIGA2    312012 5 1 0
         312012 .2 .4 .6 .8 1.0 0. .0053686 .0063474 .0073403 .0083368
         312012 .0093342
VEL2     312013 3 1 0
         312013 .33478 .61987 1.0 0.  3.7710E+05 3.6944E+05 3.6396E+05
VEL1     312014 3 1 0
         312014 .33478 .61987 1.0 0.  1.5278E+07 1.4839E+07 1.4492E+07
BLANK
         550101 1  4 1 0 2 2001    ( GROUP 1 TOTAL REMOVAL - REFLECTOR1)
         550201 2  4 1 0 2 2002    ( GROUP 1 ABSORPTION    - REFLECTOR1)
         550301 3  4 1 0 2 2003    ( GROUP 1 DOWNSCATTER   - REFLECTOR1)
         550401 6  4 1 0 2 2004    ( GROUP 2 TOTAL REMOVAL - REFLECTOR1)
         550501 7  4 1 0 2 2005    ( GROUP 2 ABSORPTION    - REFLECTOR1)
         550601 21 4 1 0 2 2006    ( GROUP 2 VELOCITY      - REFLECTOR1)
         550701 20 4 1 0 2 2007    ( GROUP 1 VELOCITY      - REFLECTOR1)
         550102 1  4 1 0 2 2008    ( GROUP 1 TOTAL REMOVAL - REFLECTOR2)
         550202 2  4 1 0 2 2009    ( GROUP 1 ABSORPTION    - REFLECTOR2)
         550302 3  4 1 0 2 2010    ( GROUP 1 DOWNSCATTER   - REFLECTOR2)
         550402 6  4 1 0 2 2011    ( GROUP 2 TOTAL REMOVAL - REFLECTOR2)
         550502 7  4 1 0 2 2012    ( GROUP 2 ABSORPTION    - REFLECTOR2)
         550602 21 4 1 0 2 2013    ( GROUP 2 VELOCITY      - REFLECTOR2)
         550702 20 4 1 0 2 2014    ( GROUP 1 VELOCITY      - REFLECTOR2)
         99
```

Table 2.4.8-8

SIMTRAN Input File (u2c10.simtran.in) Used in Generating U2C10 Cross-Section File

```
/users/chaiko/SIMULATE/u2c10.simulate.restart 1 2 3 4 5 6 7
9999
U2C10 ATWS SIMTRAN EC-ATWS-0505 Rev 7
 1  1  1  0  6                    jdisk,ibwr,krs,krout,krin
 2  3  4  5  6  7
10 80  0  0 14100                 dimensions
 0  0  0  0  0  0  0  0           edit flags
24  0  1  1  2  2  0              iter,kdflag,kpflag,ksolv,knwtf,ktwtf,kphiwt
 6  4                            ndu,ndtf
   45.8244                       rhoref
 1 11                            lstsam / nscrm
 0.60        1.20        2.40        3.60        4.80        6.00
 7.20        8.40        9.60       10.80       12.00
33 12 12 12 12 12 12 12 12 12 12 12 12 12 12 12 12 12 12 12 12 12 12 12
33
     1.057       1.131
 1 25
  0.00  -0.10   .100   .200   .300   .400
 1 25
   0.0  -100.    60.   225.
SIGTR1   312001 5 1 0
         312001 .2 .4 .6 .8 1.0 0. .17030   .21132   .25230   .29539
         312001 .33458
SIGA1    312002 5 1 0
         312002 .2 .4 .6 .8 1.0 0. .0043117 .0043622 .0044160 .0044720
         312002 .0045297
SIGR1    312003 5 1 0
         312003 .2 .4 .6 .8 1.0 0. .0049850 .010767  .016879  .023234
         312003 .029769
SIGTR2   312004 5 1 0
         312004 .2 .4 .6 .8 1.0 0. .46027   .68728   .91722  1.14790
         312004 1.3788
SIGA2    312005 5 1 0
         312005 .2 .4 .6 .8 1.0 0. .067142  .068668  .070216  .071771
         312005 .073326
VEL2     312006 3 1 0
         312006 .33478 .61987 1.0 0.  3.7710E+05 3.6944E+05 3.6396E+05
VEL1     312007 3 1 0
         312007 .33478 .61987 1.0 0.  1.5278E+07 1.4839E+07 1.4492E+07
SIGTR1   312008 5 1 0
         312008 .2 .4 .6 .8 1.0 0. .085254  .11156   .13784   .16418
         312008 .19060
SIGA1    312009 5 1 0
         312009 .2 .4 .6 .8 1.0 0. .00048065 .00051302 .00064752
         312009 .00058343 .00062040
SIGR1    312010 5 1 0
         312010 .2 .4 .6 .8 1.0 0. .0030222 .0067297 .010649  .014724
         312010 .018915
SIGTR2   312011 5 1 0
         312011 .2 .4 .6 .8 1.0 0. .20390   .34945   .49690   .64482
         312011 .79289
SIGA2    312012 5 1 0
         312012 .2 .4 .6 .8 1.0 0. .0053686 .0063474 .0073403 .0083368
         312012 .0095342
VEL2     312013 3 1 0
         312013 .33478 .61987 1.0 0.  3.7710E+05 3.6944E+05 3.6396E+05
VEL1     312014 3 1 0
         312014 .33478 .61987 1.0 0.  1.5278E+07 1.4839E+07 1.4492E+07
BLANK
         550101 1  4 1 0 2 2001    ( GROUP 1 TOTAL REMOVAL - REFLECTOR1)
         550201 2  4 1 0 2 2002    ( GROUP 1 ABSORPTION    - REFLECTOR1)
         550301 3  4 1 0 2 2003    ( GROUP 1 DOWNSCATTER   - REFLECTOR1)
         550401 6  4 1 0 2 2004    ( GROUP 2 TOTAL REMOVAL - REFLECTOR1)
         550501 7  4 1 0 2 2005    ( GROUP 2 ABSORPTION    - REFLECTOR1)
         550601 21 4 1 0 2 2006    ( GROUP 2 VELOCITY      - REFLECTOR1)
         550701 20 4 1 0 2 2007    ( GROUP 1 VELOCITY      - REFLECTOR1)
         550102 1  4 1 0 2 2008    ( GROUP 1 TOTAL REMOVAL - REFLECTOR2)
         550202 2  4 1 0 2 2009    ( GROUP 1 ABSORPTION    - REFLECTOR2)
         550302 3  4 1 0 2 2010    ( GROUP 1 DOWNSCATTER   - REFLECTOR2)
         550402 6  4 1 0 2 2011    ( GROUP 2 TOTAL REMOVAL - REFLECTOR2)
         550502 7  4 1 0 2 2012    ( GROUP 2 ABSORPTION    - REFLECTOR2)
         550602 21 4 1 0 2 2013    ( GROUP 2 VELOCITY      - REFLECTOR2)
         550702 20 4 1 0 2 2014    ( GROUP 1 VELOCITY      - REFLECTOR2)
         99
```

Table 2.4.8-9

SIMTRAN Input File (u1c12.simtran.in) Used in Generating U1C12 Cross-Section File

```
/users/chaiko/SIMULATE/u1c12.simulate.restart 1 2 3 4 5 6 7
9999
 U1C12 ATWS SIMTRAN EC-ATWS-0505 Rev 7
  1  1  1  0  6                    jdisk,ibwr,krs,krout,krin
  2  3  4  5  6  7
 10 80  0  0 14100                 dimensions
  0  0  0  0  0  0  0  0           edit flags
 24  0  1  1  2  2  0              iter,kdflag,kpflag,ksolv,knwtf,ktwtf,kphiwt
  6  4                            ndu,ndtf
    45.8244                       rhoref
  1 11                            lstsom / nscrm
 0.60        1.20        2.40        3.60        4.80        6.00
 7.20        8.40        9.60       10.80       12.00
33 12 12 12 12 12 12 12 12 12 12 12 12 12 12 12 12 12 12 12 12 12 12 12 12 12 12
33
      1.057       1.131
  1 25
   0.00  -0.10   .100   .200   .300   .400
  1 25
    0.0  -100.    60.   225.
SIGTR1   312001 5 1 0
         312001 .2 .4 .6 .8 1.0 0. .17030   .21132   .25230   .29339
         312001 .33458
SIGA1    312002 5 1 0
         312002 .2 .4 .6 .8 1.0 0. .0043117 .0043622 .0044160 .0044720
         312002 .0045297
SIGR1    312003 5 1 0
         312003 .2 .4 .6 .8 1.0 0. .0049850 .010767  .016879  .023234
         312003 .029769
SIGTR2   312004 5 1 0
         312004 .2 .4 .6 .8 1.0 0. .46027   .68728   .91722  1.14790
         312004 1.3788
SIGA2    312005 5 1 0
         312005 .2 .4 .6 .8 1.0 0. .067142  .068668  .070216  .071771
         312005 .073326
VEL2     312006 3 1 0
         312006 .33478 .61987 1.0 0.  3.7710E+05 3.6944E+05 3.6396E+05
VEL1     312007 3 1 0
         312007 .33478 .61987 1.0 0.  1.5278E+07 1.4839E+07 1.4492E+07
SIGTR1   312008 5 1 0
         312008 .2 .4 .6 .8 1.0 0. .085254  .11156   .13784   .16418
         312008 .19060
SIGA1    312009 5 1 0
         312009 .2 .4 .6 .8 1.0 0. .00048065 .00051302 .00054752
         312009 .00058343 .00062040
SIGR1    312010 5 1 0
         312010 .2 .4 .6 .8 1.0 0. .0030222 .0067297 .010649  .014724
         312010 .018915
SIGTR2   312011 5 1 0
         312011 .2 .4 .6 .8 1.0 0. .20390   .34945   .49690   .64482
         312011 .79289
SIGA2    312012 5 1 0
         312012 .2 .4 .6 .8 1.0 0. .0053686 .0063474 .0073403 .0083368
         312012 .0095342
VEL2     312013 3 1 0
         312013 .33478 .61987 1.0 0.  3.7710E+05 3.6944E+05 3.6396E+05
VEL1     312014 3 1 0
         312014 .33478 .61987 1.0 0.  1.5278E+07 1.4839E+07 1.4492E+07
BLANK
         550101 1  4 1 0 2 2001    ( GROUP 1 TOTAL REMOVAL - REFLECTOR1)
         550201 2  4 1 0 2 2002    ( GROUP 1 ABSORPTION    - REFLECTOR1)
         550301 3  4 1 0 2 2003    ( GROUP 1 DOWNSCATTER   - REFLECTOR1)
         550401 6  4 1 0 2 2004    ( GROUP 2 TOTAL REMOVAL - REFLECTOR1)
         550501 7  4 1 0 2 2005    ( GROUP 2 ABSORPTION    - REFLECTOR1)
         550601 21 4 1 0 2 2006    ( GROUP 2 VELOCITY      - REFLECTOR1)
         550701 20 4 1 0 2 2007    ( GROUP 1 VELOCITY      - REFLECTOR1)
         550102 1  4 1 0 2 2008    ( GROUP 1 TOTAL REMOVAL - REFLECTOR2)
         550202 2  4 1 0 2 2009    ( GROUP 1 ABSORPTION    - REFLECTOR2)
         550302 3  4 1 0 2 2010    ( GROUP 1 DOWNSCATTER   - REFLECTOR2)
         550402 6  4 1 0 2 2011    ( GROUP 2 TOTAL REMOVAL - REFLECTOR2)
         550502 7  4 1 0 2 2012    ( GROUP 2 ABSORPTION    - REFLECTOR2)
         550602 21 4 1 0 2 2013    ( GROUP 2 VELOCITY      - REFLECTOR2)
         550702 20 4 1 0 2 2014    ( GROUP 1 VELOCITY      - REFLECTOR2)
         99
```

2.5 Recirculation Pump Model

A simplified pump model is used in SABRE to maintain initial rated flow conditions and to simulate the subsequent flow coast-down which results from a recirculation pump trip or a pump runback. The pressure in the downcomer region at the jet pump throat is calculated from

$$P^0 = P^* + \frac{g}{g_c}\rho_{DC}H_{th} - \frac{I_{DC}}{g_c}\frac{dW_J}{dt} + \dot{E}_p\rho_{DC}/W_{J0} \qquad \textbf{(2.5-1)}$$

where

$P^0(t)$ = downcomer fluid pressure at jet pump throat (lb_f/ft^2),

$P^*(t)$ = steam dome pressure (lb_f/ft^2),

$\rho_{DC}(t)$ = downcomer fluid density (lbm/ft^3),

$H_{th}(t)$ = height of downcomer fluid above jet pump throat (ft),

I_{DC} = downcomer fluid inertia (ft^{-1}),

W_J = jet pump flow rate = total core flow rate (lb_m/sec), and

$\dot{E}_p(t)$ = rate of mechanical energy supplied to fluid by the recirculation pump (ft·lb_f/sec).

If a recirculation pump trip occurs, the pump power $\dot{E}_p(t)$ decays exponentially according to

$$\tau_{RP}\frac{d\dot{E}_p(t)}{dt} = -\dot{E}_p(t). \qquad \textbf{(2.5-2)}$$

Under normal operation, or in the case of a single pump trip or a pump runback, the pump power response is approximated with a simple first-order lag function coupled with a proportional control model,

$$\tau_{RP}\frac{d\dot{E}_p(t)}{dt} = \dot{E}'_p(t) - \dot{E}_p(t) \qquad \textbf{(2.5-3)}$$

where

$$\dot{E}'_p(t) = \dot{E}_p(0) + G_{RP}[W_{tar} - W_J(t)]. \qquad \textbf{(2.5-4)}$$

In (2.5-4), G_{RP} is a gain factor, and W_{tar} is the target jet pump flow. W_{tar} for various recirculation pump operating conditions is supplied as part of the input data. The values specified in the base SABRE input deck (Section F.23) are listed in the following table. If there are no pump trips or runbacks, W_{tar} is equal to the initial total core flow.

Recirculation Pump Operating Conditions	Target Total Core Flow (MLb/hr)
1 pump tripped and 1 pump at normal operating speed	65
2 pumps run back to 30% speed	42
1 pump tripped and 1 pump at 30% speed	36

The values listed in the above table are generally known from plant data or from the operating cycle power flow map. That is, the total core flow is considered known under the various recirculation pump operating conditions. Hence, the purpose of the SABRE recirculation pump model is not to predict the core flow rate under various recirculation pump operating configurations, but rather to set up reactor flow conditions that are consistent with recirculation pump operation.

The recirculation pump model defined by (2.5-3) and (2.5-4) is a simple controller which forces the total core flow to the target value shown in the above table based on the recirculation pump operating conditions. The gain factor in (2.5-4) is specified within the source code and was chosen so that the calculated total core flow rate gave good agreement with the values in the above table under the indicated recirculation pump operating conditions.

2.6 Main Steam Line Model

The SABRE main steam line model computes the steam line pressure, the flow through the MSIVs, the steam flow to the main turbine, the steam flow through the bypass valves, and the steam extraction by the feedwater turbines. The mass balance for the steam line is

$$V_{SL}\frac{d\rho_{SL}}{dt} = W_{MSIV} - W_{Turb} - W_{Bypass} - W_{FWT} \qquad \textbf{(2.6-1)}$$

where

V_{SL} = Steam line volume (ft^3)[1] (see §F.26.11),
ρ_{SL} = Density of steam in steam line (Lbm/ft^3),
W_{MSIV} = Flow rate through MSIV (Lbm/sec),
W_{Turb} = Steam flow rate to main turbine (Lbm/sec),
W_{Bypass} = Flow rate through turbine bypass valves (Lbm/sec), and
W_{FWT} = Steam extraction rate by feedwater turbines (Lbm/sec).

It is assumed that the steam density changes are isentropic, and that the steam behaves as an ideal gas so that

$$\frac{\rho_{SL}}{\rho_{SL}^{o}} = \left(\frac{P_{SL}}{P_{SL}^{o}}\right)^{1/\gamma} \quad \text{and} \quad \frac{d\rho_{SL}}{dt} = \frac{\rho_{SL}}{\gamma\, P_{SL}}\frac{dP_{SL}}{dt} \qquad \textbf{(2.6-2)}$$

where

P_{SL} = Steam line pressure (psia),
γ = C_P/C_V = 1.26 for steam at conditions of interest, and
$\rho_{SL}^{o}, P_{SL}^{0}$ = Reference density and pressure.

Substituting (2.6-2) into (2.6-1) leads to

$$\frac{dP_{SL}}{dt} = \left(\frac{\gamma\, P_{SL}}{V_{SL}\,\rho_{SL}}\right)\left(W_{MSIV} - W_{Turb} - W_{Bypass} - W_{FWT}\right) \qquad \textbf{(2.6-3)}$$

From Calc. SA-MAC-003 (EC-SIMU-0501), Rev. 0, p. 3, the steam line pressure decay rate (psi/sec) due to steam extraction by the feedwater turbines and leakage/thermal losses is

[1] The steam line volume is decreased by the amount specified in §F.26.12 in the event of a turbine trip.

$$\lambda_{FW} = 2.21 + 1.8249\overline{W}_{FW} + 5.2921\overline{W}_{FW}^2 \qquad \textbf{(2.6-4)}$$

where the normalized feedwater flow rate $\overline{W}_{FW}$ = (W_{FW} / 13.3 Mlb/hr). Using this result in (2.6-3) leads to the following relation for the steam line pressure

$$\frac{dP_{SL}}{dt} = \left(\frac{\gamma P_{SL}}{V_{SL}\rho_{SL}}\right)\left(W_{MSIV} - W_{Turb} - W_{Bypass}\right) - \lambda_{FW} \qquad \textbf{(2.6-5)}$$

The steam flow through the MSIV is calculated from the following momentum equation:

$$I_{SL}\frac{dW_{MSIV}}{dt} = (144)g_c\left(P_{SD} - P_{SL}\right) - \frac{KW_{MSIV}|W_{MSIV}|}{2\rho_{MSIV}A_{MSIV}^2} \qquad \textbf{(2.6-6)}$$

where

I_{SL} = Steam line fluid inertia (ft^{-1})
W_{MSIV} = Steam flow through the MSIV (Lbm/sec),
P_{SD} = Steam dome pressure (psia),
ρ_{MSIV} = Density of steam at MSIV (Lbm/ft^3), and
A_{MSIV} = Full Open MSIV flow area (ft^2) (see §F.26.14).

The loss coefficient K in (2.6-6) is expressed as

$$K = f_m K_{MSIV} + K', \qquad \textbf{(2.6-7)}$$

where K_{MSIV} is the loss coefficient for the MSIV, and K′ is chosen so that P_{SL} is equivalent to the turbine inlet pressure. That is, given the initial steam dome pressure (§F.8) and the initial turbine-inlet pressure (§F.26.5), the value of K′ is back calculated so that the initial value of P_{SL} is equal to the initial turbine inlet pressure. The loss coefficient multiplier f_m accounts for the increased flow resistance during closure of the MSIV. The multiplier f_m is a function of valve stem position and is specified as part of the input data (see §F.25.6).

Equations (2.6-5) and (2.6-6) make up the SABRE main steam line model. In order to solve (2.6-5) and (2.6-6), expressions for the turbine steam flow W_{Turb} and turbine bypass flow W_{Bypass} need to be specified. Expressions for these two variables are provided by the pressure regulator model. A block diagram of the pressure regulator model used in SABRE is presented in Figure 2.6-1. This model describes the essential features of the Susquehanna pressure regulator. The SABRE model of the pressure regulator was developed from descriptions provided in Calc. EC-FUEL-0969, "SSES RETRAN Controller Model," and in the training manual for SSES Systems Course SY028.

In Figure 2.6-1, The Lead-Lag block is defined by the differential equation,

$$\tau_2 \frac{dy}{dt} + y = G\left(x + \tau_1 \frac{dx}{dt}\right) \qquad \textbf{(2.6-8)}$$

where x is the input to the block, y is the output, and G is the gain. The Lag block is defined by

$$\tau \frac{dy}{dt} + y = Gx. \qquad \textbf{(2.6-9)}$$

As steam line pressure changes, the turbine steam flow and the bypass steam flow will change even if there is no change in turbine control valve position and turbine bypass valve position. A decrease in steam line pressure will cause the turbine and bypass flow to decrease. The opposite effect will occur if steam line pressure increases. The actual change in flow due to a change in steam line pressure would require a detailed model of the flow resistances within the turbine and bypass system which is beyond the scope of this work. An approximate correction to the flow can be derived, however, by considering the turbine as a lumped resistance so that the turbine flow is governed by

$$P_{SL} - P_{Condenser} = \frac{K_{Turb} W_{Turb}^2}{2(144) g_c \rho_{SL} A_{Turb}^2} \qquad \textbf{(2.6-10)}$$

The steam density can be expressed as ρ_{SL} =const $P_{SL}^{1/\gamma}$. Substituting this relation into the above expression, neglecting the condenser pressure compared to the steam line pressure, and absorbing all constants into the loss factor leads to

$$W_{Turb} = \sqrt{\frac{P_{SL}^{1+1/\gamma}}{K}} \qquad \textbf{(2.6-11)}$$

The flow correction factor is obtained by dividing (2.6-11) by the initial turbine steam flow W_{Turb}^o,

$$\text{Flow Correction Factor} = \frac{W_{Turb}}{W_{Turb}^o} = \sqrt{\left(\frac{P_{SL}}{P_{SL}^0}\right)^{1+1/\gamma}}. \qquad \textbf{(2.6-12)}$$

This pressure ratio is also used to modify the bypass flow.

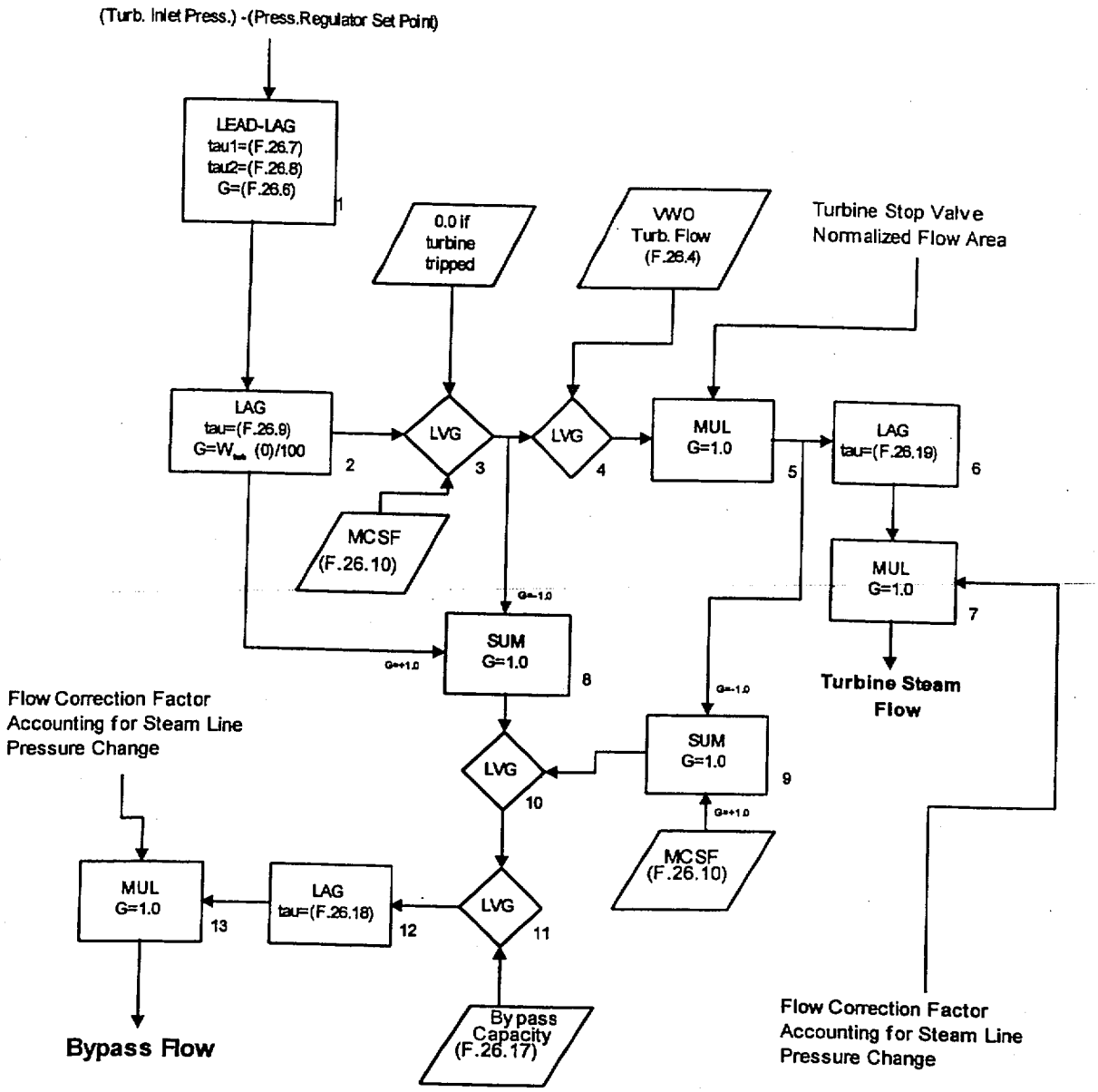

Figure 2.6-1 Block diagram of pressure regulator model used in SABRE.

2.7 Feedwater Model

A proportional control model with a first-order lag is used in SABRE to regulate feedwater flow and maintain downcomer water level near its initial value. This is a simplified approximation to the actual feedwater control system. In MSIV-closure and turbine-trip transients, where feedwater heating is lost, the decrease in feedwater enthalpy is approximated as an exponential decay following a period where there is no loss in feedwater temperature. The time constant τ_h (sec) defining the enthalpy decay is supplied as part of the code input data (see §F.24.9).

Following an MSIV closure, feedwater can continue to inject to the reactor until main steam line pressure decays to the point where the feedwater turbines can no longer generate sufficient power to overcome the vessel pressure. The feedwater turbine design specification sheet indicates that feedwater flow to the vessel can be maintained with a steam line pressure of 175 psia.[1] The rate of steam line pressure decay following an MSIV closure is computed from Eq. (2.6-5).

In the previous versions of SABRE, the rate of main steam line pressure decay following MSIV closure was computed directly from the decay constant (2.6-4). This gave correct results for MSIV closure events in which the pressure regulator operated as designed, but in the PREGO (pressure regulator failure open – see §5.7) event, this led to feedwater being available for a longer period of time than it should have been. (In the PREGO event, steam continues to be extracted by the turbine and the turbine bypass system even after the MSIVs close.) As a result, suppression pool temperatures for the PREGO ATWS event were calculated to be higher than they should have been. Since the modeling error led to conservatively high suppression pool temperatures for the PREGO event, none of the ATWS analyses performed previously with SABRE are invalid. In the present version of SABRE, this modeling error is corrected, and following MSIV closure, the main steam line pressure is obtained from the solution of (2.6-5). With the corrected model, feedwater flow is lost almost immediately on low steam line pressure following MSIV closure in the PREGO ATWS event.

Figures 2.7-1 and 2.7-2 show plant data for feedwater flow and feedwater temperature following an MSIV closure. The plant data indicates that there is no drop in temperature during the time that injection is taking place. Once injection stops, there is a very slow decay in coolant temperature presumably due to heat losses to the surroundings. Figures 2.7-1 and 2.7-2 indicate that approximately 0.1 MLb_m of feedwater is injected to the vessel, following initiation of MSIV closure, without a drop in feedwater temperature. In the SABRE code, following an MSIV closure or turbine trip, the feedwater temperature is held constant until 0.1 MLb_m of coolant are injected to the vessel. The temperature of any additional coolant injected with the feedwater system is decayed away with a time constant τ_h which is supplied as part of the SABRE code input data.

---

1 GEK-38479 (IOM 42)

Figure 2.7-1
MSIV Closure on High MSLR (Plant Data)
06/14/83
31-83070615023101

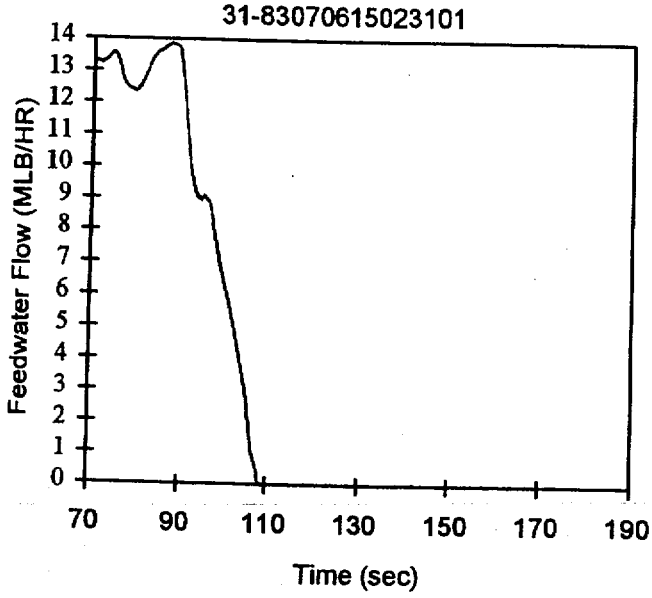

Figure 2.7-2
MSIV Closure on High MSLR (Plant Data)
06/14/83
31-83070615023101

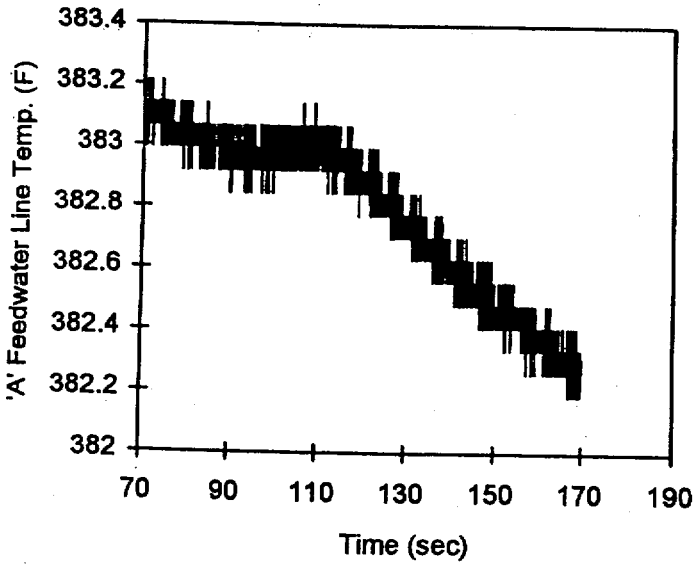

2.8 Control Rod Drive and Core Spray Models

Coolant addition to the vessel by the Control Rod Drive (CRD) system is modeled as a mass and energy source in the bypass region. The mass and energy associated with the CRD flow is deposited in the first cell (bottom cell) of the bypass region. It is assumed that the CRD flow reaches thermal equilibrium with the fluid in the lower plenum before it reaches the bypass region. This has a slight cooling effect upon the fluid in the lower plenum.

The Core Spray system is also modeled as a mass and energy source in the bottom cell of the upper plenum. Core Spray flow as a function of the pressure difference between the reactor and the suppression chamber atmosphere is specified as part of the input data. Core Spray suction is taken from the suppression pool.

2.9 HPCI and RCIC Models

SABRE includes models which describe injection by the HPCI and RCIC systems. The injection rates for these systems can be specified as constants, or the code will calculate the injection rates if the systems are operated in level control mode where the desired RPV water level is specified as part of the SABRE input data. Pump affinity equations are used in conjunction with polynomial curve fits of the pump and turbine performance curves to calculate the HPCI and RCIC turbine steam flow rates as a function of pump injection rate and RPV pressure. The enthalpy of the fluid discharged from the turbines (and deposited in the suppression pool) and the turbine speeds are also computed. Details of the HPCI and RCIC system models are described in PP&L calculation SA-MAC-002 (EC-052-0593), December, 1992.

2.10 Containment Model

The SABRE primary containment model can describe the suppression chamber and drywell pressure/temperature response to an ATWS, a small break LOCA, or a normal plant transient. SABRE models the drywell as a single control volume. The suppression chamber free volume is also described with a single temperature and pressure. Pressures within the drywell and suppression chamber are computed from the ideal gas equation of state. Heat sinks within the containment consist of the suppression pool along with the containment liner plate and structural steel. Thermal capacitance of the concrete is neglected because the heat transfer to concrete is expected to be small during the relatively short duration events (ATWS, LOCA, or plant transient) of interest. In any event, neglecting the thermal capacitance of the concrete is conservative since it leads to somewhat higher containment temperatures and pressures.

The components within the drywell and suppression chamber free volume consist of N_2 and water vapor. During an ATWS, vacuum breakers prevent the buildup of large differential pressures across the diaphragm slab by allowing steam and N_2 to flow from the suppression chamber to the drywell. In a LOCA, steam discharged into the drywell is directed through downcomer vents and condensed in the suppression pool. The suppression pool temperature calculation accounts for mass and energy from steam discharged through the downcomer vents, SRVs, and HPCI & RCIC turbines. Effects of the suppression pool cooling system and heat transfer between the containment air space and structural steel are also included in the model.

Mass balance equations for water vapor and N_2 within the drywell free volume are given by

$$\frac{dM^{g}_{W,DW}}{dt} = W_{evap,DW} + y_{W,SC}W_{vac} - W_{cond,D} + \chi W_{break} - W^{g}_{w,vent} - W_{rain,DW}\,, \qquad \textbf{(2.10-1)}$$

and

$$\frac{dM_{N,DW}}{dt} = (1 - y_{W,SC})W_{vac} - W_{N,vent}\,. \qquad \textbf{(2.10-2)}$$

Drywell average temperature is computed from the following energy balance which is taken from the COTTAP code:[1]

---

[1]Chaiko, M.A., and Murphy, M.J., "COTTAP: A Computer Code for Simulation of Thermal Transients in Secondary Containments of Boiling Water Reactors," Nuclear Technology, Vol. 94, pp. 44-55, 1991.

$$c_{DW}\frac{dT_{DW}}{dt} = Q_{Rx2} - Q_{cooler} - Q_{steel,DW} - \left[C_p\right]_{N,DW} T_{DW}\frac{dM_{N,DW}}{dt} - h^g_{W,DW}\frac{dM^g_{W,DW}}{dt}$$
$$+ T_{DW}\left(R_W\frac{dM^g_{W,DW}}{dt} + R_N\frac{dM_{N,DW}}{dt}\right) + \left[C_p\right]_{N,SC} W_{vac} y_{N,SC} T_{SC} + W_{vac} y_{W,SC} h^g_{W,SC} - W_{rain,DW}\, h^\ell_{W,sat}\left(T_{DW}\right)$$
$$+ W_{evap,DW} h^g_{W,DP} - W_{cond,DW} h_{cond,DW} - \left[C_p\right]_{N,DW} T_{DW} W_{N,vent} - h^g_{W,DW}\, W^g_{w,vent} + \chi W_{break} h^g_W\left(P_{DW}\right)$$

(2.10-3)

where c_{DW} is defined by

$$c_{DW} \equiv \left[\frac{dC_p}{dT}\right]_{N,DW} M_{N,DW} T_{DW} + \left[C_p\right]_{N,DW} M_{N,DW} + M^g_{W,DW}\frac{\partial h^g_{W,DW}}{\partial T_{DW}} - M^g_{W,DW} R_W - M_{N,DW} R_N$$

(2.10-4)

In these equations the following variable definitions are used:

$[C_p]_{N,DW}$ = Specific heat of N_2 in the drywell (Btu/Lbm-°R),

$[C_p]_{N,SC}$ = Specific heat of N_2 in the suppression chamber (Btu/Lbm·°R),

$[dC_p/dT]_{N,DW}$ = Derivative of N_2 specific heat with respect to temperature in drywell (Btu/Lbm-°R-°R),

$h_{cond,DW}$ = Enthalpy of condensate on drywell structures (Btu/Lbm),

$h^g_W\left(P_{DW}\right)$ = Enthalpy of saturated steam at drywell pressure (Btu/Lbm),

$h^g_{W,SC}$ = Enthalpy of water vapor within suppression chamber atmosphere (Btu/Lbm),

$h^g_{W,DW}$ = Enthalpy of water vapor in drywell atmosphere (Btu/Lbm),

$h^g_{W,DP}$ = Enthalpy of water vapor at surface of DW pool (Btu/Lbm),

$h^\ell_{W,sat}(T_{DW})$ = Enthalpy of saturated water at drywell atmosphere temperature (Btu/Lbm)

$M^g_{W,DW}$ = Mass of water vapor in drywell atmosphere (Lbm),

$M_{N,DW}$ = Mass of N_2 in drywell atmosphere (Lbm),

$y_{N,DW}$ = Mass fraction of N_2 in drywell atmosphere,

$y_{N,SC}$ = Mass fraction of N_2 in suppression chamber atmosphere (Lbm),

$y_{W,SC}$ = Mass fraction of water vapor in suppression chamber atmosphere,

W_{vac} = mass flow rate from suppression chamber to drywell through vacuum breakers (Lbm/sec),

$W_{rain,DW}$ = rainout rate in drywell atmosphere (Lbm/sec),

R_W = Ideal gas constant for water vapor = 0.1104 Btu/Lbm-°R,

R_N = Ideal gas constant for nitrogen = 0.0710 Btu/Lbm-°R,

T_{DW} = Drywell atmosphere temperature (°R),

$W_{cond,DW}$ = Steam condensation rate in drywell (Lbm/sec),

$W_{evap,DW}$ = Evaporation rate from water accumulated on drywell floor (lbm/sec),

$W_{N,vent}$ = Flow rate of nitrogen through downcomer vent pipes (lbm/sec),

W_{vac} = Flow rate from suppression chamber to drywell through vacuum breakers (Lbm/sec),

$W^g_{w,vent}$ = Flow rate of water vapor through downcomer vent pipes (lbm/sec),

Q_{Rx2} = Drywell heat load due to dissipation from reactor vessel (Btu/sec),

Q_{cooler} = Energy removed by drywell coolers (Btu/sec),

$Q_{steel,DW}$ = Heat transfer from drywell air to steel structures in drywell (Btu/sec), and

χ = Fraction of break flow which flashes to steam.

SABRE computes the relative humidity in the drywell from the relation

$$RH_{DW} = (100)\frac{\overline{P}_{W,DW}}{P_{sat}(T_{DW})}. \qquad \textbf{(2.10-4a)}$$

where

RH_{DW} = Relative humidity in drywell (%),
$\overline{P}_{W,DW}$ = partial pressure of water vapor in the drywell atmosphere, and
$P_{sat}(T_{DW})$ = saturation pressure of water at the drywell temperature.

If the relative humidity exceeds 100%, wet steam is beginning to form in the drywell atmosphere. When this occurs, the code removes the liquid from the atmosphere by means of a "rainout" model. The rainout rate within the drywell atmosphere is computed from the simple control model

$$W_{rain,DW} = \begin{cases} 0.0 & if\ RH_{DW} \le 100 \\ e^{20(RH_{DW}-100)} & if\ RH_{DW} > 100 \end{cases}. \qquad \textbf{(2.10-4b)}$$

The rainout rate computed from (2.10-4b) is very sensitive to the relative humidity; this prevents the RH_{DW} from exceeding 100% by any appreciable amount. Water that is removed from the atmosphere is added to the drywell pool. The same model is used to prevent relative humidity from exceeding 100% in the wetwell atmosphere.

When the pressure differential between the drywell and suppression chamber is large enough to clear the downcomer vents, the flow rate, W_{vent} (lbm/sec), through the vents is calculated from

$$W_{vent} = \sqrt{\frac{(P_{DW} - P_{SC} - \Delta P_{open})2g_c(144)\rho_{DW}A_{vent}^2}{K_{vent}}} \qquad \textbf{(2.10-5)}$$

where

P_{DW} = drywell pressure (psia),

P_{SC} = suppression chamber pressure (psia),

ΔP_{open} = differential pressure (psia) required to displace water column from vent line,

g_c = 32.2 ft-lbm/lb_f-sec^2,

ρ_{DW} = gas density in drywell (lbm/ft^3),

A_{vent} = total flow area of downcomer vents (ft^2), and

K_{vent} = loss coefficient for downcomer vent.

In order to stabilize the numerical calculation, the vent flow area A_{vent} is linearly increased over a small pressure range (2 psi):

$$A_{vent} = 0 \quad \text{if} \quad P_{DW}\text{-}P_{SC}\text{-}\Delta P_{open} < 0 \qquad \textbf{(2.10-6)}$$

$$A_{vent} = \frac{A^o_{vent}}{2}\left(P_{DW} - P_{SC} - \Delta P_{open}\right) \quad \text{if} \quad 0 \le P_{DW}\text{-}P_{SC}\text{-}\Delta P_{open} \le 2 \text{ psi} \qquad \textbf{(2.10-7)}$$

$$A_{vent} = A^o_{vent} \quad \text{if} \quad P_{DW}\text{-}P_{SC}\text{-}\Delta P_{open} > 2 \text{ psi} \qquad \textbf{(2.10-8)}$$

In Eqs. (2.10-7) and (2.10-8), A^o_{vent} is the total downcomer vent flow area when the vents are completely cleared of water.

If the suppression chamber pressure exceeds the drywell pressure by ΔP_{open} (see §F.63.3 for specification of this parameter), vacuum breakers, which are connected to 5 of the downcomer vents, will open and allow the flow of steam and nitrogen to the drywell. The loss coefficient K_{vac} for the flow path from the suppression chamber to the drywell is specified as part of the SABRE input data (see §F.63.2). This loss coefficient is based on the flow area of the 24" downcomer pipe.

In SABRE, the flow rate through the vacuum breakers W_{vac} (lbm/sec) is computed from

$$W_{vac} = 0 \quad \text{if} \quad P_{SC}\text{-}P_{DW} < \Delta P_{open} \qquad \textbf{(2.10-9)}$$

$$W_{vac} = \sqrt{\frac{A^2_{vac}\,2g_c\left(P_{SC} - P_{DW}\right)(144)\rho_{SC}}{K_{vac}}} \quad \text{if} \quad P_{SC}\text{-}P_{DW} \ge \Delta P_{open} \qquad \textbf{(2.10-10)}$$

The vacuum breakers are full open when the differential pressure reaches ΔP_{FO} (see §F.63.4). Therefore, the vacuum breaker flow area A_{vac} (ft^2) is calculated from

$$A_{vac} = 0 \qquad \text{if} \qquad P_{SC}\text{-}P_{DW} < \Delta P_{open} \tag{2.10-11}$$

$$A_{vac} = A^o_{vac}\left[\frac{P_{SC} - P_{DW} - \Delta P_{open}}{\Delta P_{FO} - \Delta P_{open}}\right] \qquad \text{if} \qquad \Delta P_{open} \le P_{SC}\text{-}P_{DW} \le \Delta P_{FO} \tag{2.10-12}$$

$$A_{vac} = A^o_{vac} \qquad \text{if} \qquad P_{SC}\text{-}P_{DW} > \Delta P_{FO} \tag{2.10-13}$$

The total full-open flow area, A^o_{vac} (ft^2), associated with flow through the vacuum breakers is 5 times the flow area of a 24" vent pipe or 10.25 ft^2 (see §F.63.1).

The mass and energy balance equations for the suppression chamber atmosphere are

$$\frac{dM^g_{W,SC}}{dt} = W_{evap,SC} - y_{W,SC}W_{vac} - W_{cond,SC} - W_{rain,SC}, \tag{2.10-14}$$

$$\frac{dM_{N,SC}}{dt} = -y_{N,SC}W_{vac} + W_{N,vent}, \tag{2.10-15}$$

and

$$c_{SC}\frac{dT_{SC}}{dt} = Q_{TP} + Q_{pool} - Q_{steel,SC} - \left[C_p\right]_{N,SC}T_{SC}\frac{dM_{N,SC}}{dt} - h^g_{W,SC}\frac{dM^g_{W,SC}}{dt} + \left(R_W\frac{dM^g_{W,SC}}{dt} + R_N\frac{dM_{N,SC}}{dt}\right)T_{SC} - \left[C_p\right]_{N,SC}W_{vac}y_{N,SC}T_{SC} - W_{vac}y^g_{W,SC}h^g_{W,SC} + W_{evap,SP}h^g_{W,SP} - W_{cond,SC}h_{cond,SC} + W_{N,vent}\left[C_p\right]_{N,SP}T_{SP} - W_{rain,SC}\,h^\ell_{W,sat}(T_{SC}) \tag{2.10-16}$$

where

$$c_{SC} \equiv \left[\frac{dC_p}{dT}\right]_{N,SC}M_{N,SC}T_{SC} + \left[C_p\right]_{N,SC}M_{N,SC} + M^g_{W,SC}\frac{dh^g_{W,SC}}{dT_{SC}} - M^g_{W,SC}R_W - M_{N,SC}R_N. \tag{2.10-17}$$

Variables not previously defined consist of

$[C_p]_{N,SC}$ = Specific heat of N_2 in the suppression chamber atmosphere (Btu/Lbm-°R),

$[C_p]_{N,SP}$ = Specific heat of N_2 evaluated at the suppression pool temperature (Btu/Lbm-°R),

$[dC_p/dT]_{N,SC}$ = Derivative of N_2 specific heat with respect to temperature in suppression chamber (Btu/Lbm-°R-°R),

$h^g_{W,SP}$ = Enthalpy of water vapor at surface of suppression pool (Btu/Lbm),

$h^g_{W,SC}$ = Enthalpy of water vapor within the suppression chamber atmosphere (Btu/Lbm),

$h_{cond,SC}$ = Enthalpy of condensate on suppression chamber structures (Btu/Lbm),

$M_{N,SC}$ = Mass of N_2 in suppression chamber atmosphere (Lbm),

$M^g_{W,SC}$ = Mass of water vapor in suppression chamber atmosphere (Lbm),

Q_{pool} = Rate of heat transfer from suppression pool to suppression chamber atmosphere (Btu/sec),

$Q_{steel,SC}$ = Rate of heat transfer from suppression chamber atmosphere to steel structures (Btu/sec),

Q_{TP} = Rate of heat transfer from SRV tail pipes to suppression chamber atmosphere (Btu/sec),

T_{SP} = Suppression pool temperature (°R),

T_{SC} = Suppression chamber atmosphere temperature (°R), and

$W_{evap,SC}$ = Evaporation rate from suppression pool (lbm/sec).

In the drywell, the structural steel is divided into 4 groups: ceiling, wall, floor, and internal structures. The ceiling, wall, and floor are all parts of the drywell liner. The drywell liner is divided into these three parts because the heat transfer coefficients between the atmosphere and the steel structures depends on the direction of heat flow. Heat transfer between the drywell atmosphere and the drywell heat sinks includes natural convection, radiation, and steam condensation effects. Forced convection heat transfer may be significant under conditions where drywell coolers are operating because of the induced circulation caused by the cooler fans. However, in most accident sequences of interest, the drywell coolers are tripped because of a LOCA signal (see §F.58 & F.59). Therefore forced convection heat transfer is neglected. Even if the drywell coolers are

operable under some conditions, it is acceptable to neglect forced convection heat transfer because it will lead to conservatively high drywell temperatures. The thermal response of steel structures is described using a lumped-parameter model.

Heat transfer within the suppression chamber is modeled in the same manner as in the drywell, except that there are no steel structures corresponding to a ceiling and a floor. In place of heat transfer to a floor, the suppression chamber atmosphere exchanges mass and energy with the suppression pool surface. There is no liner plate on the ceiling of the suppression chamber.

Natural convection and radiation heat transfer correlations for the drywell and suppression chamber atmospheres are taken from the COTTAP code.[2] The Uchida correlation is used to model condensation heat transfer when the steel temperature drops below the dew point of the atmosphere (this is also the correlation used in the COTTAP code).

The mass transfer rate between the suppression pool and the suppression chamber atmosphere is calculated from the following expression[3]

$$W_{evap,SP} = \frac{K_{W,SP}\,\rho^{g}_{W,SP}\left(P_{W,SP} - P_{W,SC}\right)A_{SP}}{\overline{P}_{N}} \qquad \textbf{(2.10-18)}$$

where

A_{SP} = Surface area of suppression pool (ft^2),

$K_{W,SP}$ = Coefficient of mass transfer for water vapor at suppression pool surface (ft/sec),

$\rho^{g}_{W,SP}$ = density of water vapor at pool surface (lb_m/ft^3),

$\overline{P}_{N}$ = average pressure of nitrogen in convective boundary layer (psia),

$P_{W,SP}$ = Partial pressure of water vapor at the surface of the suppression pool $\left(Lb_f / ft^2\right)$, and

$P_{W,SC}$ = Partial pressure of water vapor in suppression chamber atmosphere $\left(Lb_f / ft^2\right)$.

---

[2]Chaiko, M.A., and Murphy, M.J., "COTTAP: A Computer Code for Simulation of Thermal Transients in Secondary Containments of Boiling Water Reactors," Nuclear Technology, Vol. 94, pp. 44-55, 1991.
[3]Collier, J.G., Convective Boiling and Condensation, 2nd Edition, p. 324, McGraw-Hill, New York, 1972.

The mass transfer coefficient in (2.10-18) is calculated from the mass-transfer/heat-transfer analogy (Collier, p. 326)

$$K_{W,SP} = \frac{h_{Conv,SP}}{\rho^{g}_{W,SP}\left[C_p\right]^{g}_{W,SP}} \qquad \textbf{(2.10-19)}$$

where

$h_{Conv,SP}$ = Natural convection heat transfer coefficient at pool surface (Btu/ft^2-sec-°F),

$\rho^{g}_{W,SP}$ = Density of water vapor at pool surface (Lb_m/ft^3), and

$\left[C_p\right]^{g}_{W,SP}$ = Specific heat of water vapor at pool surface (Btu/Lb_m-°F).

In (2.10-19), it has been assumed that the Lewis number raised to 2/3 power is close to 1 which is generally the case.[4] In calculating the heat transfer between the suppression pool and the suppression chamber atmosphere, both natural convection and radiation effects are considered. The heat transfer coefficient for a horizontal slab is used. The rate of heat transfer from the pool to the suppression chamber atmosphere is calculated from

$$Q_{pool} = h_{pool}\left(T_{SP} - T_{SC}\right). \qquad \textbf{(2.10-20)}$$

If a large amount of energy is rapidly added to the suppression pool, then the vapor pressure of the pool can reach the total pressure of the suppression chamber atmosphere (see benchmark study in §5.2). This situation corresponds to the onset of suppression pool boiling. Under pool boiling conditions, the pressure and temperature of the suppression chamber atmosphere are no longer unknown quantities. The atmosphere pressure is equal to the vapor pressure of the pool, and the atmosphere temperature should quickly approach the pool temperature. Therefore, rather than using complicated correlations to predict the pool heat transfer and mass transfer coefficients under boiling conditions, the two coefficients are treated as parameters and are adjusted so that the heat and mass transfer rates are sufficient to maintain pressure and temperature equilibrium within the suppression chamber.

The drywell heat load from the reactor vessel Q_{Rx2} and the cooling load of the drywell coolers Q_{cool} are calculated from the following expressions:

---

[4] McQuiston, F.C., Parker, J.D., *Heating Ventilating, and Air Conditioning Analysis and Design*, 4th Edition, pp. 547-550, John Wiley, New York, 1994.

$$Q_{Rx2} = (hA)_{Rx2}[T_{Rx} - T_D] \tag{2.10-21}$$

and

$$Q_{cool} = (UA)_{cool}[T_D - T_{cool}] \tag{2.10-22}$$

where T_{Rx} is the reactor vessel temperature, which is calculated from Eq. (2.11-1) and T_{cool} is the cooling water temperature for the drywell coolers. $(hA)_{Rx2}$ is a constant which is calculated from the initial reactor heat load and the initial drywell and reactor coolant temperatures. $(UA)_{cool}$ is calculated from the initial drywell cooling load, the initial drywell temperature and the cooling water temperature; this coefficient is also maintained constant throughout the entire transient. Values of $(hA)_{Rx2}$ and $(UA)_{cool}$ are calculated in Sections D.18.5 and D.18.6.

SABRE solves a mass and energy balance for the suppression pool in order to obtain an estimate for the pool temperature during a transient simulation. Steam discharged through the SRVs and steam exhausted from the HPCI and RCIC turbines are sources of mass and energy. Under LOCA conditions, water (liquid and vapor) can also be added to the pool by means of flow through the downcomer pipes. Liquid will flow through the downcomers when the depth of the water layer on the drywell floor reaches 18". The model used in SABRE considers energy extraction by the suppression pool cooling (SPC) system, but neglects suppression pool energy losses to the surrounding walls. Mass extraction from the pool consists of HPCI, RCIC, and Core Spray suction as well as suppression pool let down. RCIC is initially aligned to the CST, but transfers to the suppression pool on low CST level. The mass and energy balance equations for the suppression pool are given by

$$\frac{dM^{\ell}_{W,SP}}{dt} = W^{g}_{SRV} + W^{g}_{HPCI} + W^{g}_{RCIC} + W^{g}_{W,vent} + W^{\ell}_{W,vent} + W^{\ell}_{cond,SC} - W^{\ell}_{HPCI} - W^{\ell}_{RCIC} - W_{CS} - W_{evap,SP} - W_{LD} + W_{rain,SC} \tag{2.10-23}$$

and

$$M^{\ell}_{W,SP}\frac{dh^{\ell}_{W,SP}}{dt} = \bar{h}_{SD}W^{g}_{SRV} + h^{g}_{HPCI}W^{g}_{HPCI} + h^{g}_{RCIC}W^{g}_{RCIC} - Q_{SPC} - Q_{pool} - h^{\ell}_{W,SP}\left(W^{\ell}_{HPCI} + W^{\ell}_{RCIC} + W_{CS} + W_{LD}\right) + h^{g}_{W,D}W^{g}_{W,vent} + h^{\ell}_{W,DP}W^{\ell}_{W,vent} + h_{cond,SC}W^{\ell}_{cond,SC} - W_{evap,SP}h^{g}_{W,SP} + W_{rain,SC}\,h^{\ell}_{W,sat}(T_{SC}) - h^{\ell}_{W,SP}\frac{dM^{\ell}_{W,SP}}{dt} \tag{2.10-24}$$

where

$M^{\ell}_{W,SP}$ = mass of water in suppression pool (Lb_m),

$h^{g}_{W,SP}$ = specific enthalpy of saturated vapor at suppression pool temperature (Btu/Lb_m),

$h^{\ell}_{W,SP}$ = specific enthalpy of suppression pool water (Btu/lb_m),

$W^{\ell}_{cond,SC}$ = Condensation rate on suppression chamber steel structures (lb_m/sec),

W^{g}_{SRV} = flow rate of steam through SRVs (lb_m/sec),

W^{g}_{HPCI} = flow rate of steam through HPCI turbine (lb_m/sec),

W^{ℓ}_{HPCI} = HPCI injection rate if HPCI suction is aligned to the suppression pool (lb_m/sec),

W^{ℓ}_{RCIC} = RCIC injection rate if RCIC suction is aligned to the suppression pool (lb_m/sec),

W_{CS} = Core spray injection rate (lb_m/sec),

W_{LD} = suppression pool letdown flow (Lb_m/sec),

W^{g}_{RCIC} = flow rate of steam through RCIC turbine (lb_m/sec),

$W^{g}_{W,vent}$ = flow rate of steam through downcomer vents (lbm/sec),

$W^{\ell}_{W,vent}$ = flow rate of liquid water through downcomer vents (lb_m/sec),

$h^{\ell}_{W,DP}$ = enthalpy of water in drywell pool (Btu/lbm),

$\bar{h}_{SD}$ = volume-weighted enthalpy in reactor steam dome region (Btu/lb_m),

h^{g}_{HPCI} = enthalpy of steam discharged from HPCI turbine (Btu/lb_m),

h^{g}_{RCIC} = enthalpy of steam discharged from RCIC turbine (Btu/lb_m),

Q_{pool} = rate of heat loss from surface of pool (Btu/sec), and

Q_{SPC} = rate of energy loss from suppression pool due to SPC system (Btu/sec).

The heat removal rate by the suppression pool cooling system is calculated from

$$Q_{SPC} = N_{Loop} 315(T_{SP} - T_{SW}) \qquad \textbf{(2.10-25)}$$

where

N_{LOOP} = number of SPC loops in operation (0, 1, or 2),

T_{SP} = suppression pool temperature (°F), and

T_{SW} = service water temperature (°F).

The service water temperature is specified as part of the input data (§F.62). The suppression pool temperature is computed as the saturation temperature of liquid water with enthalpy $h^{\ell}_{W,SP}$.

The factor, 315, in Equation (2.10-25) was determined from the containment heat removal capability of 134 x 10^6 Btu/hr per loop for 90°F service water and 208°F pool temperature (Table 6.2-2 of SSES FSAR).

During a LOCA event, water will accumulate on the drywell floor. When level reaches 18", liquid will overflow to the suppression pool through the downcomer vents. The governing equations for the drywell pool level and enthalpy are similar to (2.10-23) and (2.10-24).

2.11 Heat Capacitance of Vessel and Internals

In a reactor depressurization transient, such as an ADS blowdown, the vessel and internal structures will transfer heat to the coolant. These steel structures will effectively behave as a heat source. Vaporization occurring on the surface of the submerged parts of these structures will reduce the rate of vessel depressurization and increase the suppression pool temperature rise associated with the blowdown.

In SABRE, heat dissipation by the reactor vessel and internal steel structures is described with simple lumped-parameter models. For the reactor vessel, the governing equation is

$$M_{Rx}C_{ps}\frac{dT_{Rx}}{dt} = h_{Rx1}A_{Rx}(T_{sat} - T_{Rx}) - h_{Rx2}A_{Rx}(T_{Rx} - T_{DW}) \qquad \textbf{(2.11-1)}$$

where

M_{Rx} = mass of reactor vessel (lbm),

C_{ps} = specific heat of steel (Btu/lbm-°F),

T_{Rx} = reactor metal temperature (°F),

h_{Rx1} = coefficient for heat transfer between coolant and reactor vessel (Btu/sec-ft^2-°F),

h_{Rx2} = coefficient for heat transfer between reactor vessel and drywell atmosphere (Btu/sec-ft^2-°F),

A_{Rx} = surface area of reactor vessel (ft^2),

T_{sat} = saturation temperature of water at reactor pressure (°F), and

T_{DW} = drywell atmosphere temperature (°F).

Heat transfer between the vessel internals and the coolant is described by

$$M_{VI}C_{ps}\frac{dT_{VI}}{dt} = A_{VI}h_{VI}(T_{sat} - T_{VI}) \qquad \textbf{(2.11-2)}$$

where

M_{VI} = mass of vessel internals (excluding the fuel) (Lbm),

T_{VI} = temperature of vessel internals (°F),

h_{VI} = coefficient for heat transfer between vessel internals and reactor coolant (Btu/sec-ft^2-°F), and

A_{VI} = heat transfer area for vessel internals (ft^2).

The initial temperatures, $T_{Rx}(0)$ and $T_{VI}(0)$, are specified as the coolant saturation temperature, T_{sat}.

The heat transfer coefficients h_{Rxl} and h_{VI} depend on the reactor water level. Calculation of the heat transfer coefficients h_{Rxl} and h_{VI} is discussed in Appendix D, §D.2.

The rate of heat transfer from the steel structures to the reactor coolant is given by

$$Q_{Rxl} = h_{Rxl} A_{Rx} (T_{Rx} - T_{sat}) \quad \textbf{(2.11-3)}$$

and

$$Q_{VI} = h_{VI} A_{VI} (T_{VI} - T_{sat}) \quad \textbf{(2.11-4)}$$

In order to simplify the heat transfer model, the heat transfer rate, $Q_{Rxl} + Q_{VI}$, is added to the decay heat generation rate within the core [see Eq. (2.4.7-4)]. Although this is a very simplistic model, it does balance the steel sensible heat loss from the vessel and vessel internal structures with vapor generation during an RPV depressurization event so that the suppression pool temperature response during an RPV blowdown will be modeled correctly.

3. NUMERICAL SOLUTION OF THERMAL-HYDRAULIC EQUATIONS

3.1 Control Volume Formulation of Flow Equations

In this section, the partial diferential equations governing the reactor thermal-hydraulics are spatially integrated to obtain conservation equations in control-volume form. A diagram of a nodalized flow region is shown in Figure 3.1-1.

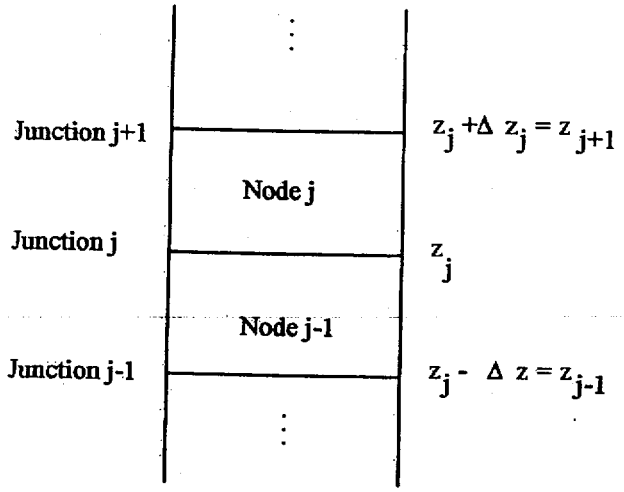

Figure 3.1-1 Nodalization Scheme for Flow Equations.

3.1.1 Nodalized Continuity Equation

For the jet pump, lower plenum, core, bypass, upper plenum, riser, and separator regions, the governing thermal-hydraulic equations are integrated as follows. Each of the terms in the continuity Equation (2.1-1) are integrated over the control volume length Δz. Integration of the first two terms in (2.1-1) is carried out as follows:

$$\int_{z_j}^{z_j+\Delta z} \frac{\partial \rho(z,t)}{\partial t} dz = \frac{d}{dt} \int_{z_j}^{z_j+\Delta z} \rho(z,t) dz = \Delta z \frac{d\rho_j(t)}{dt}, \qquad \textbf{(3.1.1-1)}$$

and

$$\int_{z_j}^{z_j+\Delta z} \frac{\partial G(z,t)}{\partial z} dz = G(z_j + \Delta z, t) - G(z_j, t) = \hat{G}_{j+1}(t) - \hat{G}_j(t) \qquad \textbf{(3.1.1-2)}$$

where

$$\rho_j(t) \equiv \frac{1}{\Delta z} \int_{z_j}^{z_j+\Delta z} \rho(z,t) dz,$$

$\hat{G}_j(t) \equiv G(z_j, t)$, and

$\hat{G}_{j+1}(t) \equiv G(z_{j+1}, t) = G(z_j + \Delta z, t)$

Integrating the right-hand-side of Equation (2-1) gives

$$\int_{z_j}^{z_j+\Delta z} \gamma_s(z,t)dz = \left[A \int_{z_j}^{z_j+\Delta z} \gamma_s(z,t)dz \right] \Big/ A = \frac{\Gamma_j(t)}{A}. \qquad \textbf{(3.1.1-3)}$$

In Equation (3.1.1-3), $\Gamma_j(t)$ (Lb/sec) is the mass source within control volume j, and A is the flow area of the control volume which is assumed to be uniform throughout the entire flow region.

Combining Equations (3.1.1-1), (3.1.1-2), and (3.1.1-3) gives the continuity equation for control volume j:

$$\Delta z \frac{d\rho_j(t)}{dt} = \hat{G}_j(t) - \hat{G}_{j+1}(t) + \frac{\Gamma_j(t)}{A} \qquad j \in \{1, 2, \ldots, N \qquad \textbf{(3.1.1-4)}$$

where N is the number of control volumes within the flow region.

Substituting the equation of state,

$$\rho_j(t) = \rho_j\left[P^*(t), \bar{h}_j(t)\right], \qquad \textbf{(3.1.1-5)}$$

where

$$\bar{h}_j(t) \equiv \frac{1}{\Delta z} \int_{z_j}^{z_j+\Delta z} \bar{h}(z,t)\, dz,$$

into Equation (3.1.1-4), leads to the following form of the nodal continuity equation:

$$\Delta z \left(\frac{\partial \rho_j}{\partial \bar{h}_j} \right) \frac{d\bar{h}_j}{dt} = \hat{G}_j(t) - \hat{G}_{j+1}(t) + \frac{\Gamma_j(t)}{A} - \Delta z \left(\frac{\partial \rho_j}{\partial P^*} \right) \frac{dP^*}{dt}. \qquad \textbf{(3.1.1-6)}$$

For certain flow regions (lower reflector region and first node in upper plenum; see Figure 2-1) it is necessary to generalize the nodal continuity equation to allow for the situation where there are multiple flow streams into or out of the control volume. The generalized continuity equation is given by

$$\Delta z\left(\frac{\partial \rho_j}{\partial \bar{h}_j}\right)\frac{d\bar{h}_j}{dt}=\sum_{p=1}^{M_j}\left[\hat{\rho}_{\ell j}\left(1-\hat{\alpha}_j\right)\hat{u}_{\ell j}+\hat{\rho}_{g j}\hat{\alpha}_j\hat{u}_{g j}\right]_p-$$

$$\sum_{p=1}^{M_{j+1}}\left[\hat{\rho}_{\ell\, j+1}\left(1-\hat{\alpha}_{j+1}\right)\hat{u}_{\ell\, j+1}+\hat{\rho}_{g\, j+1}\hat{\alpha}_{j+1}\hat{u}_{g\, j+1}\right]_p+\frac{\Gamma_j(t)}{A}-\Delta z\left(\frac{\partial \rho_j}{\partial P^*}\right)\frac{dP^*}{dt}. \tag{3.1.1-7}$$

where $j\in\{1,2,\ldots,N$ and

M_j = number of flow paths on control volume boundary defined by $z = z_j$ (z is the axial coordinate for the flow region), and

M_{j+1} = number of flow paths on the control volume boundary defined by $z=z_{j+1}=z_j+\Delta z$.

3.1.2 Nodalized Energy Equation

Each term in the energy equation (2.1-2) is integrated over the control volume length Δz in order to obtain the control-volume energy balance. For the first term the result is

$$\int_{z_j}^{z_j+\Delta z}\frac{\partial\left[\rho(z,t)\bar{h}(z,t)\right]}{\partial t}dz=\frac{d}{dt}\int_{z_j}^{z_j+\Delta z}\rho(z,t)\bar{h}(z,t)dz=\Delta z\,\rho_j(t)\frac{d\bar{h}_j(t)}{dt}+\Delta z\,\bar{h}_j(t)\frac{d\rho_j(t)}{dt}+O\left(\Delta z^2\right) \tag{3.1.2-1}$$

Derivation of the error term in Equation (3.1.2-1) is given in Appendix C. Integration of the second, third, and fourth terms leads to

$$\int_{z_j}^{z_j+\Delta z}dz\frac{\partial\left[\rho_\ell(1-\alpha)u_\ell h_\ell+\rho_g\alpha u_g h_g\right]}{\partial z}=$$
$$\left[\hat{\rho}_\ell(1-\hat{\alpha})\hat{u}_\ell\hat{h}_\ell+\hat{\rho}_g\hat{\alpha}\hat{u}_g\hat{h}_g\right]_{j+1}-\left[\hat{\rho}_\ell(1-\hat{\alpha})\hat{u}_\ell\hat{h}_\ell+\hat{\rho}_g\hat{\alpha}\hat{u}_g\hat{h}_g\right]_j, \tag{3.1.2-2}$$

$$\int_{z_j}^{z_j+\Delta z}dz\frac{1}{J}\frac{dP^*(t)}{dt}=\frac{\Delta z}{J}\frac{dP^*(t)}{dt}, \tag{3.1.2-3}$$

and

$$\int_{z_j}^{z_j+\Delta z} dz\, q'''(z,t) = \frac{1}{A}\left[A \int_{z_j}^{z_j+\Delta z} dz\, q'''(z,t)\right] = \frac{Q_j(t)}{A}, \qquad \textbf{(3.1.2-4)}$$

where $Q_j(t)$ is the heat generation rate (Btu/sec) within control volume j. Integration of the heat-flux and mass-source terms results in

$$\int_{z_j}^{z_j+\Delta z} dz \left(\frac{P_h\, q''(z,t)}{A}\right) = \left(\frac{\Delta z\, P_h}{A}\right) q_j''(t), \qquad \textbf{(3.1.2-5)}$$

where $q_j''(t)$ is the control-volume average heat flux (Btu/sec ft^2), and

$$\int_{z_j}^{z_j+\Delta z} dz\, \gamma(z,t)\, h_s(t) = \frac{h_{sj}(t)\,\Gamma_j(t)}{A}. \qquad \textbf{(3.1.2-6)}$$

The following control-volume energy balance is obtained by substituting the results in (3.1.2-1) - (3.1.2-6) and (3.1.1-5) into Equation (2.1-2):

$$\left[\Delta z\,\rho_j + \Delta z\,\bar{h}_j \frac{\partial \rho_j\left(P^*,\bar{h}_j\right)}{\partial \bar{h}_j}\right]\frac{d\bar{h}_j}{dt} = \left[\hat{\rho}_\ell\,(1-\hat{\alpha})\,\hat{u}_\ell\;\hat{h}_\ell + \hat{\rho}_g\,\hat{\alpha}\,\hat{u}_g\;\hat{h}_g\right]_j -$$

$$\left[\hat{\rho}_\ell\,(1-\hat{\alpha})\hat{u}_\ell\;\hat{h}_\ell + \hat{\rho}_g\,\hat{\alpha}\,\hat{u}_g\;\hat{h}_g\right]_{j+1} + \Delta z\left[\frac{1}{J} - \bar{h}_j\frac{\partial \rho_j}{\partial P^*}\right]\frac{dP^*}{dt} + \frac{Q_j}{A} + \frac{\Delta z\, P_h}{A} q_j'' + \frac{h_{sj}\,\Gamma_j}{A}. \qquad \textbf{(3.1.2-7)}$$

As in the case of the continuity equation, the energy balance can be generalized to allow for multiple flow paths into and out of the control volume. The generalized nodal energy equation is given by

$$\left[\Delta z\rho_j + \Delta z\bar{h}_j \frac{\partial \rho_j\left(P^*,\bar{h}_j\right)}{\partial \bar{h}_j}\right]\frac{d\bar{h}_j}{dt} = \sum_{p=1}^{M_j}\left[\hat{\rho}_{\ell j}\left(1-\hat{\alpha}_j\right)\hat{u}_{\ell j}\;\hat{h}_{\ell j} + \hat{\rho}_{gj}\,\hat{\alpha}_j\,\hat{u}_{gj}\,\hat{h}_{gj}\right]_p -$$

$$\sum_{p=1}^{M_{j+1}}\left[\hat{\rho}_{\ell\, j+1}\left(1-\hat{\alpha}_{j+1}\right)\hat{u}_{\ell\, j+1}\hat{h}_{\ell\, j+1} + \hat{\rho}_{g\, j+1}\,\hat{\alpha}_{j+1}\,\hat{u}_{g\, j+1}\,\hat{h}_{g\, j+1}\right]_p +$$

$$\Delta z\left[\frac{1}{J} - \bar{h}_j\frac{\partial \rho_j}{\partial P^*}\right]\frac{dP^*}{dt} + \frac{Q_j}{A} + \frac{\Delta z\, P_h}{A} q_j'' + \frac{h_{sj}\,\Gamma_j}{A}. \qquad \textbf{(3.1.2-8)}$$

3.1.3 Nodalized Momentum Equations

In this section, each term in the momentum equation (2.1-3) is integrated over the flow region length L in order to arrive at the overall momentum equation for the flow region.

3.1.3.1 Nodal Representation of Inertial Term

Since the length of the flow region is constant,

$$\int_0^L dz \frac{\partial G(z,t)}{\partial t} = \frac{d}{dt}\int_0^L G(z,t) \qquad \textbf{(3.1.3.1-1)}$$

Integration of the continuity equation (2-1) from z=0 to z=z leads to

$$G(z,t) = G(0,t) + \int_0^z d\xi \gamma(\xi,t) - \int_0^z d\xi \frac{\partial \rho(\xi,t)}{\partial t} \qquad \textbf{(3.1.3.1-2)}$$

Substitution of (3.1.3.1-2) into (3.1.3.1-1) gives

$$\int_0^L dz \frac{\partial G(z,t)}{\partial t} = \frac{d}{dt}\left[L\,G(0,t) + \int_0^L dz \int_0^z d\xi\, \gamma(\xi,t) - \int_0^L dz \int_0^z d\xi \frac{\partial \rho(\xi,t)}{\partial t} \right] \qquad \textbf{(3.1.3.1-3)}$$

Applying integration by parts to the double integrals in (3.1.3.1-3) gives

$$\int_0^L dz \int_0^z d\xi\, \gamma(\xi,t) = \int_0^L dz\,(L-z)\gamma(z,t) \qquad \textbf{(3.1.3.1-4)}$$

and

$$\int_0^L dz \int_0^z d\xi \frac{\partial \rho(\xi,t)}{\partial t} = \int_0^L dz\,(L-z)\frac{\partial \rho(z,t)}{\partial t} \qquad \textbf{(3.1.3.1-5)}$$

Substitution of (3.1.3.1-4) and (3.1.3.1-5) into (3.1.3.1-3) leads to

$$\int_0^L dz \frac{\partial G(z,t)}{\partial t} = \frac{d}{dt}\left[L\,G(0,t) + \int_0^L dz\,(L-z)\gamma(z,t) - \int_0^L dz\,(L-z)\frac{\partial \rho(z,t)}{\partial t} \right] \qquad \textbf{(3.1.3.1-6)}$$

We now want to develop a control-volume representation for the right-hand-side of Equation (3.1.3.1-6). Each of the terms on the RHS of (3.1.3.1-6) are evaluated below:

Nodal Approximation to 1st Term on RHS of (3.1.3.1-6)

$$L\,G(0,t) = L\,\hat{G}_1(t). \qquad \text{[Note that L=O(1)]} \qquad \textbf{(3.1.3.1-7)}$$

Nodal Approximation to 2nd Term on RHS of (3.1.3.1-6)

$$\int_0^L dz\,(L-z)\gamma(z,t) = \sum_{j=1}^{N}\int_{z_j}^{z_j+\Delta z} dz\,(L-z)\gamma(z,t) = \sum_{j=1}^{N}(L-\xi_j)\int_{z_j}^{z_j+\Delta z} dz\,\gamma(z,t) \qquad \textbf{(3.1.3.1-8)}$$

where $\xi_j \in (z_j, z_j+\Delta z)$. The mean value theorem[1] has been used in obtaining the result in Equation (3.1.3.1-8).

Expanding $(L-\xi_j)$ about z_j (the inlet of cell j) gives

$$L-\xi_j = L-z_j+(-1)(\xi_j-z_j)+\ldots \qquad \textbf{(3.1.3.1-9)}$$

Since $\xi_j \in (z_j, z_{j+1})$ and $\xi_j - z_j = O(\Delta z)$, Equation (3.1.3.1-9) can be rewritten as

$$L-\xi_j = L-z_j+O(\Delta z). \qquad \textbf{(3.1.3.1-10)}$$

Substitution of (3.1.3.1-10) into (3.1.3.1-8) leads to

$$\begin{aligned}\int_0^L dz\,(L-z)\gamma(z,t) &= \frac{1}{A}\sum_{j=1}^{N}\left\{(L-z_j)\left[A\int_{z_j}^{z_j+\Delta z} dz\,\gamma(z,t)\right]+O(\Delta z^2)\right\} \\ &= \frac{L}{A}\sum_{j=1}^{N}\left(1-\frac{z_j}{L}\right)\Gamma_j(t)+O(\Delta z) \qquad [\textit{Note that } N=O(\Delta z^{-1})]\end{aligned} \qquad \textbf{(3.1.3.1-11)}$$

Nodal Approximation to 3rd term on RHS of (3.1.3.1-6)

The following result is obtained by replacing the integral over the flow region with a summation integrals over the individual nodes:

$$\int_0^L dz(L-z)\frac{\partial\rho(z,t)}{\partial t} = \frac{d}{dt}\int_0^L dz\,(L-z)\,\rho(z,t) = \frac{d}{dt}\sum_{j=1}^{N}\int_{z_j}^{z_j+\Delta z} dz\,(L-z)\,\rho(z,t) \qquad \textbf{(3.1.3.1-12)}$$

---

1 Korn, G.A., and Korn, T.M., *Mathematical Handbook for Scientists and Engineers*, 2nd Edition, pp. 4.7-1 & 4.7-2, McGraw-Hill, NY, 1968.

From the definition of the nodal density $\rho_j(t)$, and from the mean-value theorem,

$$\rho_j(t) = \rho\left[\xi_j(t), t\right] = \frac{1}{\Delta z}\int_{z_j}^{z_j+\Delta z} dz\,\rho(z,t) \quad \textit{where} \quad \xi_j \in (z_j, z_j+\Delta z). \tag{3.1.3.1-13}$$

For the integrals in Equation (3-27), $\rho(z,t)$ is expanded about the point $z = \xi_j$ to obtain

$$\rho(z,t) = \rho(\xi_j,t) + \left(\frac{\partial\rho(z,t)}{\partial z}\right)_{z=\xi_j}(z-\xi_j) + \ldots \textit{where} \quad z \in (z_j, z_{j+1}) \tag{3.1.3.1-14}$$

With the use of Equation (3.1.3.1-13), (3.1.3.1-14) can be expressed as

$$\rho(z,t) = \rho(\xi_j,t) + O(\Delta z) = \rho_j(t) + O(\Delta z) \textit{ where } z \in (z_j, z_{j+1}) \textit{ and } j = 1,\ldots,N. \tag{3.1.3.1-15}$$

Substituting (3.1.3.1-15) into (3.1.3.1-12) gives the following result:

$$\begin{aligned}
\int_0^L dz\,(L-z)\frac{\partial\rho(z,t)}{\partial t} &= \frac{d}{dt}\sum_{j=1}^{N}\int_{z_j}^{z_j+\Delta z} dz\,(L-z)\left[\rho_j(t) + O(\Delta z)\right] \\
&= \sum_{j=1}^{N}\left\{\left[\frac{d\rho_j(t)}{dt}\right]\int_{z_j}^{z_j+\Delta z}(L-z)\,dz + O(\Delta z^2)\right\} \\
&= \sum_{j=1}^{N}\left\{\left[\frac{d\rho_j(t)}{dt}\right]\int_{z_j}^{z_j+\Delta z}(L-z)\,dz\right\} + O(\Delta z) \\
&= \Delta z\sum_{j=1}^{N}\left[\frac{d\rho_j(t)}{dt}\right]\left[L - z_j\right] - \frac{N}{2}\Delta z^2 + O(\Delta z) \\
&= \Delta z\sum_{j=1}^{N}\left[\frac{d\rho_j(t)}{dt}\right]\left[L - z_j\right] + O(\Delta z) \\
&= \Delta z\sum_{j=1}^{N}\left[\frac{\partial\rho_j}{\partial P^*}\frac{dP^*(t)}{dt} + \frac{\partial\rho_j}{\partial\bar{h}_j}\frac{d\bar{h}_j(t)}{dt}\right]\left[L - z_j\right] + O(\Delta z)
\end{aligned} \tag{3.1.3.1-16}$$

Substituting (3.1.3.1-7), (3.1.3.1-11), and (3.1.3.1-16) into (3.1.3.1-6) gives the following nodal approximation to $\int_0^L dz \frac{\partial G(z,t)}{\partial t}$:

$$\int_0^L dz \frac{\partial G(z,t)}{\partial t} = I \frac{dF(t)}{dt} + O(\Delta z) \qquad \textbf{(3.1.3.1-17)}$$

where

$$I = Fluid\ Inertia \equiv (L/A)_{Effective}, \qquad \textbf{(3.1.3.1-18)}$$

and

$$F(t) \equiv A\hat{G}_1(t) + \sum_{j=1}^{N}\left[1-\frac{z_j}{L}\right]\Gamma_j(t) - A\,\Delta z \sum_{j=1}^{N}\left[\frac{\partial \rho_j}{\partial P^*}\frac{dP^*(t)}{dt} + \frac{\partial \rho_j}{\partial \bar{h}_j}\frac{d\bar{h}_j(t)}{dt}\right]\left[1-\frac{z_j}{L}\right] + O(\Delta z) \qquad \textbf{(3.1.3.1-19)}$$

The mass sources considered in SABRE consist of the CRD flow which is deposited in the bottom cell of the bypass channel, borated water which is deposited in the top cell of the lower plenum, and Core Spray flow which is added to the bottom cell of the upper plenum region (feedwater, HPCI, and RCIC injection are included in the steam dome/downcomer model).

3.1.3.2 Nodal Representation of Convective Term

The integral of the convective term in Equation (2.1-3) can be evaluated in terms of variables defined on the region boundaries:

$$\int_0^L dz \frac{\partial\left[(1-\alpha)\rho_\ell u_\ell^2 + \alpha\,\rho_g u_g^2\right]}{\partial z} = \left[(1-\hat{\alpha})\hat{\rho}_\ell\,\hat{u}_\ell^2 + \hat{\alpha}\,\hat{\rho}_g\,\hat{u}_g^2\right]_{N+1} - \left[(1-\hat{\alpha})\hat{\rho}_\ell\,\hat{u}_\ell^2 - \hat{\alpha}\,\hat{\rho}_g\,\hat{u}_g^2\right]_1 \qquad \textbf{(3.1.3.2-1)}$$

3.1.3.3 Nodal Representation for Spatial Integral of Pressure Gradient

The integral of the pressure gradient is evaluated in terms of the channel pressure drop,

$$\int_0^L dz\, g_c \frac{\partial P(z,t)}{\partial z} = g_c\left[P(L,t) - P(0,t)\right] = g_c\left[\hat{P}_{N+1}(t) - \hat{P}_1(t)\right] \qquad \textbf{(3.1.3.3-1)}$$

3.1.3.4 Nodal Representation of Gravitational term

The total elevation head is evaluated in terms of the nodal densities as follows:

$$\int_0^L dz\ \rho(z,t)\, g = g\,\Delta z \sum_{j=1}^{N} \frac{1}{\Delta z} \int_0^L dz\ \rho(z,t) = g\ \Delta z \sum_{j=1}^{N} \rho_j(t) + O(\Delta z). \qquad \textbf{(3.1.3.4-1)}$$

3.1.3.5 Nodal Representation of Wall and Spacer Friction Terms

The wall friction integral is replaced by integrals over individual nodes:

$$\frac{f_W}{2D_h} \int_0^L dz\ \frac{G(z,t)\,|G(z,t)|\,\varphi(z,t)}{\rho_\ell(z,t)} = \frac{f_W}{2D_h} \sum_{j=1}^{N} \int_{z_j}^{z_j+\Delta z} dz\ \frac{G(z,t)|G(z,t)|\,\varphi(z,t)}{\rho_\ell(z,t)}. \qquad \textbf{(3.1.3.5-1)}$$

Following the approach used to derive Equation (3.1.3.1-15), we can obtain the following relations:

$$\varphi(z,t) = \varphi_j(t) + O(\Delta z) \ \textit{where}\ \ z \in (z_j, z_{j+1}) \ \textit{and}\ \ j = 1,\ldots,N, \qquad \textbf{(3.1.3.5-2)}$$

and

$$\rho_\ell(z,t) = \rho_{\ell j}(t) + O(\Delta z) \ \textit{where}\ \ z \in (z_j, z_{j+1}) \ \textit{and}\ \ j = 1,\ldots,N \qquad \textbf{(3.1.3.5-3)}$$

The mass flux G(z,t), where $z \in (z_j, z_{j+1})$, can be approximated by the average of the flow on the control volume boundaries:

$$G(z,t) = \frac{1}{2}\left[\hat{G}_j(t) + \hat{G}_{j+1}(t)\right] + O(\Delta z^2) \qquad \text{for}\ \ z \in (z_j, z_{j+1}). \qquad \textbf{(3.1.3.5-4)}$$

Combining Equations (3.1.3.5-1), (3.1.3.5-2), (3.1.3.5-3), and (3.1.3.5-4) leads to the following result:

$$\frac{f_W}{2D_h} \int_0^L dz\ \frac{G(z,t)|G(z,t)|\varphi(z,t)}{\rho_\ell(z,t)} = \frac{\Delta z\, f_W}{8D_h} \sum_{j=1}^{N} \frac{\left[\hat{G}_j(t) + \hat{G}_{j+1}(t)\right] \left|\hat{G}_j(t) + \hat{G}_{j+1}(t)\right|\ \varphi_j(t)}{\rho_{\ell j}(t)} + O(\Delta z) \qquad \textbf{(3.1.3.5-5)}$$

Similarly, the fuel-spacer friction term in Equation (2.1-3) can be integrated over the channel length to obtain

$$\frac{f_S}{2D_h} \int_0^L dz\ \frac{G(z,t)\,|G(z,t)|\,\Phi(z,t)}{\rho_\ell(z,t)} = \frac{\Delta z\, f_S}{8D_h} \sum_{j=1}^{N} \frac{\left[\hat{G}_j(t) + \hat{G}_{j+1}(t)\right] \left|\hat{G}_j(t) + \hat{G}_{j+1}(t)\right|\ \Phi_j(t)}{\rho_{\ell j}(t)} + O(\Delta z) \qquad \textbf{(3.1.3.5-6)}$$

3.1.3.6 Nodal Representation of Channel Inlet and Outlet Friction Terms

From the definition of the Delta function,

$$\frac{K_1}{2}\int_0^L dz \frac{G(z,t)\,|G(z,t)|\,\Phi(z,t)\,\delta(z-0)}{\rho_\ell(z,t)} = \frac{K_1}{2}\frac{G(0,t)\,|G(0,t)|\,\Phi(0,t)}{\rho_\ell(0,t)}$$
$$= \frac{K_1}{2}\frac{\hat{G}_1(t)\,|\hat{G}_1(t)|\,\hat{\Phi}_1(t)}{\hat{\rho}_{\ell 1}(t)}. \qquad \textbf{(3.1.3.6-1)}$$

Similarly, for the channel outlet friction term we have

$$\frac{K_2}{2}\int_0^L dz \frac{G(z,t)\,|G(z,t)|\,\Phi(z,t)\,\delta(z-L)}{\rho_\ell(z,t)} = \frac{K_2}{2}\frac{G(L,t)\,|G(L,t)|\,\Phi(L,t)}{\rho_\ell(L,t)}$$
$$= \frac{K_2}{2}\frac{\hat{G}_{N+1}(t)\,|\hat{G}_{N+1}(t)|\,\hat{\Phi}_{N+1}(t)}{\hat{\rho}_{\ell\,N+1}(t)}. \qquad \textbf{(3.1.3.6-2)}$$

3.1.3.7 Overall Momentum Equations

Combining the results in (3.1.3.1-17), (3.1.3.2-1), (3.1.3.3-1), (3.1.3.4-1), (3.1.3.5-5), (3.1.3.5-6), (3.1.3.6-1), and (3.1.3.6-2) yields the overall momentum equation for the flow channel,

$$I\frac{dF(t)}{dt} + M(t) = g_c\left[\hat{P}_1(t) - \hat{P}_{N+1}(t)\right] \qquad \textbf{(3.1.3.7-1)}$$

where F(t) is defined by (3.1.3.1-19), and M(t) is given by

$$M(t) \equiv \left\{ \left[1-\hat{\alpha}(t)\right] \hat{\rho}_\ell(t)\, \hat{u}_\ell^2(t) + \hat{\alpha}(t)\, \hat{\rho}_g(t)\, \hat{u}_g^2(t) \right\}_{N+1}$$

$$- \left\{ \left[1-\hat{\alpha}(t)\right] \hat{\rho}_\ell(t)\, \hat{u}_\ell^2(t) + \hat{\alpha}(t)\, \hat{\rho}_g(t)\, \hat{u}_g^2(t) \right\}_1$$

$$+ \frac{\Delta z\, f_W}{8 D_h} \sum_{j=1}^{N} \frac{\left[\hat{G}_j(t) + \hat{G}_{j+1}(t)\right] \left|\hat{G}_j(t) + \hat{G}_{j+1}(t)\right| \varphi_j(t)}{\rho_{tj}(t)}$$

$$+ \frac{\Delta z\, f_S}{8 D_h} \sum_{j=1}^{N} \frac{\left[\hat{G}_j(t) + \hat{G}_{j+1}(t)\right] \left|\hat{G}_j(t) + \hat{G}_{j+1}(t)\right| \Phi_j(t)}{\rho_{tj}(t)}$$

$$+ \frac{K_1}{2} \frac{\hat{G}_1(t) \left|\hat{G}_1(t)\right| \hat{\Phi}_1(t)}{\hat{\rho}_1^{\ell}(t)} + \frac{K_2}{2} \frac{\hat{G}_{N+1}(t) \left|\hat{G}_{N+1}(t)\right| \hat{\Phi}_{N+1}(t)}{\hat{\rho}_{N+1}^{\ell}(t)} + O(\Delta z). \qquad \textbf{(3.1.3.7-2)}$$

An overall momentum equation for the entire circulation path, from the jet pump inlet to the separator outlet, is obtained by summing the regional momentum equations (Equation 3.1.3.7-1) for the jet pump, lower plenum, mixing region, core, upper plenum, riser, and separator regions:

$$\frac{dF_{Loop}}{dt} + M_{Loop} = g_c \left(P^0 - P^*\right) + O(\Delta z) \qquad \textbf{(3.1.3.7-3)}$$

where

$$F_{Loop} \equiv \sum_{k \neq B} I_k F_k \quad \textit{and} \quad M_{Loop} \equiv \sum_{k \neq B} M_k \,. \qquad \textbf{(3.1.3.7-4)}$$

The subscript k is used here to identify the various flow regions. k can take the following values J, L, C, B, U, R, or S which refer to the jet pump, lower plenum, core, bypass, upper plenum, riser, and separator regions, respectively. In (3.1.3.7-3), P^0 is the pressure within the downcomer region at the elevation of the jet pump throat, and P^* is the steam dome pressure. In formulating the momentum equation for the natural circulation loop, the inertia associated with the upper and lower reflectors are neglected.

An additional momentum equation, independent of the unknown regional boundary pressures, can be obtained by subtracting the individual momentum equations for the core and bypass regions. The resultant expression is

$$\frac{d\left[I_C F_c(t) - I_B F_B(t)\right]}{dt} = M_B(t) - M_C(t) + O(\Delta z) \qquad \textbf{(3.1.3.7-5)}$$

Equations (3.1.3.7-3) and (3.1.3.7-5) are the momentum relations which are solved in SABRE to obtain the reactor flow behavior.

3.1.4 Nodalized Fuel and Cladding Heat Balance Equations

The regions occupied by fuel and cladding are also divided into control volumes of length Δz. Integration of the heat balance equations (2.3-1), (2.3-2) and (2.3-3) over the control volume length of the core Δz, leads to a set of ordinary differential equations for the fuel and cladding nodal temperatures $T_{fa,j}$, $T_{fb,j}$ *and* $T_{ct,j}$ respectively:

$$\left(\rho_{fa}C_{p,fa}\right)_j r_a^2 \frac{dT_{fa,j}}{dt} = -\frac{2k_{fa,j}\left(T_{fa,j}-T_{fb,j}\right)}{\ln\left(\frac{r_a+r_b}{r_a\sqrt{2}}\right)} + S_j\, r_a^2\, \overline{q}'''_{fa,j} \qquad \textbf{(3.1.4-1)}$$

$$\left(\rho_{fb}C_{p,fb}\right)_j\left(r_b^2-r_a^2\right)\frac{dT_{fb,j}}{dt} = \frac{2k_{fa,j}\left(T_{fa,j}-T_{fb,j}\right)}{\ln\left(\frac{r_a+r_b}{r_b\sqrt{2}}\right)} - \frac{\left(T_{fb,j}-T_{ct,j}\right)}{\left[\frac{\left(r_b-r_a\right)}{4r_b k_{fb,j}}+\frac{1}{2r_{ci}H_g}+\frac{\left(r_{co}-r_{ci}\right)}{4r_{co}k_{ct,j}}\right]} + \left(r_b^2-r_a^2\right)\overline{q}'''_{fb,j}, \qquad \textbf{(3.1.4-2)}$$

and

$$\left(\rho_{ct}C_{p,ct}\right)_j\left(r_{co}^2-r_{ci}^2\right)\frac{dT_{ct,j}}{dt} = \frac{\left(T_{fb,j}-T_{ct,j}\right)}{\left[\frac{\left(r_b-r_a\right)}{4r_b k_{fb,j}}+\frac{1}{2r_{ci}H_g}+\frac{\left(r_{co}-r_{ci}\right)}{4r_{co}k_{ct,j}}\right]} - \frac{\left(T_{ct,surf,j}-T_{cool,j}\right)}{\left[\frac{1}{2r_{co}H_{film,j}}\right]}, \qquad \textbf{(3.1.4-3)}$$

where

$$q'''_j(t) = \left[\frac{Q_f(t)\;S_j(t)}{N_c\,V_{f,j}}+\frac{Q_d(t)\,S_j(0)}{N_c\,V_{f,j}}\right](1-fq_1-fq_2),$$

$$q'''_{fa,j}(t) = C_s\; q'''_j(t),$$

$$q'''_{fb,j}(t) = \left(2-C_s\right) q'''_j(t),$$

$V_{f,j}$ = volume of fuel in axial control volume j of the active core region (ft^3),

fq_1 = fraction of total core power deposited in active core region as direct moderator heating,

fq_2 = fraction of total core power deposited in bypass region as direct moderator heating,

N_c = number of control volumes in active core region,

$Q_f(t)$ = total core fission power (Btu/sec),

$Q_d(t)$ = total decay heat generation rate (Btu/sec),

$S_j(t)$ = axial power shape function = (power in node j)/(average nodal power), and

C_s = fraction of pin power generated in inner radial fuel node.

Note that the subscript j defines the axial node within the active fuel region (j=1, 2, ..., 25). All other variables have been defined previously (see §2.3).

Calculation of the heat flux to the coolant within the reactor core requires determination of the clad surface temperature. The surface temperatures are calculated from (see 2.3-4)

$$\left(\rho_{ct}C_{p,ct}\right)_j\left(r_{co}^2-r_{ci}^2\right)\frac{dT_{ct,surf,j}}{dt}=\frac{\left(T_{fb,j}-T_{ct,surf,j}\right)}{\left[\frac{\left(r_b-r_a\right)}{4r_bk_{f2,j}}+\frac{1}{2r_{ci}H_g}+\frac{\left(r_{co}-r_{ci}\right)}{2r_{co}k_{ct,j}}\right]}-\frac{\left(T_{ct,surf,j}-T_{cool,j}\right)}{\left[\frac{1}{2r_{co}H_{film,j}}\right]}, \tag{3.1.4-4}$$

3.2 Calculation of the Flow Regime

In Section 3.1.3, two spatially-integrated momentum equations were derived (Equations 3.1.3.7-3 and 3.1.3.7-5). These equations define two flow rates within the reactor circulation path, namely the jet pump inlet flow rate $\hat{G}_{J1}$ and the core inlet flow rate $\hat{G}_{C1}$. Once these two flow rates are specified, the flow behavior within the entire loop is determined by continuity and energy constraints in conjunction with the flow-regime model, i.e., the Drift-Flux relation (2.1-7). The present section describes the calculational method used to determine the local reactor flow rates given the two inlet flows, $\hat{G}_{J1}$ and $\hat{G}_{C1}$.

Given the jet pump inlet flow, the outlet flow conditions for the jet pump region are computed from the nodal continuity and energy equations along with the Drift-Flux relation. Once the jet pump outlet flow is computed it defines the inlet flow to the lower plenum region. The same computation is then carried out for the lower plenum region: namely, the continuity, energy, and Drift-Flux equations are used to compute the lower-plenum outlet flow. Thus, the scheme provides a method of computing the flows sequentially as it "marches" through the circulation loop. In order to compute the flows at the outlet of the lower reflector where the flow branches into the active core and the core bypass, additional information is required; this is where the value of $\hat{G}_{C1}$ is used.

Details of the computational scheme will now be given. First, use of the Drift-Flux relation (2.1-7) will be discussed. At the j'th junction between two control volumes, this relation becomes

$$\left(\hat{\alpha}_j\,\hat{C}_{0,j}-1\right)\hat{u}_{gj}+\hat{C}_{0,j}\left(1-\hat{\alpha}_j\right)\hat{u}_{\ell j}=-\hat{V}_{gj,j} \qquad \textbf{(3.2-1)}$$

Similarly, the mass flux at junction j is given by (see Equation 2.1-6)

$$\hat{G}_j=\hat{\rho}_{\ell j}\left(1-\hat{\alpha}_j\right)\hat{u}_{\ell j}+\hat{\rho}_{gj}\,\hat{\alpha}_j\,\hat{u}_{gj} \qquad \textbf{(3.2-2)}$$

If the value of the junction mass flux is specified, then Equations (3.1-1) and (3.2-2) can be solved for the vapor and liquid velocities. Values of $\hat{\alpha}_j$, $\hat{C}_{0,j}$, $\hat{V}_{gj,j}$, $\hat{\rho}_{\ell j}$, and $\hat{\rho}_{gj}$ are determined from the adjacent volumetric values. The particular volumetric value used, i.e., the upwind or downwind value, depends on the direction of the phasic velocities. This is discussed in more detail below.

For determining junction variables from volumetric quantities, it is computationally convenient to introduce two limiting values of the coolant mass flux, $\hat{G}_{\Downarrow j}$ and $\hat{G}_{\Uparrow j}$. If $\hat{G}_j > \hat{G}_{\Uparrow j}$, then the flow regime is co-current upward. If $\hat{G}_j < \hat{G}_{\Downarrow j}$, then the flow is co-current downward. In order to obtain defining expressions for $\hat{G}_{\Uparrow j}$ and $\hat{G}_{\Downarrow j}$, Equations (3.2-1) and (3.2-2) are solved for the vapor and liquid velocities,

$$\hat{u}_{gj} = \frac{\hat{G}_j \hat{C}_{0,j} + \hat{V}_{gj,j}\ \hat{\rho}_{\ell j}}{\hat{\alpha}_j\ \hat{\rho}_{gj}\ \hat{C}_{0,j} + \left(1 - \hat{\alpha}_j \hat{C}_{0,j}\right)} \qquad \textbf{(3.2-3)}$$

and

$$\hat{u}_{\ell j} = \frac{\hat{G}_j \left(1 - \hat{\alpha}_j\ \hat{C}_{0,j}\right) - \hat{\alpha}_j\ \hat{\rho}_{gj}\ \hat{V}_{gj,j}}{\left[\hat{\alpha}_j\ \hat{\rho}_{gj}\ \hat{C}_{0,j} + \left(1 - \hat{\alpha}_j \hat{C}_{0,j}\right)\right]\left(1 - \hat{\alpha}_j\right)}. \qquad \textbf{(3.2-4)}$$

From the definition of C_0 [see Lahey & Moody, *The Thermal-Hydraulics of a Boiling Water Nuclear Reactor* (1976), p. 206], it can be seen that the quantity $(1-\alpha C_0)$ is positive or zero. Then from (3.2-4), the flow is co-current upward ($\hat{u}_{\ell j} > 0$) if the numerator in (3.2-4) is greater than zero. This leads to the following flow-regime criterion expressed in terms of the known volumetric quantities:

$$\hat{G}_j > \hat{G}_{\Uparrow j} \equiv \frac{\alpha_{j-1}\ \rho_{gj-1}\ V_{gj,j-1}}{1 - \alpha_{j-1}\ C_{0,j-1}} \qquad \textit{(Co-current upward flow).} \qquad \textbf{(3.2-5)}$$

Similarly, the flow is co-current downward if the numerator in (3.2-3) is negative,

$$\hat{G}_j < \hat{G}_{\Downarrow j} \equiv \frac{-V_{gj,j}\ \rho_j^{\ell}}{C_{0,j}} \qquad \textit{(Co-current downward flow).} \qquad \textbf{(3.2-6)}$$

Note the upwind/downwind scheme used in determining these flow-regime limits.

It follows that counter-current flow is defined by

$$\hat{G}_{\Downarrow j} < \hat{G}_j < \hat{G}_{\Uparrow j} \qquad \textit{(Counter-current flow).} \qquad \textbf{(3.2-7)}$$

In the counter-current flow regime, junction variables are calculated as a weighted average of the adjacent volumetric values. Observe that when $\hat{G}_j = \hat{G}_{\Uparrow j}$, the liquid velocity is zero because this is the dividing point between positive and negative liquid flow. Also, when $\hat{G}_j = \hat{G}_{\Downarrow j}$ the gas velocity is zero since this is the dividing point between positive and negative gas flow. Therefore,

$$\hat{w}_{gj} = 0 \quad \text{if} \quad \hat{G}_j = \hat{G}_{\Downarrow j} \qquad \textbf{(3.2-8)}$$

and

$$\hat{w}_{gj} = \hat{G}_j \hat{A}_j \quad \text{if} \quad \hat{G}_j = \hat{G}_{\Uparrow j} \qquad \textbf{(3.2-9)}$$

where

$\hat{w}_{gj}$ = mass flow rate of vapor at junction j (Lbm/sec), and

$\hat{A}_j$ = flow area of junction j (ft^2).

Given the junction mass flux, Equations (3.2-8) and (3.2-9) define the mass flow of vapor at the boundaries of the counter-current flow regime. In SABRE, the vapor flow rate within the counter-current flow regime is computed from linear interpolation, and the liquid flow rate is calculated from conservation of mass. That is

$$\hat{w}_{gj} = \frac{\hat{G}_{\Uparrow j}\left(\hat{G}_j - \hat{G}_{\Downarrow j}\right)\hat{A}_j}{\left(\hat{G}_{\Uparrow j} - \hat{G}_{\Downarrow j}\right)} \quad \text{for} \quad \hat{G}_{\Downarrow j} < \hat{G}_j < \hat{G}_{\Uparrow j} \tag{3.2-10}$$

and

$$\hat{w}_{\ell j} = \hat{G}_j \hat{A}_j - \hat{w}_{gj} \quad \text{for} \quad \hat{G}_{\Downarrow j} < \hat{G}_j < \hat{G}_{\Uparrow j}. \tag{3.2-11}$$

Table 3.2-1 summarizes the calculational scheme used to obtain junction variables from the known control volume quantities.

With the above results, description of the computational scheme for the local flow rates within the circulation loop can now be completed. In the calculation of local flows, $\hat{G}_{J1}$, $\hat{G}_{C1}$, and dP^*/dt are given (from momentum conservation and steam-dome/downcomer conservation equations). All of the remaining junction flows are then computed from continuity and energy constraints along with the Drift-Flux relation. The calculation scheme begins at the jet pump inlet. Since $\hat{G}_{J1}$ is specified, the junction variables at the inlet boundary are computed according to Table 3.2-1. The flow of mass and energy across the jet pump inlet is now defined. In order to calculate the flow of mass and energy across the outlet boundary, Equations (3.1.1-6) and (3.1.2-7) are solved for the temporal pressure derivative dP^*/dt,

$$\frac{dP^*}{dt} = \frac{d_2 a_{11} - d_1 a_{21}}{a_{11} a_{22} - a_{21} a_{12}} \tag{3.2-12}$$

where

$$a_{11} = \Delta z A \frac{\partial \rho_j}{\partial \bar{h}_j},$$

$$a_{12} = \Delta z A \frac{\partial \rho_j}{\partial P^*},$$

$$a_{21} = \Delta z A \left(\rho_j + \bar{h}_j \frac{\partial \rho_j}{\partial \bar{h}_j} \right),$$

$$a_{22} = -\Delta z A \left(\frac{1}{J} - \bar{h}_j \frac{\partial \rho_j}{\partial P^*} \right),$$

$d_1 = \quad \hat{w}_{g\,j} + \hat{w}_{\ell\,j} + \Gamma_j$, and

$d_2 = \quad \hat{w}_{g\,j}\ \hat{h}_{g\,j} + \hat{w}_{\ell\,j}\ \hat{h}_{\ell\,j} - \hat{w}_{g\,j+1}\ \hat{h}_{g\,j+1} - \hat{w}_{\ell\,j+1}\ \hat{h}_{\ell\,j+1} + Q_j + \Delta z\ P_h\ q''_j + h_{s\,j}\ \Gamma_j$.

Since $\hat{w}_{g\,j+1}$, $\hat{w}_{\ell\,j+1}$, $\hat{h}_{g\,j+1}$, and $\hat{h}_{\ell\,j+1}$ are all functions of the outlet boundary mass flux $\hat{G}_{j+1}$ (as described in Table 3.2-1), the only unknown on the RHS of Equation 3-63 is $\hat{G}_{j+1}$. As stated earlier, dP^*/dt is known at this stage of the calculation (calculation of dP^*/dt, $\hat{G}_{J1}$, and $\hat{G}_{C1}$ is discussed in the next Section). The known value of the pressure derivative is denoted as $\left(dP^*/dt\right)_0$. Subtracting $\left(dP^*/dt\right)_0$ from (3.2-12) results in the following algebraic equation for $\hat{G}_{j+1}$,

$$\Psi\left(\hat{G}_{j+1}\right) \equiv \frac{d_2\ a_{11} - d_1\ a_{21}}{a_{11}\ a_{22} - a_{21}\ a_{12}} - \left(\frac{dP^*}{dt}\right)_0 = 0 \qquad \textbf{(3.2-13)}$$

Newton's method is used to solve Equation (3.2-13) for the outlet flow, $\hat{G}_{j+1}$, of node j. A bisection procedure is used in the event the Newton's iteration fails to converge.

Once Equation (3.2-13) is solved for the jet pump region, the flow of mass and energy across the inlet boundary of the lower plenum region is determined. The solution process is then continued in a step-wise manner: equation (3.2-13) is solved for the lower plenum region to obtain the flow of mass and energy across the inlet boundary of the lower reflector region.

At the outlet of the lower reflector region, the flow branches into the core and bypass channels. Here the generalized continuity and energy equations (3.1.1-7) & (3.1.2-8) are solved. Since the inlet flow to the core $\hat{G}_{C1}$ is specified, the convective terms in (3.1.1-7) & (3.1.2-8) associated with mass and energy transport across the core inlet can be evaluated according to the scheme summarized in Table 3.2-1. The flow of mass and energy across the bypass inlet boundary can then be determined by solving the generalized form of (3.2-13). Local flows along the core and bypass channels are then computed sequentially through solution of (3.2-13). For the first node of the upper plenum, the generalized mass and energy balance equations, (3.1.1-7) & (3.1.2-8), are solved because there are two flow streams at the inlet of the upper plenum. For the riser and separator regions. there is only one flow stream on the inlet and outlet boundaries, therefore (3.1.1-6) and (3.1.2-7) are used to obtain the flow of mass and energy across the region boundaries.

Table 3.2-1

Computational Scheme for Determining Variables at Flow Junctions.

Junction Variable	Value of Junction Variable		
	$\hat{G}_j < \hat{G}_{\Downarrow j}$	$\hat{G}_{\Downarrow j} < \hat{G}_j < \hat{G}_{\Uparrow j}$	$\hat{G}_j > \hat{G}_{\Uparrow j}$
$\hat{\rho}_{\ell j}$	$\rho_{\ell\, j+1}$	$\rho_{\ell\, j+1}$	$\rho_{\ell\, j}$
$\hat{\rho}_{g j}$	$\rho_{g\, j+1}$	$\rho_{g\, j}$	$\rho_{g\, j}$
$\hat{h}_{\ell j}$	$h_{\ell\, j+1}$	$h_{\ell\, j+1}$	$h_{\ell\, j}$
$\hat{h}_{g j}$	$h_{g\, j+1}$	$h_{g j}$	$h_{g j}$
$\hat{\alpha}_j$	α_{j+1}	$\alpha_{j+1} + \frac{(\alpha_j - \alpha_{j+1})}{(\hat{G}_{\Uparrow j} - \hat{G}_{\Downarrow j})}(\hat{G}_j - \hat{G}_{\Downarrow j})$	α_j
$\hat{C}_{0,j}$	$C_{0,j+1}$	$C_{0,j+1} + \frac{(C_{0,j} - C_{0,j+1})}{(\hat{G}_{\Uparrow j} - \hat{G}_{\Downarrow j})}(\hat{G}_j - \hat{G}_{\Downarrow j})$	$C_{0,j}$
$\hat{V}_{gl,j}$	$\hat{V}_{gl,j+1}$	$V_{gl,j+1} + \frac{(V_{gl,j} - V_{gl,j+1})}{(\hat{G}_{\Uparrow j} - \hat{G}_{\Downarrow j})}(\hat{G}_j - \hat{G}_{\Downarrow j})$	$V_{gl,j}$
$\hat{w}_{g j}$	$\hat{u}_{g j}\, \hat{\alpha}_j\, \hat{\rho}_{g j}\, \hat{A}_j$	$\frac{\hat{G}_{\Uparrow j}(\hat{G}_j - \hat{G}_{\Downarrow j})\hat{A}_j}{(\hat{G}_{\Uparrow j} - \hat{G}_{\Downarrow j})}$	$\hat{u}_j^g\, \hat{\alpha}_j\, \hat{\rho}_g^j\, \hat{A}_j$
$\hat{w}_{\ell j}$	$\hat{G}_j\, \hat{A}_j - \hat{w}_{g j}$	$\hat{G}_j\, \hat{A}_j - \hat{w}_{g j}$	$\hat{G}_j\, \hat{A}_j - \hat{w}_{g j}$

Table 3.2-1 (Cont'd)
Computational Scheme for Determining Variable at Flow Junctions.

Junction Variable	Value of Junction Variable		
	$\hat{G}_j < \hat{G}_{\Downarrow j}$	$\hat{G}_{\Downarrow j} < \hat{G}_j < \hat{G}_{\Uparrow j}$	$\hat{G}_j > \hat{G}_{\Uparrow j}$
$\hat{u}_{gj}$	$\dfrac{\dfrac{\hat{C}_{0,j}\hat{G}_j}{\hat{\rho}_{\ell j}} + \hat{V}_{gj,j}}{1-\hat{\alpha}_j \hat{C}_{0,j}\left(1-\dfrac{\hat{\rho}_{gj}}{\hat{\rho}_{\ell j}}\right)}$	$\dfrac{\hat{w}_{gj}}{\hat{\alpha}_j\ \hat{\rho}_{gj}\ \hat{A}_j}$	$\dfrac{\dfrac{\hat{C}_{0,j}\hat{G}_j}{\hat{\rho}_j^{\ell}} + \hat{V}_{gj,j}}{1-\hat{\alpha}_j\ \hat{C}_{0,j}\left(1-\dfrac{\hat{\rho}_{gj}}{\hat{\rho}_{\ell j}}\right)}$
$\hat{u}_{\ell j}$	$\dfrac{\left(1-\hat{\alpha}_j\ \hat{C}_{0,j}\right)\left(\hat{G}_j - \dfrac{\hat{\alpha}_j\ \hat{\rho}_{gj}\ \hat{V}_{gj,j}}{1-\hat{\alpha}_j\hat{C}_{0,j}}\right)}{\hat{\rho}_{\ell j}\left(1-\hat{\alpha}_j\right)\left(1-\hat{\alpha}_j\ \hat{C}_{0,j}\left[1-\dfrac{\hat{\rho}_{gj}}{\hat{\rho}_{\ell j}}\right]\right)}$	$\dfrac{\hat{w}_{\ell j}}{\hat{\rho}_{\ell j}\left(1-\hat{\alpha}_j\right)\hat{A}_j}$	$\dfrac{\left(1-\hat{\alpha}_j\hat{C}_{0,j}\right)\left(\hat{G}_j - \dfrac{\hat{\alpha}_j\ \hat{\rho}_{gj}\ \hat{V}_{gj,j}}{1-\hat{\alpha}_j\hat{C}_{0,j}}\right)}{\hat{\rho}_{\ell j}\left(1-\hat{\alpha}_j\right)\left(1-\hat{\alpha}_j\ \hat{C}_{0,j}\left[1-\dfrac{\hat{\rho}_{gj}}{\hat{\rho}_{\ell j}}\right]\right)}$

3.3 Calculation of $\hat{G}_{J1}, \hat{G}_{C1}$, and dP^*/dt

In §3.2, calculation of the nodal boundary flows assumed that the jet pump inlet flow $\hat{G}_{J,1}$, core-inlet flow $\hat{G}_{C,1}$, and the rate of change of the system pressure dP^*/dt are all given. This section discusses the calculation of these three quantities.

$\hat{G}_{J,1}$ and $\hat{G}_{C,1}$ are determined from solution of the spatially-integrated momentum equations (3.1.3.7-3) and (3.1.3.7-5). Temporal integration of these two equations is accomplished using the implicit Euler's method. The finite-difference approximations for Equations (3.1.3.7-3) and (3.1.3.7-5) are

$$F_{Loop}(t) - F_{Loop}(t-\Delta t) + \Delta t \left\{ M_{Loop}(t) - g_c \left[P^0(t) - P^*(t) \right] \right\} = 0 \qquad \textbf{(3.3-1)}$$

and

$$\left[I_C F_C(t) - I_B F_B(t) \right] - \left[I_C F_C(t-\Delta t) - I_B F_B(t-\Delta t) \right] - \Delta t \left[M_B(t) - M_C(t) \right] = 0. \qquad \textbf{(3.3-2)}$$

In (3.3-1) and (3.3-2), $F_{Loop}(t)$, $M_{Loop}(t)$, and $\left[I_C F_C(t) - I_B F_B(t) \right]$ are functions of all the nodal flows throughout the reactor system as well as the rate of change of the system pressure dP^*/dt. However, as discussed in Section 3.2, all of the local flows are determined, through continuity and energy constraints, once the jet-pump-inlet flow, core-inlet flow, and rate of change of system pressure are specified. (At this stage of the calculation process, the fluid enthalpy, density, and system pressure are all known because the equations governing these variables are integrated explicitly. This is discussed further in the next section.) Consequently, there are three basic unknowns, $\hat{G}_{J1}, \hat{G}_{C1}$, *and* dP^*/dt, associated with the two relations defined by (3.1-1) and (3.3-2). The additional constraint required for closure of the system is provided by the downcomer and steam dome mass and energy relations. Solution of the full system of equations is accomplished as described below:

1. An initial estimate of $\hat{G}_{J,1}$ and $\hat{G}_{C,1}$ is provided by the values of these variables at the previous time step.

2. dP^*/dt is computed from Equations (2.2-1)-(2.2-4). In calculating dP^*/dt, the value of $\hat{G}_{S,2}$ (mass flux at the separator outlet) from the previous time step is used.

3. The nodal flowrates within the reactor are computed by the scheme described in §3.2.

4. Newton's method is used to obtain an improved estimate of $\hat{G}_{J,1}$ and $\hat{G}_{C,1}$ (a nested bisection procedure is used in the event the Newton's iteration fails to converge).

5. Steps 2-4 are repeated until convergence is obtained.

3.4 Initialization and Temporal Integration Procedures

All transient simulations are initiated at or near normal reactor operating conditions. In the initialization process, the total reactor power, total core flow (active-core flow plus core-bypass flow), reactor pressure, downcomer water level, and downcomer subcooling are specified. A SIMTRAN output file provides cross-section data for the 1-D kinetics solution. The code then calculates the neutron flux distribution, delayed-neutron precursors, and the axial power shape by solving the eigenvalue problem associated with the steady, two-group diffusion equations (see §2.4.3). It is important that the base cross-section set in the SIMTRAN output (Cross-section set 1 of 7 described in §2.4.8) correspond as close as possible to the initial conditions specified in the SABRE input deck as this will effect the accuracy of the initial flux and power distribution. This is due to the fact that the moderator density and fuel temperature perturbations Δu_j *and* $\Delta\sqrt{T_{f,j}}$ in Eq. (2.4.1-1), and in the analogous expressions for the other neutronic parameters, are all assumed to be zero at the initial reactor state.

Once the initial power distribution is determined, the initial local flow conditions are computed along with the fuel and cladding temperatures and the pump power required to maintain the specified core flow. It is implicitly assumed that the reactor is critical at the initial specified operating condition.

Since the steady-state equations are solved sequentially to obtain first the initial neutron flux distribution and then the initial flow and fuel temperature distributions, it is difficult to obtain an initial reactor state which is completely absent of small initial disturbances. Therefore, once the initial power and flow conditions are computed through sequential solution of the steady equations, a second level initialization process is initiated to remove any small perturbations which may otherwise appear at the start of the transient simulation. This second level initialization process consists of running the code in the transient mode starting at a negative time (-40 seconds) and then integrating up to t=0. The solution results for t<0 are not printed to any of the SABRE output files so that this process is transparent to the code user. During this phase of the initialization process, small adjustments are made to the value of k_{eff} in Eqs. (2.4.4.-10) and (2.4.4-12), and to the pressure regulator setpoint (see Figure 2.6-1), so that when the governing equations are integrated through negative time and reach zero, the total power and reactor pressure are as close as possible to the values specified in the SABRE input file. Typically, the adjustment to k_{eff} is on the order of a few *mk*. Printing to the SABRE output files begins when t≥0.

The transient kinetics equations are implicitly integrated as described in §2.4.4. All of the governing thermal-hydraulic equations are integrated explicitly except for the two momentum equations (3.1.3.7-3) and (3.1.3.7-5), and the equations governing the cladding surface temperature (3.1.4-4). The explicit temporal integration is carried out with Euler's method. An outline of the overall numerical solution procedure is summarized below:

1. Using the thermal-hydraulic time step size specified as part of the SABRE input data, $\bar{h}_{k,j}, P^*, P^0, W_{stm}, V_{SD}, \bar{h}_D, \bar{h}_{SD}, T_{f1,j}, T_{f2,j}, T_{cl,j}, C_i, Q_d$, and all containment parameters are obtained by explicit temporal integration.

2. Vapor and liquid-phase density and enthalpy are computed according to (2.1-8) to (2.1-10).

3. Coolant void fraction and mixture density are calculated from (2.1-4) and (2.1-5) since $\rho_\ell, \rho_g, h_\ell, h_g$, *and* $\bar{h}$ are known at this point. $\partial\rho/\partial\bar{h}$ *and* $\partial\rho/\partial P^*$ are then computed for each control volume.

4. Clad surface temperature is calculated by integrating (3.1.4-4) using the implicit Euler's method. The heat flux to the coolant is then computed. In carrying out the implicit integration of (3.1.4-4), an initial estimate for $T_{surf,j}$ is obtained from the result of the previous step.

5. The two overall momentum equations (3.1.3.7-3) and (3.1.3.7-5) are integrated implicitly (see §3.3). The temporal integration involves the solution of two coupled transcendental equations [(3.3-1) and (3.3-2)] for the jet pump and core inlet flows . These two equations are solved using a Newton's iteration scheme. Each iteration involves calculation of all the nodal flows in the reactor system. The local flows are computed according to the procedure outlined in §3.2. When convergence of the jet pump and core inlet flows is obtained, the thermal-hydraulic time step is complete.

6. After completion of a thermal-hydraulic time step, the LSODES ODE solver is called, and the 1-D kinetics equations are integrated to obtain a solution at the time corresponding to the current hydraulic solution. Once the kinetics solution is obtained at the new time level, the process begins again at Step 1.

4. DISCUSSION OF CODE LIMITATIONS

In this section, the major SABRE modeling deficiencies are identified, and the effects of these code limitations on calculational results are discussed.

4.1 Single-Channel Core Model

SABRE models the 764 fuel channels contained within the SSES reactor core as a single average-power channel with a flow area equal to the combined area of the individual channels. This modeling approach causes the code to over-predict the period of nuclear-coupled density-wave oscillations. With a single-channel model, any core flow oscillations are accompanied by oscillations of similar magnitude in the rest of the flow path inside the shroud. Thus, inertial and frictional effects in the entire flow path from the jet pump inlet to the separator outlet have a strong influence on the oscillation dynamics. In the case of a multiple core-channel model, however, not all of the individual core channels oscillate in-phase. This out-of-phase mode allows significant flow oscillations in the core channels with relatively small flow oscillations in the regions external to the core. Since the fluid inertia is smaller in this latter case, and the influence of fluid friction is more spatially concentrated, a shorter oscillation period is anticipated. A single core channel model will always over-predict the power/flow oscillation period because it is simulates all core channels oscillating in-phase.

4.2 Steam Line Model and Feedwater Controller

The SABRE code contains a single-volume steam line model; thus, the details of acoustic wave propagation within the steam lines is neglected. In addition, SABRE employs a proportional control model to simulate the effect of the feedwater control system on the reactor dynamic behavior. Although this model accounts for the basic function of the controller, which is to maintain downcomer water level in the neighborhood of the set point value, it neglects dynamics associated with the various time constants which characterize controller operation.

4.3 Separator Model

The separator model used in SABRE effects complete vapor/liquid separation at the exit of the separator region (see Figure 2-1) which is above normal water level. In actuality, the steam separators discharge liquid through a path in the side of the separator at a location below normal water level. Thus, at normal water level conditions the SABRE model under-predicts the flow path pressure drop for the liquid exiting the separator since it does not account for the hydrodynamic head associated with the liquid above the exit of the liquid discharge path. The SABRE code also neglects carry-over and carry-under effects associated with non-ideal separator operation.

4.4 Downcomer Water Level

Generally, SABRE has numerical difficulties if downcomer mixture level drops below the jet pump throat.

5. CODE BENCHMARKING

5.1 MSIV Closure with Scram—Comparison to Plant Data

In this Section, SABRE results are compared to plant data for an MSIV closure event which occurred at Susquehanna Unit 1 on 6/14/83 at 0947. The scram was the result of Main Steam Line High Radiation levels which occurred because of operational problems with the condensate demineralizers. The GETARS data for this event are logged on the General Office computer system on Tape #31; the case number is 83070615023101. Data is extracted from PP&L mainframe computer storage by typing 'cndas50 extract' in a TSO session and then following the prompts.

A summary of event-specific code input parameters used in the SABRE calculation is given in Table 5.1-1. The sequence of events calculated by SABRE is presented in Table 5.1-2. This SABRE calculation corresponds to Case 01 in the Computer Case Summary.

Comparison of SABRE results with plant data is given in Figures 5.1-1 and 5.1-2. Figure 5.1-1 shows the fission power decay as a result of the scram. With a scram time of 2.0 seconds, the SABRE-calculated core power decay shows good agreement with the plant data. Scram time in SABRE was reduced from 2.8 sec to 2.0 sec because this scram occurred early in the initial reactor fuel cycle and the neutron kinetics data used in the SABRE simulation of this case corresponds to an EOC condition. Unit 1 began commercial operation on 6-8-83, and the scram occurred on 6-14-83. At BOC some control rods are already inserted and therefore the core would shutdown considerably faster during a scram than it would at EOC. Also, at beginning of cycle, the core power is bottom peaked, and therefore, the core is more easily shutdown during a scram. This transient was simulated using a U2C7 EOC core model with the code initialized at pre-power uprate conditions. The difference in U1C1 and U2C7 neutronic response is accounted for by reducing the scram time in the SABRE input from 2.8 sec to 2.0 sec to get reasonable agreement between the predicted power response and plant data (see Table 5.1-1).

The total core flow response due to the scram and the recirculation pump runback is also displayed in Figure 5.1-1. A recirculation pump runback is initiated when level drops to +13" which leads to a slow coast down of the core flow. SABRE shows an earlier peak in core flow than the plant data.

The minimum water level predicted by SABRE (Figure 5.1-1) shows excellent agreement with the plant data (less than 1" difference) although the SABRE calculated water level tends to drop somewhat slower than the actual level.

Plant data for steam dome pressure response (Figure 5.1-1) shows an initial drop in pressure of about 25 psi caused by the rapid decrease in core void fraction associated with the scram. The SABRE calculation also shows an initial drop in reactor pressure, but the magnitude of the drop is larger. Following the initial drop in pressure, there is a rapid pressure increase due to MSIV closure. The pressure rise which is terminated before any SRVs open is halted by the onset of

steam condensation as level drops below the feedwater nozzles [-24" (see Section D.5)], and subcooled feedwater is injected directly into a region occupied by saturated steam. When the sparger nozzles are re-submerged (at about 13 seconds) as level recovers, pressure begins a second increase. The SABRE model indicates, however, that this pressure rise is also modulated by steam condensation effects. In this situation the steam condensation is a result of subcooled water exiting the steam separators. Because of the high core flow rate and low power generation (decay heat) there is no boiling within the core, and subcooled liquid fills the entire region within the shroud. Although the details of the pressure trace calculated using SABRE differ somewhat with the plant data, the overall response over the first two minutes of the transient shows good agreement.

Figure 5.1-2 presents plots of total steam flow, feedwater flow, HPCI pump flow, and HPCI turbine speed. Note that the quasi-static HPCI model cannot predict the initial spikes in HPCI flow and turbine speed exhibited by the plant data; however, the predicted response of the system does show good overall agreement with the trend of the data. In this calculation, a value of -37" (rather than -38") was used for the HPCI and RCIC initiation setpoints. The slightly higher value was used because SABRE slightly underpredicts the drop in water level due to the scram, and HPCI/RCIC would otherwise not have been initiated.

Figure 5.1-3 presents plots of the normalized thermal neutron flux during the scram. The flux is shown in the active core region (upper and lower reflector regions excluded). The change in flux during the scram is consistent with the expected response.

Table 5.1-1
Changes Made to Base 9x9 Input Deck in Appendix F

Parameter	New Value
End time (F.2.1)	120 seconds
Time steps (F.3)	Max = Min = 5 msec for t<10 sec Max = Min = 30 msec for t>10 sec
Initial power (F.6.1)	3293 MWth (pre-power uprate)
Rated core power (F.6.2)	3293 MWth (pre-power uprate)
Initial steam dome pressure (F.8)	1005 psia (to agree with plant data)
Scram on specified time (F.19.6)	0.0 sec (scram on high MSL rad.)
Scram time (F.19.10)	2.0 sec (decreased from 2.8 sec to 2.0 sec to account for fact that plant transient occurred at BOL and kinetics data corresponds to EOC). Scram time was adjusted until SABRE power decay matched reasonably close to data.
HPCI initiation on low level (F.20.2)	-37 inches
RCIC initiation on low level (F.21.2)	-37 inches
Maximum feedwater flow (F.24.7)	14.0 Mlb/hr (to agree with plant data)
Initiate MSIV closure on specified time (F.25.1)	0.0 seconds (MSIV closure on high MSL rad.)
Initial turbine inlet pressure (F.26.5)	950 psia (Dome pressure - 55 psi)[1]

[1] NEDC-32161P, "Power Uprate Engineering Report for Susquehanna Steam Electric Station Units 1 and 2," p. A.7-3.

Table 5.1-2
Sequence of Events Calculated by SABRE

```
*** Kinetics file is /d00/appl/sabre3v0/data/u2c7.simtran.out

*** SABRE data file is /home/eamac/sabre_31/input/ec-atws-0505/c01.dat

*** This is not a restart case

1   S A B R E  -  Version 3.1
    (01) MSIV Closure with scram - Compare to plant data


 t(sec)=        .000  Low-Pres Condensate Injection Inop.

 t(sec)=        .000  MSIV closure on specified time

 t(sec)=        .000  Scram initiated on specified time
                      Scram time (sec) =          2.00

 t(sec)=       2.005  All Control Rods Inserted

 t(sec)=       3.915  Level Setpoint Setdown
                      Setdown occurs when level drops to         13.00 in.
                      Delay for setpoint setdown =       .11E+02 sec

 t(sec)=       3.915  Recirc pump-A runback on low Rx lvl
                      Setpoint for Runback =         13.00 in.
                      Trip delay =      .300E+01 sec

 t(sec)=       3.915  Recirc pump-B runback on low Rx lvl
                      Setpoint for Runback =         13.00 in.
                      Trip delay =      .300E+01 sec

 t(sec)=       4.005  MSIVs are closed

 t(sec)=       8.405  HPCI initiation on Low water level
                      Setpoint for initiation =       -37.00 in.

 t(sec)=       8.405  RCIC initiation on low water level
                      Setpoint for initiation =       -37.00 in.

 t(sec)=      48.003  Main Turb Trip on high water level
                      Setpoint(inches) =        54.000

 t(sec)=      48.003  RCIC Trip on hi water level
                      Trip Setpoint =       .54E+02 in.

 t(sec)=      48.003  HPCI Trip on hi water level
                      Trip Setpoint =       .54E+02 in.

 t(sec)=      62.793  Feedwater Trip on high level
                      Trip Setpoint =       .54E+02 in.
```

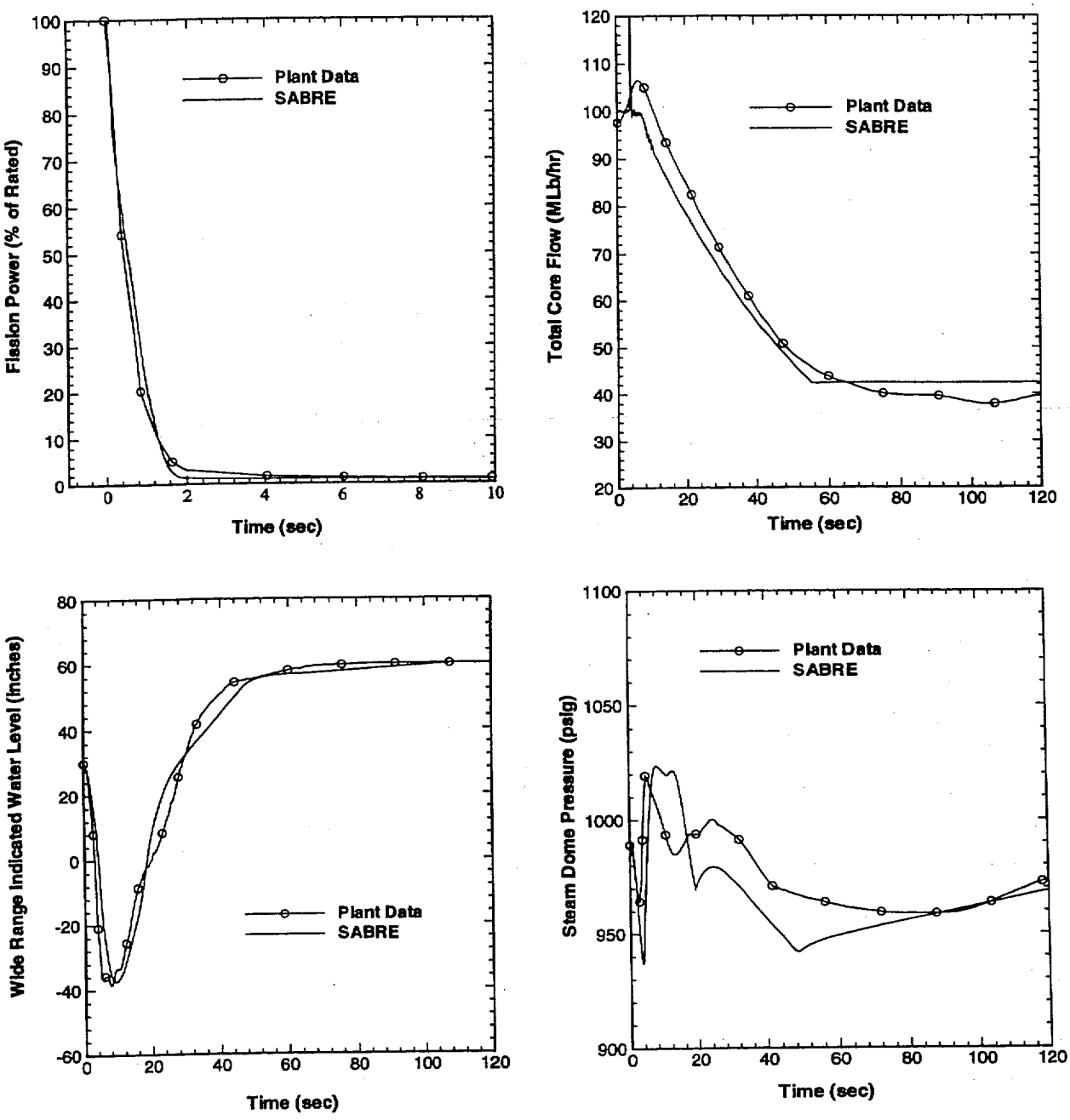

Figure 5.1-1 Comparison of SABRE results against plant data for MSIV-closure transient with scram. (SABRE Case 01)

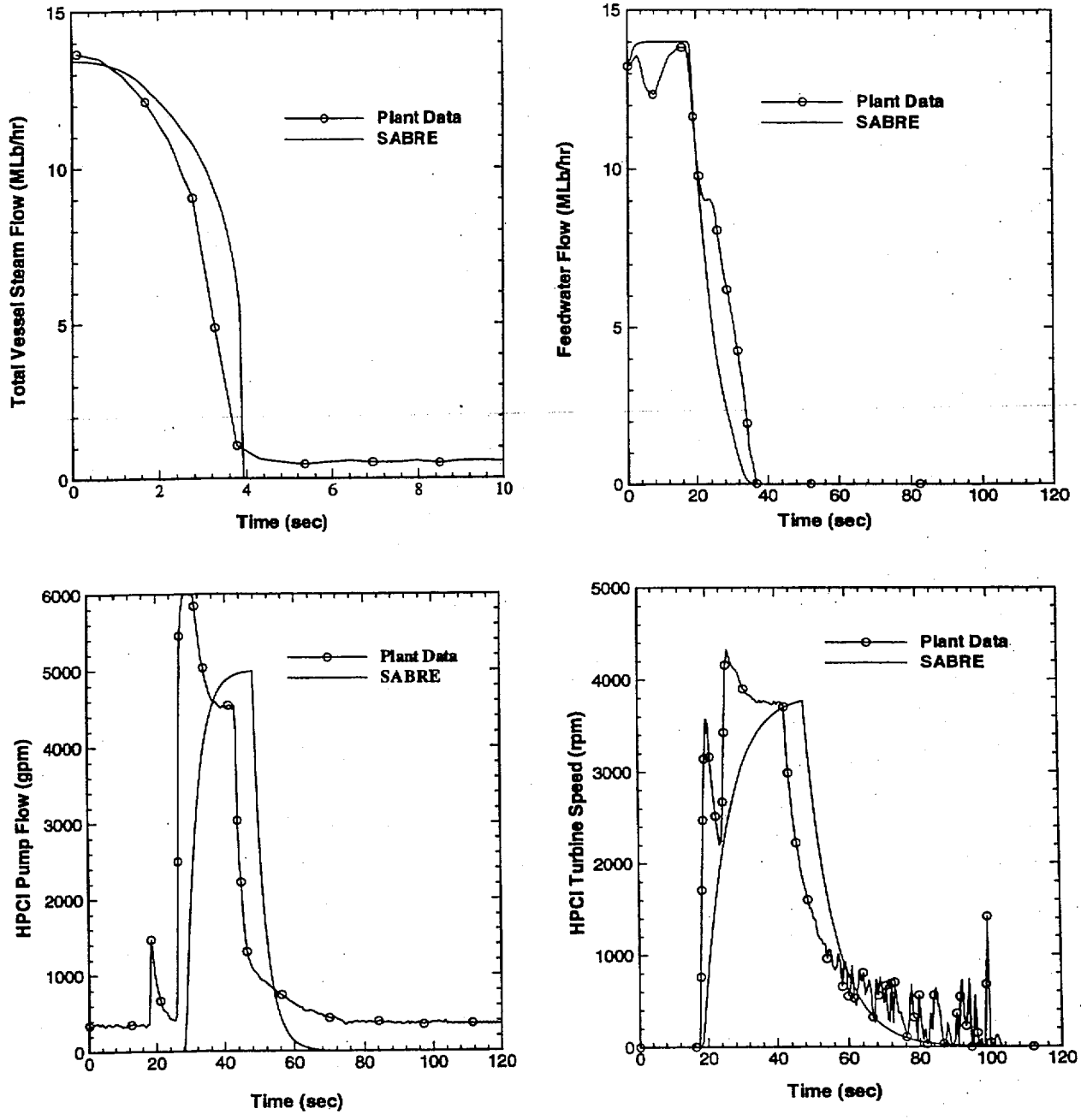

Figure 5.1-2 Comparison of SABRE results against plant data for MSIV-closure transient with scram. (SABRE Case 01)

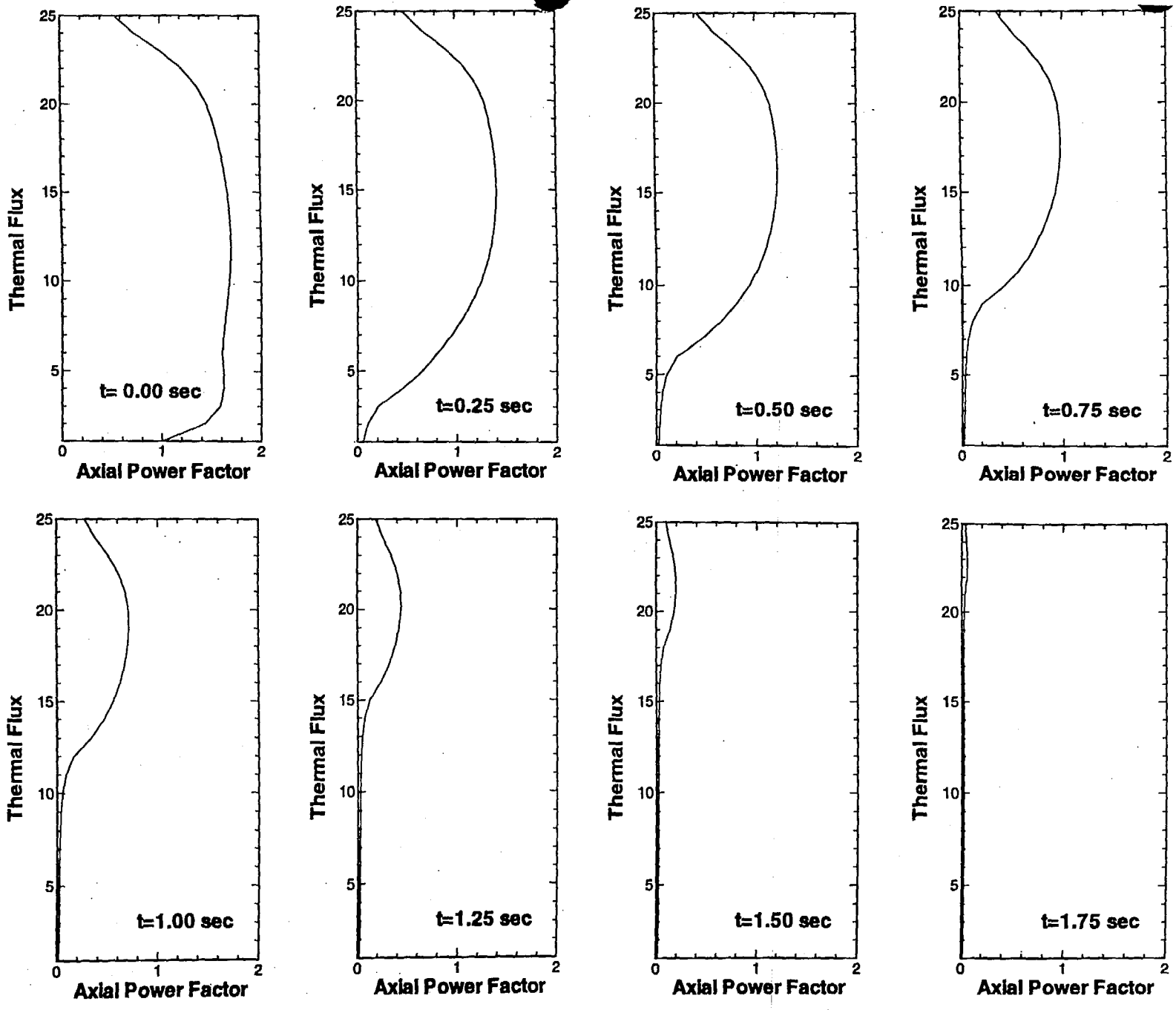

Figure 5.1-3 Change in normalized thermal neutron flux during scram. Control rods are fully inserted at t=2 seconds. (SABRE Case 01)

5.2 Containment Response for Unmitigated ATWS—Comparison to CONTAIN Code

This section presents calculation results for an MSIV-closure ATWS with no boron injection or manual control rod insertion. Makeup flow is provided by full HPCI and RCIC injection. HPCI suction is aligned to the CST for the entire event. The ATWS is initiated from 100% uprated power (3441 Mw_t) and 100 Mlb_m/hr total core flow. The core kinetics data correspond to U2C10. Changes made to the base SABRE input deck are documented in Table 5.2-1. The sequence of events for the SABRE calculation are given in Table 5.2-2. A complete listing of SABRE output is provided on microfiche (see Computer Case Summary). This SABRE calculation corresponds to SABRE Case 02 in the Computer Case Summary.

Figure 5.2-1 shows the reactor response calculated by SABRE. Plots of the containment variables are presented in Figures 5.2-2 & 5.2-3. The SABRE containment calculations are compared against results obtained with the CONTAIN code[1]. The CONTAIN input and output files for this case are given on microfiche (see CONTAIN Case 02 in Computer Case Summary). The base CONTAIN input deck is given in Appendix H. Source tables within the CONTAIN input file account for the steam addition to the suppression pool from SRV discharge as well as the heat addition/removal associated with the reactor vessel and the drywell coolers. These source tables are quite lengthy, and therefore they are not included in the base CONTAIN input deck which is presented in Appendix H (only abbreviated tables are included in the base CONTAIN input deck).

In Figure 5.2-2, the rise in drywell temperature at about 800 seconds is due to loss of drywell cooling. The rapid rise in wetwell temperature and pressure at about 1000 seconds is caused by the onset of suppression pool boiling. Once the suppression pool begins to boil, the containment pressure follows the vapor pressure of the suppression pool.

---

[1] Murata, K. K., Carroll, D. E., Washington, K. E., Gelbard, F., Valdez, G. D., Williams, D. C., and Bergeron, K. D., "User's Manual for CONTAIN 1.1: A Computer Code for Severe Nuclear Reactor Accident Containment Analysis", NUREG/CR-5026, November 1989.

Table 5.2-1
Changes Made to Base SABRE 10x10 Input Deck in Appendix G

Parameter	New Value
Problem end time (F.2.1)	2000 seconds
Time step data (F.3)	Max = 5 msec Min = 5 msec (t<30) Max = 30 msec Min = 30 msec (30<t)
Status of scram system (F.19.1)	-1 (scram and ARI are failed)
Time at which MSIV closure is initiated (F.25.1)	0.0 seconds

Table 5.2-2
Sequence of Events Calculated by SABRE

```
*** Kinetics file is /d00/appl/sabre3v0/data/u2c10.simtran.out

*** SABRE data file is /home/eamac/sabre_31/input/ec-atws-0505/c02.dat

*** This is not a restart case

1   S A B R E  -  Version 3.1
    (02) MSIVC ATWS -- NO SLC/MRI/SPC (U2C10)


 t(sec)=        .000  Scram is Failed

 t(sec)=        .000  Low-Pres Condensate Injection Inop.

 t(sec)=        .000  ARI is Failed

 t(sec)=        .000  MSIV closure on specified time

 t(sec)=       4.005  MSIVs are closed

 t(sec)=       4.345  Recirc pump-A trip on hi Rx press.
                      Setpoint for trip =      1135.00 psig
                      Trip delay =      .230E+00 sec.

 t(sec)=       4.345  Recirc pump-B trip on hi Rx press.
                      Setpoint for trip =      1135.00 psig
                      Trip delay =      .230E+00 sec.

 t(sec)=     110.953  Feedwater Trip on low Stm Line Press
                      Flow stops when press <       175.00 psia

 t(sec)=     126.313  Level Setpoint Setdown
                      Setdown occurs when level drops to        13.00 in.
                      Delay for setpoint setdown =      .11E+02 sec

 t(sec)=     160.723  HPCI initiation on Low water level
                      Setpoint for initiation =       -38.00 in.

 t(sec)=     160.723  RCIC initiation on low water level
                      Setpoint for initiation =       -38.00 in.

 t(sec)=     884.533  DW Cooler Trip on Hi DW Press
                      Trip Setpoint     =        1.720 psig
```

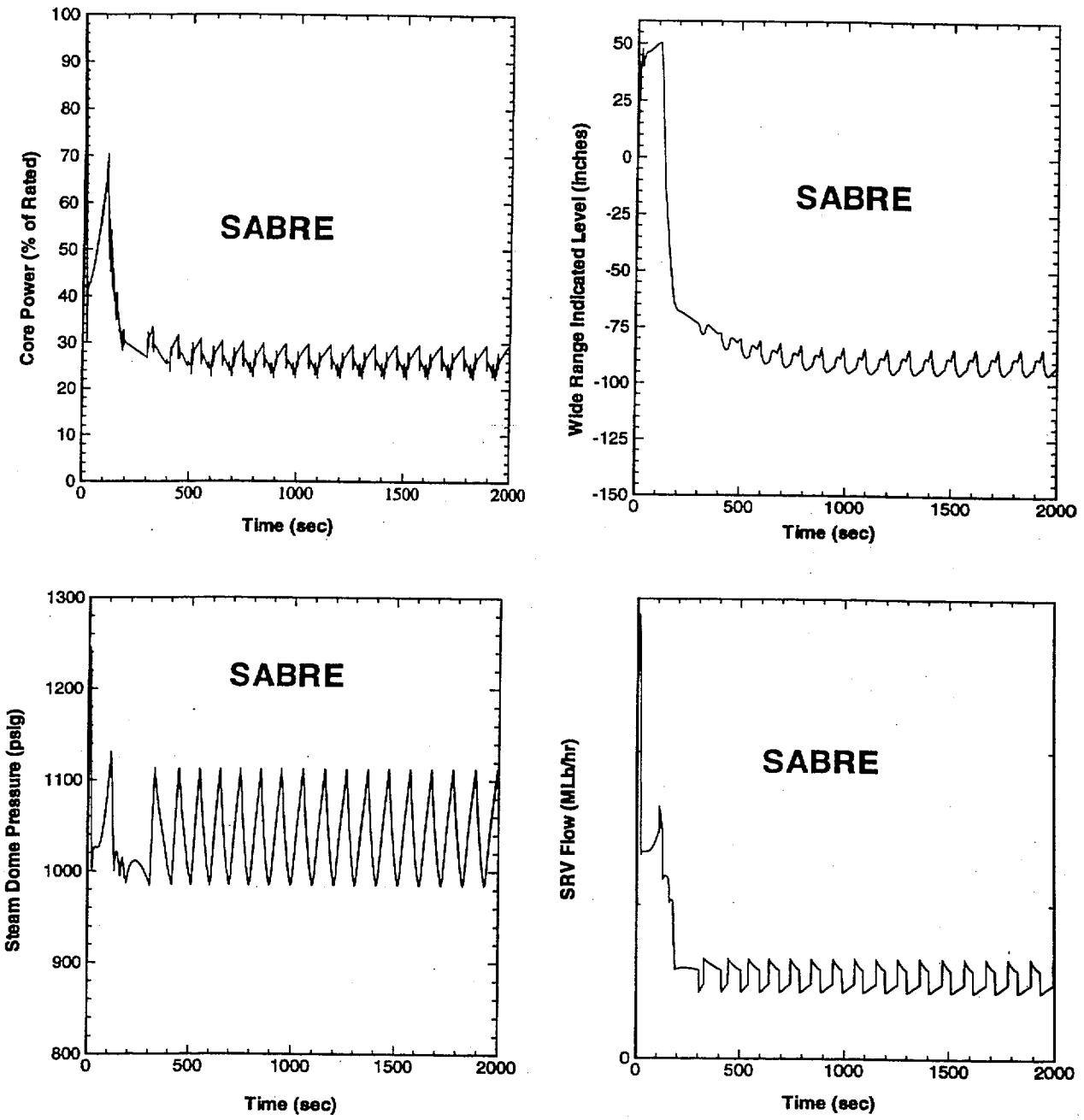

Figure 5.2-1 SABRE calculation of reactor response for unmitigated ATWS event.

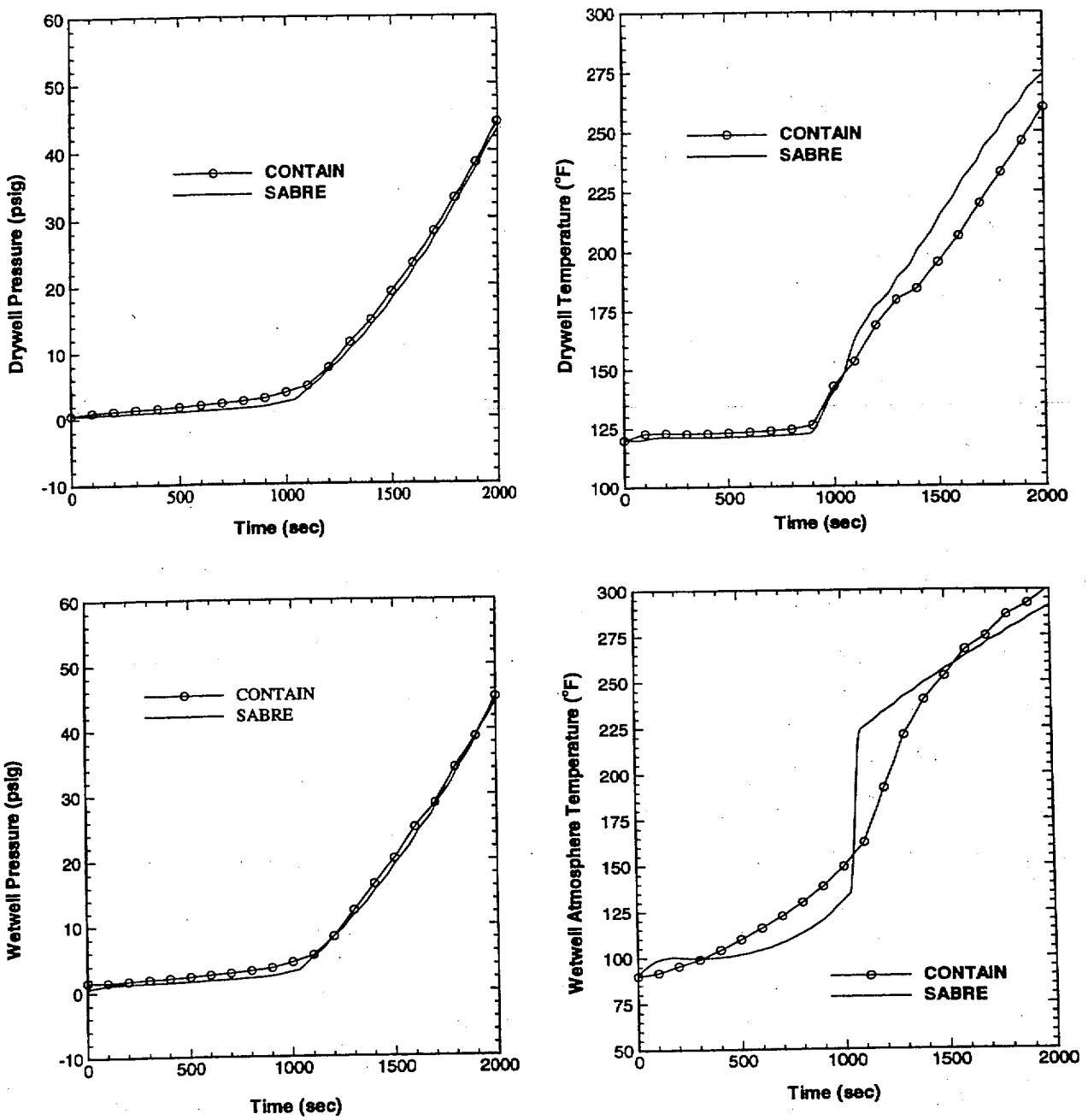

Figure 5.2-2 Comparison of SABRE and CONTAIN predictions for unmitigated MSIVC ATWS. (SABRE Case 02)

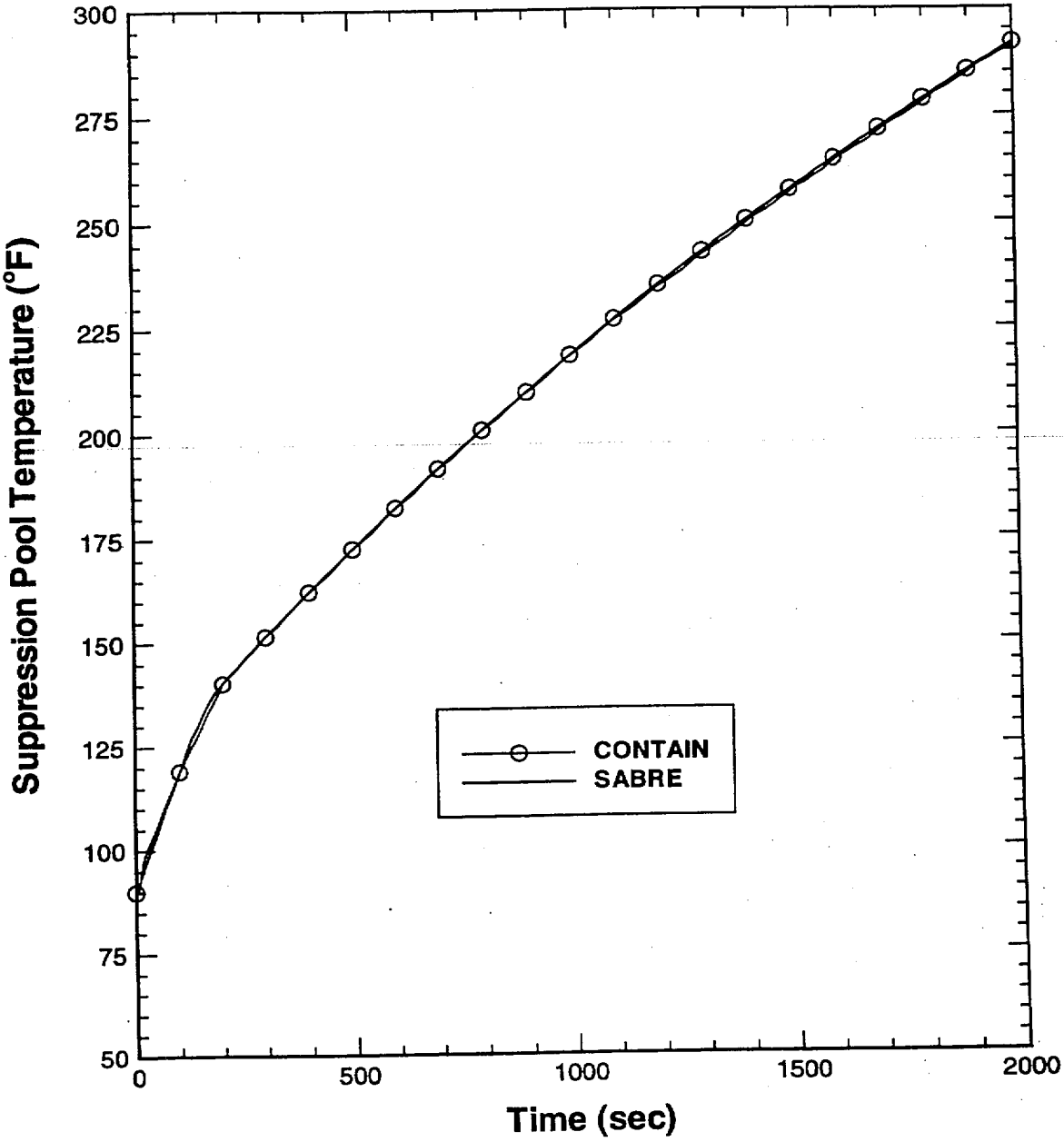

Figure 5.2-3 Comparison of SABRE and CONTAIN suppression pool temperature calculations for unmitigated MSIVC ATWS.

5.3 MSIV Closure ATWS—Comparison to PP&L RETRAN Calculations.

SABRE results for an MSIV-closure ATWS, with U2C9 kinetics data, are compared with results obtained with the PP&L RETRAN model. The RETRAN simulation is documented in Calc. NFE-2-09-003 "Unit 2 Cycle 9 Nuclear Fuels Engineering ATWS Analysis." Table 5.3-1 lists the changes made to the base SABRE model. The changes in Table 5.3-1 were made to achieve agreement with the modeling assumptions used in the RETRAN calculation. The sequence of events generated by SABRE is given in Table 5.3-2. This SABRE calculation corresponds to SABRE Case 03 in the Computer Case Summary.

Figure 5.3-1 shows a comparison of the SABRE and RETRAN calculated core power response to closure of the MSIVs. RETRAN calculates a peak power of 341% (of rated power) at 4.4 seconds, and SABRE predicts a peak power of 421% at 4.2 seconds. The SABRE calculation shows a secondary power spike of 209% which is not present in the RETRAN calculation. The secondary power spike is most likely caused by the surge in core flow predicted by SABRE following closure of the MSIVs (see Figure 5.3-2). In the SABRE model, the fluid density changes with the overall reactor pressure rather than with the local fluid pressure. The RETRAN model on the other hand contains a fully-compressible flow model, and therefore, some difference in the core flow response to a rapid pressure change is expected.

Figure 5.3-2 indicates that the total mass of steam exiting the vessel in the 30 second simulation time is somewhat larger for the SABRE calculation than it is for the RETRAN calculation. The larger mass of steam produced is consistent with the higher and more broad power spike predicted by SABRE for the transient.

The peak dome pressure calculated by SABRE is 1354 psia which occurs at 11.1 seconds. RETRAN predicts a peak pressure of 1316 psia at 7.8 seconds. This comparison shows that SABRE is conservative with regard to predicting peak vessel pressure in the MSIV closure ATWS. Included in Figure 5.3-1 is a comparison of core average heat flux and Wide Range Indicated Level. Feedwater flow is maintained constant during the transient. SABRE underpredicts the peak core-average heat flux compared to RETRAN, but the heat flux spike obtained from SABRE is much broader than that calculated by RETRAN.

Table 5.3-1
Changes Made to Base SABRE 9x9 Input Deck in Appendix F

Parameter	New Value
Time step data (F.3)	Max = 5 msec Min = 5 msec (0<t)
Initial total core flow (F.7.1)	87 Mlb/hr
Initial guess for core channel flow (F.7.2)	80 MLb/hr
Initial steam dome pressure (F.8)	1046.92 psia
Initial downcomer subcooling (F.9)	29.49 Btu/Lbm[1]
Status of scram system (F.19.1)	-1 (scram and ARI are failed)
High pressure trip for recirc. pump 'A' (F.23.7)	1214.7 psia (Table 2.2 of Ref. 1)
High pressure trip for recirc. pump 'B' (F.23.9)	1214.7 psia (Table 2.2 of Ref. 1)
Time delay for recirc. pump 'A' runback on low feedwater flow (F.23.12)	1.D+09 seconds (Neglect runback)
Time delay for recirc. pump 'A' runback on low feedwater flow (F.23.14)	1.D+09 seconds (Neglect runback)
Time delay for recirc. pump 'A' runback on low water level (F.23.16)	1.D+09 seconds (Neglect runback)
Time delay for recirc. pump 'A' runback on low water level (F.23.18)	1.D+09 seconds (Neglect runback)
MSIV closure on specified time (F.25.1)	0.0 seconds
Feedwater flow versus time flag (F.24.15)	1 (Feedwater flow is specified as afunction of time)
Feedwater flow data table (F.24.16)	Feedwater flow is specified as 14.235 Mlb/hr for the entire problem. This is the initial FW flow calculated by SABRE.
SRV actuation setpoints (F.31.4)	Used UAL values from Table 1 of Supplement 1 to GE Power Uprate Analysis (GENE-637-024-0893). For SRV 16 the opening pressure was set to 1.D+09 to make this valve inoperable (The RETRAN run had 1 SRV OOS).
Gap Conductance (F.36.4)	870 Btu/hr-ft^2-°F (to agree with RETRAN calc.)

[1] Calc. EC-ATWS-1001.

Table 5.3-2
Sequence of Events Calculated by SABRE

```
*** Kinetics file is /d00/appl/sabre3v0/data/u2c9.simtran.out

*** SABRE data file is /home/eamac/sabre_31/input/ec-atws-0505/c03.dat

*** This is not a restart case

1   S A B R E  -  Version 3.1
    (03) SSES Power Uprate MSIV-Closure ATWS U2C9 - Compare to RETRAN


 t(sec)=        .000  Scram is Failed

 t(sec)=        .000  Low-Pres Condensate Injection Inop.

 t(sec)=        .000  ARI is Failed

 t(sec)=        .000  MSIV closure on specified time

 t(sec)=        .000  Feedwater Flow determined from Table
                      Data in Table ends at t =       .10E+10 sec

 t(sec)=       4.005  MSIVs are closed

 t(sec)=       4.890  Recirc pump-A trip on hi Rx press.
                      Setpoint for trip =       1200.00 psig
                      Trip delay =      .230E+00 sec.

 t(sec)=       4.890  Recirc pump-B trip on hi Rx press.
                      Setpoint for trip =       1200.00 psig
                      Trip delay =      .230E+00 sec.

 t(sec)=      19.925  Feedwater Trip on high level
                      Trip Setpoint =       .54E+02 in.

 t(sec)=      21.325  Main Turb Trip on high water level
                      Setpoint(inches) =       54.000
```

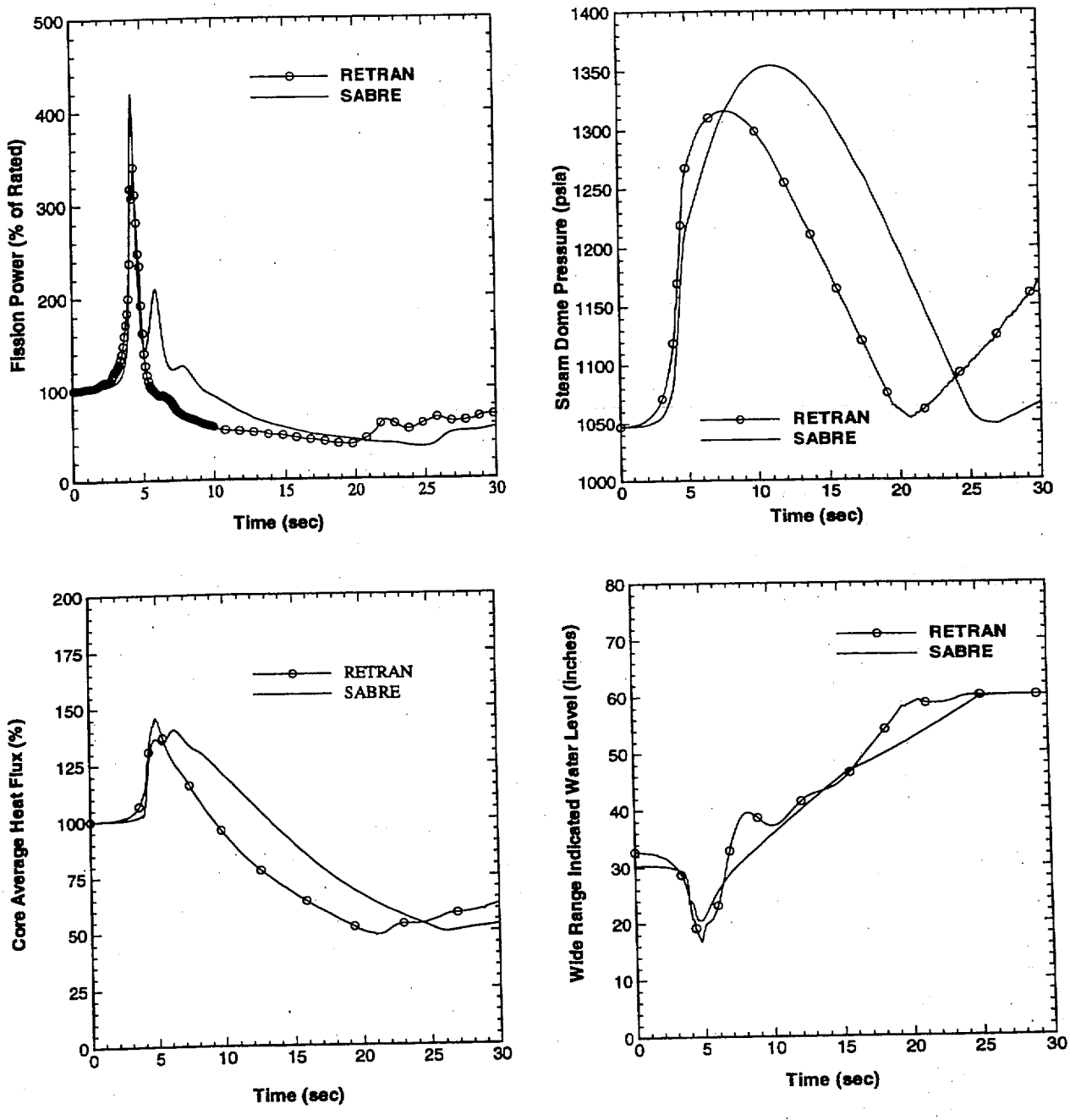

Figure 5.3-1 Comparison of SABRE and PP&L RETRAN predictions for U2C9 MSIV Closure ATWS event with one SRV out of service. (SABRE Case 03)

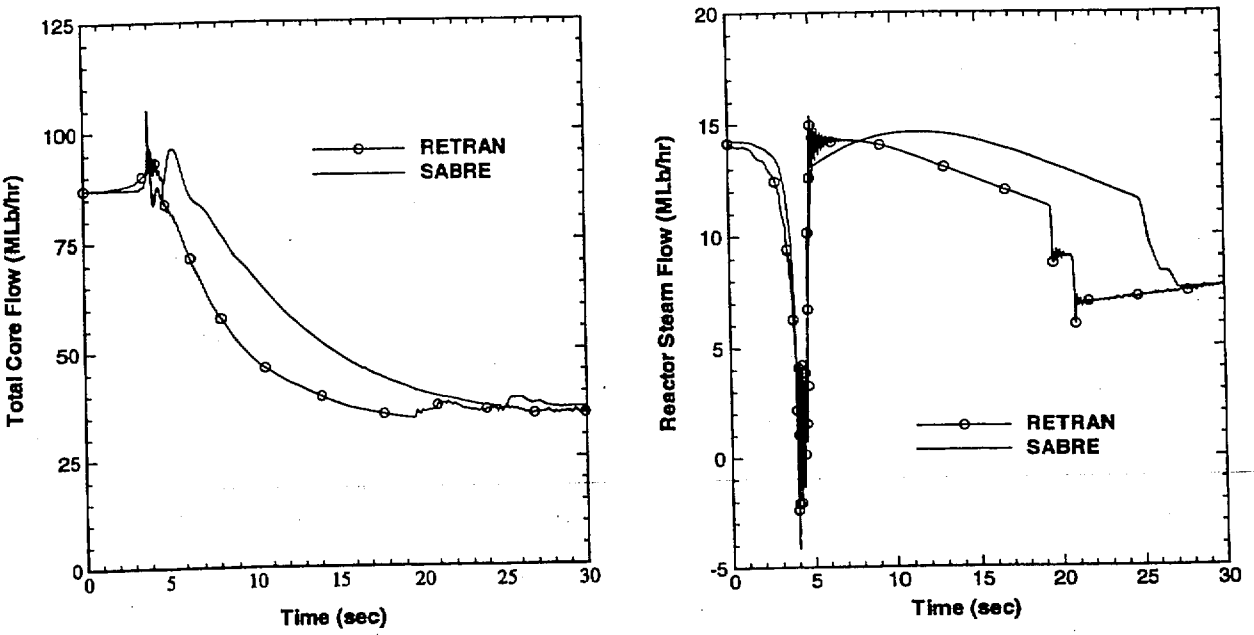

Figure 5.3-2 Comparison of SABRE and PP&L RETRAN predictions for U2C9 MSIV Closure ATWS event with one SRV out of service. (SABRE Case 03)

5.4 Inventory Boildown with Scram Failure—Comparison to SIMULATE-E

As part of the U2C9 cycle-specific ATWS analysis for Susquehanna (Calculation EC-ATWS-1001), a data base was developed for core power as a function of core channel flow, reactor pressure, and core-inlet subcooling. This data base was developed using the 3-D core simulator code SIMULATE-E. The FORTRAN program listed in Appendix M of Rev. 6 of EC-ATWS-0505 interpolates within the data base to obtain core power as a function of the three operating parameters mentioned above. Under quasi-static conditions, SABRE should compute a critical core power consistent with that predicted by SIMULATE-E. The purpose of this benchmarking study is to verify that the 1-D kinetics calculation in SABRE for core power agrees with SIMULATE-E under quasi-static conditions.

In this scenario, the scram and ARI systems are failed; recirculation pumps and feedwater are tripped at t=0. Water level beigns to fall rapidly as inventory is boiled off. RCIC is allowed to initiate on low reactor level in order to slow the rate of level decrease and thus maintain quasi-static conditions. The MSIVs remain open throughout the transient. The SABRE nuetronics model for this transient corresponds to U2C9 which is a mixed core of 9x9 and 10x10 fuel with the 9x9 fuel being the dominant fuel type. Changes made to the base 9x9 SABRE input deck are summarized in Table 5.4-1. This SABRE calculation corresponds to SABRE Case 04 in the Computer Case Summary.

The sequence of events calculated by SABRE is given in Table 5.4-2. Figure 5.4-1 shows SABRE results for core power, core channel inlet flow, downcomer level, and steam dome pressure. For this relatively "slow" transient, the SABRE calculation for core power is consistent with the power predicted by the steady-state 3-D neutronics code, SIMULATE.

Table 5.4-1
Changes Made to Base SABRE 9x9 Input Deck in Appendix F

Parameter	New Value
End time (F.2.1)	140 seconds
Time step data (F.3)	Max = 30 msec Min = 15 msec (0<t<10 sec) Max = 50 msec Min = 25 msec (10<t)
Initial total core flow (F.7.1)	87 Mlb/hr (This is the initial core flow used in the SSES ATWS analysis).[1]
Initial guess for core channel flow (F.7.2)	80 MLb/hr
Initial downcomer subcooling (F.10)	29.49 Btu/Lb[2]
Status of scram system (F.19.1)	-1 (scram and ARI failed)
HPCI operability flag (F.20.1)	0 (HPCI inoperable)
Time at which recirc. pump 'A' is tripped (F.23.1)	0 seconds.
Time at which recirc. pump 'B' is tripped (F.23.2)	0 seconds.
Time at which feedwater pumps are tripped (F.24.1)	0 seconds.
Set point for MSIV closure on low water level (F.25.2)	-129.D+09 inches (prevents MSIVs from closing on low level)
Time delay for ADS actuation (F.27.4)	102.D+09 seconds (prevent actuation of ADS)

[1] GENE-637-024-0893, Table 2.1.

[2] Calc. EC-ATWS-1001.

Table 5.4-2
Sequence of Events Calculated by SABRE

```
*** Kinetics file is /d00/appl/sabre3v0/data/u2c9.simtran.out

*** SABRE data file is /home/eamac/sabre_31/input/ec-atws-0505/c04.dat

*** This is not a restart case

1   S A B R E  -  Version 3.1
    (04) SSES Power Uprate (U2C9)-Boildown with scram failure


 t(sec)=        .000  Scram is Failed

 t(sec)=        .000  HPCI is Inoperable

 t(sec)=        .000  Low-Pres Condensate Injection Inop.

 t(sec)=        .000  ARI is Failed

 t(sec)=        .000  Feedwater Trip on specified time

 t(sec)=        .000  Recirc pump-A trip on specified time
                      Trip delay =      .000E+00 sec

 t(sec)=        .000  Recirc pump-B trip on specified time
                      Trip delay =      .000E+00 sec

 t(sec)=      33.309  RCIC initiation on low water level
                      Setpoint for initiation =        -38.00 in.

 t(sec)=      93.209  ADS timer initiation
                      Timer starts when level drops to       -129.00 in.
                      Timer runs out in      .102E+12 sec.

 t(sec)=      93.209  DW Cooler Trip on Low Rx Level
                      Trip Setpoint     =      -129.000 inches
```

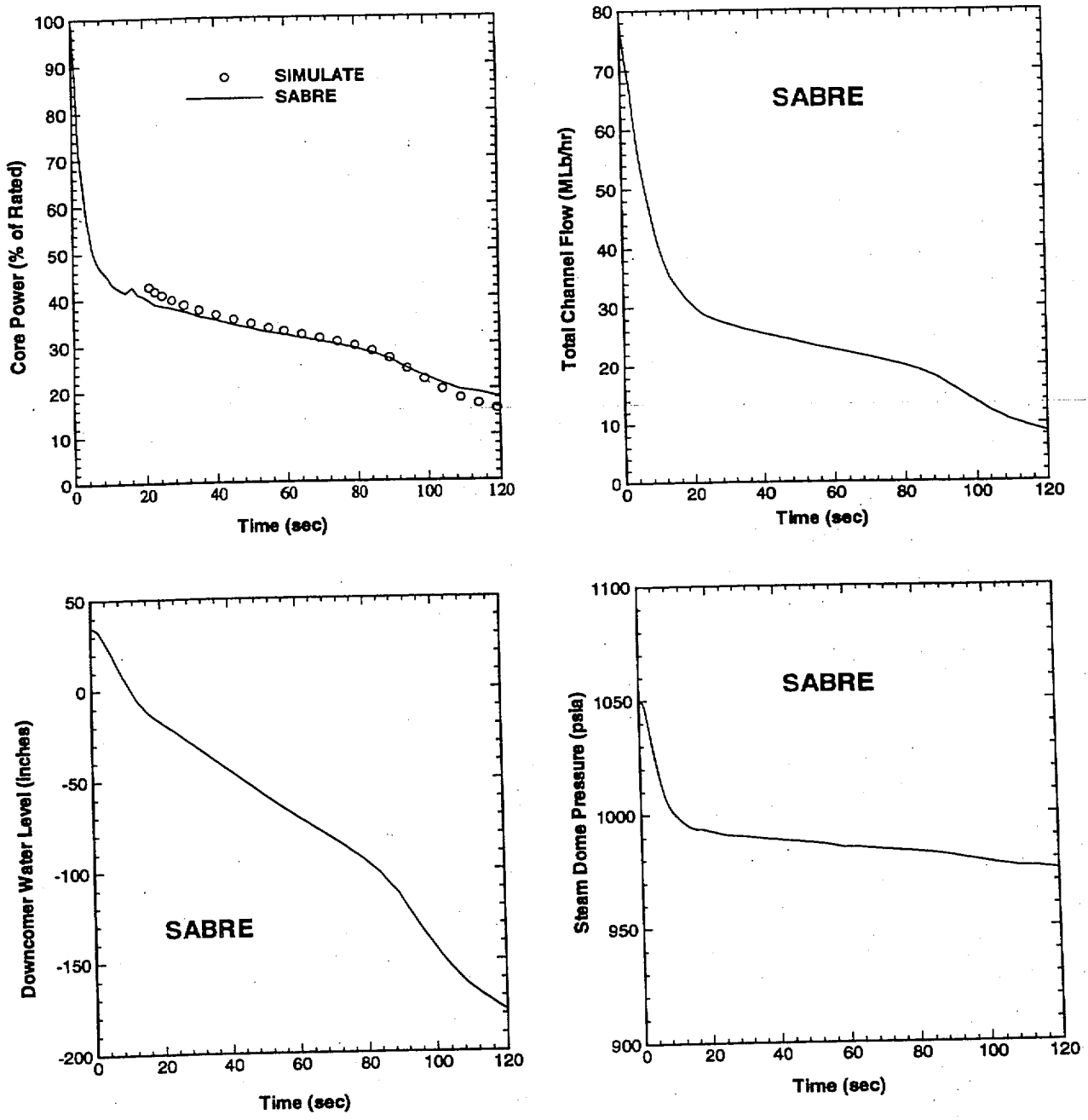

Figure 5.4-1 Comparison of SABRE core power calculation against SIMULATE-E for inventory boildown transient with scram failure (U2C9). (SABRE Case 04)

5.5 Small Break LOCA - Comparison to CONTAIN Results

In this section, the SABRE containment model is compared with CONTAIN[1] results for a small liquid break. In the SABRE code, the break flow and enthalpy can either be specified in an input table or they can be calculated (if they are calculated the break location and area are specified). A 0.02 ft^2 liquid break is specified in this benchmark study. The break is located in the downcomer region.

The reactor is initially operating at 102% power (3510 Mwt) and 100 Mlb/hr total core flow. Kinetics data corresponds to U2C10. The break occurs at t=0. Changes made to the base SABRE U2C10 input deck are identified in Table 5.5-1. The sequence of events generated by SABRE is shown in Table 5.5-2. This SABRE calculation corresponds to SABRE Case 05 in the Computer Summary. The CONTAIN calculation corresponds to CONTAIN Case 05 in the Computer Case Summary.

The CONTAIN model consists of two control volumes which represent the drywell and wetwell. The model accounts for the thermal capacitance of the steel structures within the containment. Thermal capacitance of the concrete walls is neglected in the CONTAIN model used in this benchmark study because it is also neglected in the SABRE model. As in the case of the SABRE model, the CONTAIN drywell model allows for the formation of a pool layer as water discharged from the break accumulates on the drywell floor. When the height of the pool layer reaches 18", water will overflow into the downcomer pipes and enter the suppression pool. Much of the input data for this model is taken from PP&L calculation EC-THYD-001, "CONTAIN Model for Primary Containment".

In the CONTAIN calculation, the break flow and enthalpy calculated by SABRE were used as input data. That is, the mass/enthalpy source in the CONTAIN model corresponds to the break flow/enthalpy in SABRE.

Figures 5.5-1 & 5.5-2 show a comparison of SABRE and CONTAIN results for the small break LOCA. Overall, the calculation results show good agreement for the containment temperatures, pressures, and water levels. The initial rise in suppression chamber air space temperature is caused by compression of gas in the wetwell atmosphere as nitrogen flows from the drywell to the suppression chamber. As the flow of nitrogen to the wetwell decays, the air space temperature begins to decrease as a result of heat transfer from the atmosphere to the pool. In the long term, the atmosphere temperature begins to lag the suppression pool temperature.

In Figure 5.5-2 the slightly higher drywell pool level predicted by SABRE is most likely due to the fact that SABRE calculates a somewhat higher drywell pool temperature during the first half of the transient. The higher temperature results in a decreased water density and a greater water

---

[1] Murata, K. K., Carroll, D. E., Washington, K. E., Gelbard, F., Valdez, G. D., Williams, D. C., and Bergeron, K. D., "User's Manual for CONTAIN 1.1: A Computer Code for Severe Nuclear Reactor Accident Containment Analysis", NUREG/CR-5026, November 1989.

volume. The difference in suppression pool level predictions is a very small fraction of the total pool level.

At t≈1000 sec, SABRE predicts that the break enthalpy begins to drop below the saturated liquid enthalpy corresponding to drywell temperature, i.e., the break is subcooled relative to drywell atmosphere conditions. This begins to cause a drop in drywell temperature because heat from the drywell atmosphere is transferred to the subcooled break flow. At t≈1200 sec, the drywell atmosphere becomes saturated with water (relative humidity reaches 100%) because of the decreasing atmosphere temperature. At this time "rainout" begins to occur (liquid is removed from the atmosphere) which slows the drop in drywell temperature. As the drywell temperature and pressure continue to drop from the effects of the subcooled break flow, drywell pressure finally drops below wetwell pressure at about 1600 seconds. At this time the vacuum breakers open and there is a sudden drop in the wetwell atmosphere temperature. Both codes predict vacuum breaker opening at about the same time.

Table 5.5-1
Changes Made to Base 10x10 Input Deck in Appendix G

Parameter	New Value
Problem end time (F.2.1)	3000 seconds
Hydraulic time step size (F.3)	Max = 30, Min = 15 msec for t<20 sec Max 50, Min = 25 msec for t>20 sec
Initial Power (F.6.1)	3510 MWth
Initial CST water volume (F.14)	300,000 gal
LOCA data (F.18)	Liquid break flow area = 0.02 ft^2. Break flow multiplier = 1.25.
Scram on time (F.19.6)	2.0 sec
Suppression pool level at which HPCI suction transfers to the SP (F.20.7)	1.E+09 ft (no transfer—keep suction on CST)
Time at which operator takes control of HPCI injection (F.20.14)	600 sec
RCIC operability flag (F.21.1)	0 (RCIC inoperable)
Time that recirc pump 'A' is tripped (F.23.1)	0.0 sec
Time that recirc pump 'B' is tripped (F.23.2)	0.0 sec
Time at which FW is tripped (F.24.1)	4.0 sec
Time at which MSIV closure is initiated (F.25.1)	2.0 sec
Time at which controlled cooldown of RPV is initiated (F.30.1)	600 sec
Cooldown rate (F.30.2)	90°F/hr
SRV set points (F.31.4)	Values from p. 4-16 of GENE-187-22-0992, 1993 (SAFER/GESTR-LOCA Analysis)
Initial suppression pool level (F.48)	24 ft (to agree with CONTAIN model)
SP free area vs. elevation table (F.54)	use free area of 5277 ft^2 for all elevations to agree with CONTAIN model.

Table 5.5-2
Sequence of Events Calculated by SABRE

```
*** Kinetics file is /d00/appl/sabre3v0/data/u2c10.simtran.out

*** SABRE data file is /home/eamac/sabre_31/input/ec-atws-0505/c05.dat

*** This is not a restart case

1   S A B R E  -  Version 3.1
    (02) U2C10 -- 0.02 ft2 liq break -- HPCI aligned to CST


 t(sec)=        .000  Liquid Break
                      Break Area                =         .020 ft2
                      Multiplier on break flow  =       1.250

 t(sec)=        .000  RCIC is Inoperable

 t(sec)=        .000  Low-Pres Condensate Injection Inop.

 t(sec)=        .000  Recirc pump-A trip on specified time
                      Trip delay =      .000E+00 sec

 t(sec)=        .000  Recirc pump-B trip on specified time
                      Trip delay =      .000E+00 sec

 t(sec)=       2.003  MSIV closure on specified time

 t(sec)=       2.003  Scram initiated on specified time
                      Scram time (sec) =          2.80

 t(sec)=       4.013  Feedwater Trip on specified time

 t(sec)=       4.493  HPCI initiation on Hi Drywell Press.
                      Setpoint for initiation =       .17E+01 psig

 t(sec)=       4.523  DW Cooler Trip on Hi DW Press
                      Trip Setpoint     =         1.720 psig

 t(sec)=       4.823  All Control Rods Inserted

 t(sec)=       6.016  MSIVs are closed

 t(sec)=     600.042  Operator takes control of HPCI inj.
```

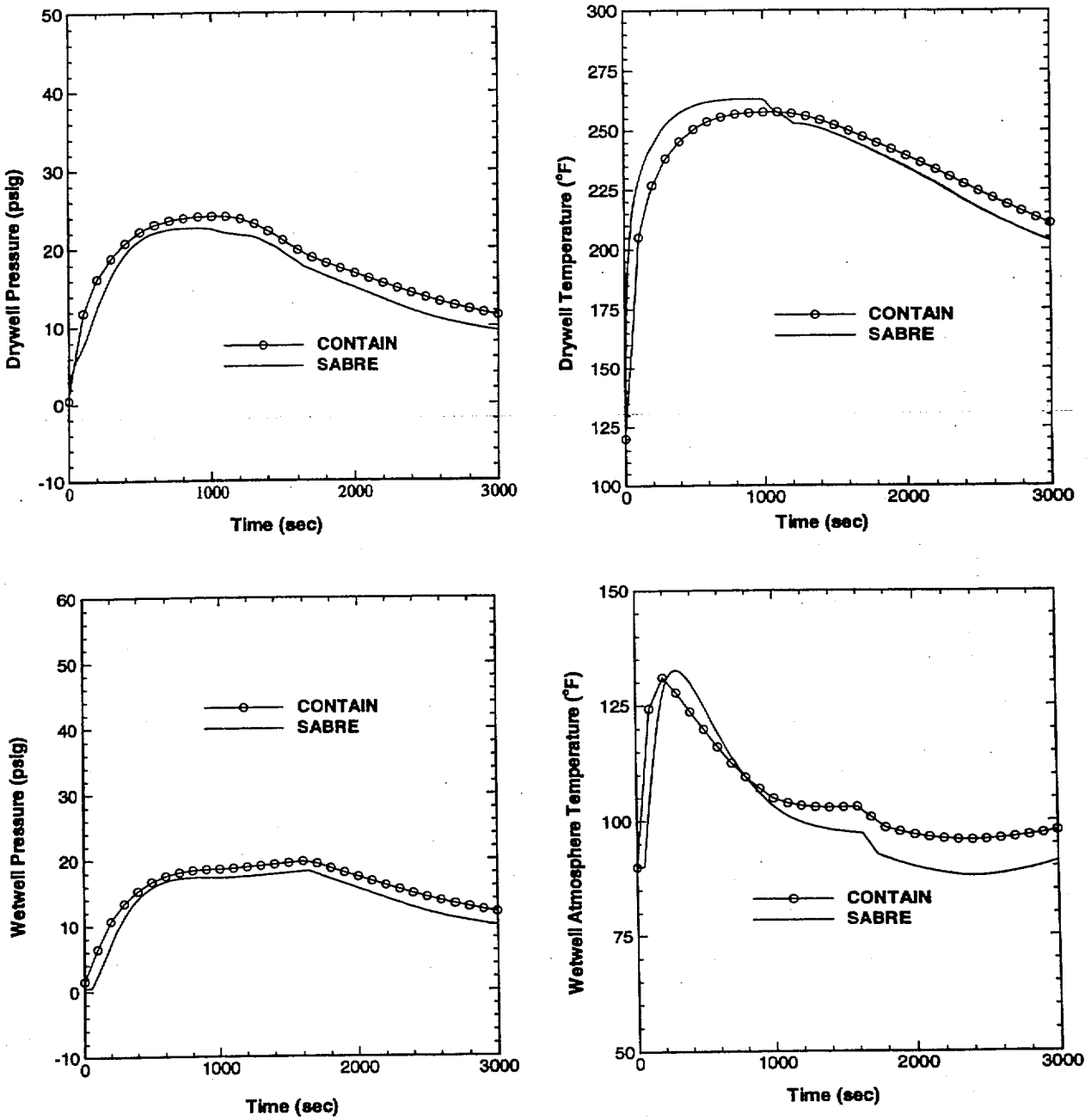

Figure 5.5-1 Comparison of SABRE and CONTAIN results for small break LOCA. (SABRE Case 05)

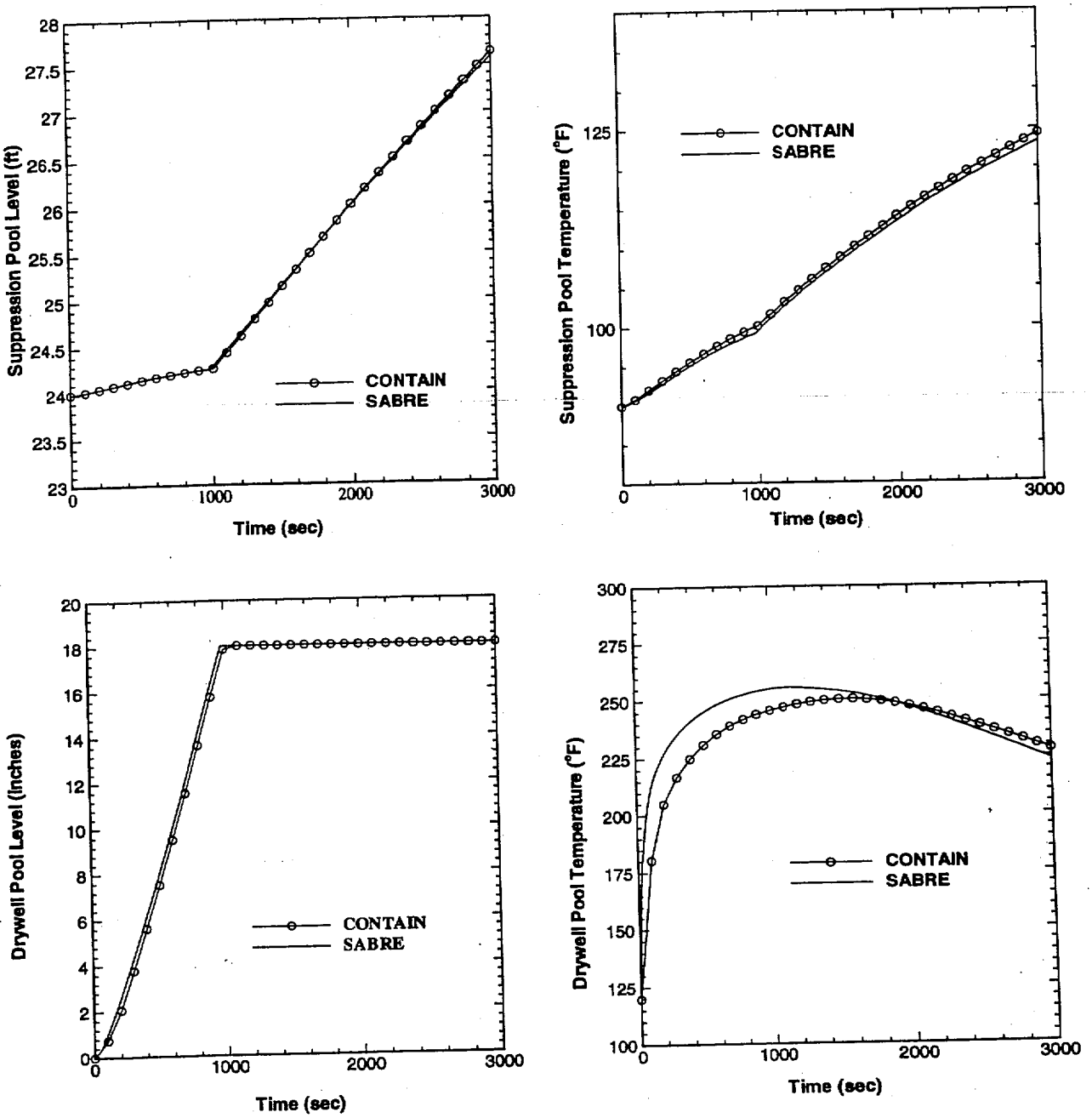

Figure 5.5-2 Comparison of SABRE and CONTAIN results for small break LOCA. (SABRE Case 05)

5.6 Turbine Trip ATWS from MEOD Rod Line - Comparison to GE TRAC Results

In this section, SABRE is compared with TRACG results for a turbine trip ATWS initiated from the MEOD (maximum extended operating domain) rod line.[1] TRACG includes a three-dimensional neutronics model with multiple core hydraulic channels and a two-fluid flow model. TRACG is considered a "state-of-the-art" computer code for simulation of BWR behavior under unstable operating regimes. The TRACG results are therefore very useful for assessing the accuracy of SABRE in predicting BWR instabilities. Both simulations are carried out with 100% turbine bypass capacity. The GE calculation was carried out with a core model consisting of 8x8 fuel. Neutronic data bases available for SABRE include a U2C7 core (full core of 9x9 fuel) and mixed 9x9/10x10 cores (mixed core of 9x9 and partial-length 10x10 fuel). The U2C7 core model is chosen for this benchmark as this is the most similar to the core model used in the GE study. Changes made to the base input deck are documented in Table 5.6-1. This SABRE calculation corresponds to SABRE Case 06 in the Computer Case Summary.

In this scenario, feedwater injection is available since the reactor is unisolated; however, feedwater heating is not maintained because of the loss of extraction steam from the turbine. The loss of feedwater heating leads to high levels of core-inlet subcooling which drives the reactor into severely unstable operation. Both TRACG and SABRE use a 60 second time constant to model the decay of feedwater temperature.

The sequence of events calculated by SABRE for this transient is presented in Table 5.6-2. Figure 5.6-1 shows the SABRE calculation results for the core-average power and core inlet subcooling. Corresponding GE results obtained with TRAC-G are presented in Figure 5.6-2. The core-inlet subcooling results show good agreement. The amplitude of the power pulses predicted by SABRE show fairly good agreement with the large-amplitude spikes calculated by TRACG. However, SABRE shows a lower frequency oscillation than TRACG and the SABRE calculation predicts a longer time to the onset of instability. The lower frequency is probably due to the higher fluid inertia associated with the single-core-channel model used in SABRE. In a multiple-channel core model such as that used in TRACG, out-of-phase channel oscillations can occur among various core channels with the flow behavior essentially decoupled from the regions above and below the core. With a single core channel model core flow oscillations necessarily involve flow oscillations in the lower and upper plena and in the riser/separator region. The greater fluid inertia associated with the single core channel model used in SABRE probably contributes to the greater core stability shown in the SABRE calculation (i.e., the longer time to the onset of instability).

---

[1]NEDO-32047, "ATWS Rule Issues Relative to Core Thermal-Hydraulic Stability", General Electric Company, January, 1992.

Table 5.6-1
Changes Made to Base SABRE 9x9 Input Deck in Appendix F

Parameter	New Value
Problem end time (F.2.1)	240 seconds
Time step data (F.3)	Max = 5 msec Min = 5 msec (0<t<10 sec) Max = 35 msec Min = 35 msec (10<t<120) Max = 25 msec Min = 25 msec (120<t<135) Max = 15 msec Min = 15 msec (135<t<180) Max = 5 msec Min = 5 msec (180<t)
Initial core power (F.6.1)	3323 MW[1]
Rated core thermal power (F.6.2)	3323 MW
Initial total core flow (F.7.1)	81.3 MLb/hr[1]
Initial guess for core channel flow (F.7.2)	75 MLb/hr
Status of scram system (F.19.1)	-1 (scram and ARI are failed)
Trip recirc. pump 'A' on specified time (F.23.1)	0.0 seconds (get recirc pump on turbine trip)
Trip recirc. pump 'A' on specified time (F.23.2)	0.0 seconds (get recirc pump on turbine trip)
High water level set point for feedwater trip (F.24.2)	54.D+09 inches (prevent loss of FW on high level oscillations)
Delay for level set point set down (F.24.12)	11.D+09 seconds (neglect set point set down)
Time at which turbine trip is initiated (F.26.1)	0.0 seconds
Maximum combined steam flow (F.26.10)	=2(F.26.4) = 2(14.631) = 29.26 Mlb/hr. (100% bypass capacity)
Turbine bypass capacity (F.26.17)	=(F.26.4) = 14.631 Mlb/hr (100% bypass capacity)
Gap Conductance (F.36.4)	870 Btu/hr-ft^2-°F (Table 2.1 of GENE-637-024-0893)

Table 5.6-2
Sequence of Events Calculated by SABRE

```
*** Kinetics file is /d00/appl/sabre3v0/data/u2c7.simtran.out

*** SABRE data file is /home/eamac/sabre_31/input/ec-atws-0505/c06.dat

*** This is not a restart case

1   S A B R E  -  Version 3.1
    (06) Turbine Trip ATWS from MEOD Rod line (u2c7) - Compare to GE


 t(sec)=        .000  Scram is Failed

 t(sec)=        .000  Low-Pres Condensate Injection Inop.

 t(sec)=        .000  ARI is Failed

 t(sec)=        .000  Main Turb Trip on specified time

 t(sec)=        .000  Recirc pump-A trip on specified time
                      Trip delay =      .000E+00 sec

 t(sec)=        .000  Recirc pump-B trip on specified time
                      Trip delay =      .000E+00 sec
```

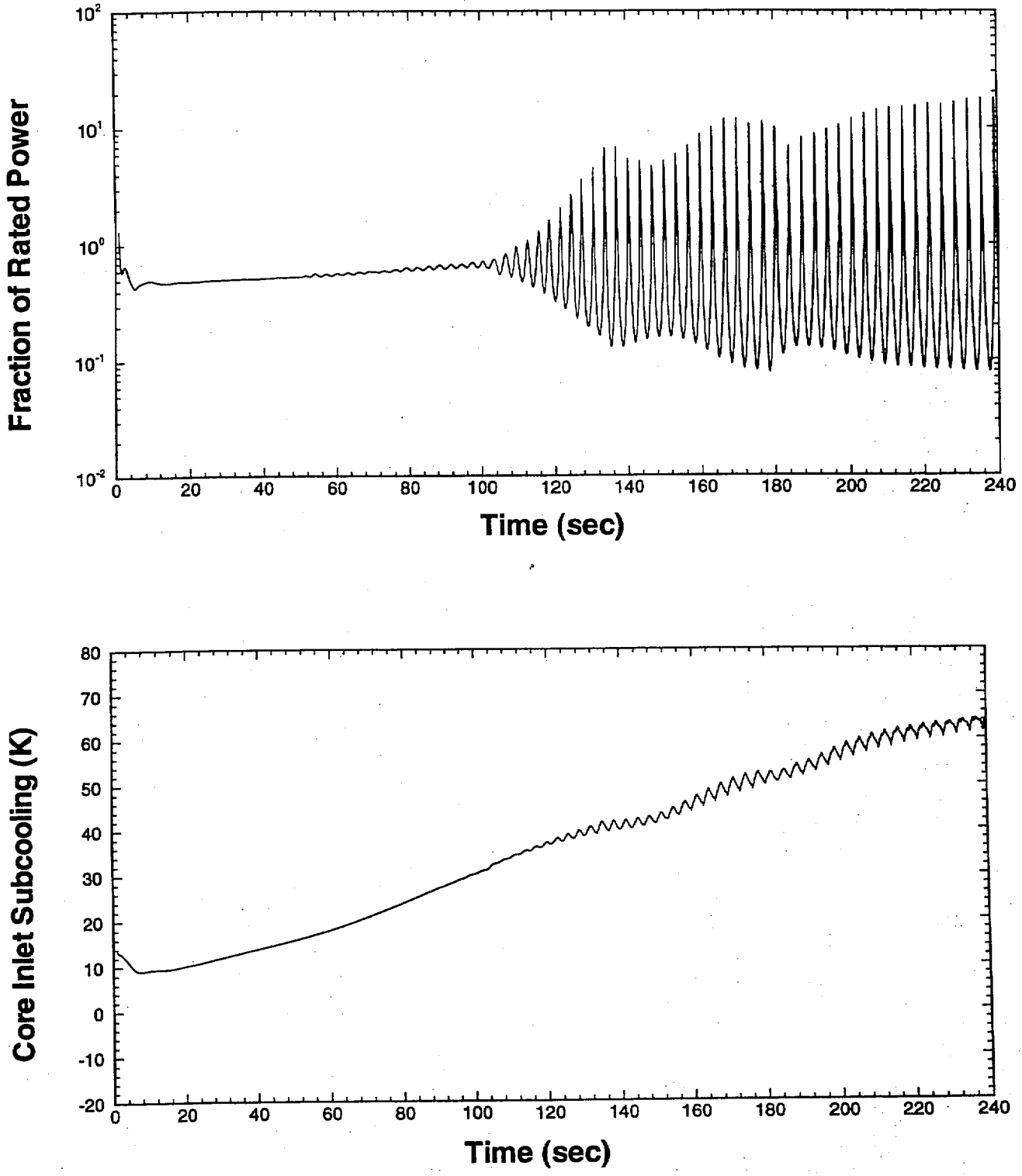

Figure 5.6-1 SABRE results for turbine trip ATWS with 100% turbine bypass capacity. U2C7 core model (9x9 core). No feedwater flow reduction. (SABRE Case 06)

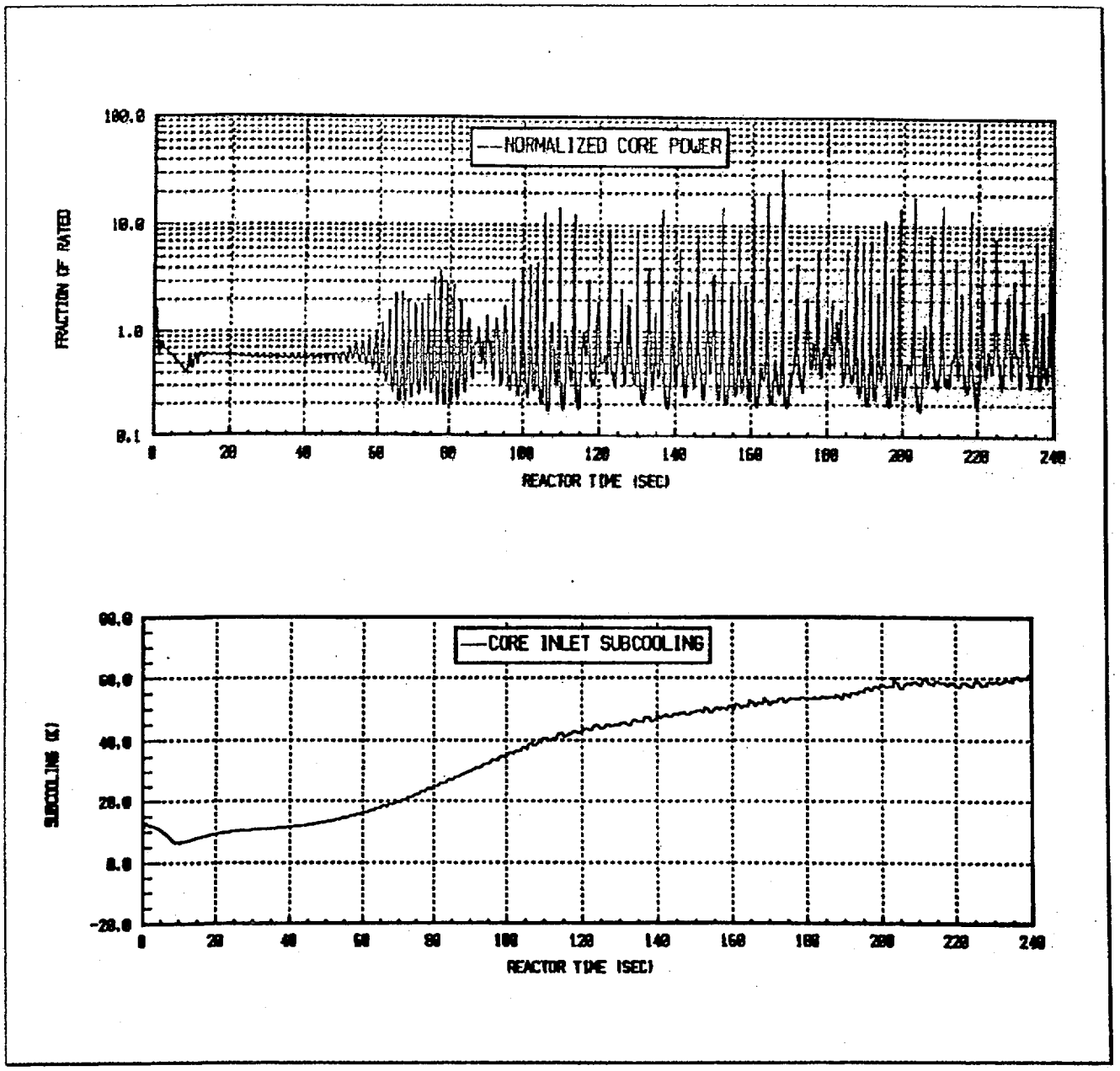

Figure 5.6-2 GE results for BWR/5 turbine trip ATWS with 100% turbine bypass capacity. (Results taken from NEDO 32047-A, "ATWS Rule Issues Relative to BWR Core Thermal-Hydraulic Stability, June 1995)

5.7 ATWS Initiated by Pressure Regulator Failure Open—Comparison to GE Results

The GE power-uprate ATWS analysis[1] for U2C7 shows that there are two limiting ATWS scenarios with regard to peak vessel pressure, peak clad temperature, and peak suppression pool temperature. These two scenarios are the MSIV-closure and PREGO ATWS events. In this benchmark study, SABRE results for an ATWS scenario initiated by pressure regulator failure to maximum demand (PREGO) are compared against the GE power uprate ATWS analysis. Section 5.8 compares SABRE against GE calculations for the MSIV-closure ATWS.

The PREGO scenario involves failure of the pressure regulator to maximum steam demand as the initiating event. Scram and ARI are failed. The reactor depressurizes until the MSIVs close on low steam line pressure. Recirculation pumps trip on high pressure following the MSIV closure, and the operator initiates boron injection to bring the reactor to Hot Shutdown. Changes made to the base 9x9 SABRE input deck are identified in Table 5.7-1. This SABRE calculation corresponds to SABRE Case 07 in the Computer Case Summary.

Following the MSIV closure, the turbine-driven feedwater pumps continue injection to the Reactor Pressure Vessel (RPV) while there is sufficient steam pressure available within the main steam lines to power the feedwater turbines. In the PREGO event, the turbine control valves and the turbine bypass valves open until steam flow reaches the maximum combined steam flow limit (see §F.26.10). When the MSIVs close on low steam line pressure, steam continues to be extracted from the steam lines and pressure drops rapidly. Consequently, the turbine-driven feedwater pumps would not operate for any significant amount of time following closure of the MSIVs. In the GE ATWS analysis for the PREGO initiating event, it was assumed that feedwater would operate for 90 seconds following the start of MSIV closure.[2] While this assumption is valid for the MSIV closure ATWS with proper operation of the pressure regulator, it is not a valid assumption for the PREGO ATWS. The assumption of feedwater operation for 90 seconds after the start of MSIV closure does not invalidate the GE Power Uprate analysis for the PREGO event because the assumption leads to a conservatively high suppression pool temperasture for the event. The availability of feedwater maintains level and fission power considerably higher than if feedwater flow was lost early in the event because of low steam line pressure. For benchmarking purposes, feedwater is maintained operable in the SABRE calculation for 90 seconds after the start of MSIV closure. This is accomplished by setting the low steam line pressure limit for feedwater operation to a negative value (see input F.24.3 in Table 5.7-1). In the GE and SABRE analyses, it is assumed that operators do not take manual control of feedwater injection prior to loss of feedwater from main-steam-line pressure decay.

Shortly after the loss of feedwater injection, HPCI and RCIC systems automatically initiate when level drops to their set points. In the SABRE calculation, HPCI and RCIC flows were adjusted to maintain downcomer water level as close as possible to the level used in the GE calculation. This was done in order to obtain a valid comparison for core power and suppression pool temperature. HPCI suction is maintained on the CST for the entire transient because the

---

[1] GENE-637-024-0893, "Evaluation of Susquehanna ATWS Performance for Power Uprate Conditions," September 1993.

[2] GENE-637-024-0893, p. A-2.

EOPs instruct the operator to manually defeat the automatic suction transfer to the suppression pool on high suppression pool level of 23.83 feet. In the GE analysis, HPCI suction was maintained on the CST.

In the SABRE calculation, the water level setpoint setdown for the feedwater system is neglected (the water level setpoint is "setdown" from +35" to +18" following a Level 3 scram signal[3]). The setpoint setdown and any recirculation pump runbacks are neglected in the SABRE calculation in order to simplify the analysis and to add conservatism.

In the GE calculation, water level was initially controlled within the target band (-80" to –110") specified by the EOPs for U2C7 but then level was allowed to drift above the level control band as the transient progressed (level was about –55" at t=1000 sec).[4] Since the GE REDY code controls water level through specification of the HPCI injection rate in the code input, it is difficult for GE to maintain constant level in their calculations. Consequently, GE allowed level to drift somewhat during the simulation. This was acceptable because with the GE methodology the somewhat higher level results in an overprediction of the suppression pool temperature.

A summary of the sequence of events calculated by SABRE is presented in Table 5.7-2. Figures 5.7-1 and 5.7-2 show a comparison of the GE and SABRE calculations for power, suppression pool temperature, steam dome pressure, core-average heat flux, indicated water level, and core-average void fraction. Key results for the PREGO ATWS are compared in Table 5.7-3.

Comparison of results in Table 5.7-3 shows that the peak suppression pool temperature predicted by SABRE differs from the GE value by only 0.5 °F (176.5 °F for GE and 176.0 °F for SABRE). This corresponds to a difference of –0.6% in the pool temperature rise which is within the margin of error of the calculation. SABRE predicts slightly higher values than GE for the steam dome pressure, and the core average heat flux.

In the SABRE calculation, the low-pressure set point (861 psig) for MSIV isolation is reached at 11.4 seconds into the event while GE predicts that pressure drops to the set point at 12.2 seconds. The most significant difference between the two calculations occurs after this point. SABRE results indicate that pressure begins to rise at about 15 seconds which is 3.6 seconds after the low-pressure isolation signal is reached. This SABRE result makes physical sense in that pressure should start to recover when the MSIVs are nearly closed (closure stroke is 4 seconds). The GE results indicate that MSIV closure begins at 14 sec and pressure begins to rise at about 18 seconds into the event.[5] This means that in the GE calculation there was a delay of nearly 2 seconds between the occurrence of the isolation signal (861 psig) and the start of MSIV closure. This delay of ~2 seconds appears too long based on the fact that the Susquehanna RETRAN model uses a delay of 0.05 seconds.[6] Outside of this discrepancy in MSIV closure time, the SABRE and GE calculations show good overall agreement particularly with regard to power and suppression pool temperature.

---

[3] Calc. EC-FUEL-0969, Section E.3.

[4] GENE-637-024-0893, Supplement 1.

[5] GENE-637-024-0893, Table A.3.1.

[6] Calc. EC-FUEL-0520 Rev. 0 (NFE-B-01-002).

Table 5.7-1
Changes Made to Base 9x9 Input Deck in Appendix F

Parameter	New Value
Problem end time (F.2.1)	1050 seconds
Time step data (F.3)	Max = 5 msec Min = 5 msec (0<t<30) Max = 30 msec Min = 30 msec (30<t)
Initial total core flow (F.7.1)	87 Mlb/hr (Table 2.1 of Ref. 1)
Initial guess for core channel flow (F.7.2)	80 MLb/hr
Initial steam dome pressure (F.8)	1053 psia (Table 2.1 of Ref. 1)
Initial downcomer subcooling (F.9)	29.49 Btu/Lbm[6]
Status of scram system (F.19.1)	-1 (scram and ARI are failed)
SP level at which HPCI suction transfers to pool (F.20.7)	23.83D+09 (prevent suction transfer to SP in accordance with EOPs)
Minimum HPCI flow (F.20.10)	250 gpm (reduced to make level control easier as power decreases)
Time at which operator takes control of HPCI injection (F.20.14)	238 sec (use operator control of HPCI to try and match GE level vs. time.
HPCI target level table (F.20.15)	Target specified to match GE water level.
Time at which operator takes control of RCIC injection (F.21.12)	238 sec (use operator control of HPCI to try and match GE level vs. time.
RCIC target level table (F.21.13)	Target specified to match GE water level.
High pressure trip for recirc. pump 'A' (F.23.7)	1214.7 psia (Table 2.2 of Ref. 1)
High pressure trip for recirc. pump 'B' (F.23.9)	1214.7 psia (Table 2.2 of Ref. 1)
Time delay for recirc. pump 'A' runback on low feedwater flow (F.23.12)	1.D+09 seconds (Neglect runback)
Time delay for recirc. pump 'A' runback on low feedwater flow (F.23.14)	1.D+09 seconds (Neglect runback)
Time delay for recirc. pump 'A' runback on low water level (F.23.16)	1.D+09 seconds (Neglect runback)
Time delay for recirc. pump 'A' runback on low water level (F.23.18)	1.D+09 seconds (Neglect runback)
Time at which manual trip of FW pumps is initiated (F.24.1)	102 sec (90 sec after start of MSIV closure) GENE-637-024-0893, p. A-2.
Minimum steam line pressure for feedwater operation (F.24.3)	-1.D+09 psia (prevent loss of FW on low steam line pressure to agree with GE analysis)
Time at which pressure regulator failure-open is initiated. (F.26.3)	0.0 seconds (to agree with GE calc.)
Maximum combined steam flow (F.26.10)	17.02 Mlb/hr (LDCN 2750)
ADS operability flag (F.27.1)	0 (EOPs instructs operator to manually defeat ADS in ATWS events)
Time at which SLCS is initiated (F.29.1)	113 seconds (Table A.3.1 of Ref. 1)
SRV actuation setpoints (F.31.4)	Used UALs per power uprate ATWS analysis.[7]
Gap Conductance (F.36.4)	870 Btu/hr-ft^2-°F (Table 2.1 of Ref. 1)
Initial suppression pool level (F.48)	22 ft. (gives water volume close to value in Table 2.1 of Ref. 1)
Time at which Loop 1 of SPC becomes effective (F.50)	1000 seconds (Table A.2.1 of Ref. 1)
Time at which Loop 2 of SPC becomes effective (F.51)	1000 seconds (Table A.2.1 of Ref. 1)

[6] Calc. EC-ATWS-1001.

[7] GENE-637-024-0893, "Evaluation of Susquehanna ATWS Performance for Power Uprate Conditions," Supplement 1, Table 1, September 1993.

Table 5.7-2
Sequence of Events Calculated by SABRE for Case 07

```
*** Kinetics file is /d00/appl/sabre3v0/data/u2c7.simtran.out

*** SABRE data file is /home/eamac/sabre_31/input/ec-atws-0505/c07.dat

*** This is not a restart case

1   S A B R E  -  Version 3.1
    (07) PREGO ATWS -- U2C7 -- Compare to GE


 t(sec)=        .000  Scram is Failed

 t(sec)=        .000  Low-Pres Condensate Injection Inop.

 t(sec)=        .000  ADS actuation is defeated

 t(sec)=        .000  ARI is Failed

 t(sec)=        .000  Press Regulator Failure Open (Max Demand)

 t(sec)=      11.430  MSIV closure on low reactor pressure
                      Setpoint(psia) =      875.700

 t(sec)=      15.430  MSIVs are closed

 t(sec)=      17.675  Level Setpoint Setdown
                      Setdown occurs when level drops to        13.00 in.
                      Delay for setpoint setdown =      .10E+10 sec

 t(sec)=      17.675  Recirc pump-A runback on low Rx lvl
                      Setpoint for Runback =        13.00 in.
                      Trip delay =     .100E+10 sec

 t(sec)=      17.675  Recirc pump-B runback on low Rx lvl
                      Setpoint for Runback =        13.00 in.
                      Trip delay =     .100E+10 sec

 t(sec)=      18.120  Recirc pump-A trip on hi Rx press.
                      Setpoint for trip =      1200.00 psig
                      Trip delay =     .230E+00 sec.

 t(sec)=      18.120  Recirc pump-B trip on hi Rx press.
                      Setpoint for trip =      1200.00 psig
                      Trip delay =     .230E+00 sec.

 t(sec)=     102.023  Feedwater Trip on specified time

 t(sec)=     113.003  SCLS Initiation
                      Number of Operable SLCS pumps =           2.
                      Transport Delay to vessel =       75.00 sec.

 t(sec)=     142.103  HPCI initiation on Low water level
                      Setpoint for initiation =      -38.00 in.

 t(sec)=     142.103  RCIC initiation on low water level
                      Setpoint for initiation =      -38.00 in.

 t(sec)=     238.013  Operator takes control of HPCI inj.

 t(sec)=     238.013  Operator takes control of RCIC inj.

 t(sec)=    1000.013  Loop 1 of Supp Pool Cool Effective
                      Service Water Temperature =       88.00 F

 t(sec)=    1000.013  Loop 2 of Supp Pool Cool Effective
                      Service Water Temperature =       88.00 F
```

Table 5.7-3
Comparison of GE and SABRE Results for U2C7 PREGO ATWS (Case 07)

Parameter	GE Calculation	SABRE Calculation	[SABRE]-[GE]	[SABRE]-[GE] (% of Rise in Temp/Press/Heat Flux)†
Peak Suppression Pool Temperature for t≤ 1050 sec	176.5 °F	176.0 °F	-0.5 °F	-0.6 %
Peak Steam Dome Pressure	1278 psia at 27 sec	1291 psia at 22.4 sec	+13 psi	+5.8 %
Peak Core Average Heat Flux (% of Rated)	141% at 24 sec	143% at 19.2 sec	+3%	+1.4%

† Based on temperature/pressure heat flux rise predicted by GE, i.e. 100%x(SABRE-GE)/GE.

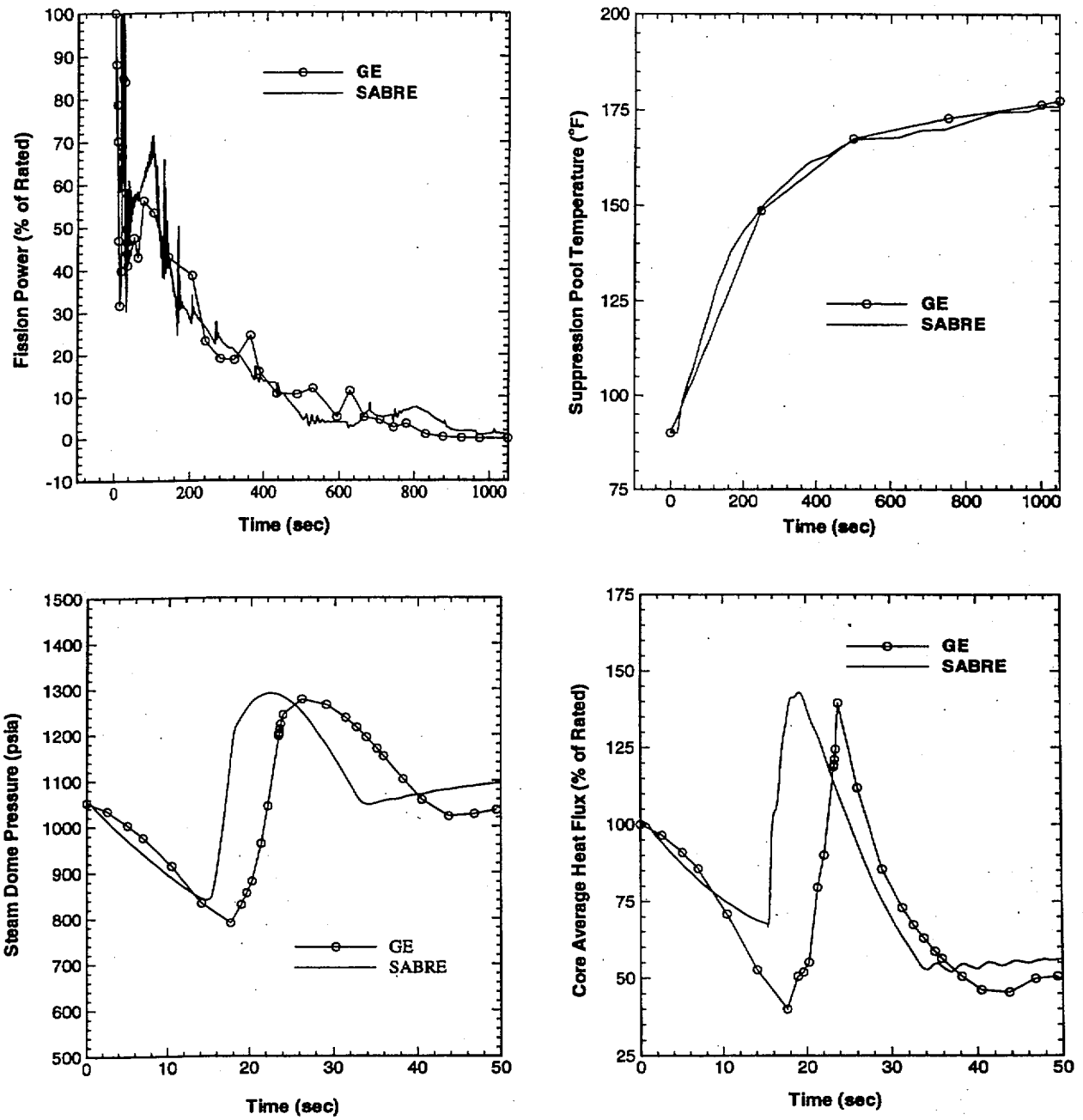

Figure 5.7-1 Comparison of SABRE and GE predictions for U2C7 PREGO ATWS event with boron injection. (SABRE Case 07)

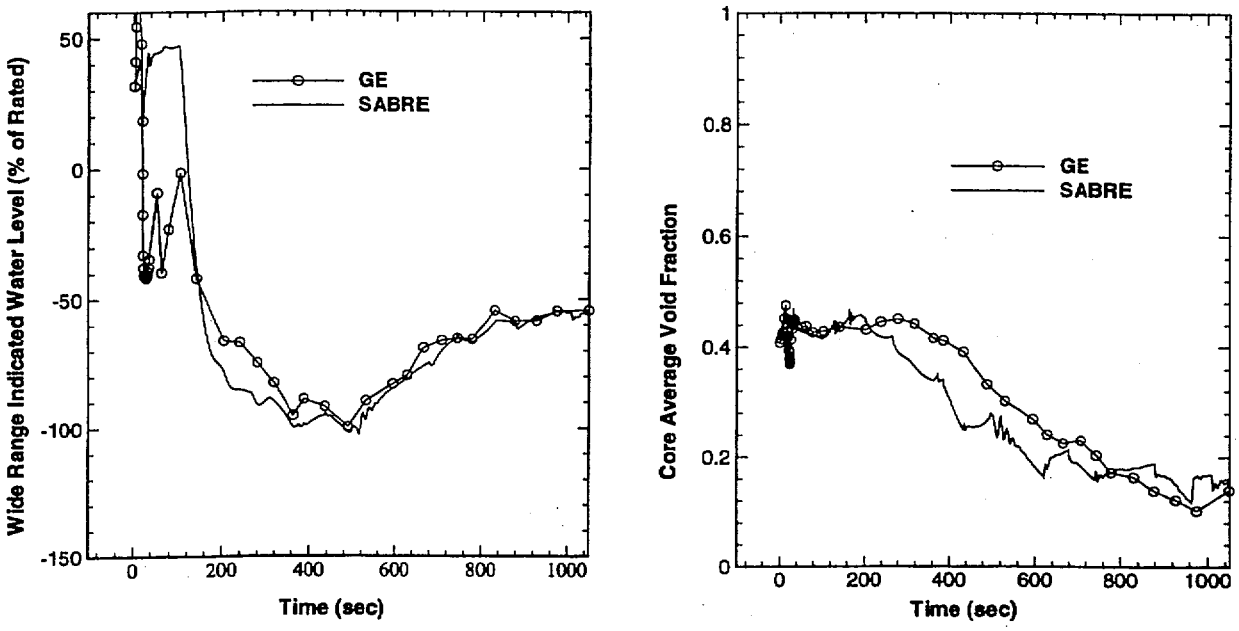

Figure 5.7-2 Comparison of SABRE and GE predictions for U2C7 PREGO ATWS event with boron injection. (SABRE Case 07)

5.8 MSIV-Closure ATWS with Boron Injection — Comparison to GE Calculations

An evaluation of the Susquehanna plant performance under ATWS conditions was performed by GE as part of the Susquehanna power uprate project.[1] In this section, SABRE results are compared against GE calculations, performed with the REDY code, for an MSIV-closure ATWS with boron injection.

Closure of the MSIVs is initiated at t=0. It is assumed that the operator does not take manual control of feedwater flow prior to its coast-down from depletion of main steam line pressure. Once feedwater flow ceases, level drops rapidly, and HPCI and RCIC systems initiate. HPCI and RCIC, with suction from the condensate storage tank (CST), are used to control level throughout the transient. SLCS is initiated at 95 seconds into the event. In this scenario water level is allowed to gradually recover as the reactor approaches the Hot Shutdown condition. Changes made to the base 9x9 SABRE input deck are shown in Table 5.8-1. The sequence of events generated by SABRE is presented in Table 5.8-2. This SABRE calculation corresponds to SABRE Case 08 in the Computer Case Summary.

GE and SABRE predictions for this event are compared in Figures 5.8-1 and 5.8-2. The SABRE calculation for the decay of fission power as a result of boron injection shows good overall agreement with the GE calculation. This is confirmed by the close agreement in suppression pool temperature. At 1000 seconds, the GE calculation predicts a suppression pool temperature of 178 °F. At the same time SABRE calculates a pool temperature of 177.3 °F. The short term steam dome pressure transient and core-average heat flux transients are compared in Figure 5.8-1 SABRE shows good agreement with the GE pressure calculation, but tends to under predict the peak heat flux. The SABRE heat flux curve is broader but less peaked. Differences between the key parameters, pool temperature, steam dome pressure, and core average heat flux are summarized in Table 5.8-3.

This case was repeated with one SRV out of service (Case 8a in Computer Case Summary). With one SRV out of service, SABRE predicts a peak steam dome pressure of 1351 psia at 10.5 seconds. GE calculates a peak dome pressure of 1340 psia at 9 seconds with one SRV out of service (Ref. 1, Table 3.1). SABRE overpredicts the pressure rise, as compared to GE, by 3.8%.

The 1-D kinetics equations in SABRE are integrated using the LSODES ordinary differential equation solver. LSODES automatically selects the time step size and method order to optimize run time and satisfy the error criteria which are specified as part of the code SABRE input data (see §F.1.5 and §F.1.6). The fluid flow and heat transfer equations in SABRE are solved using first-order, semi-implicit integration with the time step size specified by the code user. Since the hydraulic step size is part of the SABRE code input (§F.3), sensitivity studies were performed to determine the effect of variations in step size. A sensitivity study is also performed on the kinetics error control parameters.

---

[1] GENE-637-024-0893, "Evaluation of Susquehanna ATWS Performance for Power Uprate Conditions," September 1993.

The results presented in Figures 5.8-1 and 5.8-2 were obtained using hydraulic time steps of 5 msec for t<30 sec and 25 msec for t>30 sec. A smaller hydraulic step size was used for the beginning part of the transient because core power and pressure change rapidly when the MSIV closure occurs. In the remaining part of the transient, a larger time step is used because reactor conditions change more slowly as boron is injected and the core approaches Hot Shutdown condition. Sensitivity studies were performed on both the short-term time step and the long-term time step. Results of the hydraulic time step sensitivity studies are shown in Figures 5.8-3 and 5.8-4.

Figure 5.8-3 shows the power spike generated by the MSIV closure with hydraulic time steps of 1.25, 2.5, 5, and 10 msec. The maximum neutron power and peak steam dome pressure corresponding to each of these time steps is listed in the table below.

SABRE Case	Hydraulic step size (msec)	Peak Neutron Power (%)	Peak Steam Dome Pressure (psia)
08e	10	540	1310.2
08	5	516	1308.6
08f	2.5	504	1307.5
08i	1.25	497	1306.7

These results show that the incremental change in maximum power and peak pressure is decreasing as the step size decreases which indicates convergence to a solution. Also, with a hydraulic step size of 5 msec the peak power appears to be overestimated by about 4%. Because of the short duration of the power spike, the differences in peak power computed with the step sizes listed in the above table will have negligible effect on the long term suppression pool temperature response. As a result, any of the short-term step sizes ranging from 1.25 msec to 10 msec would be acceptable for the ATWS suppression pool heat-up analysis. A step size of 5 msec is recommended however because it is the best compromise between computer run time and accuracy. Aside from the peak power, there is little variation in the short-term solution with the step sizes considered.

The effect of variations in the long-term hydraulic time step size (t>30 sec) is also investigated. Figure 5.8-4 shows the suppression pool temperature response with hydraulic time steps (for t>30 sec) ranging from 20 to 40 msec. The results do not show any noticeable dependence on step size for the range of steps considered. Therefore, a long-term hydraulic step size anywhere in the range of 20 to 40 msec would be acceptable. A sensitivity was also performed on the error control parameters for the kinetics solution (RTOL and ATOL in §F.1.5 and §F.1.6, respectively) carried out with the ODE solver LSODES. SABRE Case 08 was run with RTOL=ATOL=1.D-05. In SABRE Cases 08j and 08k the values of RTOL and ATOL were set to 5.D-05 and 5.D-06, respectively. Figures 5.8-5 and 5.8-6 show that the core power and suppression pool temperature response are essentially insensitive to the changes in RTOL and ATOL.

A sensitivity study was also performed on the number of boron mixing nodes used to track the transport of borated water through the reactor core and on the boron entrainment exponent b in Equation 2.4.6-1. The number of axial nodes for boron transport through the core can range from 1 to 10 (value is selected in code input). The results in Figure 5.8-7 show that the solution is independent of the number of mixing nodes when 8 to 10 nodes are selected.

All ATWS cases in this calculation package were carried out using b=1 (linear model) in Equation 2.4.6-1 except for Cases 08l and 08m. Case 08l was run with b=1/2 and Case 08m was run with b=2. The entrainment fraction as a function of total core flow for b=1/2, b=1, and b=2 is shown in Figure 2.4.6-1. Figure 5.8-8 shows the sensitivity of the suppression pool temperature response to the entrainment exponent b. The results show that there is little change in the pool temperature response as b is varied from ½ to 2.

Table 5.8-1
Changes Made to Base SABRE 9x9 Input Deck in Appendix F

Parameter	New Value
Problem end time (F.2.1)	1000 seconds
Time step data (F.3)	Max = 5 msec Min = 5. msec(t<30) Max = 25 msec Min = 25 msec (30<t)
Initial total core flow (F.7.1)	87 Mlb/hr (Table 2.1 of Ref. 1)
Initial guess for core channel flow (F.7.2)	80 MLb/hr
Initial steam dome pressure (F.8)	1053 psia (Table 2.1 of Ref. 1)
Initial downcomer subcooling (F.9)	29.49 Btu/Lbm^2
Status of scram system (F.19.1)	-1 (scram and ARI are failed)
SP level for HPCI suction transfer to SP (F.20.7)	23.83D+09 ft. (prevents transfer)
HPCI target level table (F.20.15)	Target water level for HPCI is specified to match GE reactor water level response.
RCIC target level table (F.21.13)	Target water level for RCIC is specified to match GE reactor water level response.
High pressure trip for recirc. pump 'A' (F.23.7)	1214.7 psia (Table 2.2 of Ref. 1)
High pressure trip for recirc. pump 'B' (F.23.9)	1214.7 psia (Table 2.2 of Ref. 1)
Time delay for recirc. pump 'A' runback on low feedwater flow (F.23.12)	1.D+09 seconds (Neglect runback)
Time delay for recirc. pump 'A' runback on low feedwater flow (F.23.14)	1.D+09 seconds (Neglect runback)
Time delay for recirc. pump 'A' runback on low water level (F.23.16)	1.D+09 seconds (Neglect runback)
Time delay for recirc. pump 'A' runback on low water level (F.23.18)	1.D+09 seconds (Neglect runback)
MSIV closure on specified time (F.25.1)	0.0 seconds (to agree with GE calc.)
ADS operability flag (F.27.1)	0 (EOPs instruct operator to manually defeat ADS in ATWS events)
Time at which SLCS is initiated (F.29.1)	95 seconds (Table A.2.1 of Ref. 1)
SRV actuation setpoints (F.31.4)	Used UAL values from Table 1 of Supplement 1 to Ref. 1.
Gap Conductance (F.36.4)	870 Btu/hr-ft^2-°F (Table 2.1 of Ref. 1)
Initial suppression pool level (F.48)	22 ft. (gives water volume close to value in Table 2.1 of Ref. 1)
Time at which Loop 1 of SPC becomes effective (F.50)	1000 seconds (Table A.2.1 of Ref. 1)
Time at which Loop 2 of SPC becomes effective (F.51)	1000 seconds (Table A.2.1 of Ref. 1)

[2] Calc. EC-ATWS-1001.

Table 5.8-2
Sequence of Events Calculated by SABRE

```
*** Kinetics file is /d00/appl/sabre3v0/data/u2c7.simtran.out

*** SABRE data file is /home/eamac/sabre_31/input/ec-atws-0505/c08.dat

*** This is not a restart case

1   S A B R E  -  Version 3.1
    (08) U2C7 MSIVC ATWS -- Compare to GE


 t(sec)=       .000  Scram is Failed

 t(sec)=       .000  Low-Pres Condensate Injection Inop.

 t(sec)=       .000  ADS actuation is defeated

 t(sec)=       .000  ARI is Failed

 t(sec)=       .000  MSIV closure on specified time

 t(sec)=      4.005  MSIVs are closed

 t(sec)=      4.810  Recirc pump-A trip on hi Rx press.
                     Setpoint for trip =      1200.00 psig
                     Trip delay =     .230E+00 sec.

 t(sec)=      4.810  Recirc pump-B trip on hi Rx press.
                     Setpoint for trip =      1200.00 psig
                     Trip delay =     .230E+00 sec.

 t(sec)=     95.020  SCLS Initiation
                     Number of Operable SLCS pumps =          2.
                     Transport Delay to vessel =        75.00 sec.

 t(sec)=     98.320  Feedwater Trip on low Stm Line Press
                     Flow stops when press <       175.00 psia

 t(sec)=    110.445  Level Setpoint Setdown
                     Setdown occurs when level drops to       13.00 in.
                     Delay for setpoint setdown =      .10E+10 sec

 t(sec)=    139.045  HPCI initiation on Low water level
                     Setpoint for initiation =       -38.00 in.

 t(sec)=    139.045  RCIC initiation on low water level
                     Setpoint for initiation =       -38.00 in.

 t(sec)=    250.020  Operator takes control of HPCI inj.

 t(sec)=    250.020  Operator takes control of RCIC inj.
```

Table 5.8-3
Comparison of GE and SABRE Results for U2C7 MSIV Closure ATWS (Case 08)

Parameter	GE Calculation	SABRE Calculation	[SABRE]-[GE]	[SABRE]-[GE] (% of Temp/Press Rise)†
Suppression Pool Temperature at 1000 sec	178 °F	177.3 °F	-0.8 °F	-0.8 %
Peak Steam Dome Pressure	1313 psia at 8 sec	1309 psia at 9.5 sec	-5 psi	-2 %
Peak Core Average Heat Flux (% of Rated)	156 % at 4.4 sec	140.5 % at 6.2 sec	-15.5	-28%

† Based on temperature/pressure/heat flux rise predicted by GE, i.e., 100%x(SABRE-GE)/GE.

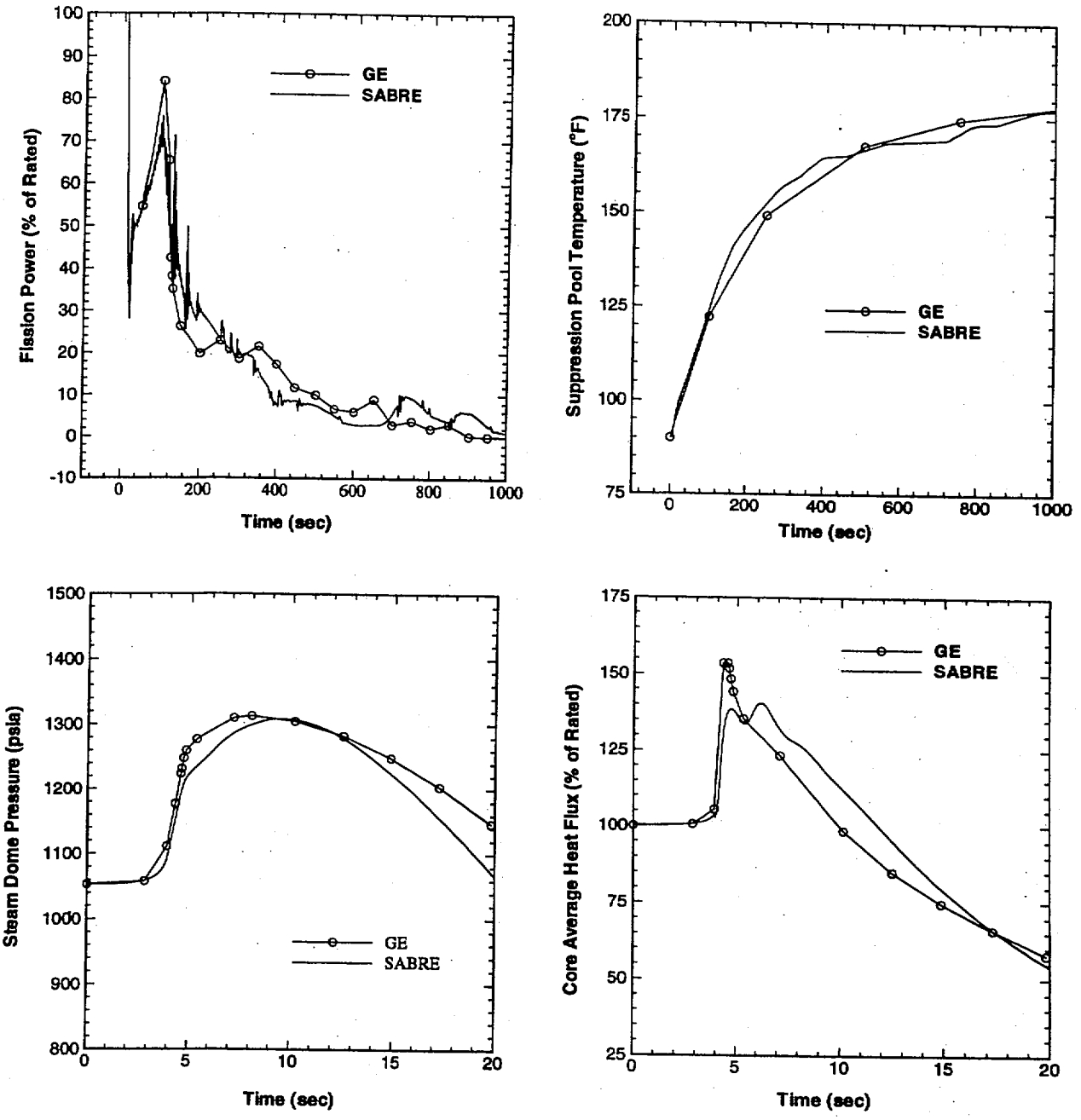

Figure 5.8-1 Comparison of SABRE and GE predictions for U2C7 MSIVC ATWS event with boron injection. (SABRE Case 08)

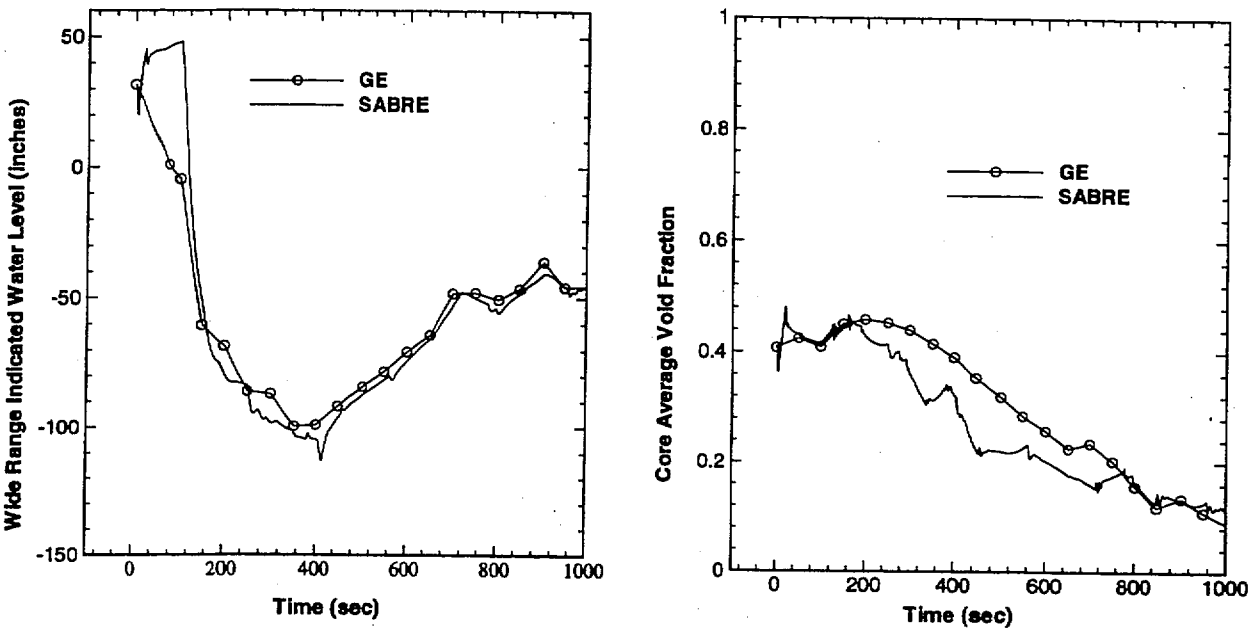

Figure 5.8-2 Comparison of SABRE and GE predictions for U2C7 MSIVC ATWS event with boron injection. (SABRE Case 08)

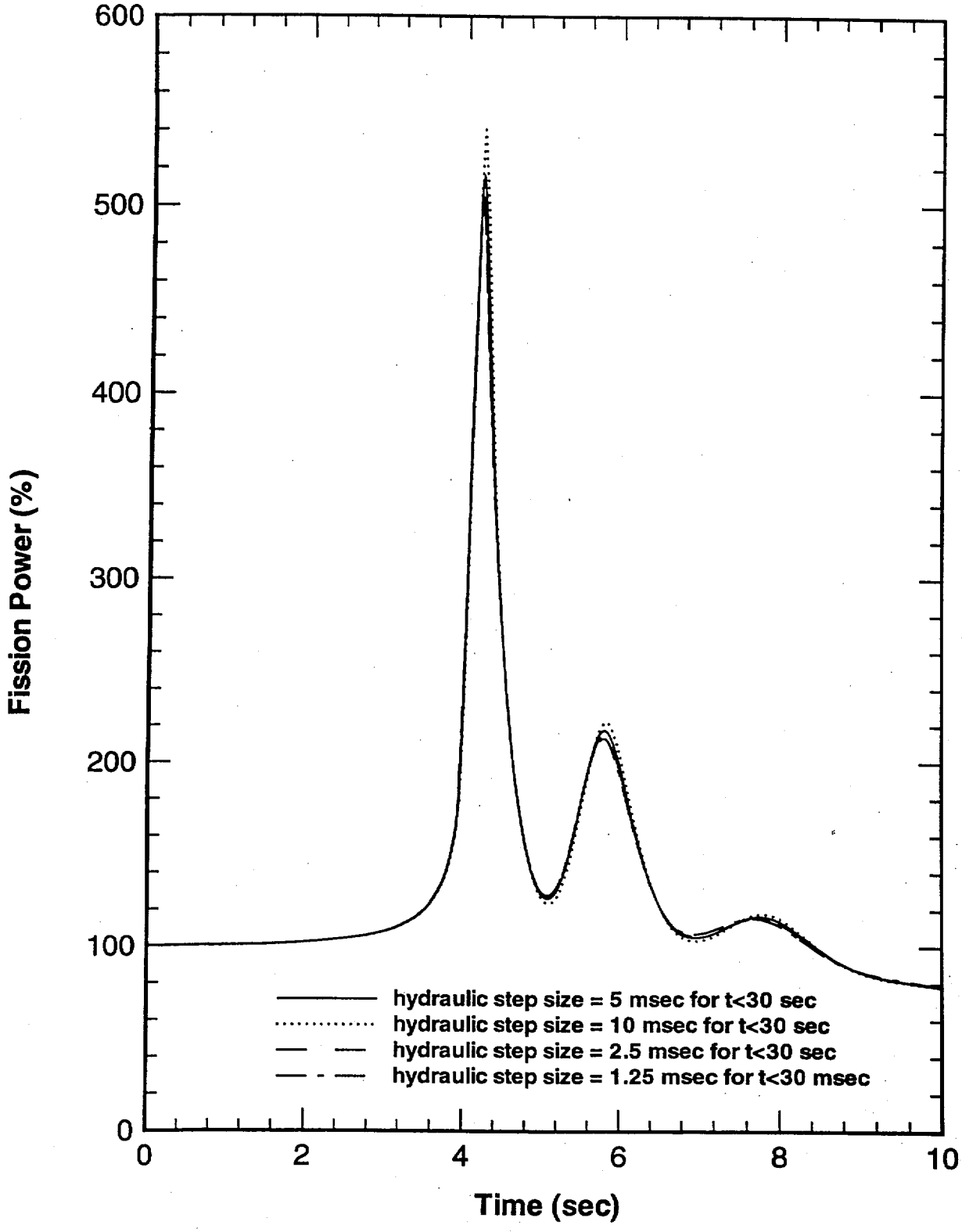

Figure 5.8-3 Effect of hydraulic time step size on power spike for MSIV closure ATWS. Time step size for kinetics solution is selected by ODE solver LSODES. (SABRE Cases 08, 08e, 08f, and 08i)

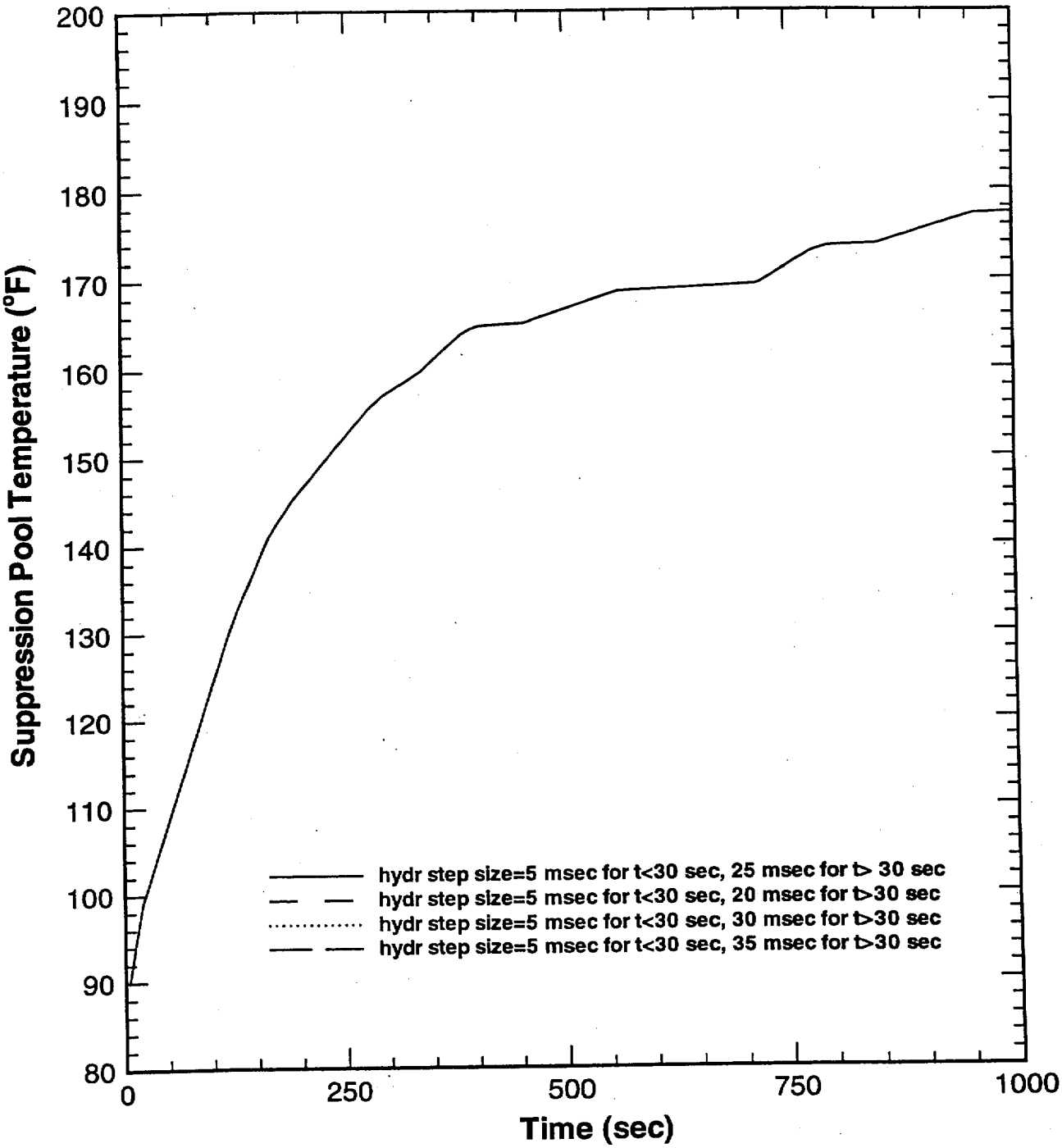

Figure 5.8-4 Effect of hydraulic time step size on suppression pool temperature response for MSIV closure ATWS. Time step size for kinetics solution is selected by ODE solver LSODES. (SABRE Cases 08, 08b, 08c, and 08d)

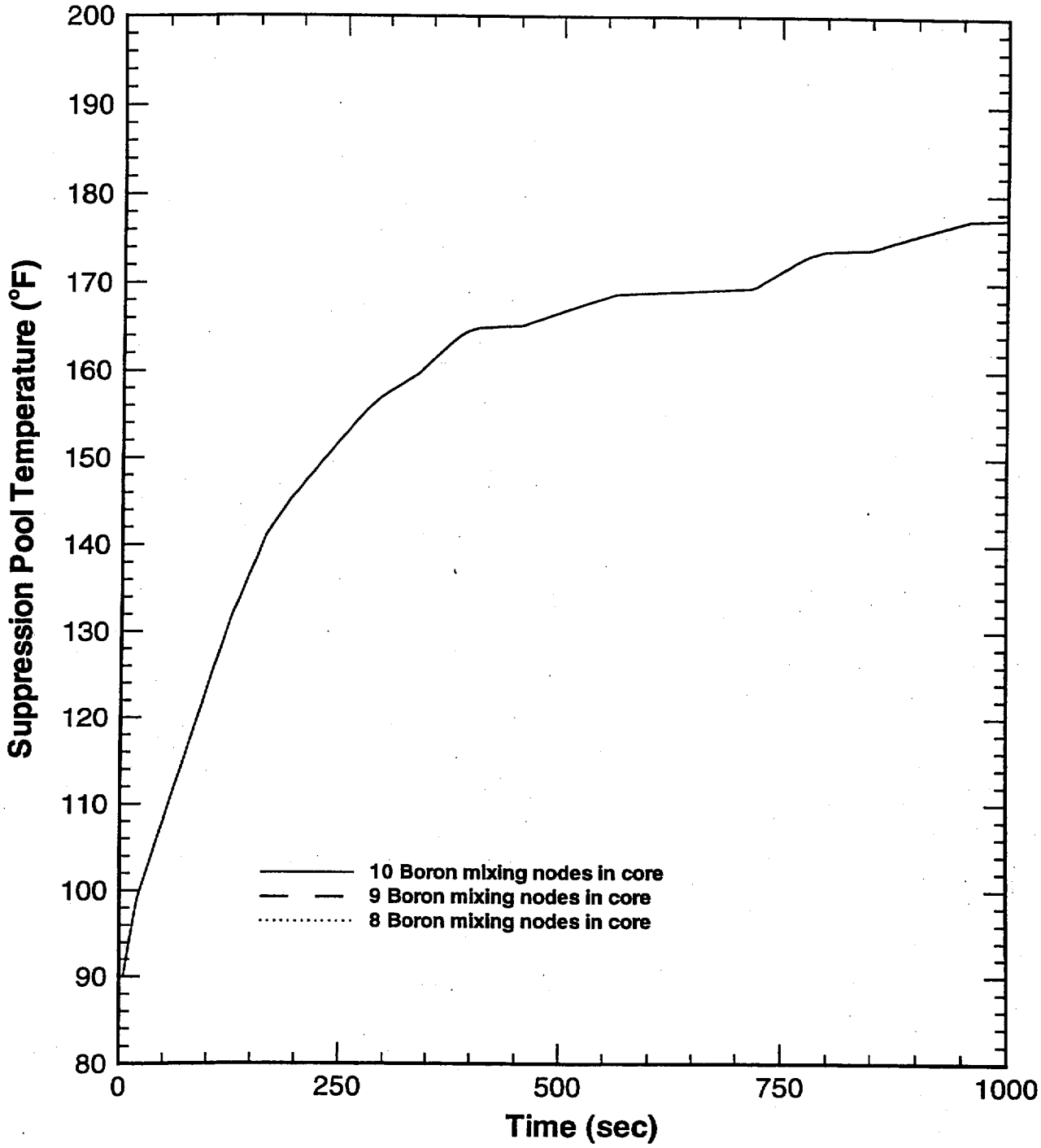

Figure 5.8-5 Effect of Boron mixing nodalization on suppression pool temperature response for MSIV closure ATWS. Time step size for kinetics solution is selected by ODE solver LSODES. Hydraulic time steps are 5 msec for t<30 sec and 25 msec for t>30 sec. (SABRE Cases 08, 08g, and 08h)

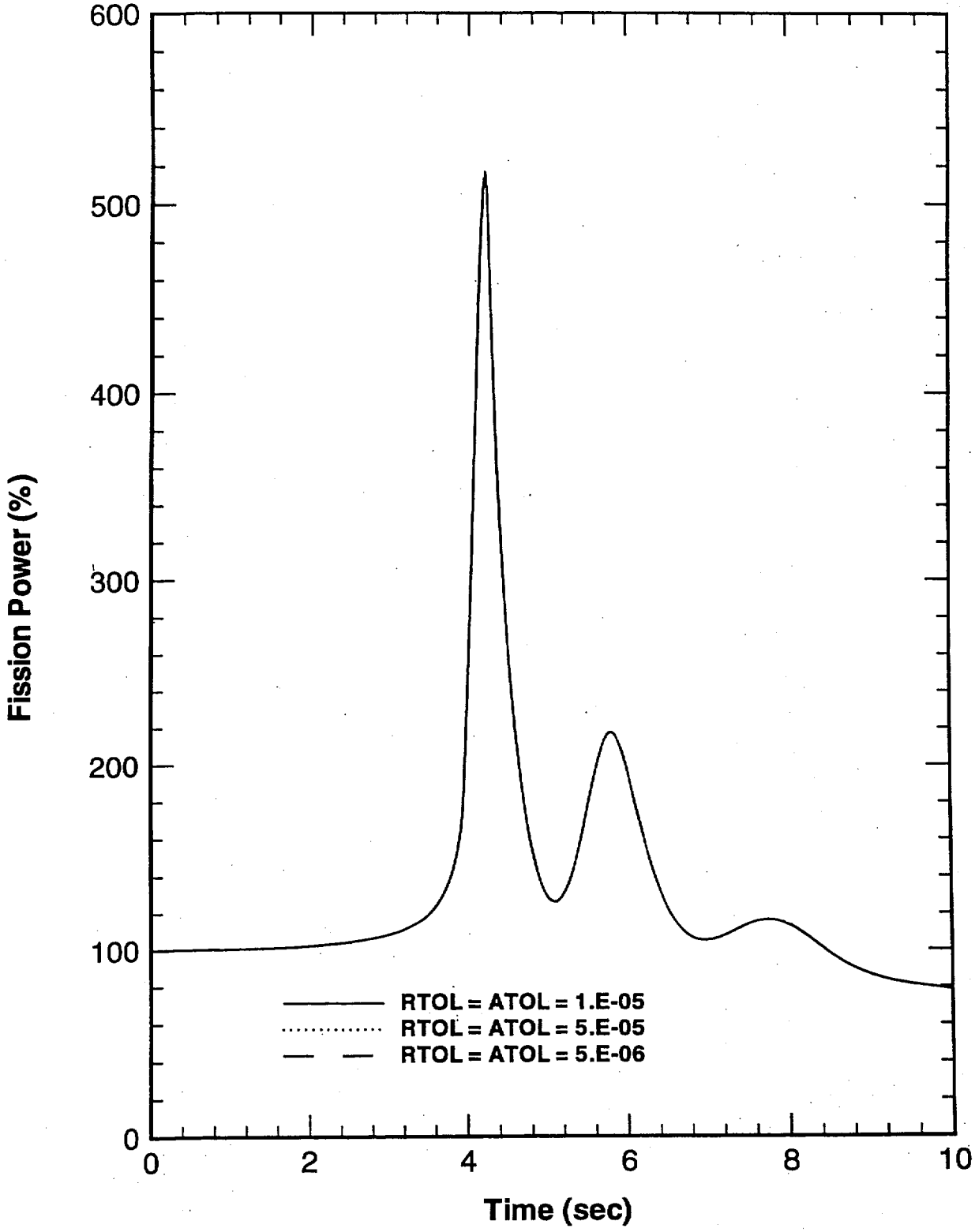

Figure 5.8-6 Effect of 1-D kinetics error control parameters RTOL and ATOL on power spike for MSIV closure ATWS. Hydraulic time steps are 5 msec for t<30 seconds and 25 msec for t>30 seconds. (SABRE Cases 08, 08j, and 08k)

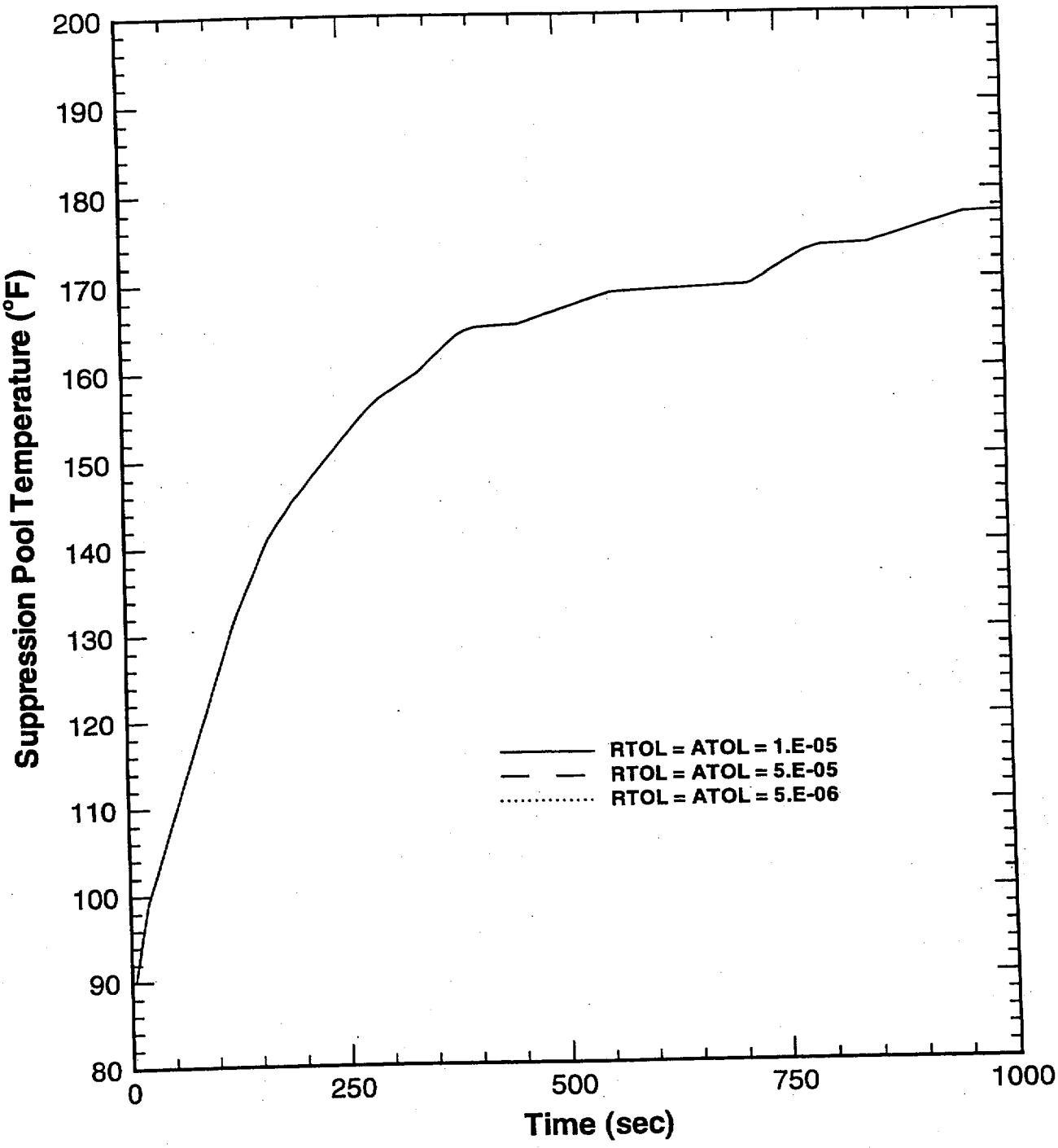

Figure 5.8-7 Effect of 1-D kinetics error control parameters RTOL and ATOL on on suppression pool temperature response for MSIV closure ATWS. Hydraulic time steps are 5 msec for t< 30 sec and 25 msec for t>30 sec. (SABRE Cases 08, 08j, and 08k)

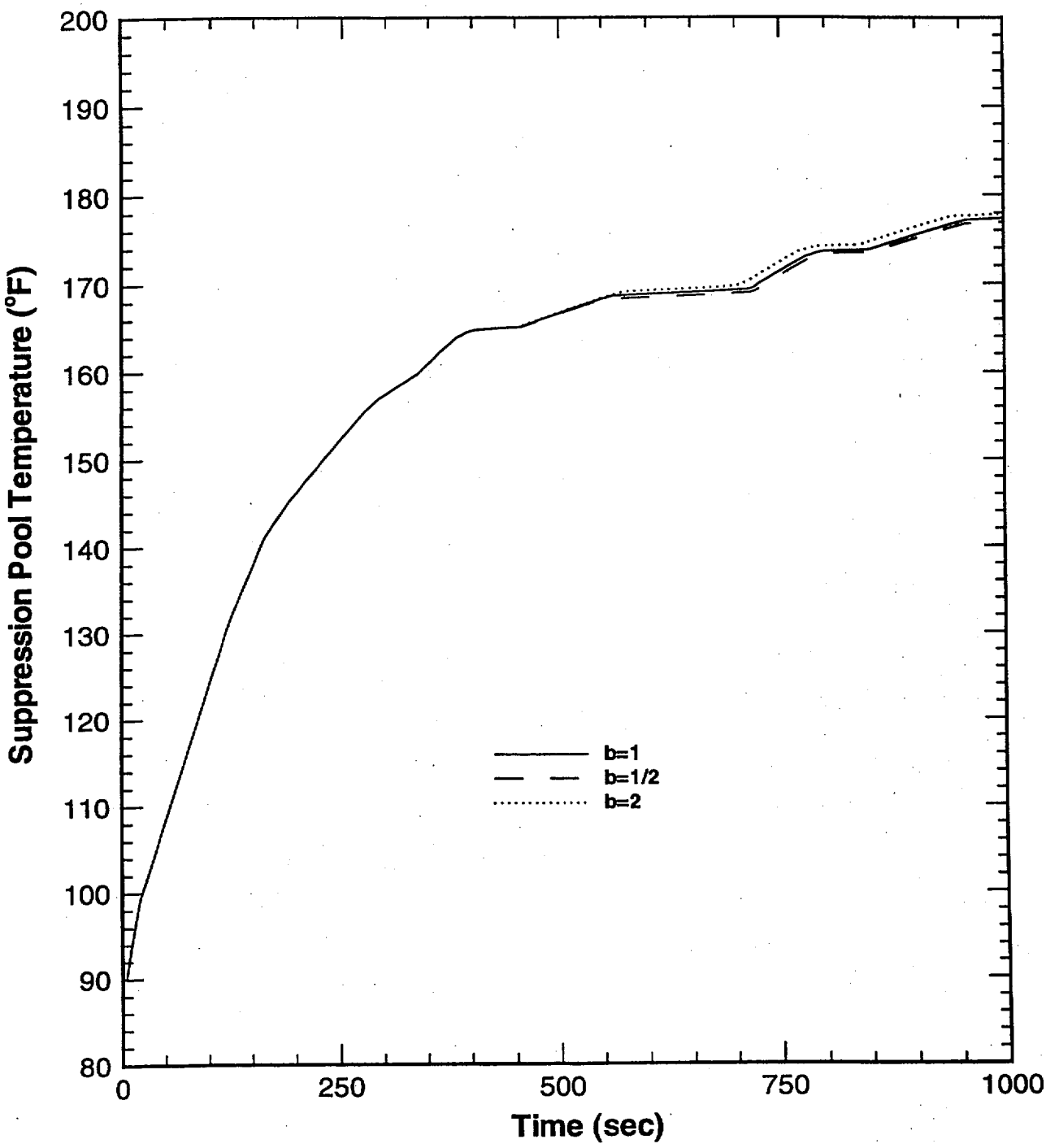

Figure 5.8-8 Effect of boron entrainment parameter b on suppression pool temperature response for MSIV closure ATWS. Hydraulic time steps are 5 msec for t< 30 sec and 25 msec for t>30 sec. (SABRE Cases 08, 08l, and 08m)

5.9 Calculation of Counter-Current Flow Limit–Comparison to Kutateladze CCFL Correlation

The Ohkawa-Lahey void model is used in the SABRE two-phase flow Calculation. In this drift-flux model, the functional form of the parameters C_o (radial concentration parameter) and V_{gj} (drift velocity) are such that the drift-flux model predicts the counter-current flow limit in agreement with the Kutateladze correlation.[1] In this section, the SABRE flow model is used to predict the counter-current flow limit (CCFL) for a heated channel with inlet flow blockage. Calculation results are compared with the Kutateladze correlation in order to verify the two-phase flow model used in SABRE. The core channel model used in this benchmark study was constructed from subroutines taken directly from the SABRE code. The FORTRAN code used for the channel flow calculation is listed in Appendix E.

In a channel with inlet flow blockage, liquid flows down into the top of the channel and replaces some or all of the water which is boiled off. If the flow is not counter-current flow limited, then a steady condition will arise in which all of the water converted to steam is replaced by the downward flowing liquid. If the channel power is high enough, however, the flow of vapor at the channel exit will restrict the downward flow of liquid (kinematic choking), and portions of the channel can become completely voided. In this situation, fuel rods can become damaged from loss of two-phase cooling.

The channel power associated with kinematic choking (CCFL) can be predicted from the Kutateladze correlation which is given by[1]

$$(j_g)^{1/2} + \left(\frac{\rho_\ell}{\rho_g}\right)^{1/4} |j_\ell|^{1/2} = V_0^{1/2}\left(\frac{\rho_\ell}{\rho_g}\right)^{1/4} \tag{5.9-1}$$

where

$$V_0 = \frac{3.2\left[gg_c\sigma\left(\rho_\ell - \rho_g\right)\right]^{1/4}}{\sqrt{\rho_\ell}}. \tag{5.9-2}$$

Just below the power level associated with CCFL, the vapor and liquid flow rates at the channel exit are given by the following energy and mass balances,

$$w_g = j_g \rho_g A = Q/\left(h_g - h_\ell\right) \tag{5.9-3}$$

and

$$w_\ell = -w_g = j_\ell \rho_\ell A. \tag{5.9-4}$$

---

[1] Ohkawa, K., and Lahey, R.T., "The Analysis of CCFL Using Drift-Flux Models," Nuclear Engineering and Design, Vol. 61, pp. 245-255, 1980.

Substituting (5.9-3) and (5.9-4) into (5.9-1) leads to the following result for the channel power associated with CCFL:

$$Q_{CCFL} = \left[\frac{V_0^{1/2} \left(\frac{\rho_\ell}{\rho_g} \right)^{1/4}}{\left(\frac{1}{(h_g - h_\ell)\rho_g A} \right)^{1/2} + \left(\frac{\rho_\ell}{\rho_g} \right)^{1/4} \left(\frac{1}{(h_g - h_\ell)\rho_\ell A} \right)^{1/2}} \right]^2 \qquad (5.9\text{-}5)$$

For a core channel with a flow area of 0.114 ft^2, and a system pressure of 1000 psia, Equation (5.9-5) predicts that the power associated with kinematic choking is 451 Btu/sec. That is, if the power of the blocked channel is less than 451 Btu/sec, the reverse flow of liquid at the channel exit will be unrestricted, and it will be equal to the inventory loss due to boiling. On the other hand, if the power exceeds 451 Btu/sec, then the flow of vapor at the channel exit will restrict the reverse flow of liquid into the channel. In this situation, there is a loss of coolant inventory accompanied by an increase in channel void fraction.

For benchmarking purposes, the core channel model developed from SABRE subroutines was run at a series of power levels some of which are below the critical power level of 451 Btu/sec and some above. Initially, the channel is filled with saturated liquid, so there is a sudden expulsion of liquid when the channel is instantaneously set to the specified power level. As the transient progresses, the liquid flow at the channel exit reverses its flow direction. A no-flow boundary condition is specified at the bottom of the channel to simulate the blockage. At the top of the channel, it is assumed that $\partial \bar{h}/\partial z = 0$, where $\bar{h}$ is the volume-weighted enthalpy of the two-phase mixture. The channel model consists of twenty-five axial nodes, and the heat addition is axially uniform.

Figure 5.9-1 shows the transient void fraction at the channel exit as a function of channel power. At 450 Btu/sec, which is just below the critical channel power predicted from Eqn. (5.9-5), the void fraction approaches a constant value as there is no restriction on liquid flow into the top of the channel. When the channel power is increased to 452 Btu/sec (1 Btu/sec above the critical power), an excursion in the void fraction occurs since liquid cannot enter the channel in sufficient amount to compensate for the inventory loss due to boiling. Figure 5.9-2 displays the liquid flow behavior at the channel exit for the same cases. The rapid decrease in reverse flow of liquid at the channel exit indicates the onset of kinematic choking. These results demonstrate that the fluid dynamics model in SABRE is consistent with the Kutateladze CCFL correlation.

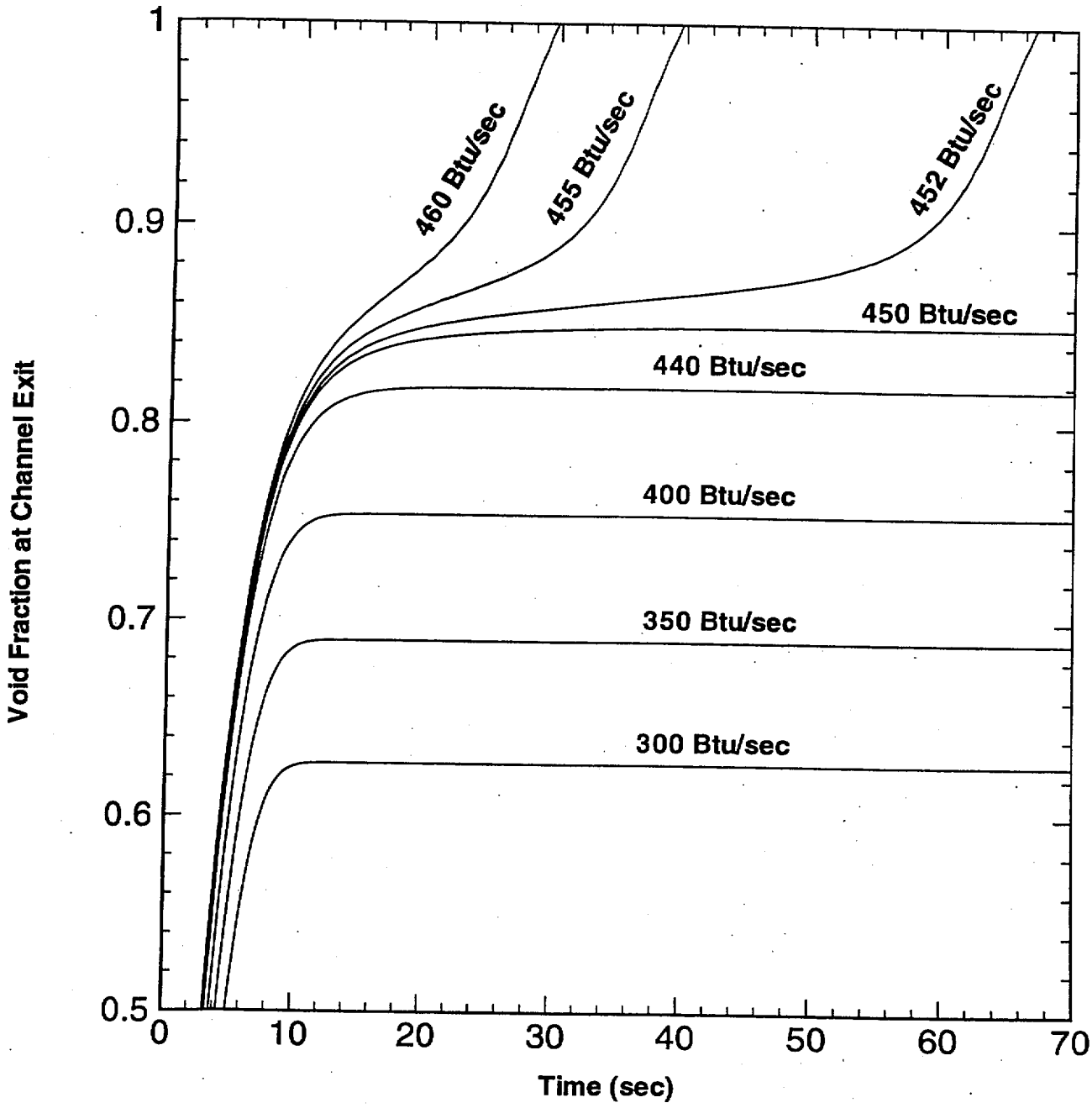

Figure 5.9-1 Prediction of channel power associated with kinematic choking by examination of void fraction response at channel exit.

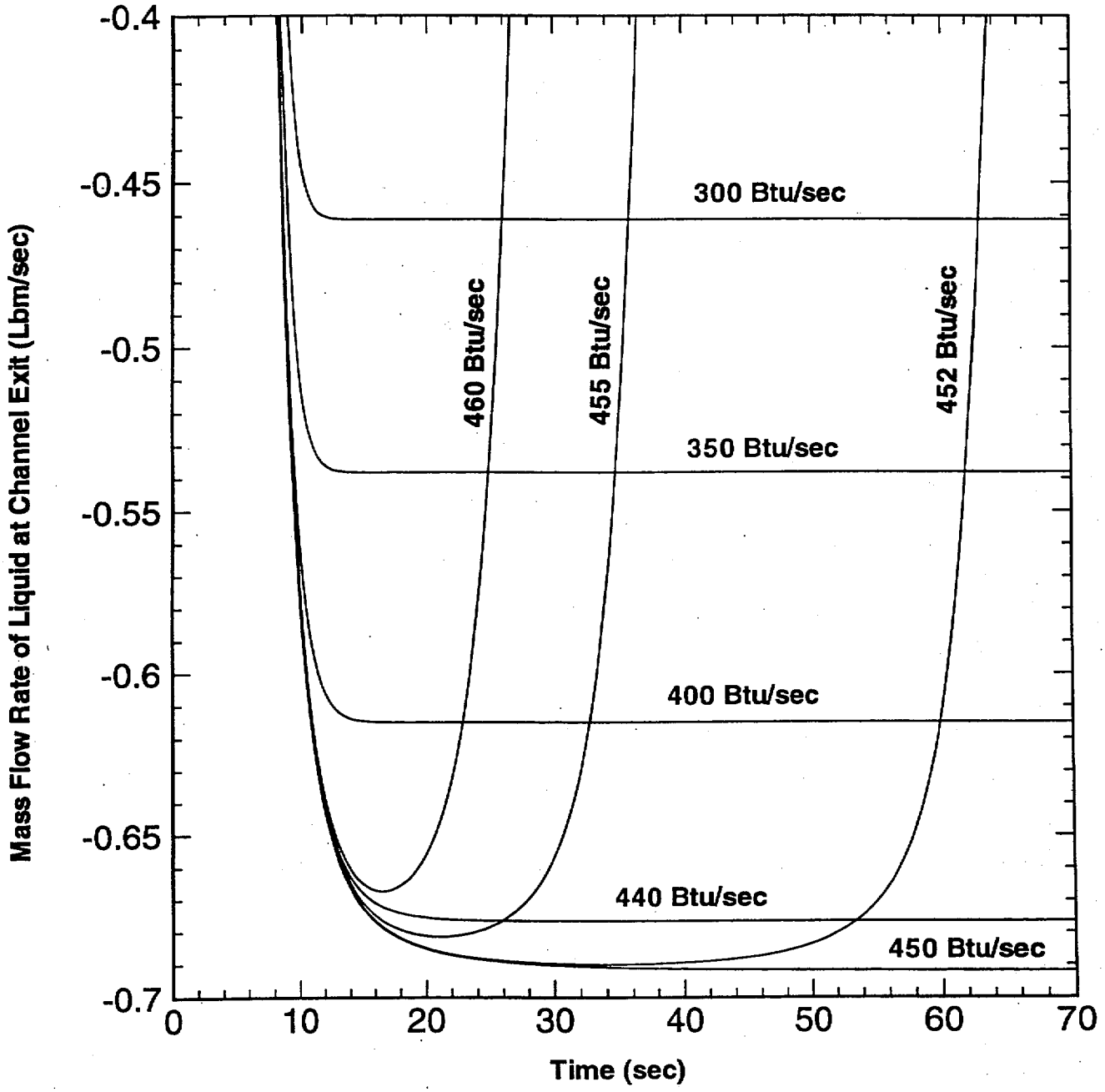

Figure 5.9-2 Prediction of channel power associated with kinematic choking by examination of liquid flow response at channel exit.

5.10 Suppression Pool Heatup from Decay Heat—Comparison to Heat Balance Calculation

Benchmarking results are presented for suppression pool heat up due to decay heat generation. In the SABRE calculation, an MSIV closure with reactor scram is initiated at t=0. Feedwater trips early in the event (45 seconds) on high RPV water level, and HPCI, with suction on the suppression pool, is used to supply coolant to the reactor. Initial reactor power is 3293 MWt, and the initial suppression pool level is 23 feet. RPV water level is controlled between 13" and 54". There is no removal of decay heat from the containment. Changes made to the base SABRE input deck are identified in Table 5.10-1. This SABRE calculation corresponds to SABRE Case 10 in the Computer Case Summary.

In this transient, reactor water level is maintained near its initial value. In addition, the reactor is not depressurized; rated reactor pressure is maintained by automatic actuation of SRVs. Since there is little change in the reactor coolant inventory, and since HPCI suction is always on the suppression pool, suppression pool mass is essentially constant. That is, water from the suppression pool is injected to the reactor, converted to steam by decay heat generation, and deposited back in the pool. Also, there is no sensible heat given off by the reactor vessel and internal structures because the reactor is maintained at high pressure.

For this situation, the rise in suppression pool temperature can easily be calculated from the following heat balance on the containment.

$$Q_{decay}(t) = M_W \int_{T_1}^{T(t)} C_{P,W}(\Theta)d\Theta + M_{S,DW}C_{P,S}\left[T(t) - T_2\right] + M_{S,WW}C_{P,S}\left[T(t) - T_1\right] \qquad (5.10\text{-}1)$$

where

$Q_{decay}(t)$ = integrated decay heat at t seconds after shutdown (Btu),
$T(t)$ = suppression pool temperature at time t (°F),
M_W = initial mass of water in suppression pool = 7.96×10^6 lbm,
$C_{P,W}$ = specific heat of water Btu/lbm-°F,
$M_{S,DW}$ = mass of steel in drywell = 1.6×10^6 lbm (§ D.18.14),
$M_{S,WW}$ = mass of steel in wetwell = 0.695×10^6 lbm (§ D.18.16),
$C_{P,S}$ = specific heat of steel = 0.14 Btu/lbm-°F (§ D.2),
T_1 = initial temperature of suppression pool and air space = 90 °F, and
T_2 = initial temperature of drywell = 120 °F.

The temperature dependence for the specific heat of water is approximated by the following linear relation[1]

[1] Data from ASME Steam Tables, 5th Edition, p. 278.

$$C_{P,W}(T) = 0.998 + 1.813x10^{-4}[T - 90].$$

In Eq. 5.10-1, the integrated decay power Q_{decay} is taken from p. 351 of PP&L Technical Report NPE-89-001, "The PP&L Approach To Risk Management And Risk Assessment (Second Revision)," January 1989. The decay power in (5.10-1) is taken from an independent source in order to provide an independent check on the decay power model used in SABRE.

Table 5.10-2 gives the suppression pool temperature as a function of time after shutdown as calculated from Eq. 5.10-1.

The sequence of events calculated by SABRE is presented in Table 5.10-3. Figure 5.10-1 compares the results in Table 5.10-2 against the SABRE calculation for suppression pool temperature. The good agreement between the results provides validation for the SABRE suppression pool temperature calculation, the containment heat structure calculation, and the SABRE decay heat model.

Table 5.10-1
Changes Made to Base 10x10 SABRE Input Deck in Appendix G

Parameter	New Value
Maximum number of time steps between detailed edits (F.1.1)	2000
Minimum number of time steps between detailed edits (F.1.2)	100
Problem end time (F.2.1)	100000 seconds
Number of print interval sets supplied (F.2.2)	1
Time step data (F.3)	Max = 5 msec Min = 5 msec (0<t<30 sec) Max = 50 msec Min = 50 msec (30<t)
Print intervals for general edits (F.5)	5000 seconds
Initial core thermal power (F.6.1)	3293 MWt
Time at which manual scram is initiated (F.19.6)	0.0
HPCI low water level initiation set point (F.20.2)	+13 inches
Time at which MSIV closure is initiated (F.25.1)	0.0
Normal CRD flow rate (F.33.1)	0.0 gpm (want injection flow from HPCI only)
Initial heat load from RPV to drywell (F.55)	0.0 Btu/sec (set to zero so all energy goes directly to SP)
Set point for loss of drywell cooling on high drywell pressure (F.58)	0.0 psig (trip drywell cooling at t=0)

Table 5.10-2
Suppression Pool Temperature Response Due to Decay Heat Addition (from Eq. 5.10-1)

Time After Shutdown (sec)	Cummulative Decay Power (Btu)	Suppression Pool Temperature (°F)
0	0.	90.0
1500	101,186,095.	102.8
2000	126,051,035.	105.8
3000	170,970,387.	111.1
4000	211,407,189.	115.9
6000	283,315,635.	124.4
8000	347,305,404.	132.0
10000	406,553,360.	139.0
15000	542,006,444.	155.0
20000	664,652,182.	169.4
30000	887,624,525.	195.6
40000	1,090,604,471.	219.3
60000	1,456,580,992.	261.8
80000	1,785,291,761.	299.7
100000	2,089,293,397.	334.5

Table 5.10-3
Sequence of Events Calculated by SABRE

```
*** Kinetics file is /d00/appl/sabre3v0/data/u2c10.simtran.out

*** SABRE data file is /home/eamac/sabre_31/input/ec-atws-0505/c10.dat

*** This is not a restart case

1   S A B R E  -  Version 3.1
    (10) Suppression pool heatup by decay heat (U2C10)


 t(sec)=        .000  Low-Pres Condensate Injection Inop.

 t(sec)=        .000  MSIV closure on specified time

 t(sec)=        .000  Scram initiated on specified time
                      Scram time (sec) =          2.80

 t(sec)=        .000  DW Cooler Trip on Hi DW Press
                      Trip Setpoint     =          .000 psig

 t(sec)=        .000  HPCI Suction Trans to SP on high SP level
                      SP water level =    23.00 ft

 t(sec)=       2.805  All Control Rods Inserted

 t(sec)=       3.090  HPCI initiation on Low water level
                      Setpoint for initiation =        13.00 in.

 t(sec)=       3.890  Level Setpoint Setdown
                      Setdown occurs when level drops to        13.00 in.
                      Delay for setpoint setdown =      .11E+02 sec

 t(sec)=       3.890  Recirc pump-A runback on low Rx lvl
                      Setpoint for Runback =        13.00 in.
                      Trip delay =      .300E+01 sec

 t(sec)=       3.890  Recirc pump-B runback on low Rx lvl
                      Setpoint for Runback =        13.00 in.
                      Trip delay =      .300E+01 sec

 t(sec)=       4.005  MSIVs are closed

 t(sec)=       8.320  RCIC initiation on low water level
                      Setpoint for initiation =       -38.00 in.

 t(sec)=       8.320  Recirc pump-A Trip on low Rx level
                      Setpoint for Trip =       -38.00 in.
                      Trip delay =      .900E+01 sec.

 t(sec)=       8.320  Recirc pump-B Trip on low Rx level
                      Setpoint for Trip =       -38.00 in.
                      Trip delay =      .900E+01 sec.

 t(sec)=      39.735  Main Turb Trip on high water level
                      Setpoint(inches) =       54.000

 t(sec)=      39.735  RCIC Trip on hi water level
                      Trip Setpoint =       .54E+02 in.

 t(sec)=      39.735  HPCI Trip on hi water level
                      Trip Setpoint =       .54E+02 in.

 t(sec)=      44.935  Feedwater Trip on high level
                      Trip Setpoint =       .54E+02 in.

 t(sec)=     801.535  HPCI initiation on Low water level
```

Setpoint for initiation = 13.00 in.

t(sec)= 931.485 HPCI Trip on hi water level
Trip Setpoint = .54E+02 in.

t(sec)= 2405.935 HPCI initiation on Low water level
Setpoint for initiation = 13.00 in.

t(sec)= 2541.285 HPCI Trip on hi water level
Trip Setpoint = .54E+02 in.

t(sec)= 4492.535 HPCI initiation on Low water level
Setpoint for initiation = 13.00 in.

t(sec)= 4628.185 HPCI Trip on hi water level
Trip Setpoint = .54E+02 in.

t(sec)= 6925.585 HPCI initiation on Low water level
Setpoint for initiation = 13.00 in.

t(sec)= 7054.185 HPCI Trip on hi water level
Trip Setpoint = .54E+02 in.

t(sec)= 9333.285 HPCI initiation on Low water level
Setpoint for initiation = 13.00 in.

t(sec)= 9442.785 HPCI Trip on hi water level
Trip Setpoint = .54E+02 in.

t(sec)= 11690.435 HPCI initiation on Low water level
Setpoint for initiation = 13.00 in.

t(sec)= 11816.285 HPCI Trip on hi water level
Trip Setpoint = .54E+02 in.

t(sec)= 14327.485 HPCI initiation on Low water level
Setpoint for initiation = 13.00 in.

t(sec)= 14438.435 HPCI Trip on hi water level
Trip Setpoint = .54E+02 in.

t(sec)= 16912.235 HPCI initiation on Low water level
Setpoint for initiation = 13.00 in.

t(sec)= 17036.135 HPCI Trip on hi water level
Trip Setpoint = .54E+02 in.

t(sec)= 19741.485 HPCI initiation on Low water level
Setpoint for initiation = 13.00 in.

t(sec)= 19854.385 HPCI Trip on hi water level
Trip Setpoint = .54E+02 in.

t(sec)= 22561.035 HPCI initiation on Low water level
Setpoint for initiation = 13.00 in.

t(sec)= 22683.485 HPCI Trip on hi water level
Trip Setpoint = .54E+02 in.

t(sec)= 25578.335 HPCI initiation on Low water level
Setpoint for initiation = 13.00 in.

t(sec)= 25692.935 HPCI Trip on hi water level
Trip Setpoint = .54E+02 in.

t(sec)= 28619.435 HPCI initiation on Low water level
Setpoint for initiation = 13.00 in.

t(sec)= 28741.185 HPCI Trip on hi water level
Trip Setpoint = .54E+02 in.

t(sec)= 31835.335 HPCI initiation on Low water level
Setpoint for initiation = 13.00 in.

t(sec)= 31951.635 HPCI Trip on hi water level
Trip Setpoint = .54E+02 in.

t(sec)= 35081.685 HPCI initiation on Low water level
Setpoint for initiation = 13.00 in.

t(sec)= 35203.035 HPCI Trip on hi water level
Trip Setpoint = .54E+02 in.

t(sec)= 38477.385 HPCI initiation on Low water level
Setpoint for initiation = 13.00 in.

t(sec)= 38595.185 HPCI Trip on hi water level
Trip Setpoint = .54E+02 in.

t(sec)= 41622.135 HPCI initiation on Low water level
Setpoint for initiation = 13.00 in.

t(sec)= 41724.585 HPCI Trip on hi water level
Trip Setpoint = .54E+02 in.

t(sec)= 44693.485 HPCI initiation on Low water level
Setpoint for initiation = 13.00 in.

t(sec)= 44806.885 HPCI Trip on hi water level
Trip Setpoint = .54E+02 in.

t(sec)= 47918.635 HPCI initiation on Low water level
Setpoint for initiation = 13.00 in.

t(sec)= 48025.635 HPCI Trip on hi water level
Trip Setpoint = .54E+02 in.

t(sec)= 51142.335 HPCI initiation on Low water level
Setpoint for initiation = 13.00 in.

t(sec)= 51254.135 HPCI Trip on hi water level
Trip Setpoint = .54E+02 in.

t(sec)= 54456.435 HPCI initiation on Low water level
Setpoint for initiation = 13.00 in.

t(sec)= 54565.885 HPCI Trip on hi water level
Trip Setpoint = .54E+02 in.

t(sec)= 57794.985 HPCI initiation on Low water level
Setpoint for initiation = 13.00 in.

t(sec)= 57906.785 HPCI Trip on hi water level
Trip Setpoint = .54E+02 in.

t(sec)= 61195.585 HPCI initiation on Low water level
Setpoint for initiation = 13.00 in.

t(sec)= 61306.585 HPCI Trip on hi water level
Trip Setpoint = .54E+02 in.

t(sec)= 64627.385 HPCI initiation on Low water level
Setpoint for initiation = 13.00 in.

t(sec)= 64739.835 HPCI Trip on hi water level
Trip Setpoint = .54E+02 in.

t(sec)= 68105.135 HPCI initiation on Low water level
Setpoint for initiation = 13.00 in.

t(sec)= 68217.485 HPCI Trip on hi water level
Trip Setpoint = .54E+02 in.

t(sec)= 71285.835 HPCI initiation on Low water level
Setpoint for initiation = 13.00 in.

t(sec)= 71381.385 HPCI Trip on hi water level
Trip Setpoint = .54E+02 in.

t(sec)= 74337.085 HPCI initiation on Low water level
Setpoint for initiation = 13.00 in.

t(sec)= 74442.585 HPCI Trip on hi water level
Trip Setpoint = .54E+02 in.

t(sec)= 77489.285 HPCI initiation on Low water level
Setpoint for initiation = 13.00 in.

t(sec)= 77589.985 HPCI Trip on hi water level
Trip Setpoint = .54E+02 in.

t(sec)= 80625.285 HPCI initiation on Low water level
Setpoint for initiation = 13.00 in.

t(sec)= 80729.535 HPCI Trip on hi water level
Trip Setpoint = .54E+02 in.

t(sec)= 83804.035 HPCI initiation on Low water level
Setpoint for initiation = 13.00 in.

t(sec)= 83907.135 HPCI Trip on hi water level
Trip Setpoint = .54E+02 in.

t(sec)= 86992.585 HPCI initiation on Low water level
Setpoint for initiation = 13.00 in.

t(sec)= 87097.185 HPCI Trip on hi water level
Trip Setpoint = .54E+02 in.

t(sec)= 90205.685 HPCI initiation on Low water level
Setpoint for initiation = 13.00 in.

t(sec)= 90310.185 HPCI Trip on hi water level
Trip Setpoint = .54E+02 in.

t(sec)= 93431.535 HPCI initiation on Low water level
Setpoint for initiation = 13.00 in.

t(sec)= 93536.935 HPCI Trip on hi water level
Trip Setpoint = .54E+02 in.

t(sec)= 96676.785 HPCI initiation on Low water level
Setpoint for initiation = 13.00 in.

t(sec)= 96782.535 HPCI Trip on hi water level
Trip Setpoint = .54E+02 in.

t(sec)= 99936.935 HPCI initiation on Low water level
Setpoint for initiation = 13.00 in.

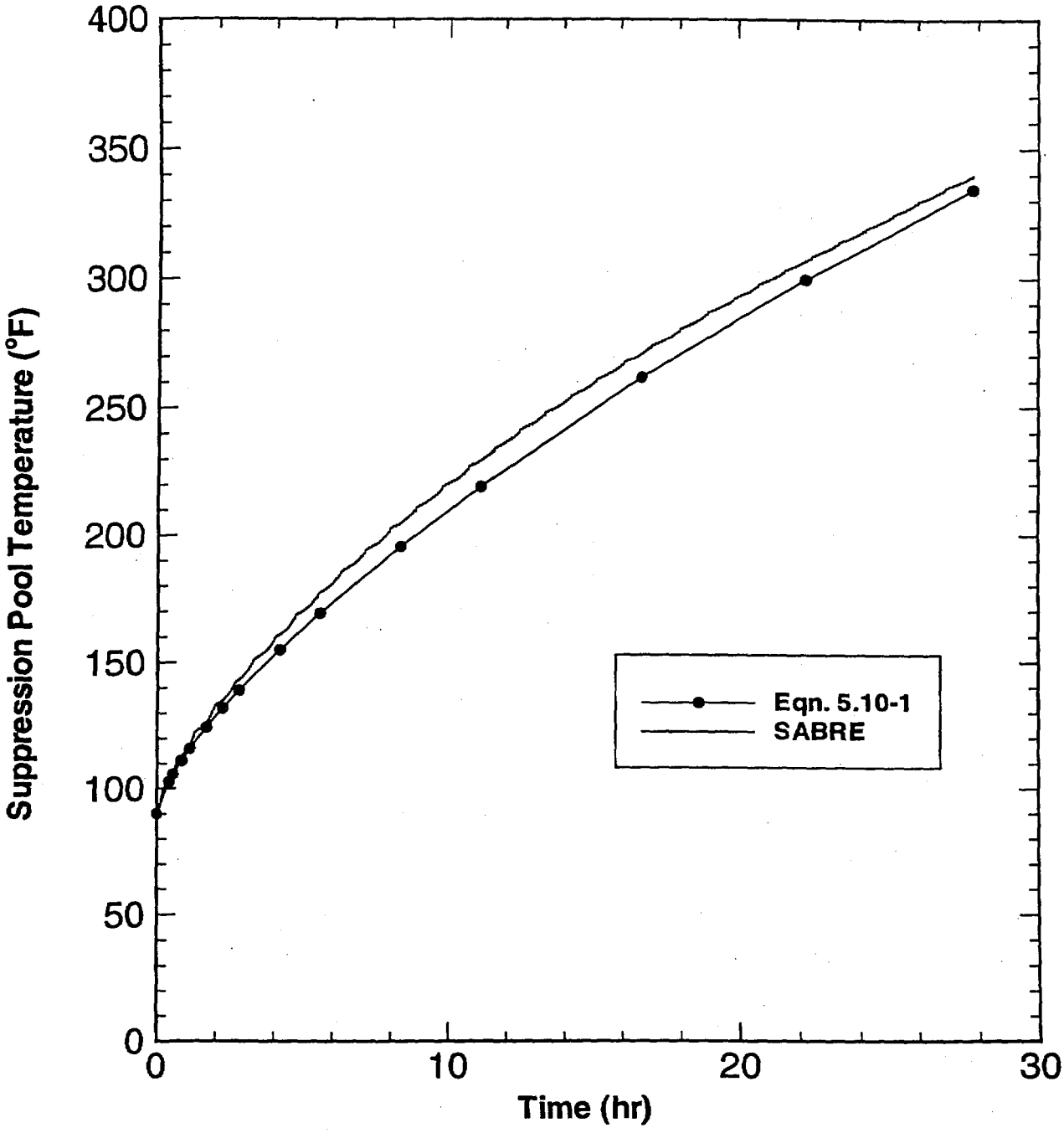

Figure 5.10-1 Comparison of SABRE-calculated suppression pool temperature against heat balance calculation (Eqn. 5.10-1) for MSIV-closure event with no decay heat removal.

5.11 Small Break LOCA - Comparison to GE SAFER/GESTR-LOCA Results

In this section, SABRE is compared with results from the GE SAFER/GESTR-LOCA Analysis for Susquehanna.[1] This benchmarking case compares break flow and reactor level with GE results for a 0.1 ft^2 liquid break in the recirculation discharge piping. In this scenario, offsite power becomes unavailable coincident with the LOCA. The GE analysis assumes that MSIVs remain open until they close on low reactor water level. This maximizes the loss of reactor coolant from the RPV. HPCI is assumed to be inoperable, and no credit is taken for RCIC injection. The water level setpoint for ADS initiation and MSIV closure used in the GE analysis is 366.5" above the bottom of the vessel which corresponds to TAF (-161"). The SABRE calculation is run until level reaches TAF. The kinetics file used in the SABRE calculation corresponds to U2C7 which is the initail power-uprate cycle. Changes made to the base input deck are documented in Table 5.11-1. This SABRE calculation corresponds to SABRE Case 11 in the Computer Case Summary.

In this scenario, a 0.1 ft^2 liquid break occurs at t=0. Feedwater injection coasts down to zero in 5 seconds as a result of the loss of offsite power. Recirculation pumps also trip at t=0 because of the loss of offsite power. Although closure of the MSIVs would follow from the LOOP, the isolation valves are maintained open in accordance with the GE calculation. GE assumes the MSIVs stay open until they close on low RPV level so as to maximize the loss of coolant inventory. The critical flow out the break is computed using the Homogeneous Equilibrium Model (HEM). In order to be consistent with the GE methodology, a flow multiplier of 1.25 is used for subcooled liquid in the SABRE calculation. The liquid at the break is subcooled in the time frame considered in this benchmark study. This critical flow model and multiplier are used by GE (GE-NE-187-22-0992, Table 3-1) for nominal LOCA calculations (not Appendix K calculations). Note that GE uses a multiplier of 1.0 in nominal calculations if the coolant is saturated.

The sequence of events calculated by SABRE for this SBLOCA is presented in Table 5.11-2. Figure 5.11-1 shows a comparison of calculation results for break flow, reactor water level, reactor pressure, and steam line flow. SABRE tends to somewhat overpredict the break flow and rate of level decrease as compared to the GE results, but overall the results show fairly good agreement.

---

[1] Pappone, D.C., "SAFER/GESTR-LOCA Analysis Basis Documentation for Susquehanna Steam Electric Station Units 1 and 2," GE-NE-187-22-0992, September, 1993.

Table 5.11-1
Changes Made to Base Input Deck in Appendix F

Parameter	New Value
Problem end time (F.2.1)	175 seconds (Run until level drops to TAF)
Hydraulic step size (F.3)	Max = Min = 5 msec for t<10 sec Max = Min = 25 msec for t>10sec
Initial core power (F.6.1)	3457 MWt (GE-NE-187-22-0992, Table 4-2)
Break Area (F.18)	0.1 ft^2 (GE-NE-187-22-0992, Section 6.1.1.3)
Break flow coefficient (F.18)	1.25 for subcooled water 1.00 for saturated water (GE-NE-187-22-0992, Table 3-1)
Time at which manual scram is initiated (F.19.6)	0.0 (scram on LOOP)
HPCI operability flag (F.20.1)	0 (HPCI is inoperable)
RCIC operability flag (F.21.1)	0 (RCIC is inoperable)
Trip recirc. pump 'A' on specified time (F.23.1)	0.0 seconds (get recirc pump trip on LOOP)
Trip recirc. pump 'B' on specified time (F.23.2)	0.0 seconds (get recirc pump trip on LOOP)
Feedwater flow versus time flag (F.24.15)	1 (Feedwater flow is specified in accordance with GE-NE-187-22-0992, Appendix C; FW starts to coast down immediately due to LOOP)
Number of points in FW flow versus time table (F.24.16)	7
Level setpoint for MSIV closure (F.25.2)	-999. (Setpoint is specified to prevent closure of MSIVs on Level 1. In GE LOCA analysis, low level setpoint is TAF, but since problem is run until level reaches TAF there is no need to close MSIVs in SABRE calculation)
ADS operability flag (F.27.1)	0 (Setpoint is specified to prevent ADS actuation on Level 1. In GE LOCA analysis, low level setpoint is TAF, but since problem is run until level reaches TAF there is no need to actuate ADS in SABRE calculation)
SRV area and actuation set points (F.31.4)	set points are specified in accordance with Table 4-5 of GE-NE-187-22-0992.
Gap Conductance (F.36.4)	870 Btu/hr-ft^2-°F. This value is appropriate for a full core of Siemens Nuclear Power (SNP) 9x9-2 fuel (Table 2.1 of GENE-637-024-0893). The GE SAFER/GESTR-LOCA Analysis for Susquehanna was carried out for SNP 9x9-2 fuel.

Table 5.11-2
Sequence of Events Calculated by SABRE

```
*** Kinetics file is /d00/appl/sabre3v0/data/u2c7.simtran.out

*** SABRE data file is /home/eamac/sabre_31/input/ec-atws-0505/c11.dat

*** This is not a restart case

1   S A B R E  -  Version 3.1
    Case 11 - 0.1 ft2 liq break LOCA (u2c7) - Benchmark to GE


 t(sec)=        .000  Liquid Break
                      Break Area                =          .100 ft2
                      Multiplier on break flow  =         1.250

 t(sec)=        .000  HPCI is Inoperable

 t(sec)=        .000  RCIC is Inoperable

 t(sec)=        .000  Low-Pres Condensate Injection Inop.

 t(sec)=        .000  ADS actuation is defeated

 t(sec)=        .000  Scram initiated on specified time
                      Scram time (sec) =          2.80

 t(sec)=        .000  Feedwater Flow determined from Table
                      Data in Table ends at t =       .10E+10 sec

 t(sec)=        .000  Recirc pump-A trip on specified time
                      Trip delay =      .000E+00 sec

 t(sec)=        .000  Recirc pump-B trip on specified time
                      Trip delay =      .000E+00 sec

 t(sec)=        .870  DW Cooler Trip on Hi DW Press
                      Trip Setpoint     =         1.720 psig

 t(sec)=       2.805  All Control Rods Inserted

 t(sec)=       4.390  Level Setpoint Setdown
                      Setdown occurs when level drops to        13.00 in.
                      Delay for setpoint setdown =      .11E+02 sec
```

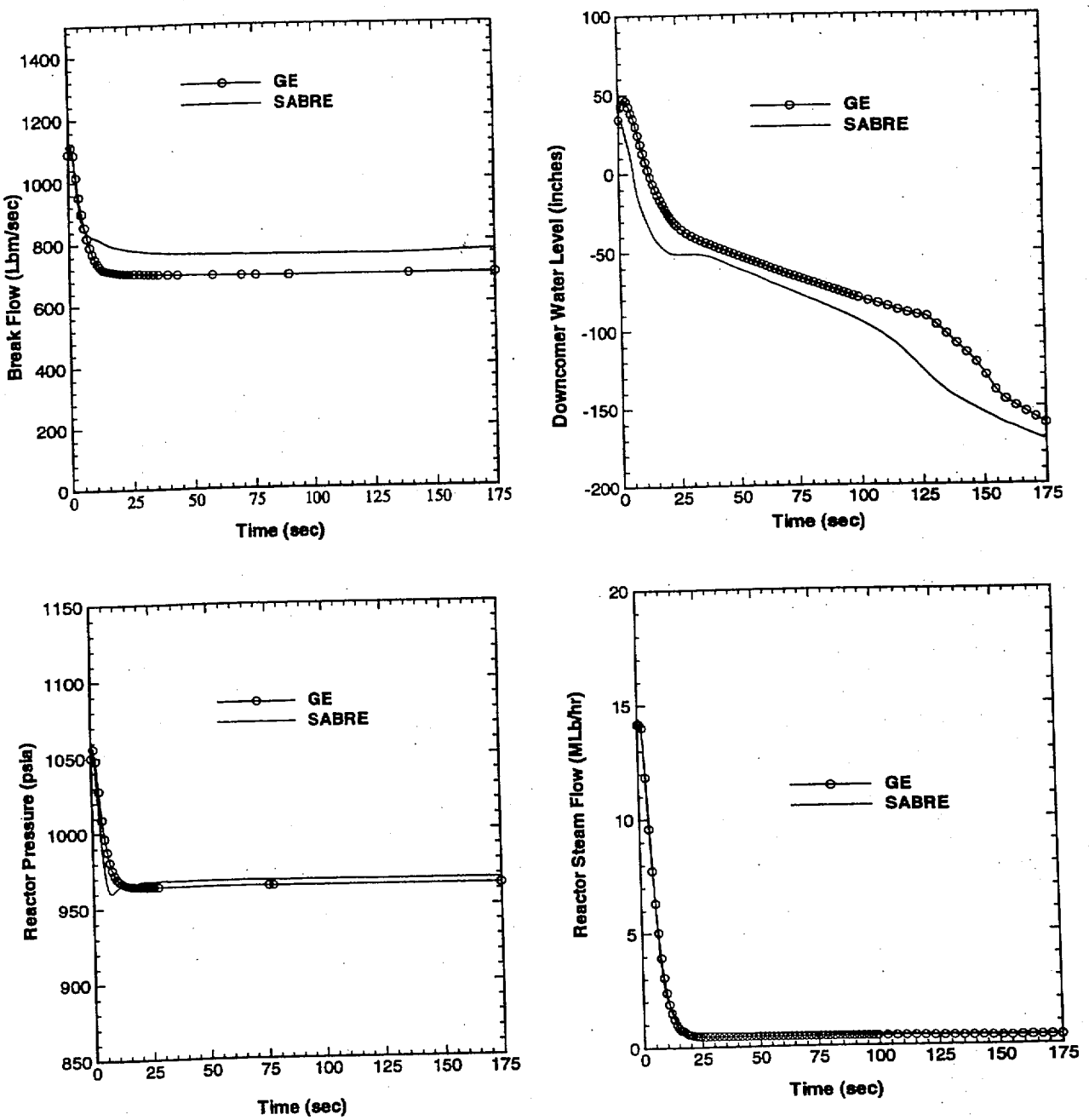

Figure 5.11-1 Comparison of SABRE results against GE SAFER/GESTR-LOCA analysis for 0.1 ft^2 liquid break. (SABRE Case 11)

5.12 Check of SABRE Mass Energy Balances with Core Spray Injection

In this test problem, the Core Spray injection table in the SABRE input deck is modified to allow initiation of Core Spray flow at 8000 gpm while the reactor is operating at normal conditions. The case is run for 250 seconds at which time conditions are essentially at steady state (there are only some minor fluctuations in core power and core flow at this time). The SABRE mass and energy balances are checked against hand calculations to ensure that the mass/energy addition associated with Core Spray injection is accounted for properly in the code. Changes made to the base input deck are documented in Table 5.12-1. This SABRE calculation corresponds to SABRE Case 12 in the Computer Case Summary.

The sequence of events calculated by SABRE for this test problem is presented in Table 5.12-2. In Table 5.12-3, the final general edit (at 250 seconds) for the run is shown. From the information in this general edit, the mass and energy balances for the first control volume in the upper plenum (the volume which receives the Core Spray injection flow) can be checked. Given the gas and liquid flow rates into the first upper plenum computaional cell, and the enthalpies associated with the inlet flows, the out flow of gas and liquid is computed by a hand calculation. The results of the hand calculation are compared to the values generated by SABRE to ensure that mass and energy are conserved.

The steady-state mass and energy balances for the first upper plenum cell are

$$W_{gU} + W_{\ell U} = W_{CS} + W_{gC} + W_{\ell C} + W_{gB} + W_{\ell B} \tag{5.12-1}$$

$$h_g W_{gU} + h_f W_{\ell U} = h_{CS} W_{CS} + h_g W_{gC} + h_f W_{\ell C} + h_g W_{gB} + h_f W_{\ell B} \tag{5.12-2}$$

where

W_{gU} = gas flow exiting Upper Plenum Cell 1 (Lbm/sec),
$W_{\ell U}$ = liquid flow exiting Upper Plenum Cell 1 (Lbm/sec),
W_{gC} = gas flow exiting Core Cell 27 (Upper Reflector) (Lbm/sec),
$W_{\ell C}$ = liquid flow exiting Core Cell 27 (Upper Reflector) (Lbm/sec),
W_{gB} = gas flow exiting Bypass Cell 5 (Lbm/sec),
$W_{\ell B}$ = liquid flow exiting Bypass Cell 5 (Lbm/sec),
h_g = saturation enthalpy of steam at reactor pressure (Btu/Lbm),
h_f = saturation enthalpy of water at reactor pressure (Btu/Lbm),
W_{CS} = core spray injection flow (Lbm/sec), and
h_{CS} = enthalpy of core spray injection flow (Btu/Lbm).

Solving (5.12-1) and (5.12-2) for W_{gU} and $W_{\ell U}$ gives

$$W_{gU} = \frac{a_{22}\, d_1 - a_{12}\, d_2}{a_{11}\, a_{22} - a_{21}\, a_{12}} \qquad (5.12\text{-}3)$$

and

$$W_{\ell U} = \frac{a_{11}\, d_2 - a_{21}\, d_1}{a_{11}\, a_{22} - a_{21}\, a_{12}} \qquad (5.12\text{-}4)$$

where

$a_{11} = 1,$
$a_{12} = 1,$
$a_{21} = h_g,$
$a_{22} = h_f,$
$d_1 = W_{CS} + W_{gC} + W_{\ell C} + W_{gB} + W_{\ell B}$, and
$d_2 = h_{CS} W_{CS} + h_g W_{gC} + h_f W_{\ell C} + h_g W_{gB} + h_f W_{\ell B}.$

The temperature of the water in the suppression pool for this case is 90 °F. The density of water at this temperature is 62.11 Lbm/ft^3. A Core Spray injection rate of 8000 gpm corresponds to

$$W_{CS} = \left(\frac{8000 gal}{\min}\right)\left(\frac{ft^3}{7.4805 gal}\right)\left(\frac{\min}{60\sec}\right)\left(\frac{62.11 Lbm}{ft^3}\right) = 1107.1 \text{ Lbm/sec.}$$

From Table 5.12-3, reactor pressure is 1021.575 psia. The gas phase and liquid phase enthalpies at this pressure are 1192.122 Btu/Lbm and 545.865 Btu/Lbm, respectively. Also, the core spray injection enthalpy is approximately the saturation enthalpy of 90°F water which is 58.018 Btu/Lbm. Using these specific enthalpies and the mass flow rates from Table 5.12-3 in Eqs. (5.12-3) and (5.12-4) results in

W_{gU} (hand calculation) = 3040.512 Lbm/sec, and
$W_{\ell U}$ (hand calculation) = 25853.32 Lbm/sec.

The SABRE calculated values from Table 5.12-3 are

W_{gU} (SABRE) = 3041.943 Lbm/sec, and
$W_{\ell U}$ (SABRE) = 25851.323 Lbm/sec.

The differences between the hand calculation and SABRE are

Δ_{gU} = (100%) (3041.943 – 3040.512)/(3040.512) = 0.05%
$\Delta_{\ell U}$ = (100%) (25851.323 – 25853.32)/(25853.32) = -0.01%

The small differences indicate that the mass and energy addition associated with the Core Spray injection is properly accounted for in SABRE.

For Core Spray injection, the injection enthalpy used in SABRE is the saturation enthalpy at the suppression pool temperature which is 58.018 Btu/Lbm in this test problem. In this problem, Core Spray injection is artificially initiated at rated reactor pressure to check the nodal mass and energy balances. If Core Spray injection could actually occur at rated reactor pressure, the injection enthalpy should be corrected for the added pressure imparted by the pump. However, in reality Core Spray only injects at low reactor pressures, and under these conditions, the enthalpy correction associated with the pump head is small and can be neglected.

Table 5.12-1
Changes Made to Base SABRE 9x9 Input Deck in Appendix F

Parameter	New Value	
Problem end time (F.2.1)	250 seconds	
Core Spray injection table (F.22a.2)	Core Spray Flow (gpm)	ΔP (psi)
	8000.	0.
	8000.	1000.
	8000.	10000.

Table 5.12-2
Sequence of Events Calculated by SABRE

```
*** Kinetics file is /d00/appl/sabre3v0/data/u2c9.simtran.out

*** SABRE data file is /home/eamac/sabre_31/input/ec-atws-0505/c12.dat

*** This is not a restart case

1   S A B R E  -  Version 3.1
    (12) Check Mass/Energy Balance with Core Spray (U2C9)


 t(sec)=        .000  Low-Pres Condensate Injection Inop.

 t(sec)=        .000  Initiation of Core Spray Flow
                      Reactor Press =      1035.30 psig
                      Supp Chamber Press =          .50 psig
```

Table 5.12-3
General Output Edit at 250 seconds

1 S A B R E - Version 3.1
0 (12) Check Mass/Energy Balance with Core Spray (U2C9)

** problem time and solver parameters

time (sec)	no. of steps	step size (sec)
250.01	16353	.0300

0*** 1-D Kinetics Results

Volume No.	Axial Power profile (fiss)	Axial Power profile (decay)	Fast Flux	Therm Flux	AbsXS_Thrm Liq_Boron (cm**-1)
25	.1665	.1514	.149008E+01	.4776567E+00	.00000E+00
24	.4933	.4487	.371805E+01	.7767447E+00	.00000E+00
23	.8539	.7770	.580333E+01	.8904190E+00	.00000E+00
22	1.0362	.9439	.723971E+01	.1106688E+01	.00000E+00
21	1.1744	1.0715	.820228E+01	.1287336E+01	.00000E+00
20	1.2737	1.1646	.882661E+01	.1423535E+01	.00000E+00
19	1.3401	1.2291	.918388E+01	.1524954E+01	.00000E+00
18	1.3830	1.2736	.933023E+01	.1597801E+01	.00000E+00
17	1.4008	1.2968	.931393E+01	.1641539E+01	.00000E+00
16	1.4204	1.3242	.918568E+01	.1606372E+01	.00000E+00
15	1.3918	1.3091	.884869E+01	.1603438E+01	.00000E+00
14	1.3471	1.2816	.836858E+01	.1583638E+01	.00000E+00
13	1.2883	1.2435	.780092E+01	.1546144E+01	.00000E+00
12	1.2177	1.1971	.718252E+01	.1493503E+01	.00000E+00
11	1.1383	1.1447	.654420E+01	.1428661E+01	.00000E+00
10	1.0568	1.0923	.591683E+01	.1357483E+01	.00000E+00
9	.9762	1.0427	.533153E+01	.1281727E+01	.00000E+00
8	.9020	.9996	.481615E+01	.1208923E+01	.00000E+00
7	.8400	.9683	.439973E+01	.1146666E+01	.00000E+00
6	.7933	.9536	.410874E+01	.1097549E+01	.00000E+00
5	.8022	.9530	.392580E+01	.1122467E+01	.00000E+00
4	.8253	.9551	.379520E+01	.1158305E+01	.00000E+00
3	.8086	.9363	.358695E+01	.1108408E+01	.00000E+00
2	.7177	.8330	.299384E+01	.9299905E+00	.00000E+00
1	.3524	.4093	.172827E+01	.6823881E+00	.00000E+00

1*** fuel/clad conditions

volume no.	avg fuel temp (degf)	clad temp (degf)	clad surface temp	heat flux (btu/ft2-sec)	film coefficient (btu/hr-ft2-f)	tcrit (deg f)	t(rewet) (deg f)
25	610.968	554.433	551.679	5.496	4395.0	570.52	642.90
24	739.025	563.054	554.926	16.282	7564.6	570.56	642.90
23	893.477	571.388	557.371	28.183	9952.3	570.67	642.90
22	977.697	575.389	558.408	34.204	10964.0	570.88	642.90
21	1044.502	578.356	559.134	38.769	11672.8	571.13	642.90
20	1094.160	580.459	559.630	42.051	12156.8	571.42	642.90
19	1128.255	581.858	559.951	44.252	12471.0	571.75	642.90
18	1150.747	582.761	560.156	45.683	12670.9	572.09	642.90
17	1160.327	583.142	560.242	46.287	12754.4	572.46	642.90
16	1171.052	583.565	560.336	46.959	12846.8	572.84	642.90
15	1156.441	582.988	560.207	46.042	12720.7	573.24	642.90
14	1133.665	582.077	560.001	44.598	12519.6	573.64	642.90
13	1104.058	580.869	559.724	42.694	12249.5	574.03	642.90
12	1069.122	579.409	559.384	40.407	11916.9	574.42	642.90
11	1030.614	577.753	558.989	37.834	11531.2	574.79	642.90
10	992.013	576.039	558.570	35.197	11122.1	575.15	642.90
9	954.792	574.332	558.141	32.596	10703.3	575.49	642.90
8	921.305	572.746	557.731	30.206	10303.5	575.81	642.90
7	893.976	571.413	557.378	28.219	9958.8	576.11	642.90
6	874.038	570.418	557.109	26.748	9695.7	576.40	642.90
5	877.678	570.601	557.159	27.018	9744.5	576.67	642.90
4	886.301	570.132	556.330	27.734	9797.9	576.85	642.90
3	875.719	567.064	553.521	27.175	9501.9	576.85	642.90
2	832.060	562.274	550.227	24.123	8793.0	576.85	642.90
1	678.794	553.557	547.878	11.893	4240.1	576.85	642.90

1volume no.	fuel temp1 (degf)	fuel temp2 (degf)	heat gen (btu/ft3-sec)	heat gen1 (btu/ft3-sec)	heat gen2 (btu/ft3-sec)
25	624.86	597.07	879.31	791.38	967.24
24	785.11	692.91	2604.86	2344.37	2865.34
23	983.66	803.23	4508.80	4057.92	4959.68
22	1094.06	861.25	5472.04	4924.84	6019.24
21	1182.60	906.30	6202.38	5582.14	6822.62
20	1248.93	939.28	6727.41	6054.67	7400.15
19	1294.71	961.68	7079.60	6371.64	7787.56
18	1325.00	976.36	7308.40	6577.56	8039.23
17	1337.94	982.59	7405.02	6664.52	8145.52
16	1352.43	989.55	7512.61	6761.35	8263.87
15	1332.69	980.07	7365.85	6629.26	8102.43
14	1301.99	965.22	7134.81	6421.33	7848.29
13	1262.20	945.80	6830.24	6147.22	7513.27
12	1215.43	922.71	6464.43	5817.99	7110.87
11	1164.13	897.00	6052.81	5447.53	6658.09
10	1112.96	870.97	5630.93	5067.84	6194.03
9	1063.90	845.61	5214.94	4693.44	5736.43
8	1019.98	822.56	4832.63	4349.37	5315.90
7	984.31	803.58	4514.79	4063.31	4966.26
6	958.38	789.64	4279.50	3851.55	4707.45
5	963.11	792.19	4322.78	3890.50	4755.06
4	974.58	797.96	4437.43	3993.68	4881.17
3	961.57	789.81	4348.03	3913.23	4782.83
2	905.77	758.30	3859.79	3473.81	4245.77
1	710.67	646.89	1895.22	1705.70	2084.74

1*** steam dome fluid conditions

vol no.	density (lb/ft3)	void fract	temp (deg f)	enthalpy (btu/lb)	w(bubl rise) (lb/sec)	w(stm line) (lb/sec)	w(cond) (lb/sec)	cond eff (%)	w-break (lbm/s)
1	2.280	1.000	547.431	1192.135	.000	3041.938	.000	.000	.00

0*** separator fluid conditions

vol no.	density (lb/ft3)	void fract	temp (deg f)	enthalpy (btu/lb)	boron conc (ppm)	gamma heat (btu/sec)	w-liquid (lb/sec)	w-gas (lb/sec)
1	19.045	.619	547.177	593.774	.000	.000	25851.293	3041.941
							25851.380	3041.937

0*** riser fluid conditions

vol no.	density (lb/ft3)	void fract	temp (deg f)	enthalpy (btu/lb)	boron conc (ppm)	gamma heat (btu/sec)	w-liquid (lb/sec)	w-gas (lb/sec)
1	18.973	.621	547.177	594.080	.000	.000	25851.380	3041.937
							25851.515	3041.932

0*** upper plenum fluid conditions

vol no.	density (lb/ft3)	void fract	temp (deg f)	enthalpy (btu/lb)	boron conc (ppm)	gamma heat (btu/sec)	w-liquid (lb/sec)	w-gas (lb/sec)
3	19.106	.618	547.177	593.511	.000	.000	25851.515	3041.932
2	21.125	.572	547.177	585.759	.000	.000	25851.680	3041.924
1	21.125	.572	547.177	585.759	.000	.000	25851.323	3041.943
							23910.489	3876.241

1*** by-pass fluid conditions

vol no.	density (lb/ft3)	void fract	temp (deg f)	enthalpy (btu/lb)	boron conc (ppm)	gamma heat (btu/sec)	w-liquid (lb/sec)	w-gas (lb/sec)
5	42.227	.093	547.177	549.090	.000	5046.392	2499.201	24.909
4	43.685	.060	547.177	547.865	.000	14636.932	2507.095	17.097
3	46.392	.000	546.076	544.430	.000	14435.574	2524.296	.000
2	46.716	.000	541.614	538.708	.000	10566.370	2524.306	.000
1	46.948	.000	538.318	534.520	.000	5747.670	2524.314	.000
							2515.479	.000

0*** core fluid conditions

vol no.	density (lb/ft3)	void fract	temp (deg f)	enthalpy (btu/lb)	boron conc (ppm)	gamma heat (btu/sec)	w-liquid (lb/sec)	w-gas (lb/sec)
27	16.548	.676	547.177	606.055	.000	.000	21411.288	3851.332
26	15.861	.692	547.177	610.109	.000	333.722	21410.798	3851.356
25	15.940	.690	547.177	609.624	.000	988.617	21439.565	3822.364
24	16.179	.684	547.177	608.187	.000	1711.219	21525.362	3736.448
23	16.610	.675	547.177	605.706	.000	2076.795	21673.900	3587.731
22	17.161	.662	547.177	602.705	.000	2353.979	21854.244	3407.240
21	17.830	.647	547.177	599.318	.000	2553.242	22058.730	3202.654
20	18.613	.629	547.177	595.659	.000	2686.908	22280.554	2980.749
19	19.512	.609	547.177	591.824	.000	2773.740	22514.007	2747.224
18	20.532	.585	547.177	587.878	.000	2810.409	22755.050	2506.149
17	21.676	.559	547.177	583.891	.000	2851.241	22999.301	2261.885
16	22.973	.530	547.177	579.854	.000	2795.538	23247.123	2014.071
15	24.405	.498	547.177	575.898	.000	2707.851	23490.138	1771.096
14	25.951	.462	547.177	572.111	.000	2592.254	23725.559	1535.740
13	27.618	.425	547.177	568.508	.000	2453.414	23950.957	1310.430
12	29.432	.383	547.177	565.047	.000	2297.186	24164.311	1097.187
11	31.393	.339	547.177	561.758	.000	2137.068	24364.110	897.521
10	33.461	.292	547.177	558.707	.000	1979.180	24550.029	711.771
9	35.679	.241	547.177	555.827	.000	1834.078	24722.274	539.742
8	38.035	.188	547.177	553.136	.000	1713.440	24881.955	380.323
7	40.533	.131	547.177	550.624	.000	1624.135	25031.177	231.390
6	43.299	.068	547.177	548.181	.000	1640.565	25172.669	90.218
5	46.388	.000	546.140	544.513	.000	1684.081	25263.243	.000
4	46.600	.000	543.225	540.768	.000	1650.152	25263.268	.000
3	46.805	.000	540.350	537.099	.000	1464.856	25263.279	.000
2	46.985	.000	537.780	533.840	.000	719.268	25263.339	.000
1	47.073	.000	536.513	532.240	.000	.000	25263.177	.000
							27778.658	.000

CC-A-[illegible]
Page 198

1*** lower plenum fluid conditions

vol no.	density (lb/ft3)	void fract	temp (deg f)	enthalpy (btu/lb)	boron conc (ppm)	gamma heat (btu/sec)	w-liquid (lb/sec)	w-gas (lb/sec)
2	47.073	.000	536.513	532.240	.000	.000	27778.658	.000
1	47.069	.000	536.573	532.316	.000	.000	27778.689	.000
							27778.718	.000

0*** jet pump fluid conditions

vol no.	density (lb/ft3)	void fract	temp (deg f)	enthalpy (btu/lb)	boron conc (ppm)	gamma heat (btu/sec)	w-liquid (lb/sec)	w-gas (lb/sec)
0	47.065	.000	536.634	532.392	.000	.000	27778.723	.000
							27778.718	.000

0*** downcomer fluid conditions

vol no.	density (lb/ft3)	void fract	temp (deg f)	enthalpy (btu/lb)	w(inject) (lb/sec)	h(inject) (btu/lb)	subcool (btu/lb)	mixture lvl (inches)	w-break (lbm/s)	boron (ppm)
1	47.065	.000	536.634	532.392	1928.169	351.879	13.461	50.796	.00	.00

0*** pressure drop results

	jet pump	lower plenum	core	by-pass	upper plenum	riser	separator
inlet (psi)	11.11	.00	.81	7.71	.00	1.54	3.79
outlet (psi)	1.18	5.40	1.09	.00	.00	.00	.00
elevation (psi)	-5.39	2.27	3.01	4.67	.71	1.34	.82
wall frict (psi)	1.68	.02	4.02	.00	.00	1.74	.36
spac frict (psi)			2.72				
spacial acc (psi)	.00	.00	.79	.00	.03	.04	-.01

1*** misc. reactor parameters

downcomer subcooling (btu/lbm)	=	13.461
downcomer collapsed level (inch)	=	50.796
steam dome pressure (psia)	=	1021.575
steam dome fluid volume (ft3)	=	8420.787
downcomer fluid volume (ft3)	=	5913.213
pressure regulator setpoint (psia)	=	966.434
downcomer bubble rise vel (ft/sec)	=	1.157
steam flow exiting vessel (lbm/sec)	=	3041.938
number of srvs open	=	0
steam condensation rate (lbm/sec)	=	.000
condensation efficiency	=	.000
core power (mw)	=	3038.40
core power (% of rated)	=	88.30
core inlet flow (mlb/hr)	=	90.92
by-pass inlet flow (mlb/hr)	=	9.06
total vessel fluid mass (lbm)	=	529466.18
crd outlet enthalpy (btu/lbm)	=	532.43